

**Continuous tall tower multispecies measurements in Europe
for quantifying and understanding
land-atmosphere carbon exchange**

Dissertation

zur Erlangung des akademischen Grades
doctor rerum naturalium (Dr. rer. nat.)

vorgelegt dem Rat der Chemisch-Geowissenschaftlichen Fakultät der
Friedrich-Schiller-Universität Jena

von Maria Elena Popa

geboren am 14 November 1974 in Oradea, Rumänien

Gutachter

1.

2.

Tag der öffentlichen Verteidigung:

Dedicated to Buni Ana

Thesis abstract

Atmospheric measurements are a tool to quantify greenhouse gas fluxes into and out of the atmosphere and to understand the underlying processes. This thesis presents measurements of greenhouse gases and related tracers from a new continental monitoring station.

Within the frame of the European project CHIOTTO, I was responsible to instrument a new tall tower monitoring station for atmospheric greenhouse gases and tracers related to the carbon cycle. For this purpose an analysis system for continuous, in-situ measurements of CO₂, CH₄, CO, N₂O and SF₆ mole fractions and O₂/N₂ ratio was designed and built at MPI-BGC, based around commercially available analysers. The challenge was to obtain a reliable, automatic system, which can run continuously without assistance, and to fulfill at the same time the high precision requirements for all the measured species. In July 2005 the measurement system was brought into operation at the final location, the tall tower station near Bialystok, in Eastern Poland.

The evaluation after 18 months of field operation confirmed the high quality of the measurements, and made possible studies of oxygen fractionation phenomena, contributing to the expertise of the presently small oxygen measurement community.

The quasi-continuous intracontinental measurements offer the possibility to study terrestrial and biogeochemical processes occurring on hourly, daily, seasonal, and annual time scales.

The record covering the first 18 months of measurements operation exhibits distinct seasonal cycles and superimposed short term variations on synoptic and diurnal time scales. The comparison of the CO₂ seasonal cycles between continental and marine sampling stations shows that the region is a sink of CO₂ during summer. The oxygen measurements in parallel with CO₂ permit quantifying the attenuation of oceanic influence over the continent, having therefore the potential to constrain the atmospheric transport and the longitudinal distribution of CO₂ sources and sinks.

Atmospheric oxygen measurements are currently used to determine the relative contribution of ocean and land biosphere to the carbon dioxide uptake. This approach is based on the stoichiometric coupling between oxygen and carbon dioxide in the processes of photosynthesis and respiration. The knowledge about the O₂:CO₂ ratio specific to the gas exchange between land biosphere and atmosphere is an essential factor for the

accuracy of this technique. There are at this time only few studies regarding this subject, and most of them based on small data sets. Using an extensive data set from the quasi-continuous measurement at the Bialystok station, I was able to examine in more detail the O₂:CO₂ ratio of the land biosphere signal and its temporal variability. The results do not correspond to the generally used average of the land biosphere O₂:CO₂ ratio, but they agree with other recent studies. This study constitutes a step towards improving the accuracy of partitioning between the land biosphere and ocean carbon uptake.

The respiration of the land biosphere represents one of the largest one-way carbon dioxide fluxes into the atmosphere. Because of its large potential variability, it is also one of the controlling factors for the net carbon exchange between the land biosphere and atmosphere. I propose a method to evaluate the night-time ecosystem respiration based on the temporal evolution of the vertical gradients of carbon dioxide. This method can provide results representative for local to regional spatial scales and it can be developed into a complementary method for the generally used eddy flux measurements.

Using the atmospheric data from the Bialystok station, I found statistically significant weekly variations of the measured gas species. The weekly periodicity can only be explained by anthropogenic influence, since there is no known natural phenomenon which could cause it. The results suggest that the observed weekly periodicity is not a local effect, but due to a large scale anthropogenic influence on atmosphere.

The mixing ratio data coupled with information about the atmospheric transport will be used to assess, by inverse modeling studies, the sources and sinks of carbon dioxide and other greenhouse gases targeted by the Kyoto Protocol at national, regional and European level. This is however an objective for the future, since it can only be achieved using data records covering many years.

In summary, this thesis contributes to the technological expertise in the developing field of atmospheric measurements, and to the understanding of processes and phenomena related to the land-atmosphere exchange of carbon dioxide and other greenhouse gases.

Kurzfassung

Messungen der Treibhausgaskonzentrationen in der Atmosphäre erlauben es, im Prinzip Treibhausgasflüsse in und aus der Atmosphäre zu quantifizieren und lassen deshalb Schlüsse auf die zugrunde liegenden Prozesse zu. Diese Doktorarbeit hat die Etablierung von Treibhausgasmessungen an einer neuen kontinentalen Messstation und die Interpretation der Messdaten zum Inhalt.

Als Teil des EU Projektes CHIOTTO war es meine Aufgabe, an einem 300 m hohen Fernsehmast in Polen Messinstrumente zu installieren, um Treibhausgase und weitere Tracer, welche mit dem Kohlenstoffzyklus zusammenhängen, zu messen. Dafür wurde ein Analysesystem basierend auf kommerziell erhältlichen Geräten entwickelt, welches quasi-kontinuierlich in-situ CO_2 , CH_4 , CO , N_2O und SF_6 Konzentrationen und das O_2/N_2 Konzentrationsverhältnis aufzeichnet. Die Herausforderung bestand darin, ein automatisiertes System zu entwickeln, welches ohne Überwachung im Stande ist zuverlässig zu messen, und welches gleichzeitig hohe Anforderungen an Messkonstanz und Genauigkeit erfüllt. Nach seiner Entwicklung, wurde das Messsystem im Juli 2005 an seinem Zielort, dem Fernsehmast in der Nähe von Bialystok in Ostpolen, installiert.

Eine Analyse des Messsystems nach 18 Monaten Laufzeit bestätigte dass das System die hohen Anforderungen an die Datenqualität erfüllt, und erlaubte es deshalb ausserdem detaillierte Studien der Fraktionierung von O_2 durchzuführen, welche international zur Erweiterung der Messexpertise in diesem Gebiet beigetragen haben.

Die gemessenen Daten erlauben es, unterschiedliche Fragen zu beantworten. In Kombination mit inversen Modellen des atmosphärischen Transports lassen sich Rückschlüsse über Quellen und Senken von CO_2 und weiterer im Kyoto Protokoll festgehaltener Treibhausgasen auf nationaler und europäischer Skala ziehen. Allerdings sollten sich dazu die Zeitreihen idealerweise über längere Zeiträume erstrecken. Des weiteren erlauben es die Daten terrestrische und biogeochemische Prozesse verbunden mit dem Kohlenstoffkreislauf auf Zeitskalen von Stunden, Tagen, Jahreszeiten und Jahren zu studieren.

Die Zeitreihen der ersten 18 Messmonate weisen saisonale Zyklen moduliert durch Variationen auf der synoptischen und Tagesskala auf. Ein Vergleich des saisonalen Zyklus von CO_2 der kontinentalen Bialystok Station mit einer marinen Station zeigt, dass die Region im Sommer eine Kohlenstoffsенке ist. Der mitgemessene Sauerstoff erlaubt es, den ozeanischen Anteil des CO_2 Signals zu schätzen. Die Sauerstoffzeitreihe enthält

deshalb wertvolle Information über vertikalen atmosphärischen Transport und somit die zonale Verteilung von CO₂ Quellen und Senken.

Atmosphärische Sauerstoffkonzentrationen werden auch dazu verwendet, den relativen Anteil der Kohlenstoffaufnahme der Ozeane im Vergleich zu dem Festland zu schätzen. Diese Methode beruht darauf, dass Sauerstoff und Kohlenstoff komplementär in die Prozesse der Photosynthese und Respiration involviert sind. Das stöchiometrische Verhältnis von O₂:CO₂ während der Aufnahme und Abgabe von Kohlenstoff zwischen organischen Kohlenstoffreservoirs und der Atmosphäre ist ein essentielles Element dieser Rechnung. Zurzeit existieren nur wenige Studien, die diese Grösse schätzen, und die meisten verwenden nur kleine Datensätze. Im Gegensatz erlaubt der umfassende Datensatz der polnischen Messstation, das O₂:CO₂ Verhältnis für Austausch mit der Landbiosphäre detaillierter zu bestimmen und seine zeitliche Variabilität zu bestimmen. Die Resultate decken sich nicht mit dem üblicherweise verwendeten Wert, aber stimmen gut mit denjenigen neuerer, unabhängiger Messungen überein. Dieses Resultat trägt deshalb dazu bei, die Genauigkeit der Trennung zwischen Ozean- und Landkohlenstoffaufnahme zu verbessern.

Die Kohlenstoffmenge welche durch Respiration der Landbiosphäre in die Atmosphäre abgegeben wird, ist einer der grössten gerichteten Flüsse im Kohlenstoffkreislauf. Aufgrund seiner potentiell hohen Variabilität ist es auch einer der Hauptfaktoren für einen potentiellen Netto Kohlenstoffverlust der Landbiosphäre. In dieser Arbeit schlage ich eine Methode zur Bestimmung der Respiration während der Nacht vor, welche auf der zeitlichen Entwicklung des vertikalen CO₂ Gradienten beruht. Die Resultate sind repräsentativ für eine Fläche von ~ 100 km² und die Methode komplementär zur Eddyflussmethode, welche in der Nacht nicht anwendbar ist.

In den Daten von der Bialystok Station habe ich signifikante Variation mit der Periode von einer Woche nachgewiesen. Diese Periode lässt sich nur durch anthropogene Einflüsse erklären, da kein anderes natürliches Phänomen welches mit dieser Periode variiert, bekannt ist. Die Resultate suggerieren, dass die Periodizität nicht ein lokaler Effekt ist, sondern durch grossskaligen anthropogenen Einfluss auf die Atmosphäre zustande kommt.

Zusammenfassend trägt diese Doktorarbeit zum einen zu der technischen Expertise in dem Gebiet der Treibhausgaskonzentrationsmessung bei, und zum andern zum Verständnis der Prozesse im Zusammenhang mit dem Austausch von Kohlendioxid und anderen Gasen zwischen der Landbiosphäre und der Atmosphäre.

Table of contents

Title page	1
Dedication page	3
Thesis abstract	5
Kurzfassung	7
Table of contents	9
List of figures and tables	13
Chapter 1. Introduction	17
1.1. Background	19
1.2. The CHIOTTO project	23
1.3. Bialystok site description	25
1.4. General information about the gas species measured at Bialystok tall tower station	26
1.5. Thesis outline	32
1.6. References	33
Chapter 2. Technical description of the measurement system	41
2.1. Introduction	43
2.2. CO ₂ and O ₂ /N ₂ measurement	44
2.2.1. Introduction	44
2.2.2. Measurement unit convention for oxygen	45
2.2.3. About oxygen fractionation	47
2.2.4. Instrument theory	50
2.2.5. Gas handling scheme	52
2.2.6. Measurement routine and calculations	64
2.2.7. Gas handling strategy for counteracting fractionation effects	68
2.3. CH ₄ , CO, N ₂ O and SF ₆ measurement	70
2.3.1. Introduction	70
2.3.2. Measurement description	71
2.4. Flask sampling	80
2.5. Meteorological measurement	81
2.6. Quality check and flagging	82
2.6.1. Quality control means	82
2.6.2. Data post-processing and flagging	83
2.7. References	84
Chapter 3. Evaluation of the measurement system performance after 18 months of operation	87
3.1. Introduction	89
3.2. Data time coverage and quality	90
3.2.1. Data time coverage	90
3.2.2. Data quality	91

3.3.	Measurement stability and precision	92
3.3.1.	Precision estimated from target measurements	92
3.3.2.	Analysers' stability and drifts	96
3.4.	Oxygen fractionation	99
3.4.1.	Stability of the high pressure cylinders	99
3.4.2.	Comparison between main and control inlet lines	105
3.5.	Comparisons between in-situ and flask samples results	110
3.6.	Summary and conclusions	115
3.7.	References	116
Chapter 4.	Overview of the atmospheric data from Bialystok tall tower station	117
4.1.	Introduction	119
4.2.	General presentation of the data series	120
4.3.	Vertical gradients of the mixing ratios	127
4.4.	Diurnal variations of atmospheric mixing ratios	131
4.4.1.	Diurnal variations of CO ₂ and O ₂ /N ₂	131
4.4.2.	Diurnal variations of CH ₄ , CO, N ₂ O and SF ₆	133
4.5.	Seasonal variations of atmospheric mixing ratios	136
4.5.1.	Data and data processing	136
4.5.2.	Seasonal variation of CO ₂ mole fraction	138
4.5.3.	Seasonal variation of O ₂ /N ₂ ratio	141
4.5.4.	Seasonal variations of CH ₄ , CO, N ₂ O and SF ₆	146
4.6.	Summary and conclusions	149
4.7.	References	151
Chapter 5.	Correlation between diurnal variations of atmospheric oxygen and carbon dioxide	153
5.1.	Background and introduction	155
5.2.	Methods	156
5.2.1.	Measurement site and data	156
5.2.2.	Data processing	159
5.2.3.	Errors affecting the calculated O ₂ :CO ₂ ratio	160
5.3.	Results and discussion	161
5.4.	Summary and conclusions	166
5.5.	References	167
Chapter 6.	Estimation of night time ecosystem respiration	169
6.1.	Introduction	171
6.2.	Data	172
6.3.	Methods for the calculation of night time CO ₂ emission	174
6.3.1.	The principle	174
6.3.2.	Method 1 – daily estimation	174
6.3.3.	Method 2 – monthly average	175
6.3.4.	Method 3 – moving time window	177
6.4.	Results and discussion	178
6.4.1.	Time series	178
6.4.2.	Comparison with the temperature function from Lloyd and Taylor (1994)	180

6.4.3.	Calculation errors	181
6.4.4.	Comment: Using the atmospheric temperature as predictor for ecosystem respiration	183
6.5.	Conclusions	183
6.6.	References	184
Chapter 7.	Weekly variations of atmospheric CO₂, CO, CH₄, N₂O and SF₆	187
7.1	Introduction	189
7.2	Data	189
7.3	Data processing and results	190
7.3.1	Correlations between the weekly cycles of the mixing ratio of different species	195
7.3.2	Correlations between the weekly cycle of mixing ratios and the meteorological parameters	198
7.4	Discussion	202
7.5	Summary and conclusions	204
7.6	References	205
Chapter 8.	Final conclusions and remarks	207
Appendices		
A 1	Europe maps: physical, land use and population density	215
A 2	Derivation of formula used to calculate the variation of O ₂ mole fraction	217
A 3	Description of the gas chromatographic method	218
A 4	MODEL-2 least squares fit	221
A 5	Supplementary figure for Chapter 7	223
	List of abbreviations and acronyms	225
	Definitions	227
	Acknowledgements	229
	Curriculum Vitae	233
	Presentations	235
	Selbständigkeitserklärung	237

List of figures and tables

Figure 1.1	Atmospheric concentrations of important long-lived greenhouse gases over the last 2,000 years	20
Figure 1.2	Global mean annual temperature between 1850 and 2005	21
Figure 1.3	Footprint area of the CHIOTTO network	23
Table 1.1	Chiotto precision and accuracy goals	24
Figure 1.4	Footprint area of the Bialystok tall tower station	25
Figure 1.5	The global carbon cycle	27
Figure 1.6	Components of the global carbon budget during the industrial period	28
Table 1.2	Atmospheric mixing ratios for the year 2005, atmospheric lifetimes and global warming potentials	32
Figure 2.1	Gas handling diagram for CO ₂ and O ₂ measurement	53
Figure 2.2	Scheme of the installation of CO ₂ and O ₂ analysers in the thermostated chamber	54
Figure 2.3	Valve switching between the two Oxzilla cells	55
Figure 2.4	The differential signal of the oxygen analyser	56
Figure 2.5	Diagram of air inlet setup for CO ₂ and O ₂ measurement	58
Figure 2.6	The two types of air inlet used for CO ₂ and O ₂ /N ₂ measurement	59
Figure 2.7	Air inlet design	59
Figure 2.8	Diagram of calibration and reference gases	60
Figure 2.9	Gas drying system	62
Figure 2.10	Cold traps design	63
Figure 2.11	Illustration of gas chromatographic measurement principle	71
Figure 2.12	The GC system diagram – LOAD position	73
Table 2.1	GC measurement specifications	74
Figure 2.13	Typical chromatogram	75
Figure 2.14	Diagram of external gas handling system for the GC measurement	76
Figure 2.15	The sample ratio calculation for the GC measurement	77
Figure 2.16	Principle scheme of the flask sampling system	81
Figure 3.1	Time coverage of the measurement at Bialystok	91
Table 3.1	Proportion of good, questionable and bad data for each gas species	92

Figure 3.2	Target gas record for the gas species measured at Bialystok	94
Table 3.2	Typical long term repeatability of Bialystok measurement	95
Figure 3.3	Comparison between the atmospheric variability and the noise of the target measurement	95
Figure 3.4	Comparison between the direct CO ₂ analyser response and the calibrated measurement result	97
Figure 3.5	CO ₂ measurement noise on different time scales	97
Figure 3.6	Evolution of the chromatogram due to accumulation of impurities inside the gas paths	98
Figure 3.7	Time evolution of the O ₂ /N ₂ ratio of the working tanks	100
Table 3.3	The O ₂ /N ₂ average drifts for the working tanks	100
Figure 3.8	O ₂ /N ₂ measurement series of the target cylinder	101
Figure 3.9	The two types of air sampling lines used for CO ₂ and O ₂ /N ₂ measurement	105
Figure 3.10	CO ₂ , O ₂ /N ₂ and APO at 300m: comparison between the main and control sampling lines	107
Figure 3.11	The difference between the air sampled through the main and control lines from the 300m height	108
Figure 3.12	The APO difference between the air sampled through the main and control lines from the 30m height	108
Figure 3.13	Difference between the interpolated value of the in-situ measurement results and the measured flask value	112
Table 3.4	Results of the t-tests for the differences between in-situ measurement and the flask samples results	113
Figure 4.1	Time series of CO ₂ and O ₂ /N ₂ measurement	121
Figure 4.2	Time series of CH ₄ measurement	122
Figure 4.3	Time series of CO measurement	123
Figure 4.4	Time series of N ₂ O measurement	124
Figure 4.5	Time series of SF ₆ measurement	125
Figure 4.6	Interval selected from the SF ₆ record, including two pollution events and the corresponding air mass back-trajectories	126
Figure 4.7	Variations of the vertical gradients of CO ₂ mole fraction, atmospheric temperature, potential temperature and the potential temperature gradients typical for the warm season	128
Figure 4.8	Variations of the vertical gradients of CO ₂ mole fraction and the potential temperature gradients typical for the cold season	129
Figure 4.9	Average summer and winter vertical profiles of CO ₂ mole fraction at different times of day	130

Figure 4.10	Vertical profiles of CO ₂ , CH ₄ , CO, N ₂ O and SF ₆ representative for day and night time, during summer	131
Figure 4.11	Average daily cycle of CO ₂ mole fraction during Apr – Sep-2006	132
Figure 4.12	Monthly averaged diurnal cycles of CO ₂ and O ₂ /N ₂ , for different sampling heights above ground level	133
Figure 4.13	Average diurnal variation of CO ₂ , CH ₄ , CO, N ₂ O and SF ₆ for the period Jun – Sep-2006	135
Table 4.1	Location and coordinates of the sampling stations	136
Figure 4.14	Location of the sampling stations	137
Figure 4.15	Seasonal harmonic fit to the CO ₂ data from Bialystok	139
Figure 4.16	Four-harmonic seasonal components of the CO ₂ mole fraction at BIK	139
Figure 4.17	Four-harmonic seasonal components of the CO ₂ mole fraction at different sampling stations	140
Figure 4.18	Seasonal cycles of CO ₂ , O ₂ /N ₂ and APO at BIK, for two sampling heights	141
Figure 4.19	Seasonal cycles of CO ₂ , O ₂ /N ₂ , and the oceanic and land biosphere components of the O ₂ /N ₂ , at BIK and SIS	145
Figure 4.20	O ₂ /N ₂ versus CO ₂ for SIS and BIK	146
Figure 4.21	Two harmonic components of the curve fit to the CH ₄ , CO, N ₂ O and SF ₆ afternoon data	147
Figure 4.22	Seasonal curve fit to the SF ₆ afternoon data	148
Figure 5.1	Summer typical day – night variation of CO ₂ and O ₂ /N ₂ for different sampling heights	157
Figure 5.2	Illustration of CO ₂ and O ₂ /N ₂ variations over 24-hours and the corresponding O ₂ :CO ₂ ratio calculated as slope of a linear fit	159
Figure 5.3	Diurnal O ₂ :CO ₂ ratio at 30m height in the vegetation intervals in 2005 and 2006	161
Figure 5.4	Diurnal O ₂ :CO ₂ ratio at 30m height in the vegetation intervals compared to the daily averaged meteorological parameters	164
Figure 5.5	Daily O ₂ :CO ₂ at 30, 90 and 300m above ground level	165
Figure 6.1	Land cover map of the area surrounding the BIK tower	172
Figure 6.2	Example of CO ₂ measured in air sampled at different heights above ground, over a 24-hours interval	173
Figure 6.3	Night time CO ₂ emission calculation for the daily step method	175
Figure 6.4	Illustration of the monthly calculation method	176
Figure 6.5	Monthly averaged diurnal CO ₂ variation	176

Figure 6.6	Illustration of the moving time window method	177
Figure 6.7	Night time respiration calculated by three methods	178
Figure 6.8	CO ₂ emission versus mean atmospheric temperature	179
Figure 6.9	Respiration versus atmospheric temperature and the fitted Lloyd curves for the three calculation methods	180
Figure 6.10	The respiration normalized to R ₁₀ and the normalized function of temperature	181
Figure 7.1	Example of CO ₂ measurement results in the cold and warm seasons	190
Table 7.1	Sample characteristics for each sampling height	191
Figure 7.2	CO ₂ averages for each day of week	191
Figure 7.3	The distribution of the CO ₂ concentration data compared with the normal distribution	192
Figure 7.4	Multiple comparison based on Kruskal-Wallis ANOVA for the CO ₂ concentration in air sampled at 300m agl.	193
Figure 7.5	Multiple comparison tests for the CO ₂ concentration versus day of week, for the sampling heights 5, 30, 90 and 180m agl.	193
Figure 7.6	Distribution of the measurement time for each day of the week, for the 300m sampling height.	194
Figure 7.7	Winter weekly variation for CH ₄ , CO, CO ₂ , N ₂ O and SF ₆	196
Figure 7.8	Weekly CO and CH ₄ versus CO ₂	197
Figure 7.9	Summer weekly variation for CH ₄ , CO, CO ₂ , N ₂ O and SF ₆	198
Figure 7.10	Anomalies of mixing ratio and meteorological parameters function of day of week for winter and summer time	199
Figure 7.11	Correlations between the weekly cycle of each gas species and the weekly cycle of the meteorological parameters	201

Chapter 1.

Introduction

1.1	Background	19
1.2	The CHIOTTO project	23
1.3	Bialystok site description	25
1.4	General information about the gas species measured at Bialystok tall tower station	26
1.5	Thesis outline	32
1.6	References	33

1.1 Background

The greenhouse effect is a natural process by which some constituents of the atmosphere absorb the infrared radiation emitted by the Earth surface, having as direct result the warming of the lower to mid-troposphere. The phenomenon was discovered as early as 1827 by J. Fourier and firstly quantified in 1896 by S. Arrhenius.

The gases in the atmosphere that significantly absorb infrared radiation are referred to as “greenhouse gases”. Naturally occurring greenhouse gases include water vapor, tropospheric ozone (O₃), carbon dioxide (CO₂), methane (CH₄), and nitrous oxide (N₂O). Natural abundances of greenhouse gases are responsible for a warming of the Earth surface on the order of 33°C.

The amount of heat energy added to the earth and to the lower atmosphere by the greenhouse effect is depending on the concentration of greenhouse gases in the atmosphere. Arrhenius (1896) estimated that the Earth temperature would increase by 5 - 6 degrees in case of doubling CO₂ concentration.

Since the industrial era began, atmospheric concentrations of CO₂ and other greenhouse gases have increased rapidly (e.g. Neftel et al., 1994, Keeling and Whorf, 2005). For example, global mean concentration of CO₂ in the atmosphere has reached a record (379 ppm) in 2005, higher than observed over the past half-million years, and has done so at an extremely fast rate (Barnola et al., 2003). Global surface air temperature has also increased by 0.74 ± 0.18 °C over the past 100 years (estimated for the period 1906 – 2005 from HadCRUT3 dataset, Brohan et al., 2006) and the temperature increase rate has accelerated in the recent decades (figure 1.2). There is also evidence for changes over the last century in other climate aspects like precipitation, frequency of extreme events, sea level, ice and snow coverage (summarized in Trenberth et al., 2007).

Recognizing the problem of potential global climate change, the World Meteorological Organization (WMO) and the United Nations Environment Programme (UNEP) established in 1988 the Intergovernmental Panel on Climate Change (IPCC), with the mission to assess scientific, technical and socio-economic information relevant for the understanding of climate change, its potential impacts and options for adaptation and mitigation.

In the last decades it became increasingly clear that the observed climate changes are mostly anthropogenic, as a result of the enhanced atmospheric greenhouse gas concentrations caused by fossil fuel burning, cement manufacture, increase in agricultural

and industrial production due to fast growth in human population (e.g. Levitus et al., 2001, Barnett et al., 2001, Stott et al., 2001, Tett et al., 2002, Stone et al., 2007). It became also clear that strong global action is necessary in order to reduce future human impact on climate. The Montreal Protocol on substances that deplete the ozone layer (entered into force on 01-Jan-1989), following which the CFC's emissions were strongly reduced, was an example of successful international cooperation.

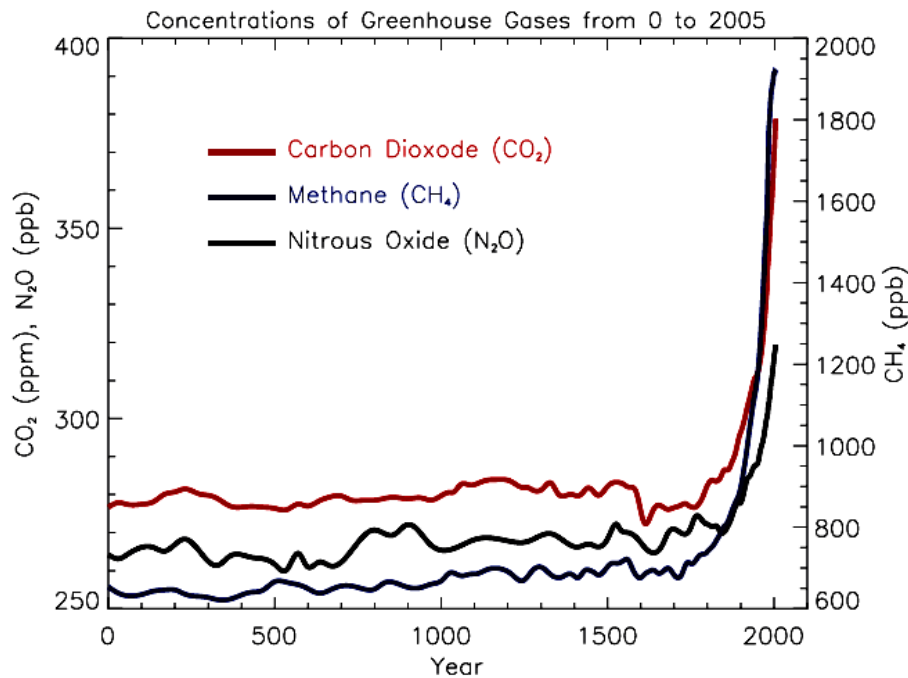


Figure 1.1 Atmospheric concentrations of important long-lived greenhouse gases over the last 2,000 years. The figure is from Forster et al., 2007.

A next step was the Kyoto Protocol (negotiated in December 1997), by which industrialized nations have committed to make substantial reductions in their emissions of greenhouse gases by 2012. As of December 2006, a total of 169 countries and other governmental entities have ratified the agreement. The target gases of the Kyoto protocol (the “Kyoto” gases) are: CO₂, CH₄, N₂O, SF₆, HFCs and PFCs.

For scientific as well as for political reasons it is important to estimate how the climate will evolve in the future, for different emission scenarios of various gases. Mathematical models allow in principle examination of the response of the coupled land surface climate system to a range of possible future atmospheric greenhouse gas concentration evolutions. However the accuracy of the models' projections is dependent on the knowledge about the actual state and about the processes which govern the changes.

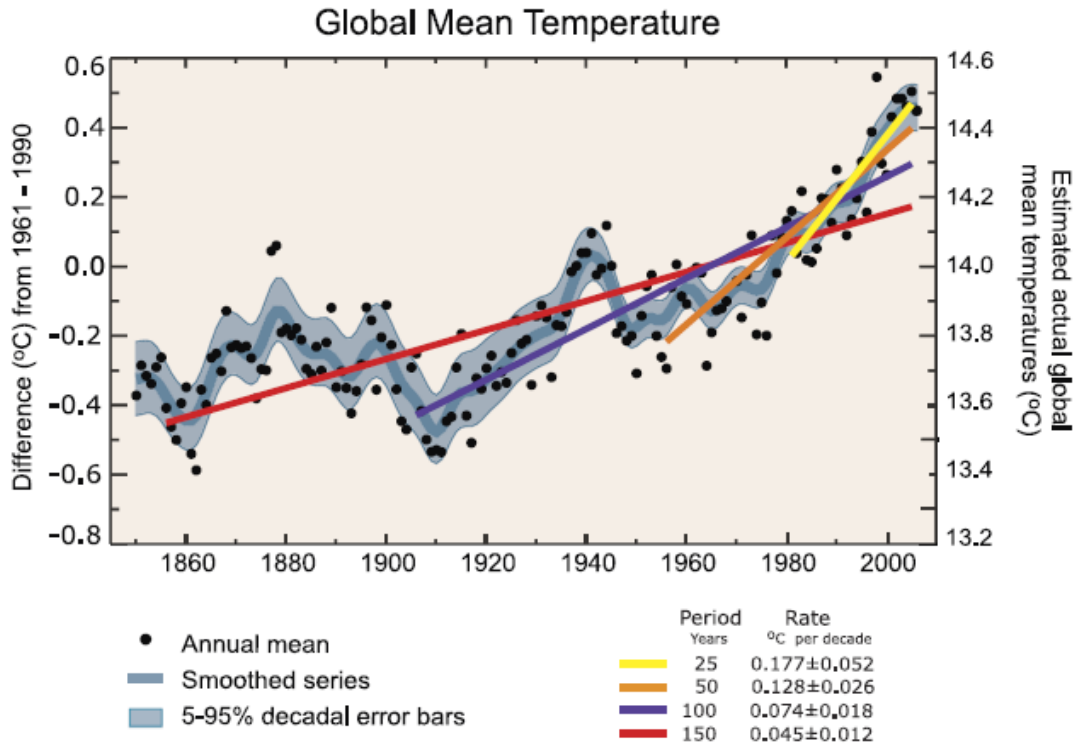


Figure 1.2 Global mean annual temperature between 1850 and 2005 in absolute value (right axis) and relative to the 1961 to 1990 mean (left axis). The figure is from Forster et al., 2007 and is based on the dataset HadCRUT3 (Brohan et al., 2006)

One way to increase our knowledge is by direct measurements of the atmospheric composition. This is because the spatial and temporal variation of the concentrations of greenhouse gases in the atmosphere carries information about (i) spatial distribution and intensity of fluxes into and out of the atmosphere (sources and sinks), (ii) factors controlling the time variations of fluxes and (iii) interactions and feedbacks of different processes and variables. Using atmospheric concentration measurements together with information about atmospheric transport, it is possible to estimate the strength and location of the contributing fluxes. The method is called “atmospheric inversion” and has been greatly developed in the past two decades (e.g. Tans et al., 1989, 1990, Enting and Mansbridge, 1991, Enting et al., 1995, Fan et al., 1998, Rayner et al., 1999, Bousquet et al., 1999a, 1999b; Heimann and Kaminski, 1999, Kaminski and Heimann, 2001, Gurney et al., 2002; Roedenbeck et al., 2003a, 2003b, Gerbig et al., 2003a, 2003b).

Monitoring of the atmospheric concentration of CO₂ has been started in 1958 by C. D. Keeling from the Scripps Institution of Oceanography (SIO) at Mauna Loa Observatory, Hawaii, which is in the present the longest continuous atmospheric CO₂

record (e.g. Keeling et al., 1976, Keeling and Whorf, 2005). Many other monitoring stations and networks have been developed in the mean time and are currently in operation, including besides CO₂ measurements of other greenhouse gases like CH₄, N₂O, SF₆ (e.g. SIO air sampling network, NOAA CMDL CCGG cooperative air sampling network, GAW network of measurement stations, CSIRO measurement program). Long observational records already exist from various stations all over the world.

Traditionally, most of the measurement stations are remotely located. Continental stations have been avoided because the large concentration variability in the vicinity of strong sources makes the data difficult to interpret. The signal measured at a remote location is representative for hemispheric or global scale, but has already lost part of the spatial and temporal resolution due to the strong mixing of the lower troposphere. In the recent years inverse modeling studies have identified the lack of continental stations as strong limitation in resolving the longitudinal sources and sinks distribution (Fan et al., 1998, Prentice et al., 2000, Schimel et al., 2001, Gloor et al., 2000).

Tans (1991) proposed a strategy to address the need of continental measurements, overcoming the main problems associated with them, by measuring CO₂ and other gas species on tall towers. To infer fluxes at regional level, it is useful to sample close to the earth surface (in the boundary layer), where the proximity to sources and sinks results in large signals with high temporal resolution. If the gases are measured at sufficient height above ground (ideally few hundred meters to avoid local influences), the signal integrates fluxes from a footprint on the order of 500 to 1000 km around (Gloor et al., 2001). Sampling continuously from different heights above ground permits to separate the local from regional signals (Gloor et al., 2000).

Following this strategy, NOAA-CMDL (now NOAA/ESRL GMD) started in 1992 a measurement program in North –America using 300-500 meters tall towers (Bakwin et al 1995, 1998, *NOAA ESRL GMD Tall Tower and Aircraft Network*). Also in 1992 measurements from a tall tower at Tsukuba, Japan have been started (Inoue and Matsueda, 2001). In Europe tall tower measurements have been put into operation at Cabauw, Netherlands in 1992 (Vermeulen et al, 1997), Hegyhátsál, Hungary in 1994 (Haszpra et al., 2001), Norunda, Sweden in 1994 (Lundin et al., 1999), Ochsenkopf in 2002 (Jordan et al., 2005).

Starting in 2002, the project CHIOTTO incorporated the existing tall towers and added new ones, creating a coherent monitoring network in Europe.

1.2 The CHIOTTO project

CHIOTTO (Continuous High-precision Tall Tower Observations of Greenhouse Gases in Europe) was an EU funded project (EVK2-CT-2002-00163, 1-Nov-2002 – 1-May-2006, <http://www.chiotto.org>), having the objective to build an infrastructure for continuous monitoring of the concentrations of greenhouse gases on the European continent above the surface layer using tall towers. Nine tall towers are part of the network, covering a big part of Europe (see figure 1.3). The footprint (i.e. the area which significantly influences the short term concentration variations in the sampled air) of this network was estimated using atmospheric transport model calculations.

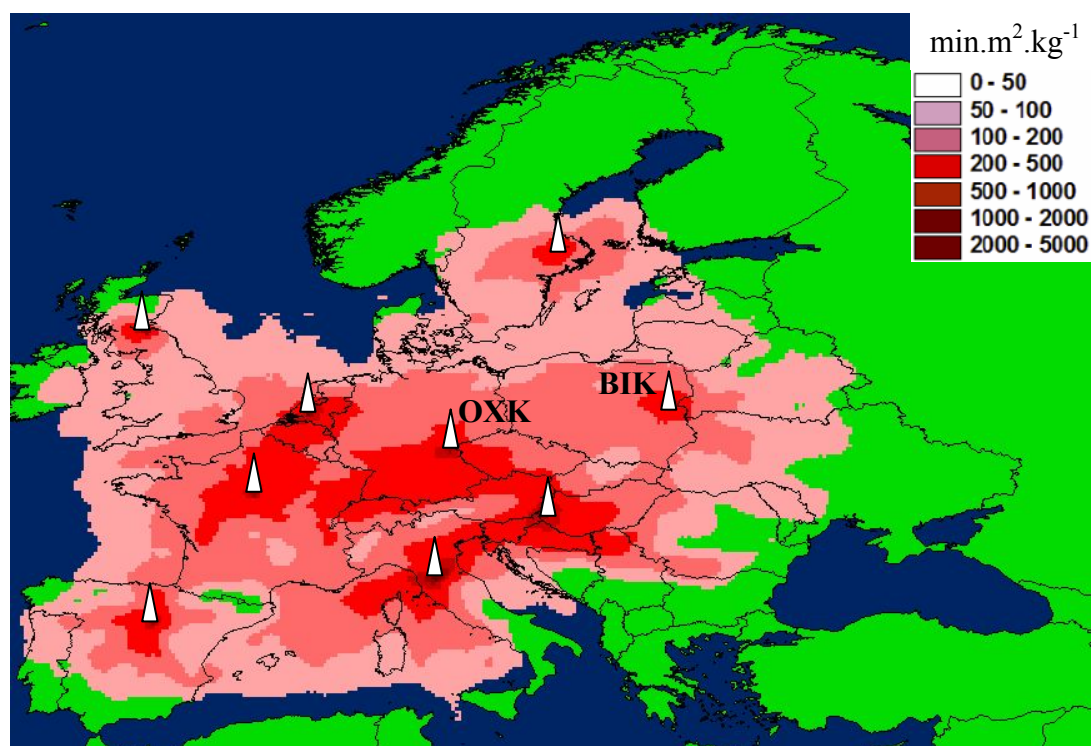


Figure 1.3 Footprint area of the CHIOTTO network estimated with COMET transport model (Vermeulen et al., 2006), for the year 2005 (figure courtesy to A. Vermeulen, ECN Netherlands). The tall tower locations are marked by white triangles.

The approach of the project was to measure continuously the mixing ratio of CO₂ and other greenhouse gases or species related to the carbon cycle like CH₄, CO, N₂O and SF₆ at different heights in the boundary layer, using tall towers. The mixing ratio data coupled with information about atmospheric transport (inverse modeling technique) will be used to obtain regionally representative carbon flux estimates for Europe. This was also considered an important step towards a fully operational continuous observing

system in the framework of the Kyoto Protocol for quantifying sources and sinks of the most important greenhouse gases over Europe.

One of the strengths of the CHIOTTO project was to create a harmonized monitoring network, for which partial standardization of the equipment and of the measurement procedures was required. The precision and accuracy goals (listed in table 1.1), common for all the participants, were established taking into account the WMO recommendations (WMO, 2003).

Table 1.1 Chiotto precision and accuracy goals

Gas species	CHIOTTO Intra-laboratory instrumental precision	CHIOTTO Inter-laboratory calibration scale accuracy	WMO Inter-laboratory comparability
CO ₂	0.1 ppm	0.1 ppm	± 0.1 ppm
O ₂ /N ₂	5 permeg	10 permeg	± 1 permeg
CH ₄	2 ppb	3 ppb	± 2 ppb
CO	1 ppb	3 ppb	± 2 ppb
N ₂ O	0.1 ppb	0.2 ppb	± 0.2 ppb
SF ₆	0.1 ppt	0.2 ppt	-

The CHIOTTO measurement network continues to be operated as an integral part of the atmospheric component of the European project CarboEurope-IP, which has officially started in January 2004 (Contract No. GOCE-CT-2003-505572, www.carboeurope.org).

MPI-BGC Jena contributed to the CHIOTTO project by developing an already existing tall tower station at Ochsenkopf, Germany (OXK) and by setting up a new tall tower measurement station near Bialystok, in Eastern Poland (BIK). These are the only two stations of the CHIOTTO network which, besides the analysis of trace species (CO₂, CH₄, CO, N₂O, SF₆), have also the capability to perform in-situ high-precision atmospheric oxygen measurements.

As part of the MPI-BGC group lead by A. Manning and M. Gloor, I was in charge to set up the new measurement station at Bialystok. The measurement setup follows the project requirements for the equipment and the guidelines regarding the measurement and calibration procedures. The already existing tall tower station at Ochsenkopf, although it

had to be stopped in 2004 due to technical problems, provided useful experience for the design of the new measurement system. The measurement station at Bialystok became operational in August 2005, after a long measurement test phase at the institute in Jena. The system measures quasi-continuously the atmospheric mole fractions of CO₂, CH₄, CO, N₂O, SF₆ and the O₂/N₂ ratio, as well as meteorological parameters (atmospheric pressure, temperature, humidity; wind speed and direction).

1.3 Bialystok site description

The measurement station is located at a 300 m tall tower near Bialystok, in Eastern Poland (Lat 53°14'N, Long 23°01'E, Alt 180 m). The area within a few hundred kilometers around the tower is flat, with a maximal elevation of 250 m above sea level. The land is covered by crops (about 60%), pastures and forest; there is no significant local industry. The nearest town Bialystok with ~300000 inhabitants is situated at about 20 km SE from the tower.

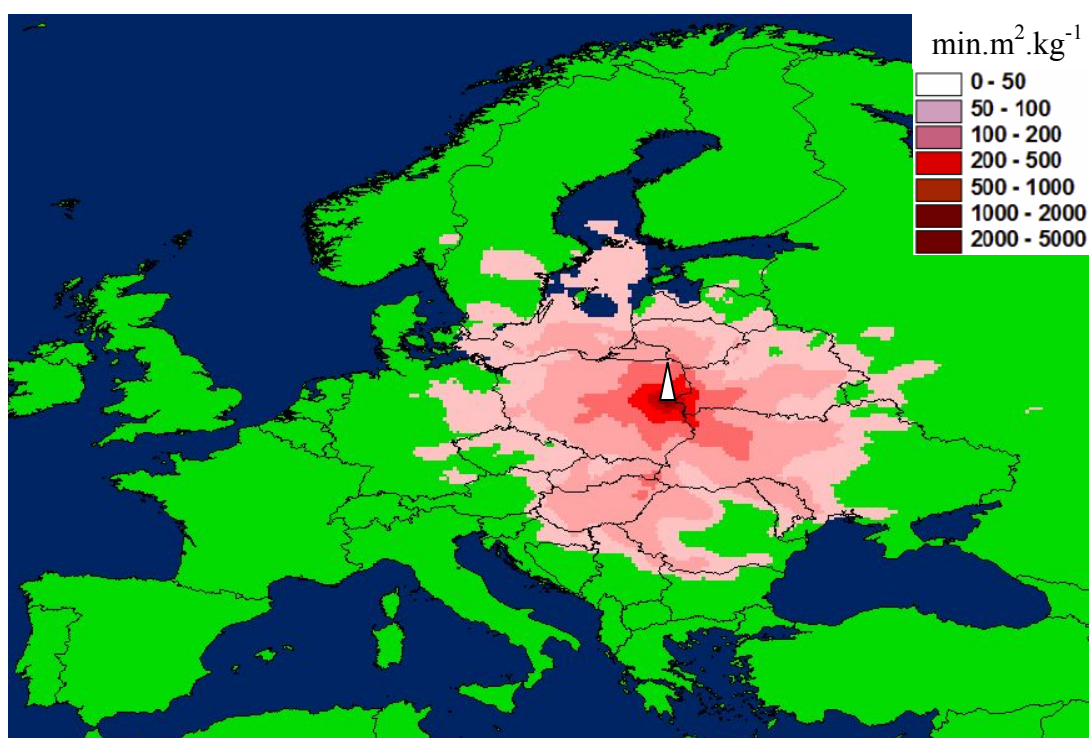


Figure 1.4 Footprint area of the Bialystok tall tower station (level 300 m agl) estimated with COMET transport model, for the year 2005 (figure courtesy to Alex Vermeulen, ECN Netherlands). The tall tower location is marked by the white triangle.

The climate is continental, with four seasons and large difference between summer and winter temperatures. The movement of air masses is not altered by high obstacles (e.g. mountains) thus it follows the general average West-East pattern of this latitude. The average influence area for the air sampled at Bialystok tower at 300 m above ground, as calculated for the year 2005 using the COMET transport model, is illustrated in figure 1.4.

Europe maps illustrating the topography, land use and population density are attached in Appendix 1, for a better perspective of the relative position of the Bialystok station.

1.4 General information about the gas species measured at Bialystok station

Carbon dioxide (CO₂) is the greenhouse gas which accounts presently for the largest anthropogenic increase in radiative forcing.

The atmospheric concentration of CO₂ is closely related to the biogeochemical carbon cycle which involves the exchange of carbon with the terrestrial biosphere, the ocean and the marine biosphere, as well as on longer time scales interactions with sediments and the lithosphere (figure 1.5). The CO₂ in the atmosphere constitutes only a small fraction of the total carbon stored in the other reservoirs.

Currently, humans are emitting about 6.5 PgC /yr to the atmosphere from fossil fuel burning and cement production (Marland et al., 2007), and about 2 PgC /yr from land use change (Houghton, 2003). The anthropogenic CO₂ emissions are small compared to the natural fluxes, but they are still strong enough to produce disequilibrium. It is this disequilibrium which leads to accumulation of CO₂ in the atmosphere and thus to enhancement of the CO₂ greenhouse effect.

The atmospheric CO₂ mixing ratio increased from a range of 275 to 285 ppm in the pre-industrial time (AD 1000–1750) (Etheridge et al., 1996) to about 382 ppm in 2007 (globally averaged over NOAA/GMD marine surface sites, Dr. Pieter Tans, NOAA/ESRL, www.esrl.noaa.gov/gmd/ccgg/trends). Measurements of air entrapped in ice cores show that the present CO₂ concentration has not been reached during the past 420,000 years (Petit et al. 1999, Barnola et al., 2003). The average growth rate of atmospheric CO₂ determined by direct instrumental measurements over the period 1960 to 2005 was 1.4 ppm / year and rose to 1.9 ppm / year over the 1995 to 2005 decade.

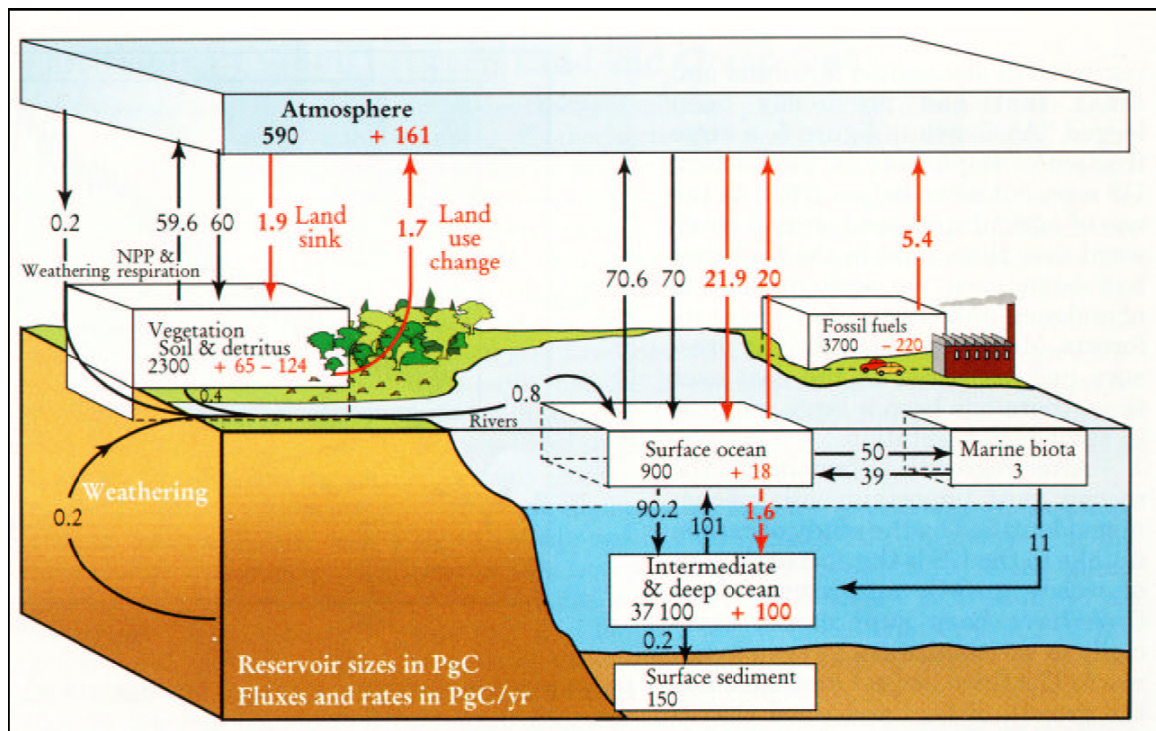


Figure 1.5 The global carbon cycle. Arrows show the fluxes ((in petagrams of carbon per year, 1 Pg = 10^{15} g) between the atmosphere, the land and the ocean, averaged over the 1980s. Anthropogenic fluxes are in red, natural fluxes in black. Within the boxes, black numbers give the preindustrial sizes of the reservoirs and red numbers denote changes resulting from human activities since preindustrial times. The figure is from Sarmiento and Gruber, 2002.

The observed increase in atmospheric concentration does not represent the whole anthropogenic emission (figure 1.6). Comparisons of the atmospheric growth rate with the estimated industrial emissions (Andres et al., 1996, Marland et al., 2007) show that only about half of the CO_2 emitted since 1950s remained in the atmosphere. The rest has been taken up by the land biosphere and the oceans, which are the main sinks of CO_2 on time scales of tens or hundreds of years.

Efforts have been made to determine the relative contributions of the ocean and the land biosphere to the CO_2 uptake. The question is important because the storage into these two reservoirs is essentially different. The carbon stored into the land biosphere is sensitive to climate and human intervention, thus it can rapidly return into the atmosphere as CO_2 , for example by biomass burning, deforestation or, hypothetically, due to land biosphere response to the global warming. In contrast, if CO_2 is taken up by the oceans,

most of the carbon is not likely to reenter the atmosphere soon, because of the slow mixing time of the oceans. Thus on longer time scales the ocean uptake may be more important for attenuating the effect of anthropogenic emissions. Estimations using different methods showed that, over the last decades, the anthropogenic CO₂ has been taken up by the land biosphere and ocean in comparable proportions (e.g. Battle et al., 2000, Rayner et al., 1999, Le Quéré et al., 2003, Manning and Keeling, 2006).

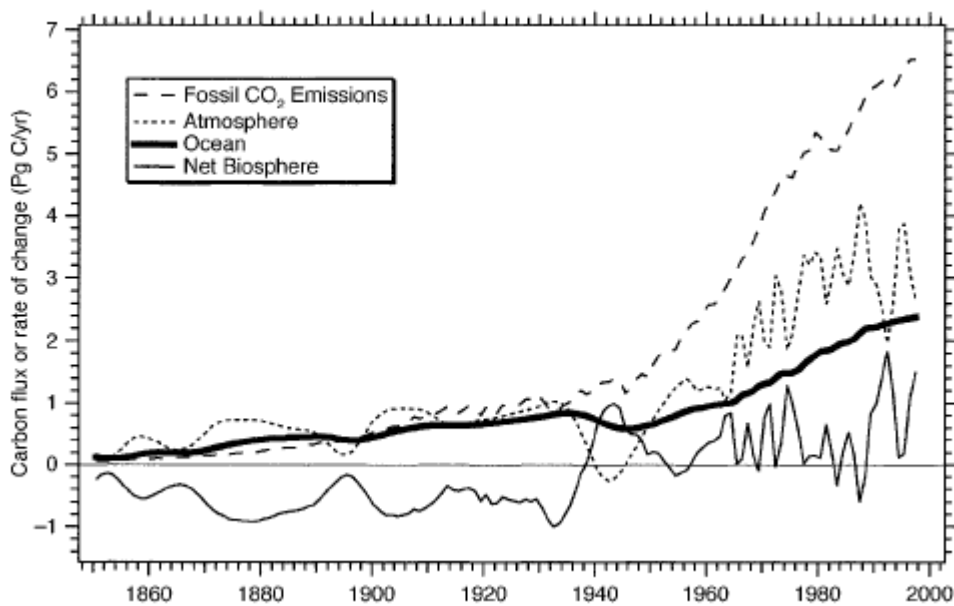


Figure 1.6 Components of the global carbon budget during the industrial period: emissions from fossil-fuel burning and cement production (Andres et al. 2000) are partitioned into the observed atmospheric increase (from Keeling et al. 1995), ocean uptake (model estimate using the ocean C-cycle model HAMOCC3, updated from Maier-Reimer, 1993), and a residual component inferred to represent the net balance of the terrestrial biosphere. The figure is from Prentice et al., 2000.

Methane (CH₄) is the second most important anthropogenic greenhouse gas after CO₂ in terms of radiative forcing (Ramaswamy et al., 2001). The natural sources of methane to the atmosphere include wetlands, termites, oceans, cud chewing animals, biomass burning and volcanoes. Human activities that produce CH₄ include energy production from coal and natural gas, waste disposal in landfills, raising ruminant animals, rice agriculture and biomass burning (Rasmussen and Khalil, 1984). Anthropogenic sources are estimated to account presently for more than 60% of the total emissions to the

atmosphere. The main sinks are the chemical oxidation in the troposphere and the uptake by soils. The residence time of CH₄ in the atmosphere is about 12 years (Forster et al., 2007).

The atmospheric CH₄ mixing ratio increased from 715 ppb in pre-industrial times (AD 1700–1800) (Etheridge et al., 1992, 2002) to 1774 ppb in 2005 (global average from NOAA/GMD flask sampling network, Forster et al., 2007). Over the past two decades, the CH₄ growth rate in the atmosphere has slowed (e.g. Dlugokencky et al., 2003), for reasons which are not yet clear.

Nitrous oxide (N₂O) is a greenhouse gas which had a globally averaged atmospheric concentration of about 270 ± 5 ppb in pre-industrial time (Flückiger et al., 1999) and reached 319 ppb in 2005 (Forster et al., 2007). Direct atmospheric measurements show that N₂O has been increasing with a rate of 0.26% per year in the past few decades. Although it has a lower concentration than CO₂, N₂O is an important greenhouse gas because of its long residence time in the atmosphere (114 years, Montzka et al., 2003) and its high energy absorption capacity per molecule. Presently the N₂O sources from anthropogenic activities (biomass burning, fossil fuel combustion, industrial production of adipic and nitric acids, the use of nitrogen fertilizer in agriculture) are approximately equal to the natural sources (chemical oxidation of ammonia in the atmosphere, microbes, bacteria). The main sinks are photodissociation in the stratosphere and reactions with excited atomic oxygen, affecting in this way the stratospheric chemistry.

Sulfur hexafluoride (SF₆) is the strongest greenhouse gas that has been evaluated, having a global warming potential of 22800 over a 100 year period (Forster et al., 2007). SF₆ does not have significant natural sources, its pre-industrial concentration being estimated at less than 0.04 ppt (Maiss and Brenninkmeijer, 1998). SF₆ is used by the electrical industry as dielectric medium for high voltage equipment, in semiconductor industry as an etchant and in the magnesium and aluminium industry. It is also deliberately released as an inert tracer to study atmospheric and oceanic transport processes.

Systematic atmospheric measurements go back to 1978 based on the air archive Cape Grim, Tasmania (Fraser et al., 1991). They show a strong increase in atmospheric SF₆ concentration, from 0.6 ppt in 1978 (Maiss et al., 1996) to more than 6 ppt in 2007.

The chemical stability of SF₆, which makes it interesting for some applications, leads also to a very long atmospheric lifetime of about 3200 years (Ravishankara et al., 1993). Thus the present atmospheric accumulation is practically irreversible for thousands of years.

Its chemical stability, the possibility to measure it with high precision and the relatively well known sources have made SF₆ one of the most attractive tracers for atmospheric transport and mixing studies (e.g. Maiss et al., 1996, Denning et al., 1999, Gloor et al., 2007).

Carbon monoxide (CO) is a trace gas with average atmospheric lifetime of about 60 days. The natural CO sources are oxidation of hydrocarbons, emissions from oceans, volcanoes and degradation of plants. Anthropogenic sources include fossil fuel burning and oxidation of hydrocarbons and account at present for more than 50% of the total emissions. Almost all the CO emitted into the atmosphere each year is removed by reactions with OH radicals (85%), by soil uptake (10%), and by diffusion into the stratosphere (Khalil and Rasmussen, 1990).

In the troposphere CO is the main controller of the concentration of OH radicals and thus of the oxidation capacity of the troposphere. It is estimated that about 75% of the OH radicals are consumed by the reaction with CO (Thompson, 1992). CO affects in this way the global cycles of natural and anthropogenic trace gases that are removed from the atmosphere by reaction with OH, for example methane. The chemical reactions of CO may produce significant amounts of ozone in the troposphere (e.g. Fishman and Crutzen, 1978, Fishman et al., 1980).

The direct radiative impact of CO on the atmosphere (the “direct” greenhouse effect) is not significant. However, CO is important because of its indirect greenhouse effect by increasing tropospheric ozone and methane concentrations, and because of its multiple effects on tropospheric chemistry.

Measurements of atmospheric **oxygen** constitute a valuable tool to study the carbon cycle. The atmospheric oxygen content is modified by fossil fuel burning, gas exchange between the atmosphere and the terrestrial biosphere, and by gas exchange with the oceans. The variations of atmospheric oxygen are on the same order of magnitude as those of CO₂. Because of the large atmospheric oxygen background (~21%), observing these variations necessitates a very high relative measurement precision. In the past decades measurements with the required precision became available (e.g. Keeling et al.,

1996, Battle et al., 2000, Tohjima et al., 2003). These measurements revealed a long term decrease in atmospheric oxygen content, modulated by a distinct seasonal cycle.

The long term oxygen decrease is mainly dependent on the consumption by fossil fuel burning and on the net release from the land biosphere. The changes in atmospheric CO₂ and oxygen are inversely coupled during biosphere respiration and photosynthesis, and in the processes of combustion. It is considered so far that the average O₂:CO₂ mole exchange ratio between the land biota and atmosphere is 1.1 (Severinghaus, 1995); for the fossil fuel burning an average global ratio of about 1.4 moles of O₂ consumed per mole of CO₂ produced was estimated (Keeling, 1988a). The consumption of fossil fuel is relatively well known, so that the corresponding oxygen consumption can be estimated. But the measured decrease in atmospheric oxygen is smaller than what would be expected based on the amount of fossil fuel burned. Thus a source of oxygen exists, and this is presently considered to be the release from the land biosphere. In this way the corresponding uptake of CO₂ by the land biosphere and by oceans can be estimated (Machta, 1980, Keeling, 1988b, Keeling and Shertz, 1992, Keeling et al., 1993, Keeling et al., 1996, Bender et al., 1996, Langenfelds et al., 1999, Bender et al., 2005, Battle et al., 2000, Tohjima et al., 2003, Manning and Keeling, 2006).

The seasonal variations of oxygen are determined by the gas exchange between the ocean and atmosphere and to the seasonal cycle of the land biosphere. The oceanic component of the oxygen seasonal cycle can be estimated by subtracting the land biosphere component, based on parallel measurements of CO₂ seasonal variation. The oceanic induced seasonal variations of oxygen and the spatial gradients of atmospheric oxygen have been used to study biological productivity in the ocean (Keeling and Shertz, 1992, Bender et al., 1996, Balkanski et al., 1999), gas exchange between the ocean and the atmosphere (Keeling et al., 1998) and oceanic transport (Stephens et al., 1998, Gruber et al., 2001).

The concept of global warming potential (GWP) was developed to compare the ability of different greenhouse gases to trap heat in the troposphere. The definition of GWP for a particular greenhouse gas is the ratio of heat trapped by one unit mass of the greenhouse gas to that of one unit mass of CO₂ over a specified time period. The value of the GWP depends on the length of the time interval considered. The values of the global warming potential and the atmospheric lifetimes for the species of interest for this work are listed in table 1.2, as estimated in IPCC 2007 (Forster et al., 2007).

Table 1.2 Atmospheric mixing ratios for the year 2005, atmospheric lifetimes and global warming potentials (GWP) over 100-years time horizon as assessed by IPCC 2007

Species	Mixing ratio in 2005 (IPCC 2007)	Atmospheric lifetime (years)	GWP - 100 years (IPCC 2007)
CO ₂	379 ± 0.65 ppm	50-200	1
CH ₄	1774 ± 1.8 ppb	12	25
N ₂ O	319 ± 0.12 ppb	114	298
SF ₆	5.6 ± 0.038 ppt	3200	22800

1.5 Thesis outline

I was responsible to design, optimize and bring into operation the measurement system for the new Bialystok tall tower station. The system measures quasi-continuously the atmospheric mole fractions of CO₂, CH₄, CO, N₂O, SF₆ and the O₂/N₂ ratio, as well as meteorological parameters (atmospheric pressure, temperature, humidity; wind speed and direction). **Chapter 2** is a detailed technical description of the measurement principles and the instrumental setup. Although based on commercial analysers, the resulted measurement system is able to reach a much higher precision than the factory specifications of individual instruments. Careful gas handling and special measurement and quality assurance procedures play an important role in achieving this performance.

After an intensive testing and optimization phase which took place at MPI-BGC Jena, the measurement system was installed and put into operation at the final location in eastern Poland in summer 2005. **Chapter 3** presents an evaluation of the technical performance of the measurement system, after the first 18 months of operation at the field site. Although technical problems appeared from time to time, the data coverage for the first year of measurement is satisfying. The typical precision achieved, calculated for the whole time interval, is within or close to the Chiotto precision targets. The evaluation has also discovered some issues which have to be more studied in the future, like the oxygen fractionation and the stability of the composition of standard gases in high pressure gas cylinders.

Chapter 4 is an overview of the general features of the measurement data collected at Bialystok tall tower station in the first 18 months of operation. Typical

variability patterns, like the vertical gradients of the mixing ratios, and the diurnal and seasonal variations, are described.

Some specific, interesting aspects apparent in the measurement data are analyzed in detail in the following three chapters.

Chapter 5 is an analysis of the correlation between the observed variations of the atmospheric oxygen and carbon dioxide on diurnal time scale. The resulted O₂:CO₂ ratios are unexpected in comparison to the values generally used in present, but they are compatible with some more recent published results.

Chapter 6 proposes a method to estimate the night-time CO₂ flux due to land biosphere respiration. The method can potentially be used complementarily to the Eddy flux measurements. The results so far are in the expected range of absolute flux values and in good agreement with results from other estimates regarding the dependence on temperature.

A weekly cycle was observed in the measured mixing ratios of most of the species measured, which is correlated with a similar variation of some of the meteorological parameters. Although an anthropogenic reason is suspected, the meteorological parameters could also be the source of this effect. **Chapter 7** is an analysis of this finding.

At last **Chapter 8** contains the conclusions regarding the results obtained so far and the reliability of this type of measurement, with some ideas about possibilities to continue and develop this work.

1.6 References

- Andres R. J., Marland G., Fung I., and Matthews E. (1996) A 1° x 1° distribution of carbon dioxide emissions from fossil fuel consumption and cement manufacture, 1950-1990. *Global Biogeochemical Cycles* 10(3), 419-429.
- Andres R. J., Marland G., Boden T., and Bischof S. (2000) Carbon dioxide emissions from fossil fuel consumption and cement manufacture, 1751-1991, and an estimate of their isotopic composition and latitudinal distribution. In: *The Carbon Cycle*, [Wigley, T.M.L. and D.S. Schimel (eds.)]. Cambridge University Press, New York, pp. 53-62.
- Arrhenius S. (1896) On the Influence of Carbonic Acid in the Air upon the Temperature of the Ground, *London, Edinburgh, and Dublin Philosophical Magazine and Journal of Science (fifth series)*, April 1896. vol 41, 237-275

- Bakwin P. S., Tans P. P., Hurst D. F., and Zhao C. L. (1998) Measurements of carbon dioxide on very tall towers: results of the NOAA/CMDL program. *Tellus Series B-Chemical & Physical Meteorology* 50(5), 401-415.
- Bakwin P. S., Tans P. P., Zhao C. L., Ussler W., and Quesnell E. (1995) Measurements of carbon dioxide on a very tall tower. *Tellus Series B-Chemical & Physical Meteorology* 47(5), 535-549.
- Balkanski Y., Monfray P., Battle M., and Heimann M. (1999) Ocean primary production derived from satellite data: An evaluation with atmospheric oxygen measurements. *Global Biogeochemical Cycles* 13(2), 257-271.
- Barnett T. P., Pierce D. W., and Schnur R. (2001) Detection of anthropogenic climate change in the world's oceans. *Science* 292(5515), 270-274.
- Barnola J.-M., Raynaud D., Lorius C., and Barkov N.I. (2003) Historical CO₂ record from the Vostok ice core. In *Trends: A Compendium of Data on Global Change*. Carbon Dioxide Information Analysis Center, Oak Ridge National Laboratory, U.S. Department of Energy, Oak Ridge, Tenn., U.S.A.
- Battle M., Bender M. L., Tans P. P., White J. W. C., Ellis J. T., Conway T., and Francey R. J. (2000) Global carbon sinks and their variability inferred from atmospheric O₂ and δC^{13} . *Science* 287(5462), 2467-2470.
- Bender M., Ellis T., Tans P., Francey R., and Lowe D. (1996) Variability in the O₂/N₂ ratio of Southern Hemisphere air, 1991-1994 - Implications for the carbon cycle. *Global Biogeochemical Cycles* 10(1), 9-21.
- Bender M. L., Ho D. T., Hendricks M. B., Mika R., Battle M. O., Tans P. P., Conway T. J., Sturtevant B., and Cassar N. (2005) Atmospheric O₂/N₂ changes, 1993-2002: Implications for the partitioning of fossil fuel CO₂ sequestration. *Global Biogeochemical Cycles* 19(4), B4017.
- Bousquet P., Ciais P., Peylin P., Ramonet M., and Monfray P. (1999) Inverse modeling of annual atmospheric CO₂ sources and sinks 1. Method and control inversion. *Journal of Geophysical Research-Atmospheres* 104(D21), 26161-26178.
- Bousquet P., Peylin P., Ciais P., Ramonet M., and Monfray P. (1999) Inverse modeling of annual atmospheric CO₂ sources and sinks 2. Sensitivity study. *Journal of Geophysical Research-Atmospheres* 104(D21), 26179-26193.
- Brohan P., Kennedy J. J., Harris I., Tett S. F. B., and Jones P. D. (2006) Uncertainty estimates in regional and global observed temperature changes: A new data set from 1850. *Journal of Geophysical Research-Atmospheres* 111(D12), -.
- Denning A. S., Holzer M., Gurney K. R., Heimann M., Law R. M., Rayner P. J., Fung I. Y., Fan S. M., Taguchi S., Friedlingstein P., Balkanski Y., Taylor J., Maiss M., and Levin I. (1999) Three-dimensional transport and concentration of SF₆ - A model intercomparison study (TransCom 2). *Tellus Series B-Chemical and Physical Meteorology* 51(2), 266-297.
- Dlugokencky E. J., Houweling S., Bruhwiler L., Masarie K. A., Lang P. M., Miller J. B., and Tans P. P. (2003) Atmospheric methane levels off: Temporary pause or a new steady-state? *Geophysical Research Letters* 30(19), -.

- Enting I. G. and Mansbridge J. V. (1991) Latitudinal distribution of sources and sinks of CO₂ - results of an inversion study. *Tellus Series B-Chemical and Physical Meteorology* 43(2), 156-170.
- Enting I. G., Trudinger C. M., and Francey R. J. (1995) A synthesis inversion of the concentration and delta C¹³ of atmospheric CO₂. *Tellus Series B-Chemical and Physical Meteorology* 47(1-2), 35-52.
- Etheridge D. M., Pearman G. I., and Fraser P. J. (1992) Changes in tropospheric methane between 1841 and 1978 from a high accumulation-rate antarctic ice core. *Tellus Series B-Chemical and Physical Meteorology* 44(4), 282-294.
- Etheridge D.M., Steele L.P., Francey R.J., and Langenfelds R.L. (2002) Historical CH₄ records since about 1000 A.D. from ice core data. In *Trends: A Compendium of Data on Global Change*. Carbon Dioxide Information Analysis Center, Oak Ridge National Laboratory, U.S. Department of Energy, Oak Ridge, Tenn., U.S.A.
- Etheridge D. M., Steele L. P., Langenfelds R. L., Francey R. J., Barnola J. M., and Morgan V. I. (1996) Natural and anthropogenic changes in atmospheric CO₂ over the last 1000 years from air in antarctic ice and firn. *Journal of Geophysical Research-Atmospheres* 101(D2), 4115-4128.
- Fan S., Gloor M., Mahlman J., Pacala S., Sarmiento J., Takahashi T., and Tans P. (1998) A large terrestrial carbon sink in North America implied by atmospheric and oceanic carbon dioxide data and models. *Science* 282(5388), 442-446.
- Fishman J. and Crutzen P. J. (1978) Origin of ozone in troposphere. *Nature* 274(5674), 855-858.
- Fishman J., Seiler W., and Haagenson P. (1980) Simultaneous presence of O₃ and CO bands in the troposphere. *Tellus* 32(5), 456-463.
- Forster P., Ramaswamy V., Artaxo P., Berntsen T., Betts R., Fahey D.W., Haywood J., Lean J., Lowe D.C., Myhre G., Nganga J., Prinn R., Raga G., Schulz M. and Van Dorland R. (2007): Changes in Atmospheric Constituents and in Radiative Forcing. In: *Climate Change 2007: The Physical Science Basis. Contribution of Working Group I to the Fourth Assessment Report of the Intergovernmental Panel on Climate Change* [Solomon, S., D. Qin, M. Manning, Z. Chen, M. Marquis, K.B. Averyt, M. Tignor and H.L. Miller (eds.)]. Cambridge University Press, Cambridge, United Kingdom and New York, NY, USA.
- Fourier J.-B.J. (1827) Memoire sur les temperatures du globe terrestre et des espaces planetaires, *Mémoires de l'Académie Royale des Sciences de l'Institut de France* VII. 570-604.
- Fraser P.J., Langenfelds R., Derek N., Porter L. W. (1991) Studies in air archiving techniques. Part 1: Long term stability of atmospheric trace gases in dry, natural air stored in high pressure, surface treated aluminium cylinders. In: *Baseline Atmospheric Program (Australia) 1989*. [Wilson, R. and Gras J. L. (eds.)]. Department of the Arts, Sport, the Environment, Tourism and Territories and CSIRO. 16-29.
- Gerbig C., Lin J. C., Wofsy S. C., Daube B. C., Andrews A. E., Stephens B. B., Bakwin P. S., and Grainger C. A. (2003a) Toward constraining regional-scale fluxes of CO₂ with atmospheric observations over a continent: 1. Observed spatial

- variability from airborne platforms. *Journal of Geophysical Research-Atmospheres* 108(D24), 4756.
- Gerbig C., Lin J. C., Wofsy S. C., Daube B. C., Andrews A. E., Stephens B. B., Bakwin P. S., and Grainger C. A. (2003b) Toward constraining regional-scale fluxes of CO₂ with atmospheric observations over a continent: 2. Analysis of COBRA data using a receptor-oriented framework. *Journal of Geophysical Research-Atmospheres* 108(D24), 4757.
- Gloor M., Bakwin P., Hurst D., Lock L., Draxler R., and Tans P. (2001) What is the concentration footprint of a tall tower? *Journal of Geophysical Research-Atmospheres* 106(D16), 17831-17840.
- Gloor M., Dlugokencky E., Brenninkmeijer C., Horowitz L., Hurst D. F., Dutton G., Crevoisier C., Machida T., and Tans P. (2007) Three-dimensional SF₆ data and tropospheric transport simulations: Signals, modeling accuracy, and implications for inverse modeling, *Journal of Geophysical Research-Atmospheres* 112, D15112.
- Gloor M., Fan S. M., Pacala S., and Sarmiento J. (2000) Optimal sampling of the atmosphere for purpose of inverse modeling: A model study. *Global Biogeochemical Cycles* 14(1), 407-428.
- Gruber N., Gloor M., Fan S. M., and Sarmiento J. L. (2001) Air-sea flux of oxygen estimated from bulk data: Implications for the marine and atmospheric oxygen cycles [Review]. *Global Biogeochemical Cycles* 15(4), 783-803.
- Gurney K. R., Law R. M., Denning A. S., Rayner P. J., Baker D., Bousquet P., Bruhwiler L., Chen Y. H., Ciais P., Fan S., Fung I. Y., Gloor M., Heimann M., Higuchi K., John J., Maki T., Maksyutov S., Masarie K., Peylin P., Prather M., Pak B. C., Randerson J., Sarmiento J., Taguchi S., Takahashi T., and et al. (2002) Towards robust regional estimates of CO₂ sources and sinks using atmospheric transport models. *Nature* 415(6872), 626-630.
- Haszpra L., Barcza Z., Bakwin P.S., Berger B.W., Davis K.J., Weidinger T. (2001) Measuring system for the long-term monitoring of biosphere/atmosphere exchange of carbon dioxide. *Journal of Geophysical Research* 106D, 3057–3070.
- Heimann M. and Kaminski T. (1999) Inverse modeling approaches to infer surface trace gas fluxes from observed atmospheric mixing ratios. In: *Approaches to scaling of trace gas fluxes in ecosystems*. [Bouwman AF (eds.)]. Vol. 24, Elsevier, Amsterdam. pp. 275-295
- Houghton R. A. (2003) Revised estimates of the annual net flux of carbon to the atmosphere from changes in land use and land management 1850-2000. *Tellus Series B-Chemical and Physical Meteorology* 55(2), 378-390.
- Inoue H.Y. and Matsueda H. (2001) Measurements of atmospheric CO₂ from a meteorological tower in Tsukuba, Japan. *Tellus B* 53(3), 205-219.
- Jordan A., Schultz U., Seifert T., Gloor M., Manning A., Heimann M., Schulze E.-D. (2005) Continuous GC measurements of trace gases at the Ochsenkopf monitoring station, *Proceedings of the 12th IAEA/WMO meeting of CO₂ experts, Toronto, Sept. 2003, WMO-GAW Report 161*, ed. D. Worthy and L. Huang;
- Kaminski T. and Heimann M. (2001) Inverse modeling of atmospheric carbon dioxide fluxes. *Science* 294(5541), U1-U1.

- Keeling C.D., Bacastow R.B., Bainbridge A.E., Ekdahl C.A., Guenther P.R., and Waterman L.S. (1976) Atmospheric carbon dioxide variations at Mauna Loa Observatory, Hawaii. *Tellus* 28, 538-551.
- Keeling C. D., Whorf T. P., Wahlen M., and Vanderpligt J. (1995) Interannual extremes in the rate of rise of atmospheric carbon dioxide since 1980. *Nature* 375(6533), 666-670.
- Keeling, C.D. and Whorf T.P. (2005) Atmospheric CO₂ records from sites in the SIO air sampling network. In *Trends: A Compendium of Data on Global Change*. Carbon Dioxide Information Analysis Center, Oak Ridge National Laboratory, U.S. Department of Energy, Oak Ridge, Tenn., U.S.A.
- Keeling R. F. (1988a) *Development of an interferometric oxygen analyzer*. Ph.D. thesis, Harvard University, Cambridge, Mass., 178pp.
- Keeling R. F. (1988b) Measuring correlations between atmospheric oxygen and carbon dioxide mole fractions - a preliminary study in urban air. *Journal of Atmospheric Chemistry* 7(2), 153-176.
- Keeling R. F., Najjar R. P., Bender M. L., and Tans P. P. (1993) What atmospheric oxygen measurements can tell us about the global carbon cycle. *Global Biogeochemical Cycles* 7(1), 37-67.
- Keeling R. F., Piper S. C., and Heimann M. (1996) Global and hemispheric CO₂ sinks deduced from changes in atmospheric O₂ concentration. *Nature* 381(6579), 218-221.
- Keeling R. F. and Shertz S. R. (1992) Seasonal and interannual variations in atmospheric oxygen and implications for the global carbon cycle. *Nature* 358(6389), 723-727.
- Keeling R. F., Stephens B. B., Najjar R. G., Doney S. C., Archer D., and Heimann M. (1998) Seasonal variations in the atmospheric O₂/N₂ ratio in relation to the kinetics of air-sea gas exchange. *Global Biogeochemical Cycles* 12(1), 141-163.
- Khalil M. A. K. and Rasmussen R. A. (1990) The global cycle of carbon monoxide - trends and mass balance. *Chemosphere* 20(1-2), 227-242.
- Langenfelds R. L., Francey R. J., Steele L. P., Battle M., Keeling R. F., and Budd W. F. (1999) Partitioning of the global fossil CO₂ sink using a 19-year trend in atmospheric O₂. *Geophysical Research Letters* 26(13), 1897-1900.
- Le Quere C., Aumont O., Bopp L., Bousquet P., Ciais P., Francey R., Heimann M., Keeling C. D., Keeling R. F., Kheshgi H., Peylin P., Piper S. C., Prentice I. C., and Rayner P. J. (2003) Two decades of ocean CO₂ sink and variability. *Tellus Series B-Chemical & Physical Meteorology* 55(2), 649-656.
- Levitus S., Antonov J. I., Wang J. L., Delworth T. L., Dixon K. W., and Broccoli A. J. (2001) Anthropogenic warming of Earth's climate system. *Science* 292(5515), 267-270.
- Lundin L. C., Halldin S., Lindroth A., Cienciala E., Grelle A., Hjelm P., Kellner E., Lundberg A., Molder M., Moren A. S., Nord T., Seibert J., and Stahl M. (1999) Continuous long-term measurements of soil-plant-atmosphere variables at a forest site. *Agricultural & Forest Meteorology* 98-9(Special Issue SI), 53-73.

- Machta L. E. (1980) Oxygen depletion. In *Carbon Dioxide Effects Research and Assessment Program: Proceedings of the International Meeting on Stable Isotopes in Tree-Ring Research* [Jacoby (ed.)]. U.S. Dept. of Energy, 125–127.
- Maier-Reimer E. (1993) Geochemical cycles in an ocean general circulation model - preindustrial tracer distributions. *Global Biogeochemical Cycles* 7(3), 645-677.
- Maiss M. and Brenninkmeijer C. A. M. (1998) Atmospheric SF₆: trends, sources, and prospects. *Environ. Sci. Technol.* 32(20), 3077-3086.
- Maiss M., Steele L. P., Francey R. J., Fraser P. J., Langenfelds R. L., Trivett N. B. A., and Levin I. (1996) Sulfur hexafluoride - A powerful new atmospheric tracer. *Atmospheric Environment* 30(10-11), 1621-1629.
- Manning A. C. and Keeling R. F. (2006) Global oceanic and land biotic carbon sinks from the Scripps atmospheric oxygen flask sampling network. *Tellus Series B-Chemical and Physical Meteorology* 58(2), 95-116.
- Marland G., Boden T.A., and Andres R. J. (2007) Global, regional, and national fossil fuel CO₂ emissions. In *Trends: A Compendium of Data on Global Change*. Carbon Dioxide Information Analysis Center, Oak Ridge National Laboratory, U.S. Department of Energy, Oak Ridge, Tenn., U.S.A.
- Neftel A., Friedli H., Moor E., Lötscher H., Oeschger H., Siegenthaler U., and Stauffer B. (1994) Historical CO₂ record from the Siple Station ice core. In *Trends: A Compendium of Data on Global Change*. Carbon Dioxide Information Analysis Center, Oak Ridge National Laboratory, U.S. Department of Energy, Oak Ridge, Tenn., U.S.A.
- Petit J. R., Jouzel J., Raynaud D., Barkov N. I., Barnola J. M., Basile I., Bender M., Chappellaz J., Davis M., Delaygue G., Delmotte M., Kotlyakov V. M., Legrand M., Lipenkov V. Y., Lorius C., Pepin L., Ritz C., Saltzman E., and Stievenard M. (1999) Climate and atmospheric history of the past 420,000 years from the Vostok ice core, Antarctica. *Nature* 399(6735), 429-436.
- Prentice I. C., Heimann M., and Sitch S. (2000) The carbon balance of the terrestrial biosphere: Ecosystem models and atmospheric observations. *Ecological Applications* 10(6), 1553-1573.
- Rasmussen R. A. and Khalil M. A. K. (1984) Atmospheric methane in the recent and ancient atmospheres - concentrations, trends, and interhemispheric gradient. *Journal of Geophysical Research-Atmospheres* 89(ND7), 1599-1605.
- Ravishankara A. R., Solomon S., Turnipseed A. A., and Warren R. F. (1993) Atmospheric lifetimes of long-lived halogenated species. *Science* 259(5092), 194-199.
- Ramaswamy V., et al. (2001) Radiative forcing of climate change. In: *Climate Change 2001: The Scientific Basis. Contribution of Working Group I to the Third Assessment Report of the Intergovernmental Panel on Climate Change* [Houghton, J.T., et al. (eds.)]. Cambridge University Press, Cambridge, United Kingdom and New York, NY, USA, pp. 349–416.
- Rayner P. J., Enting I. G., Francey R. J., and Langenfelds R. (1999) Reconstructing the recent carbon cycle from atmospheric CO₂, delta C¹³ and O₂/N₂ observations. *Tellus Series B-Chemical and Physical Meteorology* 51(2), 213-232.

- Rodenbeck C., Houweling S., Gloor M., and Heimann M. (2003a) CO₂ flux history 1982-2001 inferred from atmospheric data using a global inversion of atmospheric transport. *Atmospheric Chemistry & Physics* 3, 1919-1964.
- Rodenbeck C., Houweling S., Gloor M., and Heimann M. (2003b) Time-dependent atmospheric CO₂ inversions based on interannually varying tracer transport. *Tellus Series B-Chemical & Physical Meteorology* 55(2), 488-497.
- Sarmiento J. L. and Gruber N. (2002) Sinks for anthropogenic carbon. *Physics Today* 55(8), 30-36.
- Schimel D. S., House J. I., Hibbard K. A., Bousquet P., Ciais P., Peylin P., Braswell B. H., Apps M. J., Baker D., Bondeau A., Canadell J., Churkina G., Cramer W., Denning A. S., Field C. B., Friedlingstein P., Goodale C., Heimann M., Houghton R. A., Melillo J. M., Moore B., Murdiyarso D., Noble I., Pacala S. W., Prentice I. C., Raupach M. R., Rayner P. J., Scholes R. J., Steffen W. L., and Wirth C. (2001) Recent patterns and mechanisms of carbon exchange by terrestrial ecosystems. *Nature* 414(6860), 169-172.
- Severinghaus J. P. (1995) *Studies of the terrestrial O₂ and carbon cycles in sand dune gases and in biosphere 2*. Ph.D. thesis, Columbia University, 148 pp.
- Stephens B. B., Keeling R. F., Heimann M., Six K. D., Murnane R., and Caldeira K. (1998) Testing global ocean carbon cycle models using measurements of atmospheric O₂ and CO₂ concentration. *Global Biogeochemical Cycles* 12(2), 213-230.
- Stone D. A., Allen M. R., and Stott P. A. (2007) A multimodel update on the detection and attribution of global surface warming. *Journal of Climate* 20(3), 517-530.
- Stott P. A., Tett S. F. B., Jones G. S., Allen M. R., Ingram W. J., and Mitchell J. F. B. (2001) Attribution of twentieth century temperature change to natural and anthropogenic causes. *Climate Dynamics* 17(1), 1-21.
- Tans P. P. (1991) Uncertainties in the global carbon-cycle. *Pure and Applied Chemistry* 63(5), 766-768.
- Tans P. P., Conway T. J., and Nakazawa T. (1989) Latitudinal distribution of the sources and sinks of atmospheric carbon dioxide derived from surface observations and an atmospheric transport model. *Journal of Geophysical Research-Atmospheres* 94(D4), 5151-5172.
- Tans P. P., Fung I. Y., and Takahashi T. (1990) Observational constraints on the global atmospheric CO₂ budget. *Science* 247(4949), 1431-1438.
- Tett S. F. B., Jones G. S., Stott P. A., Hill D. C., Mitchell J. F. B., Allen M. R., Ingram W. J., Johns T. C., Johnson C. E., Jones A., Roberts D. L., Sexton D. M. H., and Woodage M. J. (2002) Estimation of natural and anthropogenic contributions to twentieth century temperature change. *Journal of Geophysical Research-Atmospheres* 107(D16), -.
- Thompson A. M. (1992) The oxidizing capacity of the earth's atmosphere - probable past and future changes. *Science* 256(5060), 1157-1165.
- Tohjima Y., Mukai H., Machida T., and Nojiri Y. (2003) Gas-chromatographic measurements of the atmospheric oxygen/nitrogen ratio at Hateruma Island and Cape Ochi-ishi, Japan. *Geophysical Research Letters* 30(12), 1653.

- Trenberth K.E., Jones P.D., Ambenje P., Bojariu R., Easterling D., Klein Tank A., Parker D., Rahimzadeh F., Renwick J.A., Rusticucci M., Soden B. and Zhai P. (2007) Observations: Surface and Atmospheric Climate Change. In: *Climate Change 2007: The Physical Science Basis. Contribution of Working Group I to the Fourth Assessment Report of the Intergovernmental Panel on Climate Change* [Solomon, S., D. Qin, M. Manning, Z. Chen, M. Marquis, K.B. Averyt, M. Tignor and H.L. Miller (eds.)]. Cambridge University Press, Cambridge, United Kingdom and New York, NY, USA.
- Vermeulen A.T., Hensen A., den Ouden A.C.B., Pieterse G. (1997) Validation of methane emission inventories for NW-Europe. Petten, ECN, Report ECN-C--96-088.
- Vermeulen, A. T., Pieterse, G., Hensen, A., van den Bulk, W. C. M., and Erisman, J. W. (2006) COMET: a Lagrangian transport model for greenhouse gas emission estimation – forward model technique and performance for methane, *Atmos. Chem. Phys. Discuss.*, 6, 8727-8779.
- WMO (2003) Report of the 11th WMO/IAEA Meeting of Experts on Carbon Dioxide Concentration and Related Tracer Measurement Techniques, Tokyo, Japan, 25-28 Sep. 2001, Tech. Rep. 148, World Meteorological Organisation - Global Atmospheric Watch, Geneva, Switzerland.

Chapter 2.

Technical description of the measurement system for atmospheric CO₂, O₂/N₂, CH₄, CO, N₂O and SF₆

2.1	Introduction	43
2.2	CO ₂ and O ₂ /N ₂ measurement	44
2.2.1	Introduction	44
2.2.2	Measurement unit convention for oxygen	45
2.2.3	On oxygen fractionation	47
2.2.4	Instrument theory	50
2.2.5	Gas handling scheme	52
2.2.6	Measurement routine and calculations	64
2.2.7	Gas handling strategy for counteracting fractionation effects	68
2.3	CH ₄ , CO, N ₂ O and SF ₆ measurement	70
2.3.1	Introduction	70
2.3.2	Measurement description	71
2.4	Flask sampling	80
2.5	Meteorological measurement	81
2.6	Quality check and flagging	82
2.6.1	Quality control means	82
2.6.2	Data post-processing and flagging	83
2.7	References	84

Abstract

An analysis system for continuous atmospheric measurements was designed and built at Max Planck Institute for Biogeochemistry Jena, Germany in order to set up a new tall tower station near Bialystok, Poland (Lat 53°14'N, Long 23°01'E, Alt 180 m), as part of the CHIOTTO tall tower network.

The system is designed to measure quasi-continuously the mole fractions of CO₂, CO, CH₄, N₂O and SF₆ and the O₂/N₂ ratio in air sampled at five heights of the tower ranging from 5 to 300 m. The measurement devices are: an Oxzilla oxygen fuel cell analyzer, a LiCor-7000 NDIR CO₂ analyzer, an Agilent gas chromatograph (GC) with flame ionization detector (FID) for CH₄ and CO and electronic capture detector (ECD) for N₂O and SF₆. Meteorological parameters are measured at the same heights of the tower in order to help interpreting the mixing ratio data. Additional flask samples are filled regularly for analysis at MPI-BGC laboratory.

The challenge was to build a reliable automatic system which can run continuously without assistance and to fulfill at the same time the high precision requirements for all the measured species.

I present in what follows the technical setup of the Bialystok measurement system, including the main working parameters and some fine tuning directions which lead to the performance achieved. I describe as well the quality check means and procedures, and the data processing and flagging method.

2.1 Introduction

The Bialystok tall tower measurement station was set up under the EU project CHIOTTO (Continuous High-precision Tall Tower Observations of greenhouse gases) as part of a tall tower network covering Europe. The project provided guidelines for the choice of equipment and for the measurement and calibration procedures. The target precision of the measurements was common for all the partners and established taking into account the WMO recommendations (see Table 1.1 in Chapter 1). The measurement system from the already existing tall tower station at Ochsenkopf (partly described by Jordan et al., 2005) was also a source of helpful experience for the design of the new measurement system.

The measurement system was designed and built in laboratory, and tested in the measurement container when it was located at the institute in Jena. The challenge was not only to reach the high precision targets, but also to build an automatic system, robust enough to run continuously and unattended at a remote location. In June 2005 it was partly uninstalled and transported to the final site – a 300 m tall television tower near Bialystok, Poland. Here the final installation and testing was done; the continuous measurement is running since end of July 2005.

The system measures quasi-continuously the mixing ratios of CO₂, CH₄, CO, N₂O and SF₆ and the O₂/N₂ ratio in air sampled from five heights of the tower, between 5 and 300 m above ground level. The main part of the measurement system is installed inside a thermally controlled container, at the base of the tower. The air sampling inlets are fixed on the tower at different heights (5, 30, 90, 180, and 300 m) and atmospheric air is aspirated continuously by pumps installed in the measurement container, and directed to the instruments. There are two almost independent modules; one of them measures CO₂ mole fraction and O₂/N₂ ratio, using a LiCor 7000 CO₂ analyser and an Oxzilla oxygen analyser, and the other measures the mole fractions of CH₄, CO, N₂O and SF₆ by a gas chromatographic method. The connection between the two consists in using the same calibration gases, which requires partial coordination. Auxiliary system parameters used to verify the system performance, like pressures, temperatures, flows, are monitored and recorded together with the mixing ratio data for the posterior quality check.

Meteorological parameters are measured at different heights above ground. The meteorological sensors are installed on the tower and the data are transmitted to the

computer in the measurement container via a CAN-BUS system. Additional flask samples are filled weekly and measured at the MPI-BGC Jena Gas- and IsoLab.

The measurement is fully automated by a custom written Labview software, running unassisted. Using the ISDN link with pcAnywhere software the computers can be accessed and controlled remotely. A short maintenance and check is done about once per week by a local technician and a general maintenance is necessary every few months.

2.2 CO₂ and oxygen measurement

2.2.1 Introduction

CO₂ is accumulating in the atmosphere at an average rate of 1.5 to 2 ppm/year (e.g. Forster et al., 2007). In order to distinguish such small trends in the background air, the atmospheric CO₂ mixing ratio has to be measured with a precision of the order of 0.1 ppm or better (WMO, 2003). There are already well established methods for measuring atmospheric CO₂ mixing ratio, the most frequently used being the techniques based on infrared absorption (e.g. Keeling, 1960) and gas chromatography. Still to reach the required precision level demands very thorough optimization of the instrumental parameters, laboratory conditions and referencing strategy.

The measurement of atmospheric oxygen variations is especially challenging for two reasons. First, the variation which has to be detected (on the order of parts per million) is very small relative to the background atmospheric concentration of about 21%, which means the necessary relative precision is very high. The second reason is that oxygen concentration can be strongly influenced inside the measurement system, by various processes: pressure and temperature induced fractionation, chemical reactions, adsorption and desorption on internal surfaces of tubing and equipment, diffusion through some materials. Some of these effects and the special procedures necessary to counteract them are described later in detail.

Several oxygen measurement methods which can achieve a precision on the order of ppm have been developed in the past years, using various principles: interferometry (Keeling, 1988a, b), mass spectrometry (Bender et al., 1994a), paramagnetism (Manning et al., 1999), fuel cell (Stephens et al., 2001), vacuum ultraviolet absorption (Stephens, 1999), zirconium oxide electrode electrochemical technique (Bloom et al., 1989), gas

chromatography (Tohjima, 2000). Also, special gas handling procedures to avoid fractionation effects have been studied and applied for high precision oxygen measurements (e.g. Keeling et al., 1998).

The measurement system described here uses a LiCor-7000 infrared CO₂ analyser coupled with an Oxzilla FC-2 fuel cell oxygen analyser (Sable Systems). The setup has been developed having as starting point the technique introduced by Stephens et al. (2001, 2007) and the further experience achieved by A. Manning (MPI-BGC, now at University of East Anglia, Norwich, UK), and R. Thompson (NIWA, NZ, now at MPI-BGC, Jena).

The long phase of careful testing and optimization lead to 3-minute measurement precisions of about 0.1 ppm for CO₂ and 5 permeg for O₂/N₂ ratio. As shown in detail in Chapter 3, this precision level was confirmed after the first 18 months of operation in field conditions, after the system was deployed at the final location.

2.2.2 Measurement unit convention for oxygen

A particularity of atmospheric oxygen measurements is that the O₂ variations are usually reported as O₂/N₂ ratio and not as mole fraction. The O₂/N₂ ratio is expressed in “permeg”, a relative unit defined by comparison with an arbitrary standard (Keeling & Shertz, 1992).

$$\delta O_2/N_2 \text{ (permeg)} = \left(\frac{(O_2/N_2)_{\text{sample}}}{(O_2/N_2)_{\text{reference}}} - 1 \right) \times 10^6$$

The reason for this convention is the “dilution” effect, illustrated in what follows. Supposing we have M_{air} moles of air, containing M_{O_2} moles of oxygen and M_{N_2} moles of nitrogen. The corresponding mole fractions of O₂ and N₂ are X_{O_2} and X_{N_2} :

$$X_{\text{O}_2} = M_{\text{O}_2} / M_{\text{air}} \quad ; \quad X_{\text{N}_2} = M_{\text{N}_2} / M_{\text{air}}$$

Suppose we add a number of moles of another compound M_X . The new number of moles of air will be:

$$M_{air_new} = M_{air} + M_X$$

As the number of moles of O₂ and N₂ did not change, the O₂/N₂ ratio is not affected by the addition of M_X. In contrast, the mole fraction of both O₂ and N₂ has changed, the new mole fractions being:

$$X_{O_2_new} = \frac{M_{O_2}}{M_{air} + M_X} < X_{O_2} \quad ; \quad X_{N_2_new} = \frac{M_{N_2}}{M_{air} + M_X} < X_{N_2}$$

In conclusion, the mixing ratio of oxygen in air does not represent well the oxygen fluxes in and out of the atmosphere, since it can be altered by variations of other air components (for example CO₂), without the oxygen quantity actually changing.

A better estimator of oxygen fluxes is the O₂/N₂ ratio defined above, which's changes can only be due to changes in number of moles of oxygen or nitrogen, according to:

$$\Delta(\delta O_2 / N_2) = \left(\frac{\Delta M_{O_2}}{X_{O_2}} - \frac{\Delta M_{N_2}}{X_{N_2}} \right) \times \frac{10^6}{M_{air}} \quad (\text{Manning \& Keeling, 2006})$$

where ΔM_{O_2} and ΔM_{N_2} are the changes in number of moles of O₂ and N₂.

If we have one mole of air, adding or extracting one micromole of oxygen - without changing the quantity of any of the other compounds - would change the O₂/N₂ ratio by about 4.8 permeg.

In many cases the changes in the O₂/N₂ ratio can be considered as being caused only by changes in the oxygen number of moles. This is possible mainly because the atmospheric nitrogen variations are much smaller than oxygen variations (Keeling and Shertz, 1992). Additionally, the effect on O₂/N₂ ratio of one mole change in nitrogen is roughly four times smaller than the effect of one mole change in oxygen, as can be easily seen from the relation above.

2.2.3 On oxygen fractionation

Fractionation is a term originating from isotope measurements and means essentially the separation of different components of an initially homogenous mixture. In the case of O₂/N₂ measurements the term fractionation refers to the separation of oxygen with respect to nitrogen (or to the bulk of air).

The relative precision required for the atmospheric oxygen measurements is in the range where measurement artifacts like fractionation effects become important. The measurement strategy must therefore be adapted in order to minimize fractionation effects and to make possible their surveillance. Various authors (e.g. Keeling et al., 1998, Sturm et al. 2006, Manning, 2001) studied in detail fractionation-related problems of the atmospheric oxygen measurements and proposed methods to minimize them. Some of the oxygen fractionation mechanisms, which are relevant for this work, are summarized in what follows based on literature sources. The gas handling procedures employed to counteract fractionation effects are presented in the paragraph 2.2.7.

Thermal fractionation

In areas where temperature gradients exist and gas transport is dominated by molecular diffusion, thermal diffusion leads to accumulation of heavier molecules (in this case the oxygen) in the colder region (Chapman and Dootson, 1917, Grew and Ibbs, 1952, Chapman and Cowling, 1970). The steady state is reached when the flux due to thermal diffusion in one direction is balanced by the flux driven by concentration diffusion in the opposite direction. For small temperature gradients the following equation is a good approximation of the magnitude of the effect (from Keeling et al., 1998):

$$\delta O_2 / N_2 (\text{permeg}) = (-\alpha \Delta T / T) \times 10^6$$

where:

- $\delta O_2 / N_2$ – fractionation effect in permeg
- α = 0.018 (Grew and Ibbs, 1952)
- T – absolute temperature (K)
- ΔT – temperature difference

The effect of a 1°C temperature difference in steady state is thus on the order of 60 permeg.

Fractionation of O₂/N₂ observed at tee-junctions and air inlets has been attributed to thermal diffusion (Manning, 2001, Sturm et al. 2006).

Pressure induced fractionation

In areas where pressure gradients exist, the heavier molecules accumulate in regions with higher pressure. The fractionation effect due to pressure gradients can be estimated using the following equation:

$$\delta O_2 / N_2 (\text{permeg}) = \frac{m_{O_2} - m_{N_2}}{m_{air}} \times \frac{\Delta p}{p} \times 10^6$$

where:

$\delta O_2/N_2$	– fractionation effect in permeg
$m_{O_2} = 32$	– molecular mass of oxygen
$m_{N_2} = 28$	– molecular mass of nitrogen
$m_{air} \cong 29$	– molecular mass of air
$\Delta p/p$	– relative pressure difference

The effect of a relative pressure difference of 1‰ (e.g. p = 1 bar and Δp = 1 mbar) is thus in steady state 138 permeg.

Fractionation due to humidity gradients

By molecular diffusion, oxygen tends to accumulate in regions with higher absolute humidity. The fractionation effect due to water content gradients can be estimated using the following equation:

$$\delta O_2 / N_2 (\text{permeg}) = \left(\frac{D_{N_2:H_2O}}{D_{O_2:H_2O}} - 1 \right) \times \Delta X_{H_2O} \times 10^6$$

where:

$\delta O_2/N_2$	– fractionation effect in permeg
$D_{N_2:H_2O}$	– diffusivity of nitrogen to water vapor
$D_{O_2:H_2O}$	– diffusivity of oxygen to water vapor
$\frac{D_{N_2:H_2O}}{D_{O_2:H_2O}} = 0.965$	(Severinghaus et al., 1996)
ΔX_{H_2O}	– gradient of water vapor mole fraction

Considering air at 20°C and 1 bar pressure, a water content gradient of 11.5 mmol/mol (corresponding to the difference between 100% and 50% relative humidity) leads to a fractionation effect of about 400 permeg.

Fractionation at flow through small orifices (leaks)

When gas flows through an orifice with the dimension smaller than the mean free path of the gas molecules, the dominant transport mechanism is Knudsen diffusion. The molecular flow is proportional to the partial pressure difference and to the molecular velocity, which varies inversely with the square root of the molecular weight (Dushman, 1962). The ratio of the O₂ to N₂ which flow through a leak is thus $(28/32)^{1/2} = 0.946$ smaller than the O₂/N₂ ratio upstream of the leak.

Fractionation by differential physical adsorption onto surfaces

Oxygen and nitrogen can be differently adsorbed onto certain surfaces due to different surface affinities of the two gases. Physical adsorption is typically reversible and pressure dependent, i.e. the gases are adsorbed when pressure increases and are desorbed when pressure decreases. The effect of differential adsorption and desorption can be observed as changes of the O₂/N₂ ratio with pressure, for example in air extracted from high pressure cylinders.

Chemical reactions

Oxygen can be affected by reactions with materials inside the gas paths. Tests made by Keeling et al. (1998) showed a strong downwards drift of O₂/N₂ in glass flasks unpurified with grease. Thus the choice of the materials and the cleaning procedures (for example of gas tubing and high pressure cylinders) must take into account the possible chemical reactions.

Permeation through solid materials

Sturm et al. (2004) studied the permeation of different gases through various polymeric O-ring seals in the presence of partial pressure differences. Experimentally, they found that the gas inside flask samples can be significantly affected during storage, depending on the materials and geometry of flasks and valves, and on partial pressure differences between sample and surrounding air. The permeation coefficient is specific

for gas-solid combinations. Similar permeation phenomena can also affect the sampled air inside a system for continuous measurement, for example if tubing or other parts made of polymeric materials are used. The problem can be counteracted by adequate choice of materials and equipments.

Gravimetric fractionation

Gravimetric fractionation is a particular case of pressure fractionation, i.e. it is due to the pressure gradients induced by gravitation. Thus the fractionation of gases due to gravitational settling leads to enrichment of heavier gas species at the bottom of a gas mixture column (Dalton, 1826, Gibbs, 1928, Craig et al., 1988). Gravimetric fractionation was observed for example in air contained in snow or ice (e.g. Craig et al., 1988, Sowers et al., 1989, Schwander et al., 1989, Bender et al., 1994b), and in soil gases (Severinghaus et al., 1996). Of interest in this work is the fractionation of air components in high pressure gas cylinders, particularly the fractionation of oxygen with respect to nitrogen. As estimated by Keeling et al. (1998), at barometric equilibrium the O_2/N_2 ratio at the top of a gas cylinder with a height of 1 m, positioned vertically, would be 17 permeg lower than the ratio at the bottom.

2.2.4 Instrument theory

Oxzilla oxygen analyser

Oxzilla FC-2 is a differential oxygen analyser based on two Max-250 oxygen sensors, produced by Maxtec. The Max-250 sensors are galvanic electrochemical cells, containing a lead anode, a gold cathode and a weak acid electrolyte. The sample air can get in contact with the electrolyte via a permeable Teflon membrane. The oxygen contained in air react with the H^+ ions contained in the solution, producing water and an electron flux. The electrical current obtained is proportional to the partial pressure of oxygen, and thus with the oxygen mole fraction in air. Because of using a weak acid electrolyte, the MAX-250 sensors are not affected by chemical interferences of CO , CO_2 and NO_x . Some factory specifications for MAX-250 oxygen sensors are listed bellow:

- life time: > 900000 $O_2\%$ hours
- range: 0 – 100% oxygen
- response time: <15 sec for 90%

- <25 sec for 97%
- accuracy: $\pm 2.0\%$ full scale over operating temperature range
 $\pm 1.0\%$ full scale at constant temperature and pressure
- pressure effect: $\pm 2\%$ from the full scale for 0.5...1.5 atm
- stability: less than 1% drift (full range) over 8 hours at constant temperature and pressure
- materials: o-ring: BUNA-N
housing: CPVC plastic

As a remark, 1% from the full scale means 10000 ppm, which is few orders of magnitude larger than our necessary precision.

There are two factors which can strongly influence the fuel cells signal: temperature and pressure. Moreover, each sensor has a unique response to pressure and temperature fluctuations. Thus the effect will not be compensated alone by using two sensors in a differential measurement mode. However, the setup presented in this chapter does mostly counteract this problem.

LiCor CO₂ analyser

The LiCor model LI-7000 is a closed path, non-dispersive, infrared (NDIR) gas analyser. The analyser is based on the CO₂ property to absorb infrared radiation (IR). The gas flows through a cell positioned between an IR source and an IR detector. The infrared radiation passes through the sample cell and is absorbed by the CO₂ contained in air. The attenuation of the radiation is proportional to the CO₂ mole fraction in air.

LI-7000 has two gas cells and thus offers the possibility to be used in a differential measurement mode. The same IR source serves both the sample and the reference gas paths, the same IR beam being split to pass through both cells. This cancels out the effect of eventual temporal variations of the infrared source intensity on the measurement result.

The analyser has two IR detectors which measure simultaneously the water and CO₂ content in the same gas stream, in the IR windows centered on 4.255 μm for CO₂ and 2.595 μm for water. The CO₂ result is corrected for water interference, using the result of the water measurement.

Some of the relevant factory specifications for LI-7000 are listed below.

- sample cell volume: 10.86 cm³

CO₂ Analyzer Specifications

- range: 0-3000 ppm

- accuracy: 1% nominal
- zero drift (with temperature): ± 0.3 ppm/ $^{\circ}$ C
- span drift: $\pm 0.2\%$ of reading/ $^{\circ}$ C
- resolution: 0.01 μ mol/mol
- noise CO₂ @1Hz, 370ppm: RMS noise: 26 ppb
peak to peak noise: 182 ppb

H₂O Analyzer Specifications

- accuracy: 1%.
- zero drift: ± 0.02 mmol/mol/ $^{\circ}$ C
- span drift: $\pm 0.4\%$ of reading/ $^{\circ}$ C

2.2.5 Gas handling scheme

General description

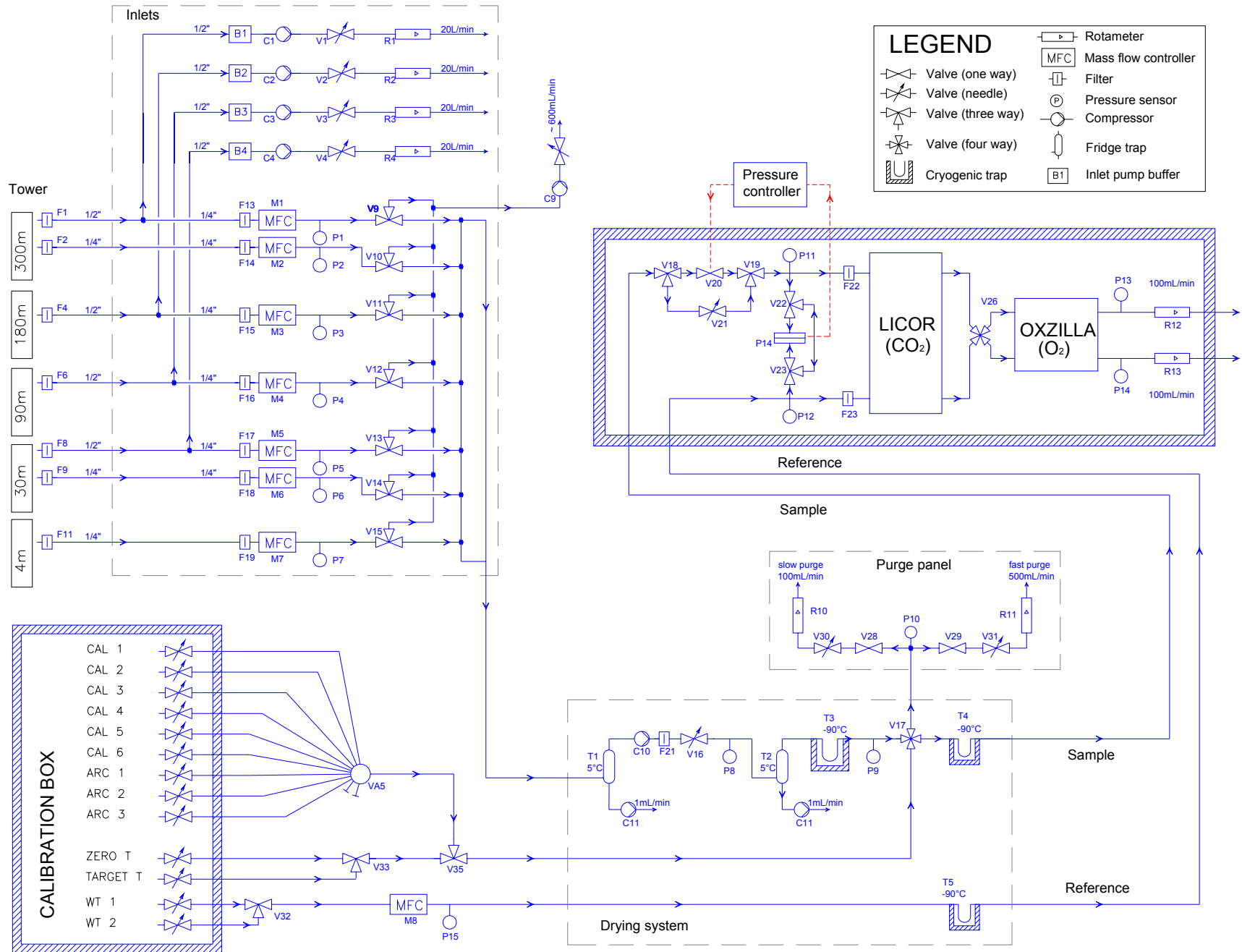
Atmospheric air sampled from the tower is measured alternately with calibration gases, by the CO₂ and oxygen analysers.

As shown before, the response of the fuel cell oxygen analyser is proportional to the oxygen mole fraction in air, while the oxygen measurement results are usually expressed as O₂/N₂ ratio. Thus the measured mole fraction must be afterward converted to O₂/N₂ ratio.

The mole fraction of oxygen in air is affected by dilution with other gases contained in air. It is therefore necessary either to eliminate the potentially interfering compounds or to keep their mole fraction constant, or to measure them in parallel and correct the oxygen results. When measuring atmospheric air, the gases which can have a significant dilution effect are the CO₂ and the water. The natural variations of argon and other species are small enough that they can be neglected.

In this setup, the CO₂ and oxygen analysers are installed in series, measuring the same gas stream (similar to Stephens et al. 2001, 2007). The measured CO₂ mole fraction is used to correct for the dilution effect when the oxygen result is converted from mole fraction to O₂/N₂ ratio. The water effect is minimized by drying the air and gases measured to a very low and constant dewpoint, as described later.

Figure 2.1 (next page) Gas handling diagram for CO₂ and O₂ measurement



The installation and optimization of CO₂ and O₂ analysers

The same gas stream is measured successively, first by the LiCor CO₂ analyser (which does not affect the composition of the measured gas) and then by the Oxzilla oxygen analyser. This is partly being done because, as explained before, the CO₂ mole fraction is needed to compute the O₂/N₂ ratio.

The measurement is differential, which means that the sample is measured in parallel with a reference gas from a high pressure cylinder (WT) and the difference between the two lines is used to compute the mole fraction.

The CO₂ and O₂ analysers are very sensitive to temperature variations. To minimize the effect of ambient temperature fluctuations, the analysers and some of the pressure controlling parts have been installed inside a self made thermostated chamber which maintains the temperature constant in a range of $\pm 0.05^\circ\text{C}$.

Both analysers give signals proportional to the partial pressure of the measured species. For this reason it is necessary that the sample and the reference gases are permanently maintained at the same pressure, otherwise a pressure difference between the two lines could erroneously be interpreted as concentration difference.

The pressure control is implemented by a differential pressure sensor (MKS 223BD, Pdiff in figure 2.2) connected to a controller (MKS 250E, sensitivity 0.001 mbar)

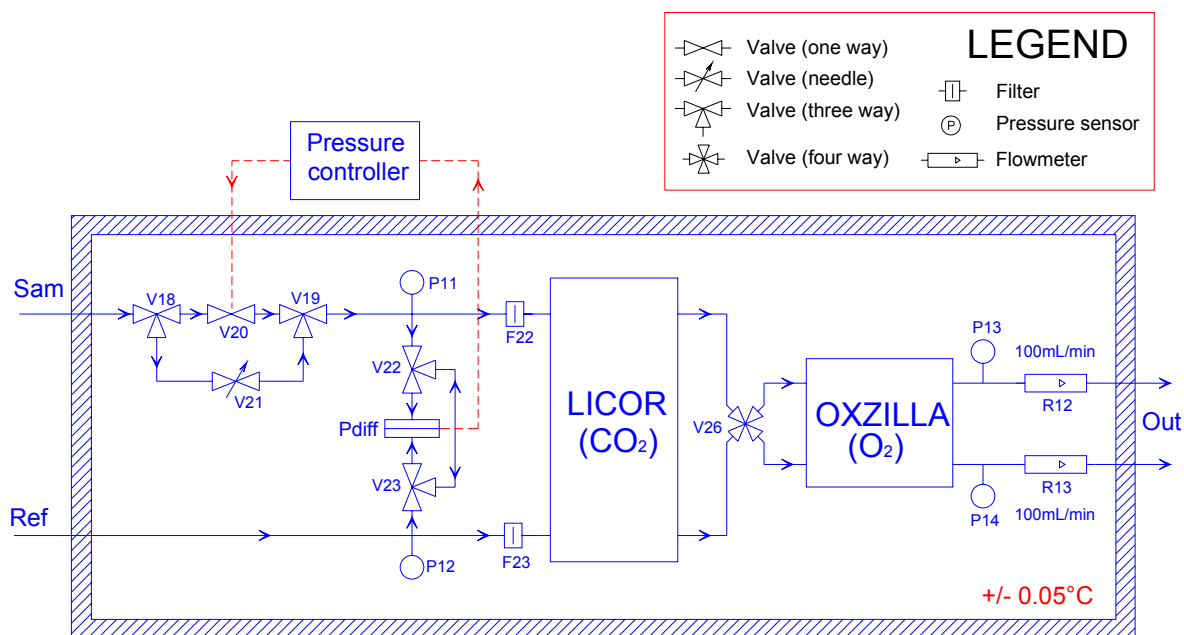


Figure 2.2 Scheme of the installation of CO₂ and O₂ analysers in the thermostated chamber

which adjusts an electronic valve (MKS 248A, V20). As the differential pressure sensor is very sensitive to damage by large pressure differences (the full range is 10 mbar) a protection by-pass is switched automatically if the pressure difference between the two lines becomes accidentally too high (V18, V19, V21, V22, V23).

The inline pressure follows the fluctuations of atmospheric pressure. Changes in the absolute pressure affect the analysers' responses, even if the differential pressure between the sample and the reference lines is maintained constant. The CO₂ analyzer measures the pressure inside the sample cell and uses the result for computing the CO₂ dry air mixing ratio, based on factory calibration coefficients. The measurement range of the pressure sensor limits the allowed pressure inside the LiCor's cells to maximally 115 kPa. The oxygen analyser partly counteracts the effect by measuring the atmospheric pressure and correcting the oxygen result.

Because of intrinsic chemical properties, the two fuel cells used for the oxygen measurement react slightly different to the fluctuations of atmospheric pressure. Moreover, the small temperature fluctuations and the ageing have a different effect on each cell. This makes the differential signal unstable on time intervals longer than few minutes.

To get stability over longer time, we adapted a solution which has already been used (B. Stephens, A. Manning, R. Thompson). A four way valve installed before the oxygen analyser switches every 90 seconds the sample and the reference gases. That means: first the sample is measured by the cell 1 and the reference by cell 2; after that the valve is switched and the sample will be measured by cell 2 and the reference gas by cell 1. The switching is illustrated in figure 2.3.

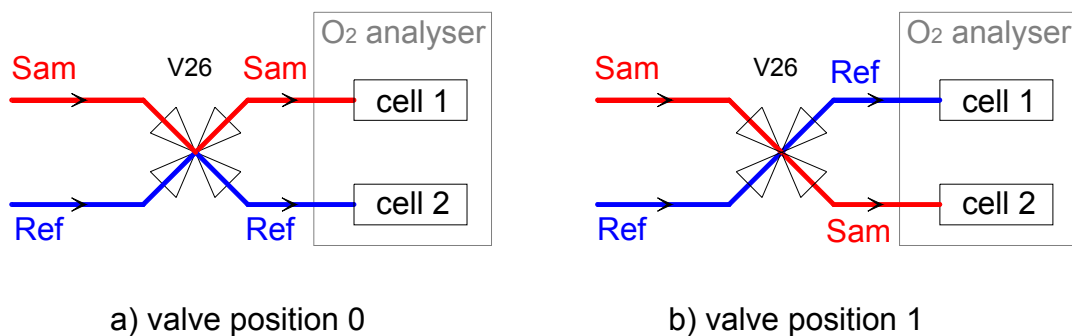


Figure 2.3 Valve switching between the two Oxzilla cells

Instead of a four way valve, a combination of four three way solenoid valves (Numatech Series S) has been included in the system, specially designed to have symmetric gas paths, similar pressure drops (in order to minimize the pressure fluctuations) and no dead space in both switching positions. The difference between cells for the two switching positions is used further to calculate the oxygen concentration, as shown further.

The analysers transmit data via RS-232 connection with a frequency of 1Hz. Figure 2.7 illustrates the differential signal of the oxygen analyser, with the switching between the sample and reference every 90 seconds marked by the black vertical lines.

Measurements from the first 40 seconds after each switch are rejected, as this time is necessary for pressure equilibration and for the gas paths flushing. The grey areas mark the measurement points which are not taken into account. The data in the white windows are used to compute the averages shown in red. The difference between the measurement averages for the two switching positions (A – B1), calculated for each 3 minutes interval, is used further as oxygen raw signal.

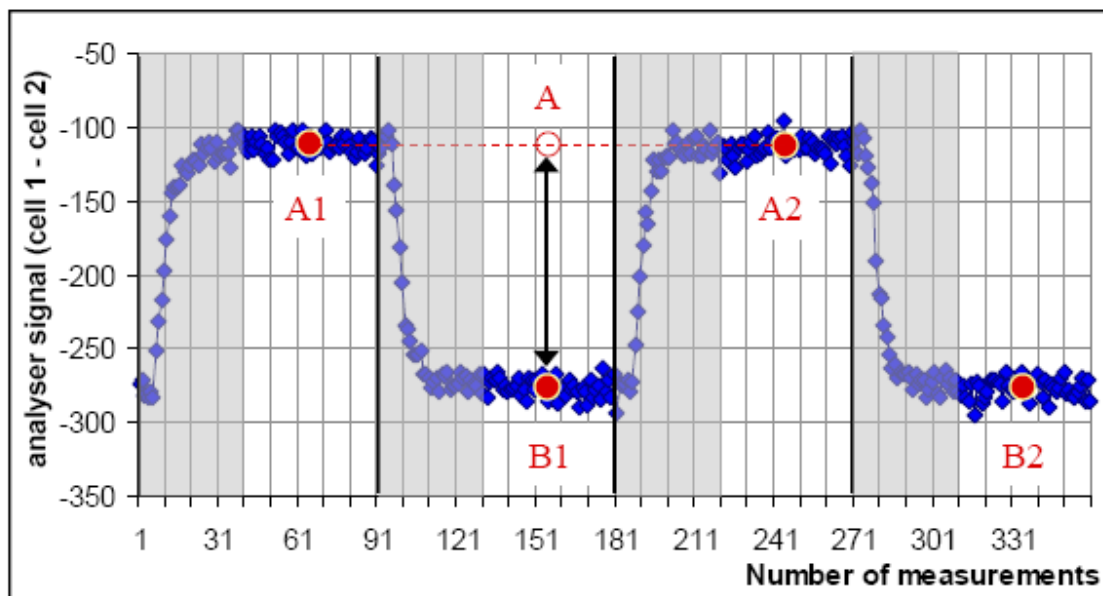


Figure 2.4 The differential signal of the oxygen analyser

As it can be seen in figure 2.4, the equilibration time after a valve switch is usually around 20 seconds. Moreover, in this particular example the difference between the two gases was bigger than 300 permeg, which is larger than the usual situation and thus requests a longer flushing time. The 40-second data rejection window was decided

following extensive lab tests and is meant to cover even the most extreme variations possible.

The LI-7000 CO₂ analyzer is built to measure both water and CO₂ in the same gas and to correct the CO₂ result using the measured water concentration. In our case, the water content in the measured gas is very low, on the order of 0.5 ppm or less. At this level the noise of the water sensor proved to be few orders of magnitude bigger than the actual signal and to induce a significant error to the CO₂ result, rather than improving it. Setting the water value to zero in the analyser's software cancelled the water measurement and reduced the short term noise of the CO₂ signal. The error induced on the CO₂ result because no water correction is applied, is insignificant given the low water content of the measured gas (the gas stream is dried before being measured, as it will be shown in a later paragraph).

Following the careful pressure and temperature control, and after the water measurement was disabled, the short term peak-to peak noise of the LiCor signal when measuring constant gas with a sampling frequency of 1Hz is on the order of 0.02 – 0.03 ppm (the instrument resolution is 0.01 ppm). When averaging a number of 50 measurement points, the standard error of the mean is about 0.004 ppm, which is much smaller than the typical precision achieved (as it will be shown in Chapter 3, paragraph 3.3).

For the oxygen analyser, the typical short term noise at a sampling frequency of 1Hz is about 15 instrument units, which is equivalent after calibration to about 8 ppm. When averaging the results of 50 measurement points, the standard error of the mean is on the order of 1 ppm. As will be shown later, this is on the same order of magnitude with the typical precision we achieve with this measurement. This means that the analyser's noise is one of the main limiting factors for the precision.

Air inlet system

The air is sampled continuously from 5 heights on the tower: 5 m, 30 m, 90 m, 180 m and 300 m. Two different types of inlet lines are used, named "A" and "B" respectively in the figures; the configuration difference is shown in figure 2.6. The main (type A) inlet lines from 30 m, 90 m, 180 m and 300 m levels are made of 1/2" Dekabon tubing; the sampled air is driven by piston pumps (model Thomas CD607) at a flow rate of about 20 L/min. The reason to use such a high flow rate is to get a short residence time of the ambient air in the tubing (in order to minimize eventual diffusion and absorption

effects) and to minimize the effect of oxygen thermal fractionation at inlets. A stream of 100 ml/min (controlled by Mass flow controllers Analyt GFC 171S) is then separated for the measurement via a tee-junction and the rest is flushed outside.

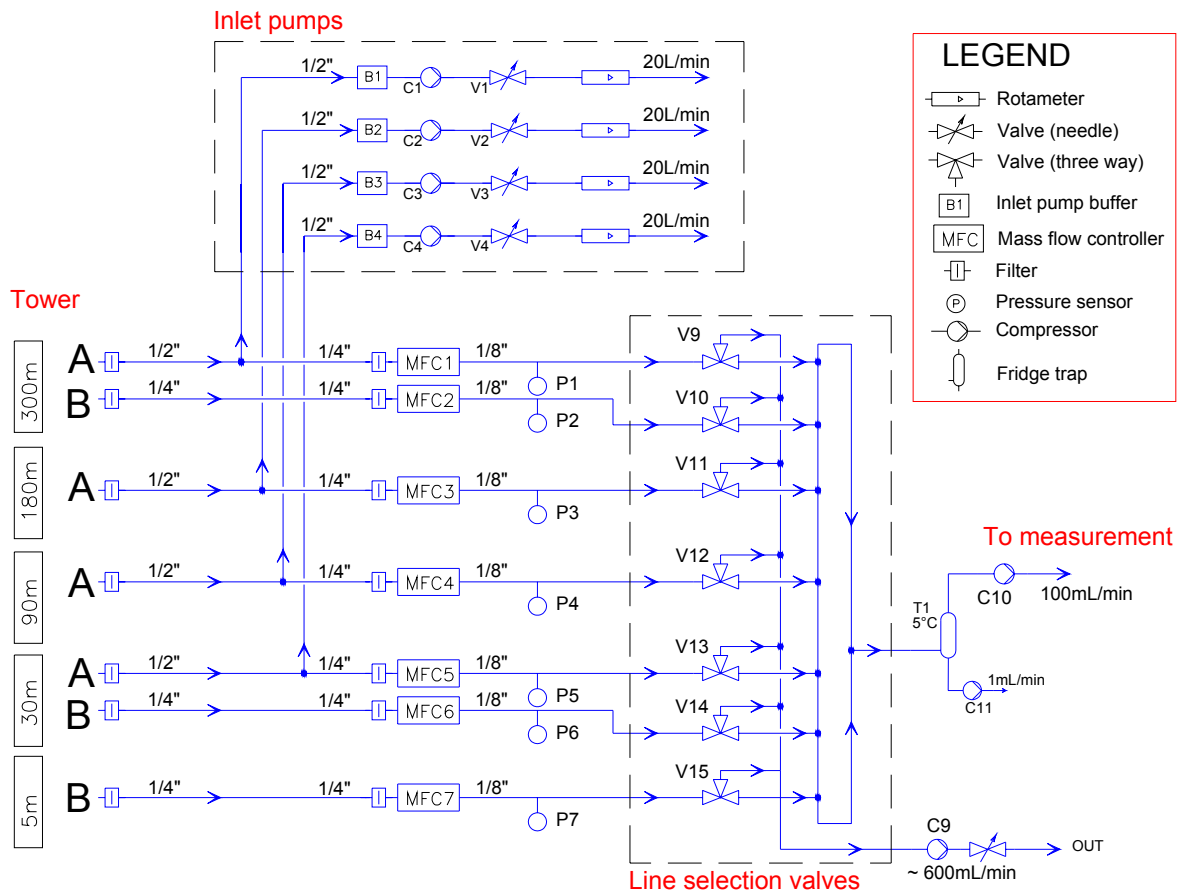


Figure 2.5 Diagram of air inlet setup for CO₂ and O₂ measurement

The two additional “control” sampling lines (type B) from 30 m and 300 m levels use 1/4” tubing, without inlet pump and without tee. The control lines’ purpose is to be used as a check for the main sampling lines, in order to detect a possible oxygen fractionation or any other problems, like broken tubing or blocked inlet filters. The air flow on these lines is only 100 ml/min thus the travel time through the tubing is longer (about 30 min for the 300 m level) and time corrections must be made for comparisons between lines. The sampling line from the 5 m height is also of type B.

A three way solenoid valves system (Numatech Series S) controlled by the Labview program selects one line to be measured, while the other ones are continuously flushed at constant flow to avoid the air stagnating into the tubing. The selected air stream is then driven to the drying system by a KNF Neuberger N05 diaphragm pump with aluminum head and Teflon coated diaphragm. This type of pump has been tested, and it proved not to alter the O₂ and CO₂ composition of an air stream which passed through it (Manning, 2001).

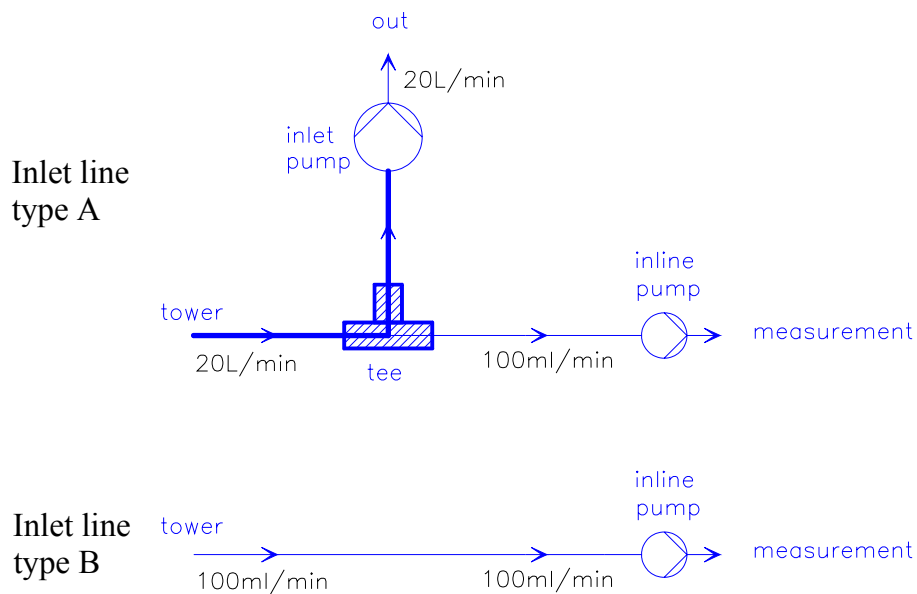


Figure 2.6 The two types of air inlet used for CO₂ and O₂/N₂ measurement

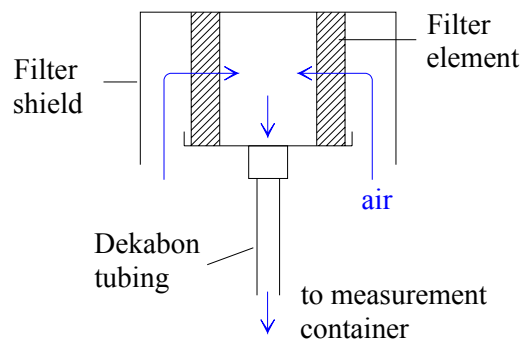


Figure 2.7 Air inlet design

Calibration and reference gases

For calibration and reference we use high pressure cylinders filled with air by the MPI-BGC Jena gas facility. Some specifications of the gas cylinders are listed below.

Cylinder: type *Luxfer P2806Z*; material *Aluminum alloy*; volume: *50L*; maximum work pressure: *200bar*

Cylinder valve: type *Rotarex-Ceodeux D20030163*; material *Brass*; seat *PCTFE*

Cylinder pressure regulator: type *Scott Model 51-14C (high purity, two stages)*; material *Nickel plated brass, SS diaphragm*

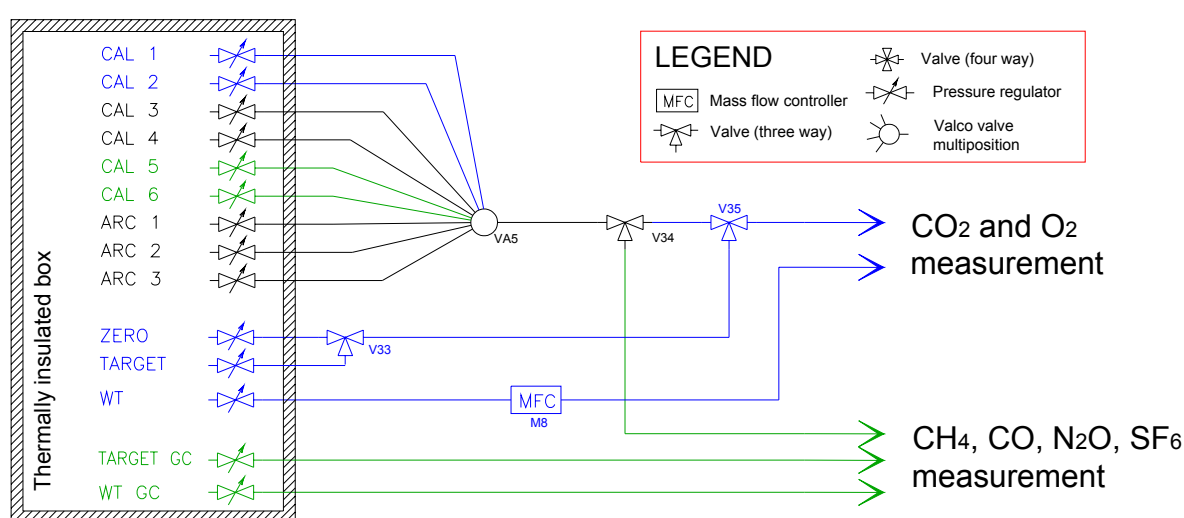


Figure 2.8 Diagram of calibration and reference gases
Blue – used only for the O₂/N₂ and CO₂ measurement system
Green – used only for the gas chromatographic measurement
Black – shared by the two measurement systems

The **working tank** (WT) provides the reference gas for the differential measurement. It contains air with concentration in the normal atmospheric range and with an initial pressure of 200 bar. The flow of the reference gas is maintained at 100 ml/min by a mass flow controller (M8 in figure, type Analyt GFC 171S). The lifetime of one working tank is about two months.

The main calibration is done at intervals of about 40 hours, using the set of four **calibration standard gases** CAL1 – CAL4, which cover the atmospheric concentration

range. Two of these cylinders are shared with the gas chromatographic measurement. The lifetime of the calibration cylinders is estimated to be 2 – 3 years.

Only for CO₂, there is a more frequent **zero** calibration, which corrects for eventual short term drifts. The name of this gas does not mean that it has zero CO₂ concentration (actually the zero calibration gas has a CO₂ concentration in the normal atmospheric range), but that it is being used to correct the zero term of the calibration curve, as explained in more detail in the paragraph 2.2.6.

The **archive** standard gases (ARC1...ARC3) are meant to propagate the measurement scale on long term, on the order of 10...20 years. They are not used for routine measurement calibration, but only for comparisons with the calibration gases, in order to detect any eventual evolution. This type of calibration will be implemented in 2007 and will take place once every few months, or when any of the calibration gases will be replaced.

The purpose of the **target** measurement (TT) is to verify the stability of the measurement on short, medium and long term and to signalize eventual measurement problems. Also, the target measurement result on long term provides an evaluation of the measurement repeatability. This measurement it is not used for any calibration or corrections.

All the gases are measured in Jena laboratories against primary standards traceable to SIO scale for O₂/N₂ ratio and the NOAA/ESRL GMD X2005 scale for CO₂.

The selection of the calibration gases is made by a multiposition 12 port Valco valve (VA5 in figure) with 1/16" fittings, controlled by Labview software via serial port. The three-way valves (V33, V34 and V35) are solenoid type Numatech Series S.

The gas cylinders are stored in horizontal position, inside an insulated box, for thermal stability. The horizontal storage of cylinders and the thermal stability is particularly important for oxygen, to avoid shifts caused by gravimetric or thermal fractionation (Keeling et al., 1998). The regulators are installed outside insulated box and connected to the cylinder valves via 1/16" Nickel tubing (length 1.5 – 2 m).

Air drying system

Air drying is important for the oxygen concentration measurement, because of the dilution effect. Each ppm of water added into air would replace 0.21 ppm of oxygen. The dilution effect of water on CO₂ mole fraction is much smaller: 1 ppm water modifies the CO₂ mole fraction with about 0.00037 ppm, which is not distinguishable within the

sensitivity of this measurement. However, the water can influence the CO₂ measurement by IR absorption interference.

The ambient air is dried by four-stage cooling, as shown in figure 2.9. The construction of the three types of cold traps used is shown in figure 2.10.

The first two traps (T1 and T2) are placed inside a refrigerator, at a temperature of about 5°C. These traps are made in glass and filled with glass beads (borosilicate, diameter 4mm). The purpose of the glass beads is to increase the condense surface and to decrease the volume which has to be flushed. The water condenses on the glass beads and on the traps walls and is continuously eliminated by a peristaltic pump (C11 in figure 2.9).

The pressure inside the trap T1 is about 700 mbar abs. The purpose of the first trap is to eliminate part of the water from the sampled air, mainly for the protection of the sensitive diaphragm pump (C10 in figure 2.9) situated after it. The second glass trap T2 is installed after the pump C10, at a pressure of about 1600 mbar abs. The higher pressure makes it more efficient in eliminating the water. The dewpoint of air after leaving the trap T2 is between 2 and 10°C.

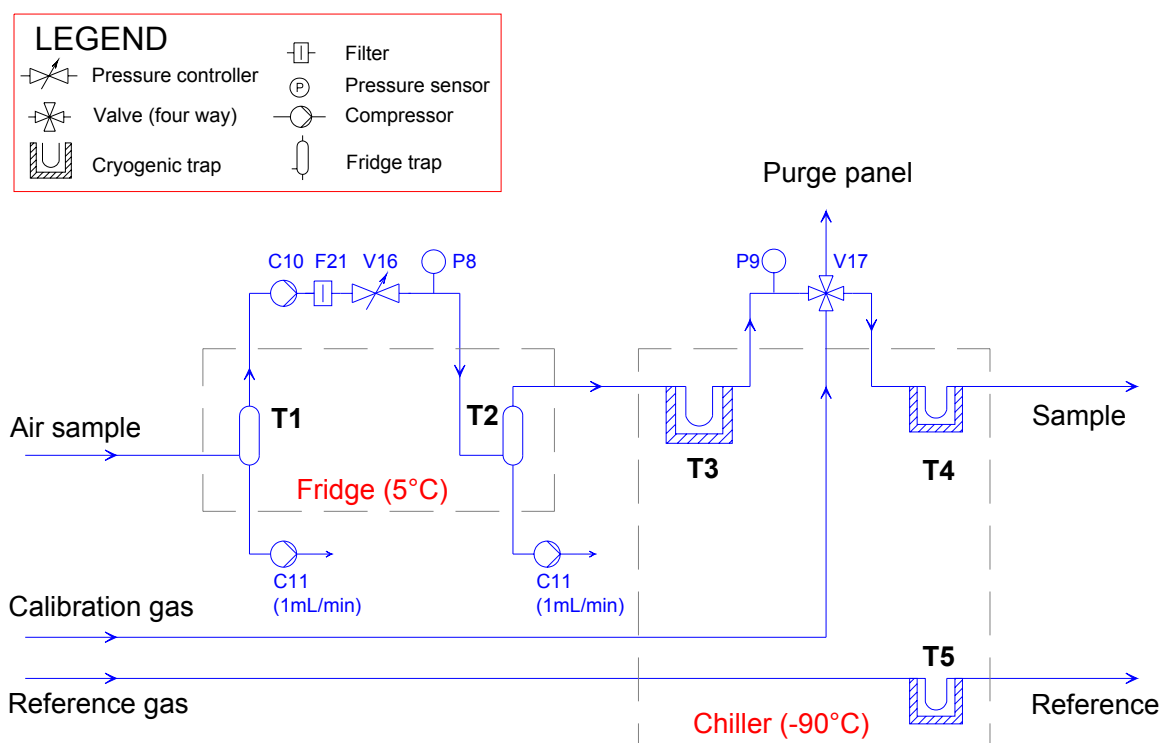


Figure 2.9 Gas drying system

After the bulk of the water has been eliminated, the air passes two more cold traps (T3 and T4), situated inside a cryogenic cooler (Kinetics Thermal, VT 490), at a temperature of about -90°C . The construction of the chiller traps T3 and T4 is described in figure 2.10 b and 2.10 c respectively. The trap T3 is filled with the same type of glass beads like T1 and T2. Most of the water still existing in the air is frozen in the trap T3 which has to be cleaned and dried by a technician at one to two weeks intervals.

The traps T1 – T3 are used only for the drying of the ambient air. After these three stages, the air has a dewpoint between -70 and -80°C , in the same range as the gas from cylinders. The last stage of drying is the trap T4, common for air, target gas and calibration gases. The function of the last trap is to get the same dewpoint for the measured air and gases. A similar role plays the trap T5, installed in the same cryogenic cooler on the reference gas line.

Measurements made during summertime, in conditions of high atmospheric humidity, have shown the final dewpoint of the sampled air after the trap T4 to be at least -82°C . This implies that the air or gas contains a maximum of 0.4 ppm of water when leaving the drying system. The dilution effect on oxygen is therefore at most 0.1 ppm, which is ten times smaller than the typical precision achieved.

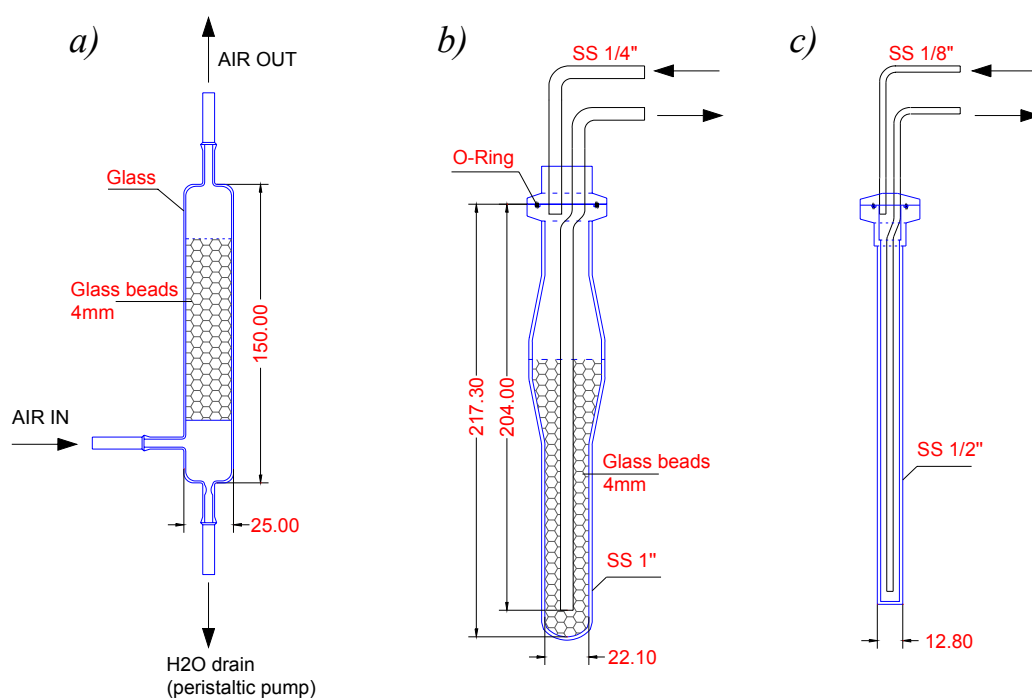


Figure 2.10 Cold traps design. a) Fridge trap (T1, T2); b) Chiller big trap (T3); c) Chiller small trap (T4, T5). Figure courtesy to U. Schultz, MPI-BGC.

2.2.6 Measurement routine and calculations

Software

The measurement system is automated, being controlled by custom written Labview software. The program controls the valves according to the chosen measurement sequence and registers the data from analysers and the system diagnostic parameters (flows, pressures, temperatures). In addition, the Labview program calculates in real time the CO₂ mixing ratio and O₂/N₂ ratio, based on calibration parameters and the raw signal from analysers.

Measurement routine

Both analysers provide direct concentration results. However, the direct results are not stable and precise enough and are used only as raw signals. The software registers these raw signals and calculates the CO₂ mole fraction and O₂/N₂ ratio using the external calibration.

The measurement is organized in cycles, which are user defined series of air samples, calibration and reference gases.

In normal operation, the program is set to repeat a certain measurement sequence composed by air samples from different heights, target and zero gases (the “air cycle”). A typical measurement sequence is:

0 1 2 3 4 5 6 Z T 3 6 0 4 2 T

where the numbers 0 – 6 are the codes used by the Labview software for the air sampling lines (0 = 300 m – line A; 1 = 300 m – line B; 2 = 180 m; 3 = 90 m; 4 = 30 m – line A; 5 = 30 m – line B; 6 = 5 m); Z and T are the codes for zero calibration respective target measurement. The measurement order for the different sampling heights and gases changes, e.g. the target tank is being measured first time after the zero cylinder and second time after the air line “2”. The idea of this scheme is to detect eventual systematic errors due to insufficient flushing of the common gas paths.

Each of the codes from the example above stands for a series of six times 3-minute measurements (the total measurement of one line lasts 18 minutes), thus six values are obtained. After switching between different gases or air coming from different heights, a certain time is necessary for the common gas paths to be flushed and for pressure stabilization. This time was determined experimentally to be about 5 minutes. In the actual setup, the first three measurement points (9 min) are discarded, taking into

account a safety range for the equilibration time. The total number of six measurements for each sampling line was decided as follows: because three measurement points have to be discarded, the remaining three measurements represent a minimal number of data points which can be used to monitor eventual systematic errors, in case the equilibration time will become longer than 9 minutes.

Every time when the zero cylinder is measured, the CO₂ calibration coefficients are updated as explained in the next paragraph “Calculation of CO₂ mole fraction” and the following measurements (in this example target cylinder T) are calibrated using the new coefficients.

There is a different sequence for the main calibration, using the four calibration gases. The calibration cycle is set to be repeated every 40 hours, but the program does not start the calibration cycle until the previous air cycle was completed. The 40-hour setting implies that the calibration is performed at different times of the day. The rationale is to avoid systematic errors associated to the eventual dependence of the measurement on any 24-hours influence, like room temperature.

The calibration cycle is structured partly differently from the air cycle. At the start of the calibration sequence, the Valco valve VA5 (see figure 2.8) selects the first calibration gas and the program switches the system valves to send the gas to the purge panel (see figure 2.1). This is necessary for the flushing of the cylinder regulator (because the air was stagnating inside, thus absorption / desorption effects are possible) and of part of the gas paths. A “fast purge” step at 500 ml/min is followed by a “slow purge” step at 100 ml/min. The “slow purge” step brings the flow close to the normal measurement flow. After this, the calibration gas is directed to the measurement system and measured 12 times in a row (12 x 3-minute), for 36 minutes in total. From these 12 measurements, the first 6 (18 minutes) are discarded as this time interval is necessary for the common gas paths to be flushed and for pressure stabilization. The last 6 measurement points undergo a standard deviation check (threshold 4 x stdev) and any outlier is discarded. The average of the remaining measurement points is the result used further. By averaging the measurement results, the standard error of the final result is in principle smaller than the noise of each measurement. This is important for calibration, which has to be more precise than the normal measurement.

The same purge – measurement sequence is repeated for each of the four calibration gases. The measurement results of the four cylinders are used to compute the new calibration coefficients. A simple real-time quality check of the calibration result is

done and the program decides if the calibration is accepted or rejected. This eliminates only the large calibration failures, due for example by the breakdown of the calibration valve VA5. If the calibration was rejected, the old calibration continues to be used. If the calibration was accepted, the new coefficients will be used until the next calibration.

Calculation of CO₂ mole fraction

For CO₂ the calibration curve is calculated as a two degrees polynomial fitting, obtaining:

$$y = a * x^2 + b * x + c,$$

where: a, b, c = calibration coefficients
 x = measured (analyser) signal
 y = mole fraction

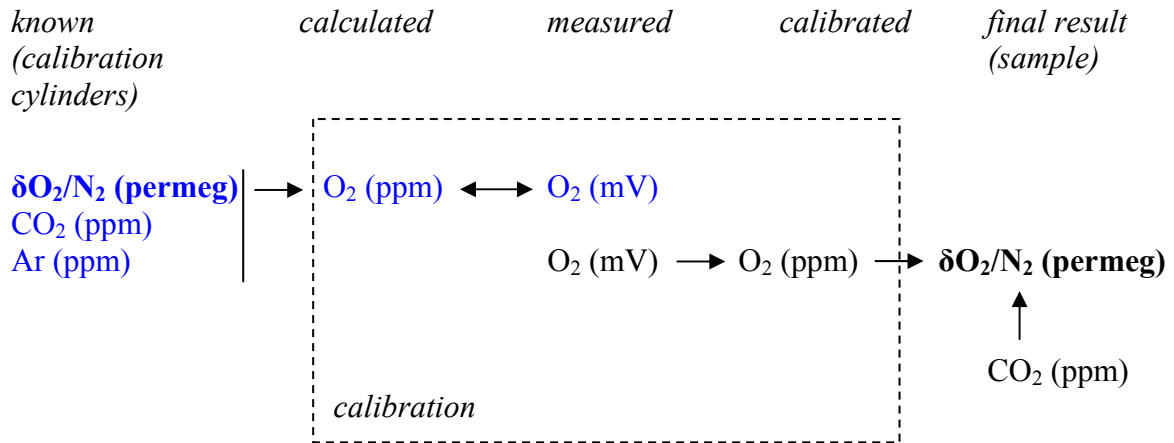
Every few hours a zero calibration takes place. The zero tank is measured after the calibration and its mole fraction value is calculated using the a, b, c coefficients obtained from calibration. After few hours, the zero tank is measured again and a new value is obtained, possibly different from the previous one. This difference is used as correction for the “zero” term c and the new assigned value for c coefficient will be used to calculate the measured air mole fraction until the next zero calibration.

Calculation of O₂/N₂ ratio

As explained before, the oxygen measurement results are usually expressed in terms of O₂/N₂ ratio, and not in oxygen mole fraction. The O₂/N₂ ratio unit is “permeg”, a relative unit defined by comparison with an arbitrary standard:

$$\delta O_2/N_2 (\text{permeg}) = \left(\frac{(O_2/N_2)_{\text{sample}}}{(O_2/N_2)_{\text{reference}}} - 1 \right) \times 10^6$$

On the other hand, the fuel cell analyser response is proportional to the mole fraction of oxygen in air. The conversion between the two measures must take into account the dilution effect on the mole fraction (explained in the paragraph 2.2.2). The calculation path is illustrated in the following scheme, where the blue letters refer to calibration gases.



The calculation steps are:

- Calculation of calibration gases mole fraction to obtain O₂ (ppm) for calibration gases
- Measurement calibration to obtain O₂ (ppm) for air sample
- Calculation of O₂/N₂ ratio for air sample

The calculation for each step is explained in detail in what follows.

a) Calculation of calibration gases mole fraction

Note: in what follows we do not consider the absolute mole fraction for oxygen, but the difference between the mole fraction of interest and the reference mole fraction of $X_{O_2}^0 = 0.20946$ (Machta & Huges, 1970).

The difference between oxygen mole fraction of calibration gases and the reference oxygen mole fraction is calculated for each calibration gas from the ratio values (permeg) with corrections for CO₂ and Ar mole fractions. The correction for argon is necessary in this case because its concentration was strongly modified in the process of production the calibration cylinders.

The formula used is:

$$\Delta X_{O_2}(\text{ppm}) = \delta O_2 / N_2(\text{permeg}) \times X_{O_2}^0 \times (1 - X_{O_2}^0) - ((CO_2 - CO_{2ref}) + \Delta X_{Ar}) \times X_{O_2}^0$$

where:

ΔX_{O_2} (ppm) = mole fraction difference corresponding to $\delta O_2/N_2$ (permeg)

$X_{O_2}^0 = 0.20946$ (reference mole fraction of oxygen in air)

CO_{2ref} = 363.29 ppm (specific to SIO O₂/N₂ scale)

ΔX_{Ar} (ppm) = difference between Ar mole fraction of sample and the normal atmospheric value ($Ar_{ref} = 0.945\%$)

A derivation of this formula is given as Appendix 2.

b) Calibration

We use four calibration gases, for which the ratio (permeg) is known and the ppm values calculated as explained before. By measuring the four calibration gases, we obtain the parameters of the linear regression of oxygen analyser signal against the cylinders oxygen mole fraction. When measuring sample air, these parameters are used to compute the sample mole fraction.

c) Calculation of O₂/N₂ ratio for air sample

The result of air measurement following calibration is expressed as mole fraction and a conversion to O₂/N₂ ratio is necessary. The formula is the reverse of the one used at point a), with the CO₂ correction but this time without the Ar correction. Argon correction is not needed when measuring atmospheric air since its concentration variations in air are too small to affect the oxygen measurement significantly.

$$\delta O_2/N_2 (\text{permeg}) = \frac{\Delta X_{O_2} (\text{ppm}) + (CO_2 - CO_{2ref}) \times X_{O_2}^0}{X_{O_2}^0 \times (1 - X_{O_2}^0)}$$

where:

ΔX_{O_2} (ppm) = mole fraction difference

$X_{O_2}^0 = 0.20946$ (reference mole fraction of oxygen in air)

CO₂ (ppm) = CO₂ mole fraction measured in the same air sample

CO_{2ref} = 363.29 ppm (specific to SIO scale)

2.2.7 Gas handling strategy for counteracting fractionation effects

As shown in the paragraph 2.2.3, oxygen gradients due to various fractionation mechanisms may occur in different parts of the system. For example oxygen tends to accumulate in the regions with lower temperature, higher humidity or higher pressure.

Other potential fractionation mechanisms are the flow through orifices with dimensions smaller than the free molecular path (leaks) and the differential adsorption of O₂ and N₂ on solid surfaces as discussed in section 2.2.3.

The existence of pressure and temperature gradients cannot be avoided in all cases. For example the room temperature is around 25°C but the sampled air is driven at some stage through cryogenic traps at about -90°C. The flow of gases through the measurement system is not possible without the existence of pressure gradients.

A strategy for minimizing fractionation effects which has been successfully employed (e.g. Keeling et al. 1998) is to expose the sample and the reference gases to pressure, temperature and humidity gradients only under conditions of steady flow. Mass balance ensures that the relative flows of oxygen and nitrogen into any region must equal the relative flows out of the region even if concentration gradients exist within the region itself. The implementation of this strategy at Bialystok measurement system follows the methods previously applied by A. Manning for the tall tower station at Ochsenkopf, Germany.

The gas handling scheme was designed to keep the pressure and flow variations minimal. Continuous flow is maintained on all of the air sampling lines from the tower, whether they are selected for measurement or not. The inline flows and pressures are actively controlled. However, when switching between inlet lines, in some situations, small pressure fluctuations may occur and the observed effects on the oxygen results can go up to 20 permeg variations and for up to 12 minutes after switching, while the effect on CO₂ is not noticeable. A careful quality check is thus necessary to eliminate eventual erroneous data points.

Temperature fluctuations are diminished by an air conditioning system which keeps room temperature variations in a range of ±1°C. The gas cylinders are placed inside a thermally insulated box, to minimize the spatial and temporal temperature gradients. Also, the CO₂ and oxygen analysers, together with the sensitive pressure control parts are installed in a self made thermostated box.

No plastic is being used within the gas flow paths in order to avoid O₂/N₂ changes due to differential permeation. The whole system is carefully leak checked to avoid gas loss which would change the remaining gas composition.

The main air sampling lines from the tower contain tee-junctions which are potential thermal or pressure fractionation locations. To have the possibility to detect and study eventual fractionation inside the tees, additional “control” inlet lines with a

different design (without tees) have been installed at two heights of the tower. The double sampling lines provide also a possibility to detect eventual thermal fractionation at inlet. Although the inlet configuration is similar, the flow at inlet is greatly different: 20 L/min for the main lines and 100 ml/min for the control lines. Thermal fractionation depends strongly on flow rate, therefore it is likely to be negligible at a flow rate of 20 L/min but it can be significant at 100 ml/min. A detailed description of the inlet system is provided in paragraph 2.2.5, and results of the comparison between the main and the control sampling lines are presented in Chapter 3, paragraph 3.4.2.

For the calibration and target gases it is not possible to keep continuous flow. In this case, the calibration measurement starts with a purge step for flushing the regulator and the tubing as described in the paragraph 2.2.6.

2.3 CH₄, CO, N₂O and SF₆ measurement

2.3.1 Introduction

There are several gas chromatographic systems for CH₄, N₂O and SF₆ analysis that have been described in the literature (e.g. Worthy et al., 2003). High precision CO measurement with a GC-FID has been implemented only recently at the Canadian baseline stations by D. Worthy. Optimization of such a system to meet the precision targets set by Chiotto project on long term is a challenging task, even under laboratory conditions.

The design of the gas handling system and the gas chromatograph setup for N₂O and SF₆ had as a starting point the measurement implemented before at another tall tower station (Ochsenkopf, Germany - Jordan et al., 2005). The CH₄ and CO measurement method was developed starting from Dough Worthy's setup described in the Canadian Baseline Program Report. To get the required precision necessitated careful testing and optimization of sample loop and GC columns dimensions, gas flow, temperature and pressure parameters and of the valves switching schedule. Another challenge was to get the gas chromatograph based system stable and reliable enough to be running continuously without an operator's assistance.

2.3.2 Measurement description

Gas chromatograph setup

As principle, the gas chromatographic (GC) measurement consists in two main steps: the separation of the air sample in different components (which is done by packed chromatographic columns) and the detection and quantification of the components of interest. Different species are retained differently by the columns, so they elute at different time intervals and they are carried to the detector by the carrier gas. The detector outputs a signal which is proportional to the amount of the species of interest. The integration of this signal over a specific period of time gives the total amount of the measured species in the sampled air. The columns, detectors and carrier gases are chosen depending on which chemical species have to be measured. For this particular measurement, a flame ionization detector (FID) with N_2 carrier gas is used for CH_4 and CO detection and an electronic capture detector (ECD) for N_2O and SF_6 , with $ArCH_4$ as carrier gas.

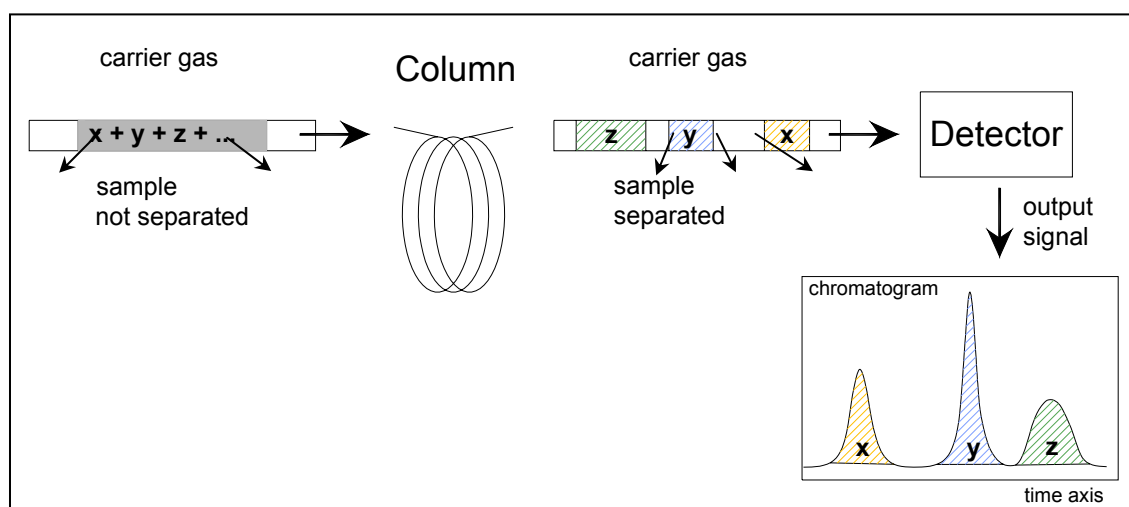


Figure 2.11 Illustration of gas chromatographic measurement principle

The main components of the GC system (shown in figure 2.9) are:

- Hewlett Packard model 6890 gas chromatograph equipped with:
 - flame ionization detector (FID) for CH_4 and CO
 - electronic capture detector (ECD) for N_2O and SF_6

- Hewlett Packard model 5790 heated nickel catalyst unit (methaniser)
- 4 packed columns
- 2 sample loops
- Single instrument GC Chemstation software
- 3 Valco 10 port - 2 positions and 1 Valco 4 port - 2 positions valves with 1/16" fittings and microelectric actuator
- 1 oven (Kendro Lab Products)
- 1 mass flow controller (Analyt GFC 171S)
- H₂ supply:
 - H₂ cylinder (purity 99.999%)
 - H₂ purifier (Molsieve 13X, 160 ml, self-made)
- N₂ supply:
 - Jun-Air compressor with buffer volume
 - N₂ generator (Parker UHP 76-94)
 - N₂ purifier (Aeronex or NuPure)
 - backup N₂ cylinder (99.999%)
- Zero air supply:
 - Jun-Air compressor with buffer volume
 - Zero air generator (Parker 75-83)
 - Zero air purifier (Sofnocat and Molsieve 13X, 200 ml, self-made)
 - backup zero air cylinder (synthetic air, 20.5% O₂ in N₂, hydrocarbon free)
- ArCH₄ supply:
 - P5 (5% CH₄ in Ar) cylinders (ECD quality)
 - ArCH₄ purifier (Aeronex or NuPure)

The FID sample loop is a stainless steel tube with a volume of 15 ml. The air sample flows through the sample loop with about 100 ml/min and the pressure near atmospheric pressure. When the two position Valco valve VV1 switches, the air volume contained in the sample loop is transferred to and carried through the columns by the carrier gas, where CH₄ and CO are separated. The CH₄ elutes about one minute later than the air bulk and the CO delay is about two minutes. The separated sample is lead to the FID, which detects directly the CH₄. After the CH₄ peak has been detected, the valve VV3 switches to lead the rest of the sample through "methaniser", a NiO catalyst which

converts the CO into methane using H₂, in order to make its detection possible. In this way both CH₄ and CO are detected by the FID as CH₄, and what differentiates them is the retention time.

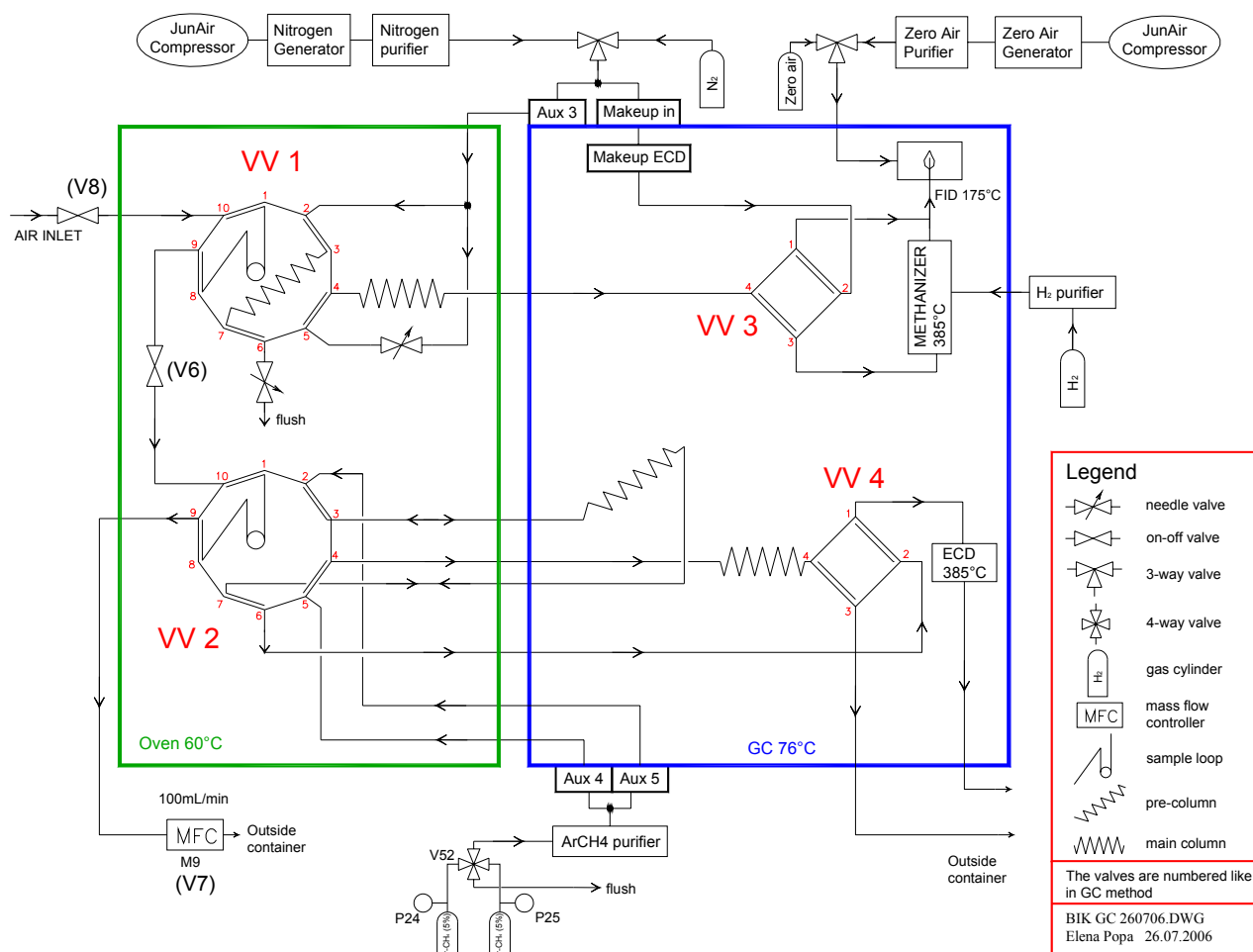


Figure 2.12 The GC system diagram – LOAD position

After CH₄ and CO have eluted, the pre-column is flushed by reversing the carrier gas flow direction to eliminate any eventual late eluting compounds which would affect the following measurement. While the CH₄ and CO reach the detector, the flushing of the sample loop with gas for the next measurement already starts.

The sample loop for the ECD (25 ml) is installed in series with the FID sample loop, and flushed with the air sample in the same time. The switching of VV2 leads the sample through the pre-column and main column. One of the first eluting compounds is

oxygen, which is vented by valve VV4 in order to protect the ECD detector; then VV4 switches, sending the rest of the gas eluting from the column to the detector. N₂O and SF₆ are both directly detected by the ECD with a difference in retention times of about 1 min.

The technical parameters of the GC measurement are summarized in Table 2.1.

Table 2.1 GC measurement specifications

Specific	CH ₄ and CO	N ₂ O and SF ₆
Detector, temperature	FID, 175°C	ECD, 385°C
	Ni catalyst, 385°C	
	H ₂ flow 50 ml/min	
	Air flow 320 ml/min	
Oven temperature	60°C	76°C
Sample loop	15 ml	25 ml
Precolumn	SS, 4ft, 1/8" O.D., Molsieve 5A, 80-100 mesh	SS, 6ft, 3/16" O.D., Hayesep Q, 80-100 mesh
Column	SS, 4ft, 1/8" O.D., Unibeads 1S, 60-80 mesh	SS, 12ft, 3/16" O.D., Hayesep Q, 80-100 mesh
Carrier gas	N ₂	P5 (5% CH ₄ in Ar)
Run time	7 min	7 min

Figure 2.13 is an example of a typical chromatogram, with the signals from both detectors overlapped. Both area and height of the peaks are proportional to the mole fraction of the species. The best precision for mole fraction calculation in case of CH₄ and N₂O is obtained when using the peak area, while for CO and SF₆ the peak heights lead to better results.

The chromatograph has its own software (HP Chemstation) which controls the measurement according to the predefined method. A measurement "method" specifies the flow, pressure, temperature and valves switching steps which are necessary for the measurement of one sample, together with the integration parameters for computing the peak characteristics. The Chemstation software registers the signal from the detectors with a frequency of 20 Hz and calculates the peaks area and height. For each measurement a report is created containing the integration results and other additional parameters which are useful for diagnosis and quality check.

The parameters of the currently used method are described in Appendix 3.

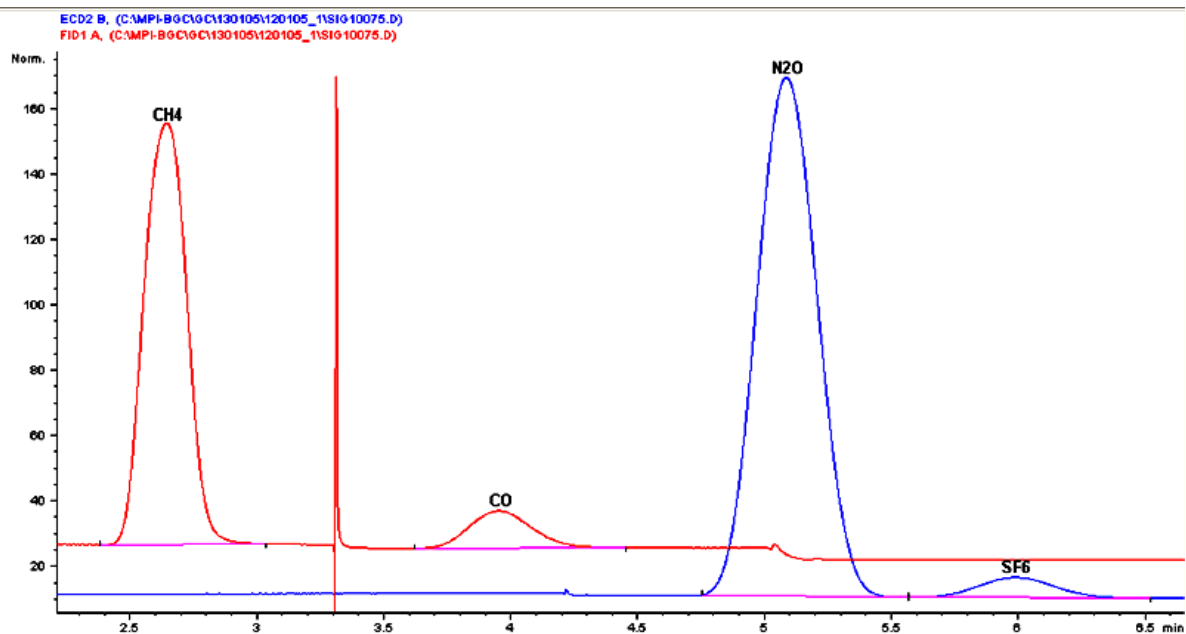


Figure 2.13 Typical chromatogram

Gas handling scheme

The diagram of the measurement setup for CH₄, CO, N₂O and SF₆ is shown in Figure 2.14; the detailed diagram of the gas chromatograph itself was shown in Figure 2.12.

Like for the CO₂ and O₂ measurement, the air is sampled from 5 heights of the tower: 5 m, 30 m, 90 m, 180 m and 300 m. The flow in the inlet lines (Dekabon 1/2") is continuous, 100 ml/min for the 5 m level and 20 L/min for the other lines. From each of the inlet lines a stream of 100 ml/min is taken and the rest is flushed outside. One of the sample lines is selected for measurement by a solenoid valves combination (Numatech Series S) while the other lines are maintained at constant flow. The sampled air is first dried cryogenically to a dewpoint of about -80°C, in a similar way with the one described before for CO₂ and O₂/N₂ measurement, and then driven to the gas chromatograph inlet.

The air sample is measured alternately with a reference gas from a high pressure cylinder, called working tank (WT), as illustrated in Figure 2.15. The ratio between the area or height of the sample air peak and the bracketing working tank peaks is the intermediary result used further to compute the mixing ratio.

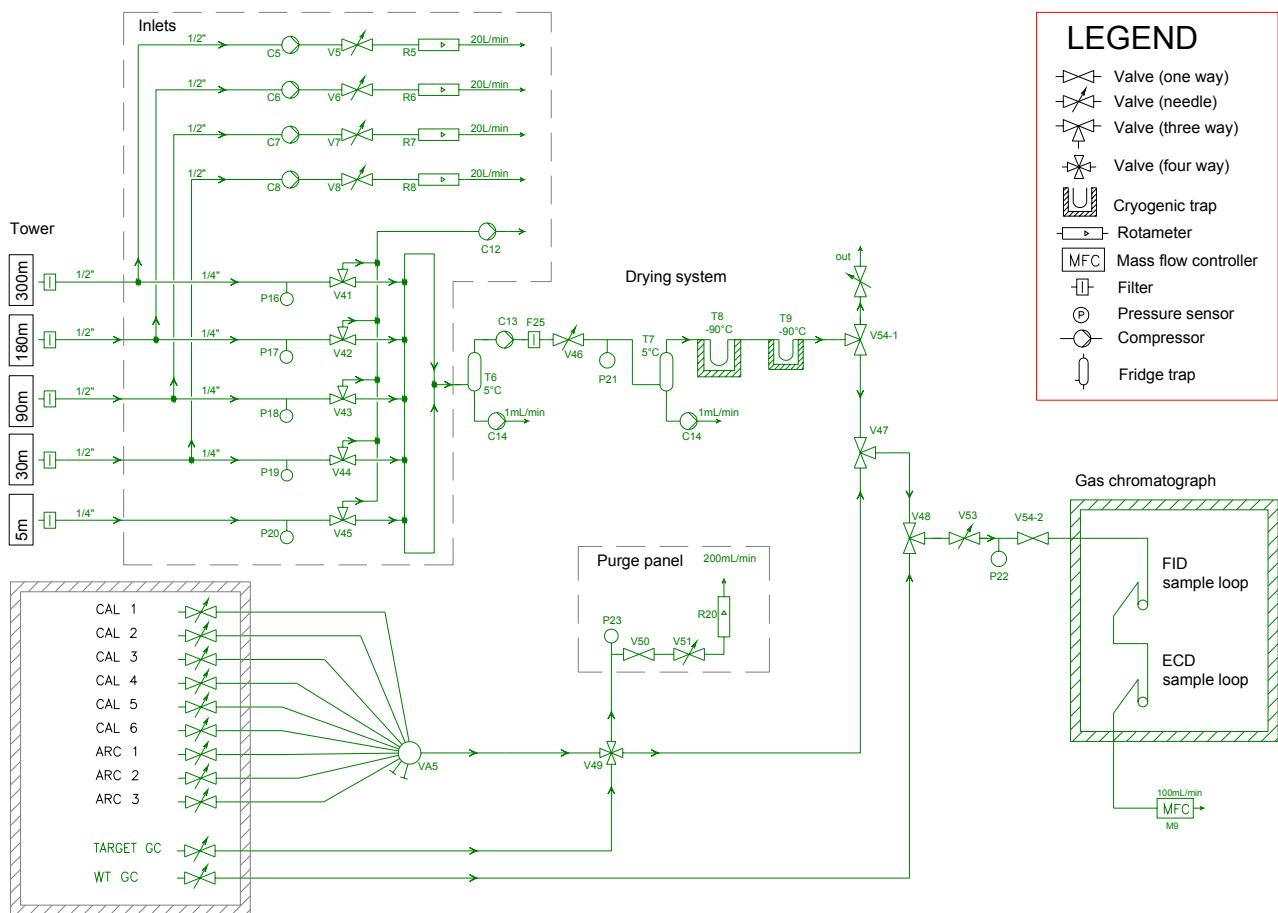


Figure 2.14 Diagram of external gas handling system for the GC measurement

The reference and calibration gases have a dewpoint between -60 and -70°C , and they do not pass through the drying system for the following reason. By contrast to the CO_2 and O_2/N_2 measurement system, (where the flow is continuous for both sample and reference lines), the GC measurement alternates the sample and the reference measurements and the gas flows through only when the injection into the sample loops is being done. The gas stagnating into the chiller traps would lead to faster blocking of traps with ice. For the atmospheric sample the solution is the continuous flushing of the gas path, the air being eliminated into the room via the valve V54-1 except of the air injection time interval. For the calibration and reference gases, a similar solution is not convenient, because it would significantly decrease the gas cylinders lifetime.

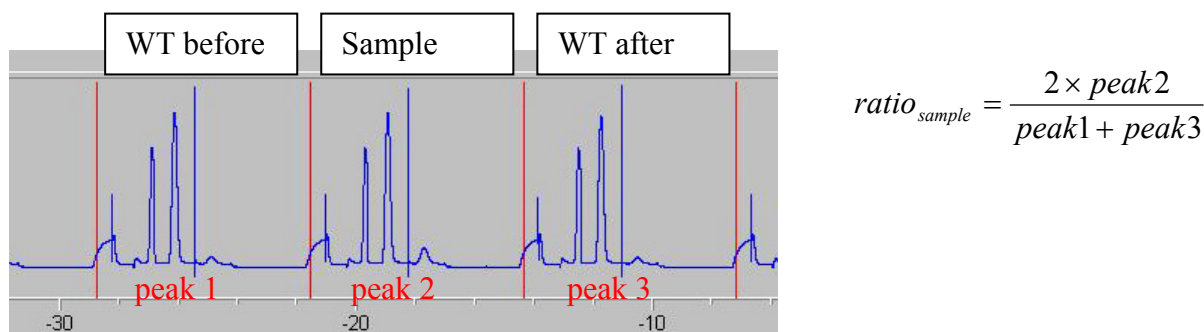


Figure 2.15 The sample ratio calculation for the GC measurement

Calibration

The calibration is done using a set of four high pressure aluminum cylinders (Luxfer, 50 L, 130 bar), calibrated at MPI-BGC Jena GasLab and traceable to internationally recognized scales maintained by NOAA/ESRL GMD (for CH₄, CO and SF₆) and CSIRO (N₂O). For CH₄, CO and SF₆ the calibration gas mole fractions cover the normal atmospheric range. In the case of CO, the calibration gas mole fractions range between 100 and 450 ppb, while the atmospheric mole fraction can reach sometimes much higher values, on the order of 600-800 ppb. This has to be taken into account as potential supplementary error for the measurement results which are outside of the calibration range. However, linearity tests made for the FID detector (for the range 50-500 ppb with CO and 400-2500 ppb with CH₄) did not show any non-linearity detectable within the sensitivity of this measurement. Based on this, it has been decided not to exclude the measurement results which are outside of the calibration range.

Each calibration gas is first flushed for 5 minutes through the valve V49 and the purge panel, and then measured six times; the result used further is the average of the six measurements. So far no systematic differences between the first measurement and the following five measurements have been observed, thus no measurement is excluded for insufficient flushing reasons. A standard deviation check is done by the Labview program and any eventual outlier from the series of six results is flagged as “bad” and excluded from calculation.

The regular calibration takes place at intervals of about 120 hours. The stability of the system over long term was tested before the final installation and the conclusion was that the time between two consecutive calibrations can safely be longer than one month.

The 120 hours interval is redundant and was decided considering a potentially unstable environment. A non-regular forced calibration can also be made when necessary, for example after changes in the measurement system.

System control, data logging and calculation

The automation and data processing is done partly by the GC instrument Chemstation software and partly by the same Labview program which controls the CO₂ and O₂/N₂ measurement.

The Chemstation software manages the general GC measurement and operation: controls the measurement parameters according to the method, processes the detectors signals, registers the results in reports and manages eventual dangerous malfunctions. The chromatograph is equipped with 8 valve closures (four 24 DC voltage, 2 current and 2 TTL contact closures) which make it possible for the Chemstation software to control the 4 Valco valves, the mass flow controller valve, the air inlet valve and to launch a starting signal to Labview.

Although the GC Chemstation program has its own calibration possibility, this was not flexible and precise enough to obtain sufficiently precise results. Also, two of the calibration gases are shared with the CO₂ measurement system which required coordinated calibration timing for the two systems. For this reason the calibration is controlled and computed by the main Labview program. The alternation of reference gas with ambient air, target and calibration gases is also controlled by Labview, because the GC does not have enough control possibilities for the necessary number of selection valves.

After each measurement, the Labview software reads the file reports created by Chemstation and extract the raw data – peaks area and height - to compute the mole fraction. Labview writes the final data files containing the mole fraction results and adding flags that result from a first level real time quality check. A series of other parameters are registered and checked for measurement quality diagnoses: pressures, baseline levels, retention times, methaniser efficiency and calibration linearity.

Optimization and fine tuning

The gas chromatograph was first installed, tested and optimized in the lab, to achieve a good instrument performance. Some of the main optimization directions which led to the presently achieved precision are presented in what follows.

Special attention had to be paid to the measurement of CO and CH₄, as there had not been any such system at the institute yet. Major problems with CO detection turned out to require intensive conditioning of the chromatographic columns with repeated cycles of ambient to high temperature (225°C).

The signal to noise ratio is one of the main factors determining the measurement precision, especially in the case of small peaks like CO and SF₆. The first step to improve it was achieving a smooth and stable baseline. The baseline quality proved to be strongly dependent on carrier gases quality but also on the external environment parameters, like pressure and temperature. Using high purity gases with additional filters, keeping the gas paths continuously flushed and stabilizing the external temperature resulted in a substantial decrease in baseline variations. Subsequently a series of tests was performed to optimize the measurement method parameters – pressures, temperature, flows and valves switching – to obtain big and well defined peaks for the species measured.

The sensitivity of the detectors can undergo big fluctuations caused partly by variations in atmospheric pressure. Especially the ECD detector proved to be quite unstable in time, having sensitivity variations of up to 30% over less than one hour. Measuring alternately the working tank with the sample air drastically reduces the problem, as the sensitivity variations affect both measurements.

One concern was the possible dilution of the actual sample with traces of the previously measured gas, if the common gas paths would not be flushed sufficiently. For adjusting the flushing times for all the system components, measurement tests have been done using gases with very different concentrations. The tests consisted in measuring gases in series like AAAA-BBBB...where A and B are gases with different concentrations. The flushing was considered good enough when the first measurement of gas B did not show any systematic difference from the following three. In the final method setup, the flushing time used is about 20% longer than the minimum flushing time established by these tests.

The peak integration made by Chemstation was one of the main limitations for precision. The integration parameters have been adjusted using long datasets of constant gas measurements with concentrations spanning the atmospheric range. Each dataset (containing repeated measurements of only one gas) was reprocessed with different sets of integration parameters. The set of integration parameters which gave the best results in terms of standard deviation for all datasets was chosen for further use. The finally

achieved precision was up to ten times better than the one obtained with parameters automatically chosen by Chemstation program.

The linearity of the detectors for the measured species has been tested in the common atmospheric range. The FID proved to be linear in the detection limit for the whole range covered by CO and CH₄ (about 50 to 2500 ppb). In case of ECD, the concentration level of SF₆ gives linear response, while for N₂O the signal response to concentration variation can be non-linear, even for the small range of 315 – 328 ppb covered by calibration. Following these tests, the calibration for CH₄, CO and SF₆ is done by linear fitting, and for N₂O by second degree polynomial fitting.

2.4 Flask sampling

An automated flask sampler was installed in the measurement container by a team from NIWA – New Zealand, built to fill two flasks at the same time. The principle diagram of the flask sampling system is presented in figure 2.16. Up to eight flask pairs can be installed in the sampling system, but only one pair can be filled at a time.

The air is sampled from the 30 m and 300 m levels of the tower via two dedicated sampling lines similar to the ones for continuous measurement. The inlet lines are continuously flushed at a flow of about 20 L/min, to avoid air stagnating inside the tubing; in this way flask sampling can take place at any moment without additional preconditioning of the inlet lines being necessary. When the sampling takes place, the air is directed through a cryogenic trap which removes the water up to a dewpoint of -75 to -80°C.

The flask sampling system is controlled by custom Labview software and can be programmed to take samples without an operator being present.

The flasks are installed in the sampling system during the technician visit and left with the valves open. The sampling takes place unassisted, at the programmed date and time. The sampling starts with a sampler “line flushing” step of three minutes at a flow of 4 L/min and pressure of 1.8 bar abs. The flask is then flushed for 10 minutes (flow 2 L/min, pressure 1.6 – 1.8 bar abs), after which the flow is stopped and the flask is left under pressure. The technician closes the sample valves and uninstalls the filled flasks at a future visit. The long time during which the flasks are installed in the sampling system

with the flask valves open (up to two months) imposes strict requirements on the tightness of the system.

We use 1 L glass flasks equipped with two PCTFE sealed valves (Normag, Ilmenau), preconditioned with dried air at 1.8 bar in MPI-BGC laboratory. The flasks are analyzed in the MPI-BGC Gas- and Iso-Lab for CO₂, O₂/N₂, CH₄, CO, N₂O, SF₆, ¹³C and ¹⁸O.

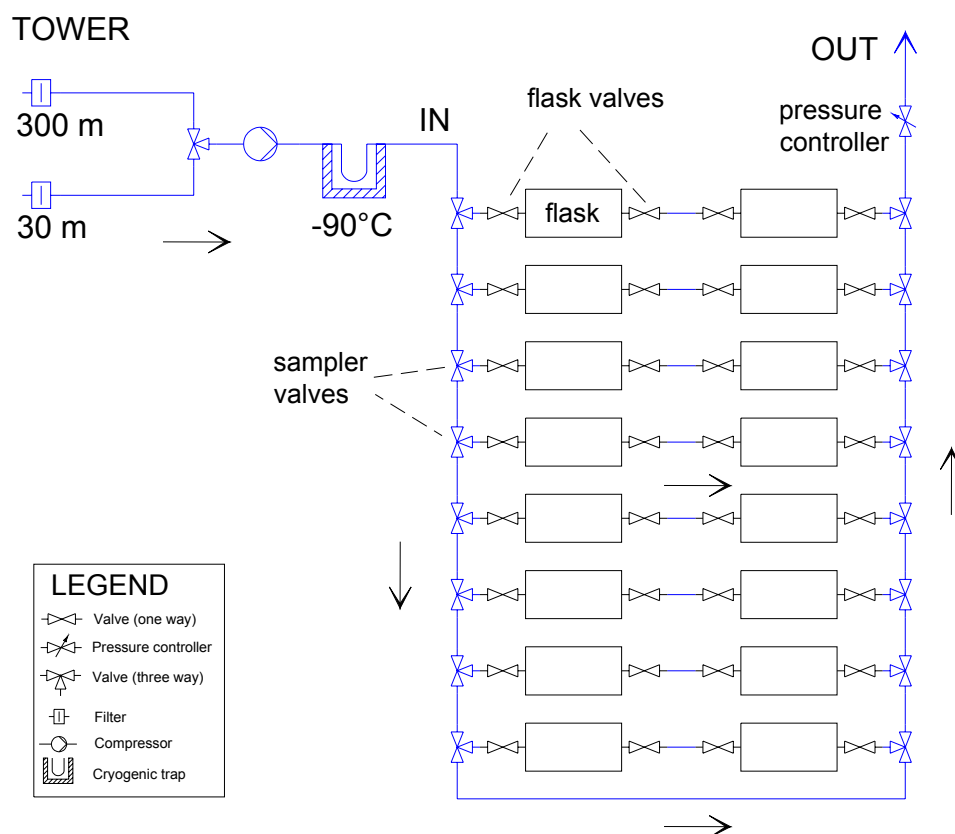


Figure 2.16 Principle scheme of the flask sampling system

2.5 Meteorological measurement

Meteorological parameters are measured at different levels on the tower and the data are transmitted to the main Labview program by CAN-Bus system. The measured parameters are:

- wind speed and direction at 300 m and 75 m
- atmospheric pressure at 30 m, 300 m
- atmospheric temperature at 5 m, 30 m, 90 m, 180 m, 300 m

- atmospheric humidity at 30 m, 300 m

The meteorological data are registered in the data files every 90 seconds, together with the results of the CO₂ and O₂/N₂ measurement.

2.6 Quality check and flagging

2.6.1 Quality control means

In order to assess the measurement quality and to discover and repair eventual failures one needs clear means to verify the measurement. Also, some of the technical parameters of the measurement (pressures, flows) can slowly evolve in time, a fact that requires some settings to be adjusted from time to time. For the Bialystok measurement system we tried to set up a coherent and complete scheme, for both real time and post-processing quality check.

A primary quality check tool is the monitoring of various system diagnostic parameters which are used for real time flagging and which are re-checked again in posterior data verification. The data from 28 pressure sensors, 7 temperature sensors, and 2 flow sensors, are registered every 90 seconds in dedicated files. Each action of the program, for example the switching of any of the 60 valves, is registered in additional log files.

The target measurement is a means to monitor the measurement and to indicate eventual problems, and also to determine the characteristic precision. It consists in measuring periodically (usually 4 to 6 hours) a constant gas with known concentrations, from a high pressure cylinder.

During a normal measurement sequence, gases with different concentrations are measured alternately, flowing through the same path. A potential problem is the dilution of the sample with the previous measured gas, if the flushing time was not long enough to clean the gas paths below the detection limits. Careful tests were made at the initial setup for adjusting the flushing time, however, this issue needs to be verified continuously. As a check, each air line is measured at least three times consecutively. Any systematic shift between the first air measurement and the following ones would be an indication for an insufficient flushing of the common air path. The same check is done for the calibration, in which case each cylinder is measured six times.

Another reason for repeatedly measuring the calibration gases is that the calibration has to be more precise than the sample measurement; by using the mean of six values, the standard error is about 2.5 times smaller than the typical standard error of one measurement. This gives also the possibility of real time quality check and eventual exclusion of any wrong measurement in the calibration cycle.

For the gas chromatographic measurement the reference gas peak result is another important parameter to monitor, as it should be quite constant and the measurement frequency is high (once every 14 minutes). It can have some “normal” fluctuations caused by atmospheric pressure or room temperature variations but, in the same time, an unusual result can indicate a measurement problem, like detector sensitivity variations, injection problems, or GC leaks.

2.6.2 Data post-processing and flagging

A first data flagging is done in real-time by the Labview program, based on some of the diagnostic parameters. This first check has mainly the purpose to rapidly signal eventual problems. The final quality check is done a posteriori based on more complete information.

All the intermediary data files resulted from the measurements and calculations are stored. In some situations it is necessary that the calculation is redone starting from any intermediary step, or even from the raw Labview or Chemstation data. The Chemstation program stores the information for each measurement in a separated folder and has the possibility to re-integrate any signal using any new set of integration parameters.

After the eventual necessary re-calculation has been done, the final results are quality flagged. The flagging is based on user registered events (work or changes in the system, any other known events) and on the system diagnostic parameters. All the steps done for a data set post-processing are registered in a log file, in such way that the processing can be redone based on this information. Also, all the original and intermediary files are stored and a new reprocessing creates new files versions without overwriting the old ones.

2.7 References

- Bender M. L., Battle M., and Keeling R. F. (1998) The O₂ balance of the atmosphere: A tool for studying the fate of fossil-fuel CO₂ [review]. *Annual Review of Energy & the Environment* 23, 207-223.
- Bender M. L., Sowers T., Barnola J.-M., and Chappellaz J. (1994b) Changes in the O₂/N₂ ratio of the atmosphere during recent decades reflected in the composition of air in the firm at Vostok Station, Antarctica, *Geophys. Res. Lett.*, 21(3), 189–192.
- Bender M. L., Tans P. P., Ellis J. T., Orchardo J., and Habfast K. (1994a) A high precision isotope ratio mass spectrometry method for measuring the O₂/N₂ ratio of air. *Geochimica et Cosmochimica Acta* 58(21), 4751-4758.
- Bloom A. J., Caldwell R. M., Finazzo J., Warner R. L., and Weissbart J. (1989) Oxygen and carbon dioxide fluxes from barley shoots depend on nitrate assimilation *Plant Physiol.* 91(1), 352-356.
- Chapman S. and Cowling T.G. (1970) *The mathematical theory of non-uniform gases*. Cambridge Univ. Press, Cambridge.
- Chapman S. and Dootson F. W. (1917) Thermal diffusion. *Phil. Mag.* 33, 248.
- Craig H., Horibe Y., and Sowers T. (1988) Gravitational separation of gases and isotopes in polar ice caps. *Science* 242(4886), 1675-1678.
- Dalton J. (1826) On the constitution of the atmosphere. *Philos. Trans. R. Soc. London* 116, 174.
- Dushman S. (1962) *Scientific Foundations of Vacuum Technique*, Wiley.
- Forster, P., Ramaswamy V., Artaxo P., Berntsen T., Betts R., Fahey D.W., Haywood J., Lean J., Lowe D.C., Myhre G., Nganga J., Prinn R., Raga G., Schulz M. and Van Dorland R. (2007): Changes in Atmospheric Constituents and in Radiative Forcing. In: *Climate Change 2007: The Physical Science Basis. Contribution of Working Group I to the Fourth Assessment Report of the Intergovernmental Panel on Climate Change* [Solomon, S., D. Qin, M. Manning, Z. Chen, M. Marquis, K.B. Averyt, M. Tignor and H.L. Miller (eds.)]. Cambridge University Press, Cambridge, United Kingdom and New York, NY, USA.
- Gibbs J. W. (1928) *Collected works, Vol. 1 Thermodynamics*, Yale
- Grew K. E. and Ibbs T. L. (1952) *Thermal Diffusion in Gases*. Cambridge Univ. Press, New York. 143 p.
- Jordan A., Schultz U., Seifert T., Gloor M., Manning A., Heimann M., Schulze E.-D. (2005) Continuous GC measurements of trace gases at the Ochsenkopf monitoring station, *Proceedings of the 12th IAEA/WMO meeting of CO₂ experts, Toronto, Sept. 2003, WMO-GAW Report 161*, ed. D. Worthy and L. Huang;
- Keeling C. D. (1960) The concentration and isotopic abundances of carbon dioxide in the atmosphere. *Tellus* 12(2), 200-203.

- Keeling, R. F. (1988a) *Development of an interferometric oxygen analyzer for precise measurement of the atmospheric O₂ mole fraction*. Ph.D. thesis, Harvard University, Cambridge, Massachusetts.
- Keeling R. F. (1988b) Measuring correlations between atmospheric oxygen and carbon dioxide mole fractions: a preliminary study in urban air. *Journal of Atmospheric Chemistry* 7(2), 153-176.
- Keeling R. F., Manning A. C., McEvoy E. M., and Shertz S. R. (1998) Methods for measuring changes in atmospheric O₂ concentration and their application in southern hemisphere air. *Journal of Geophysical Research-Atmospheres* 103(D3), 3381-3397.
- Keeling R. F. and Shertz S. R. (1992) Seasonal and interannual variations in atmospheric oxygen and implications for the global carbon cycle. *Nature* 358(6389), 723-727.
- Manning, A. C. (2001) *Temporal variability of atmospheric oxygen from both continuous measurements and a flask sampling network: Tools for studying the global carbon cycle*, Ph.D. thesis, University of California, San Diego, California
- Manning A. C. and Keeling R. F. (2006) Global oceanic and land biotic carbon sinks from the Scripps atmospheric oxygen flask sampling network. *Tellus Series B-Chemical & Physical Meteorology* 58(2), 95-116.
- Manning A. C., Keeling R. F., and Severinghaus J. P. (1999) Precise atmospheric oxygen measurements with a paramagnetic oxygen analyzer. *Global Biogeochemical Cycles* 13(4), 1107-1115.
- Schwander J. (1989) The transformation of snow to ice and the occlusion of gases. In: Oeschger, H., Langway Jr., C.C. (Eds.), *The Environmental Record in Glaciers and Ice Sheets*. Wiley, New York, pp. 53-67.
- Severinghaus J. P., Bender M. L., Keeling R. F., and Broecker W. S. (1996) Fractionation of soil gases by diffusion of water vapor, gravitational settling, and thermal diffusion. *Geochimica et Cosmochimica Acta* 60(6), 1005-1018.
- Sowers T., Bender M., and Raynaud D. (1989) Elemental and isotopic composition of occluded O₂ and N₂ in polar ice. *Journal of Geophysical Research-Atmospheres* 94(D4), 5137-5150.
- Stephens B.B. (1999) *Field-based atmospheric oxygen measurements and the ocean carbon cycle*. Ph.D. thesis, 221 pp., University of California, San Diego.
- Stephens B., Bakwin P., Tans P., and Teclaw R. (2001) Measurements of atmospheric O₂ variations at the WLEF tall-tower site. In *Sixth International Carbon Dioxide Conference, Extended Abstracts*, vol. I, Tohoku Univ., Sendai, Japan, 78-80.
- Stephens B. B., Bakwin P. S., Tans P. P., Teclaw R. M., and Baumann D. D. (2007) Application of a differential fuel-cell analyzer for measuring atmospheric oxygen variations. *Journal of Atmospheric and Oceanic Technology* 24(1), 82-94.
- Sturm P., Leuenberger M., Sirignano C., Neubert R. E. M., Meijer H. A. J., Langenfelds R., Brand W. A., and Tohjima Y. (2004) Permeation of atmospheric gases through polymer o-rings used in flasks for air sampling. *Journal of Geophysical Research-Atmospheres* 109(D4), -.
- Sturm P., Leuenberger M. and Valentino F.L. (2006) On thermal fractionation effects at air intakes. *13th WMO/IAEA Meeting of Experts on Carbon Dioxide*

Concentration and Related Tracers Measurement Techniques, Boulder, Colorado, USA, 19-22 September 2005. WMO-GAW Report 168, ed. S. Toru.

Tohjima Y. (2000) Method for measuring changes in the atmospheric O₂/N₂ ratio by a gas chromatograph equipped with a thermal conductivity detector. *Journal of Geophysical Research-Atmospheres* 105(D11), 14575-14584.

WMO (2003), *Report of the 11th WMO/IAEA Meeting of Experts on Carbon Dioxide Concentration and Related Tracer Measurement Techniques, Tokyo, Japan, 25-28 Sep. 2001, Tech. Rep. 148.* World Meteorological Organisation - Global Atmospheric Watch, Geneva, Switzerland.

Chapter 3.

Evaluation of the measurement system performance after 18 months of operation

3.1	Introduction	89
3.2	Data time coverage and quality	90
3.2.1	Data time coverage	90
3.2.2	Data quality	91
3.3	Measurement stability and precision	92
3.3.1	Precision estimated from target measurements	92
3.3.2	Analysers' stability and drifts	96
3.4	Oxygen fractionation	99
3.4.1	Stability of the high pressure cylinders	99
3.4.2	Comparison between main and control inlet lines	105
3.5	Comparisons between in-situ and flask samples results	110
3.6	Summary and conclusions	115
3.7	References	116

Abstract

One year and a half of operation in field conditions provide sufficient data for a first estimation of the technical performance of the greenhouse gas measurement system installed at the Bialystok tall tower station.

The average measurement precision estimated based on the long term repeatability of the target measurement, the data coverage and the data quality during this time interval are satisfactory. The methods applied to counteract inherent instabilities and drifts of various components of the measurement system proved to be effective. As the measurement system had still been adjusted during this time, even better results are expected in the future regarding the coverage and the quality of the measurement.

Comparisons between the in-situ measurement and the flask samples results are used here as a means to verify the accuracy of the in-situ measurement. With the exception of the CO results, no systematic differences have been found between the two types of measurement.

Following this study, potential measurement problems have been identified. The decrease of the O₂/N₂ ratio inside some of the high pressure gas cylinders and the differences between parallel sampling lines from the same height of the tower are related to oxygen fractionation phenomena. There is a difference of about 10 ppb between the CO mixing ratio measured in-situ and the flask samples results, which can be only partly explained by changes in the flask samples during storage. These constitute objects of study for the future.

3.1 Introduction

The measurement system for atmospheric gases described in Chapter 2 was built and extensively tested at MPI-BGC Jena, before being transported and reinstalled at the final location near Bialystok, Poland. The first evaluation of the technical performance was done while the system was still located in Jena. However, not all the final field conditions could be simulated in Jena. Also new difficulties appeared, related to particular conditions at the Bialystok tall tower site (for example electrical power instability, difficult access on the tower especially at the 300 m level, difficult transport of equipment and high pressure gas cylinders). The distance between the measurement location and the Jena institute made immediate interventions in case of system malfunctioning impossible.

Therefore a realistic assessment of the measurement system performance can only be done after the system has been working for a while in field conditions. A general evaluation is presented in this chapter, using the data from the first 18 months of measurement.

Data

The main Labview software which controls the measurement is meant to calculate the final mixing ratio results, and to perform a first level quality check. At the start of this measurement, not all the necessary program features were implemented yet. A large part of the data had to be recalculated in order to correct or replace faulty calibrations and mistakes in the Labview calculations, or in case of update of the calibration scales.

The calibration scales for all the gases have been updated few times in this 18-month interval, by changing the values assigned to the calibration gases. For CO₂ and O₂/N₂, the data for the air measurement have been recalculated, but not all the auxiliary data (like for example the target measurement). The results of the gas chromatograph measured species (CH₄, CO, N₂O and SF₆) have all been corrected for changes of the calibration scales.

The data have been quality checked based on technical diagnostic parameters recorded together with the concentration data (pressures, temperatures, flows) and on known events registered by users (power failures, technical maintenance, etc). Impossible or improbable values have been flagged as “bad” or “questionable”.

3.2 Data time coverage and quality

3.2.1 Data time coverage

In order to get a quantitative estimate for the time coverage of the gas measurement, the number of the existing measurement points for each day was compared to the maximum possible number of measurements per day (282 for CO₂, O₂/N₂ and meteorological measurements; 96 for CH₄, CO, N₂O and SF₆). The days when the number of measurement points equals at least half of the maximum (at least 141 measurement points for CO₂, O₂/N₂ and meteorological parameters, and at least 48 measurement points for the GC measured species) are marked as “good”. The time coverage is calculated as ratio between the number of “good” days and the total number of days in the interval considered (549 in this case).

Figure 3.1*a* illustrates the time coverage of the gas measurements for the period between 1-Aug-2005 and 1-Feb-2007. Some short data gaps (few days) are unavoidable being due to the maintenance done every two to four months. Though, some longer data gaps can be observed, for example in May for both measurement systems and around January 2006 for the GC species. In the interval 9-May-2006 to 9-Jun-2006 the main computer broke and had to be replaced; in this time no measurement was running. In Dec-2005 an impure ArCH₄ carrier gas cylinder contaminated the gas paths of the ECD detector used for the N₂O and SF₆ measurement. These had to be cleaned and partly rebuilt before the ECD detector could be properly used again in February 2006. Also, in January 2006 the gas chromatograph computer was damaged and had to be replaced.

Some of the technical problems have been caused by local power failures or instability. Also, the Valco valves with microelectric actuator, used in the gas chromatograph system, proved to be a constant source of problems.

The time coverage of the meteorological measurement is presented in figure 3.1*b*. The pressure labeled “p_{ground}” is the atmospheric pressure measured as additional parameter by the oxygen analyser at the ground level. All the other parameters shown are measured by the meteorological measurement system which is described in Chapter 2.

As it can be seen in the figure 3.1, the meteorological measurement stopped in September 2006, except for the atmospheric pressure independently measured by the oxygen analyser. The cause was the malfunctioning of the equipment at 300 m level of the tower. The problem was particularly difficult to handle because the access to the 300

m level is hard and possible only two times per year for several hours. At the moment of writing this thesis, part of the meteorological measurement has been restored.

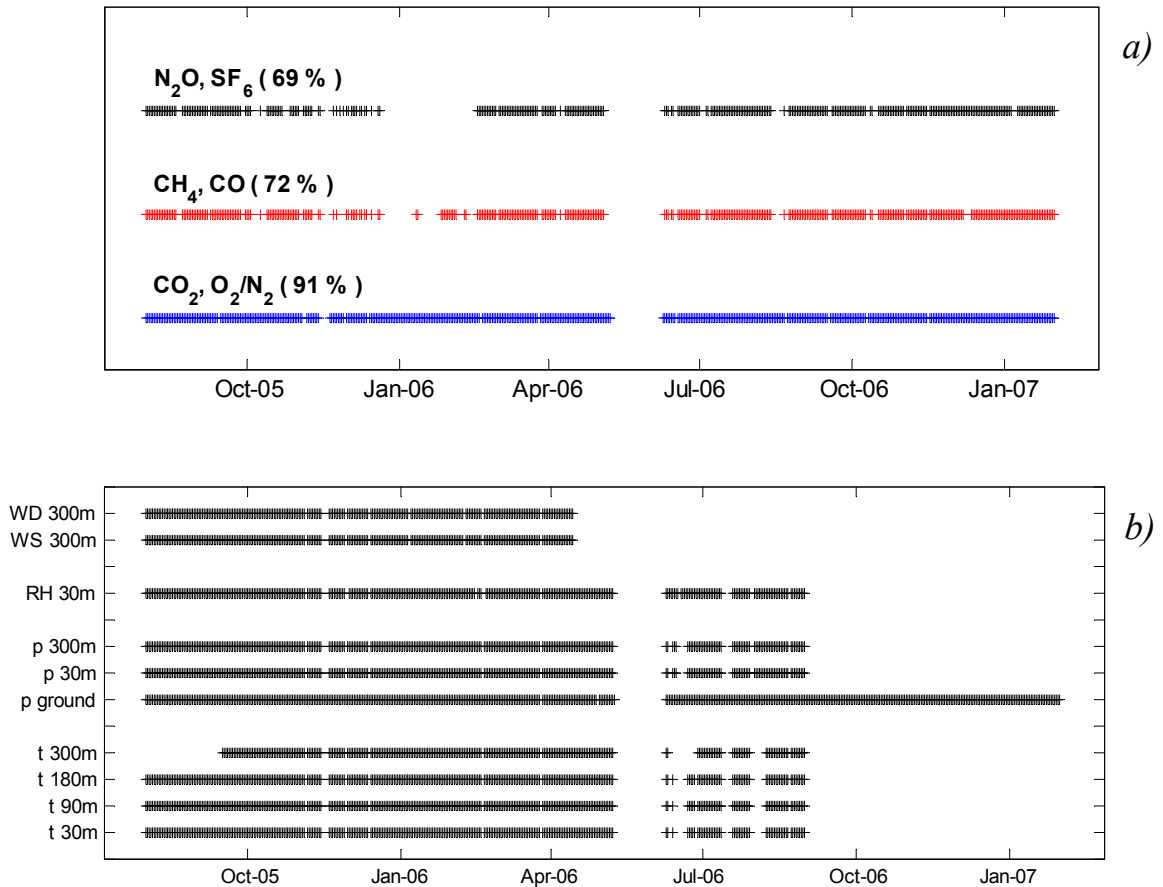


Figure 3.1 a) Time coverage for CO₂ and O₂/N₂ measurement (blue), for CH₄ and CO (red), and for N₂O and SF₆ (black); b) Time coverage of the meteorological measurement. Notations: WD – wind direction; WS – wind speed; RH – relative atmospheric humidity; p – atmospheric pressure; t – atmospheric temperature

3.2.2 Data quality

The number of measurement points considered above shows only the time when the measurement system was functioning without information about the quality of the data. The measurement results for the time interval between July 2005 and 1-Feb-2007 have been quality checked and to each measurement point a “flag” was assigned, which specifies if the datum is “good”, “questionable” or “bad”. Table 3.1 shows the proportion

of good (flag 0), questionable (flag 1) and bad (flag 2) data, as separated by the quality check.

The quality check was primarily based on registered diagnostic parameters of the system (pressures, temperatures, flows etc) and on known events (maintenance, broken parts, power failures). Next the data values have been verified and the impossible or improbable values were marked as “bad” or “questionable”.

The flag 2 (“bad”) corresponds to known technical problems or to impossible data values (for example negative concentration results). The routine and event maintenance time intervals are marked with flag 2, the same as the measurements other than normal routine (various technical tests, measurements of cylinders for inter-comparisons etc). For the GC species, in some time periods, the first measurement after the switch between sampling lines from different heights of the tower had to be discarded because it appeared that the flushing time of the gas paths was not sufficient. This is accounted here as flag 2.

Flag 1 was assigned when any known or suspected technical problem could have affected the data, and to improbable data values. The flag 1 may be changed in the future after a further investigation either to flag 2 or flag 0. The rest of the data received flag 0.

Table 3.1 Proportion of good, questionable and bad data for each gas species

	CO ₂	O ₂ /N ₂	CH ₄	CO	N ₂ O	SF ₆
Total measurements	156466	156466	38939	38939	37283	37283
flag 0 (%)	70.8	70.6	64.7	68.2	64.4	66.5
flag 1 (%)	22.4	22.5	31.2	27.7	30.3	28.1
flag 2 (%)	6.7	6.9	4.1	4.1	5.4	5.4

3.3 Measurement stability and precision

3.3.1 Precision estimated from target measurements

The target measurement (described in Chapter 2) consists in analyzing periodically a constant gas from a high pressure cylinder, with the immediate purpose to signal any measurement problem. An additional use of this measurement is to determine

the medium and long term repeatability, which is a measure of typical measurement precision.

The routine target measurement for the CO₂ and O₂/N₂ analysis system was implemented in Aug-2005. Since then, the target gas was measured once every 3 to 6 hours. The measurement sequence is set up so that the target follows different gases or air sampled from different heights. This is done as a diagnostic, in order to reveal eventual insufficient gas paths flushing time (in such case the target result will be correlated to the result of the previous measurement) and for prevention, to avoid any systematic error in the target measurement by dilution with the previous gas.

As explained before, CO₂ and O₂/N₂ data for the air measurement have been in large part recalculated and additionally corrected for the CO₂ calibration scale updates. The results of the target measurement before Feb-2006 have not been corrected at the moment of writing this thesis. Only some of the data were dismissed following the quality check. Thus these results cannot be fully representative for the precision of the air measurement, since they did not undergo the same processing steps.

Figure 3.2 (*a* and *b*) shows the CO₂ and O₂/N₂ target measurement for the whole measurement period considered in this work. A significant drift can be observed in the CO₂ series, mostly due to adjustments of the calibration scale. The large variations in 2005 for CO₂ and O₂/N₂ are due to errors in the real time calculation (errors which have been corrected in case of the air measurement data). However, even with this problem, the standard deviation of the whole CO₂ data set is 0.11 ppm, close to the project precision goal of 0.1 ppm, and for O₂/N₂ is 6.87 permeg. If the data before Feb-2006 are not taken into account, the standard deviation of CO₂ and O₂/N₂ data become 0.095 ppm and 4.81 permeg respectively.

The target measurement for the gas chromatograph was implemented later, in Nov-2005 and takes place roughly once every 3 hours. The results of the target measurement have been processed in parallel with the air measurement record and suffered similar corrections and calibration scale updates. The target record for the GC measured species (CH₄, CO, N₂O, SF₆) is shown in figure 3.2, c-f.

Table 3.2 summarizes the standard deviations of the target results, which are used as estimate of mean measurement precision for the whole set of data. For CO₂ and O₂/N₂, the standard deviation in table 3.2 was calculated only using the data after Feb-2006. Because the measurement station was set up as part of the Chiotto tall tower network, the

third column in Table 3.2 contains for comparison the precision required within this project. As a note, these values cannot be interpreted as accuracy estimation.

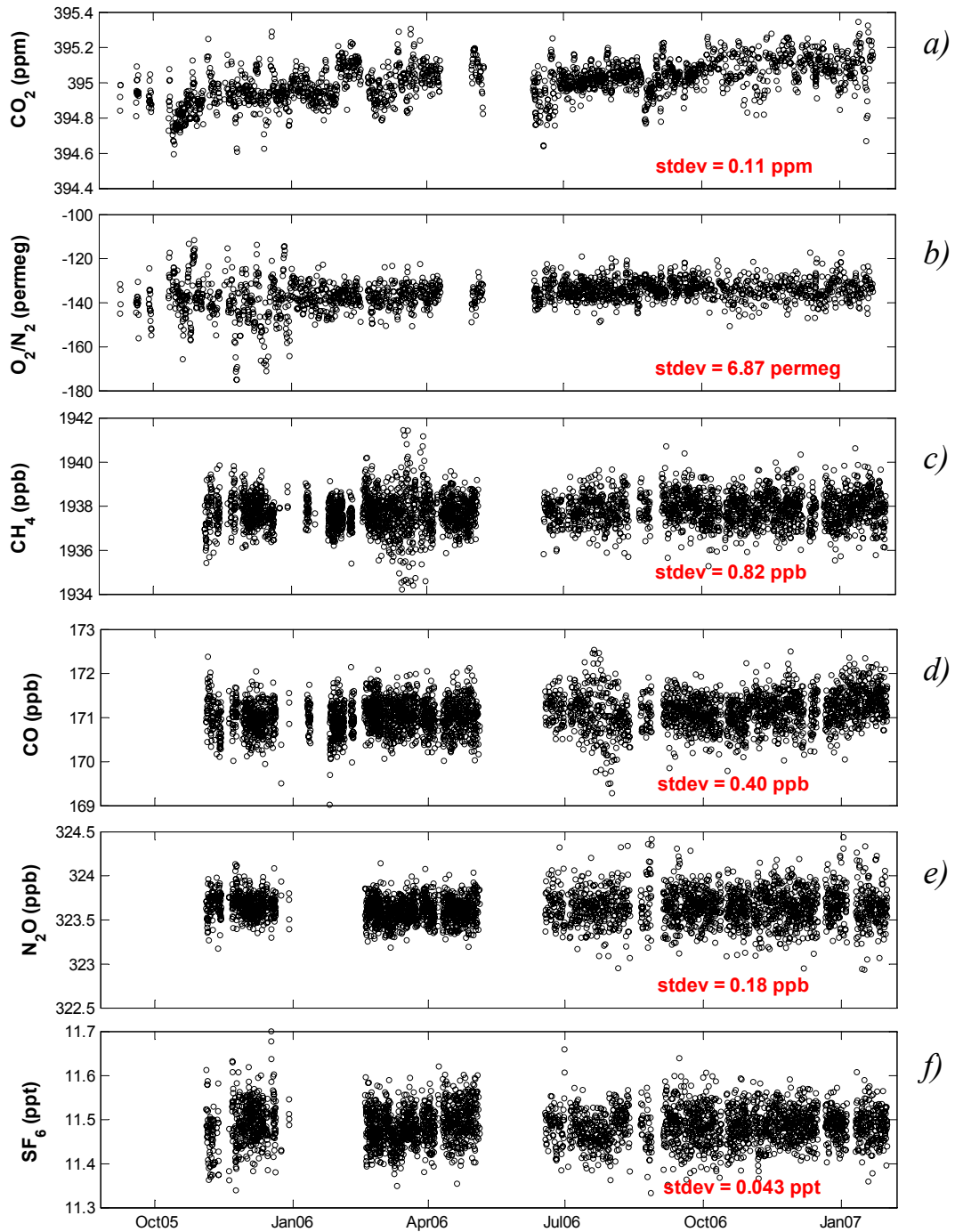


Figure 3.2 Target gas record for the gas species measured at Bialystok

Table 3.2 Typical long term repeatability of Bialystok measurement compared with the CHIOTTO project precision goals.

Species	Specific repeatability (stdev)	CHIOTTO precision goals
CO ₂	0.095 ppm	0.1 ppm
O ₂ /N ₂	4.81 permeg	5 permeg
CH ₄	0.82 ppb	2 ppb
CO	0.40 ppb	1 ppb
N ₂ O	0.18 ppb	0.1 ppb
SF ₆	0.043 ppt	0.1 ppt

Comparison between the measurement noise and the magnitude of the atmospheric signals

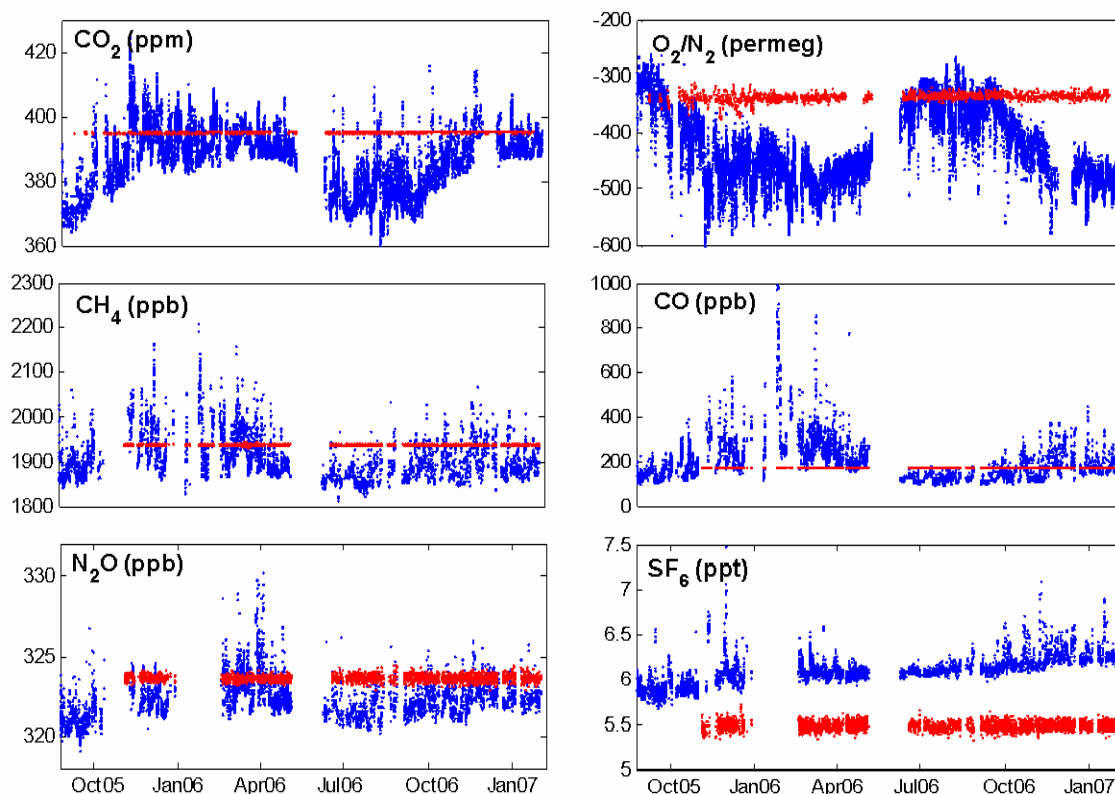


Figure 3.3 Comparison between the atmospheric variability and the noise of the target measurement. In order to use the same y-scale, the values of O₂/N₂ target measurement have been adjusted with -200 permeg and the values of SF₆ target measurement with -6 ppb.

The variability of the target measurement results can be assumed as the “noise” of the measurement. However, a more important aspect than the absolute value of noise itself is its ratio to the signal which has to be measured. Figure 3.3 shows overlapped the measurement of air sampled from 300 m height and the target data. The air from 300 m is used for comparison, because it has the lowest natural variability between all the sampling heights (which means the smallest signal amplitude). In case of CO₂, CH₄ and CO, the target noise is insignificant when compared with the atmospheric signals. For N₂O, the noise is comparable with the atmospheric signal. In the case of SF₆, only few signals can be distinguished that are larger than the measurement noise. This suggest that, although the precision of this SF₆ measurement is very good in its absolute value, it might be still not enough to distinguish eventual small variations in the measured air.

3.3.2 Analysers’ stability and drifts

The CO₂ analyser

Looking again at figure 3.2, a general upwards trend can be observed in the CO₂ target results. This is mainly due to successive calibration scale changes, as the target values have not yet been updated.

Shorter term instabilities are also present, on the order of days or weeks, which usually follow the maintenance of the CO₂ instrument. Immediately after the restart of the measurement, the CO₂ target values are lower than the average and they slowly increase during the following 2 – 4 weeks up to the normal value.

A possible explanation is as follows. Because of the gradual accumulation of impurities in the measurement cells, the LiCor signal always presents a drift downwards. In stable conditions, the maximal drift observed is on the order of 0.15 ppm during the 40 hours between two successive calibrations. The “zero calibration” done at approximately 3 hours intervals reduces this effect to about 0.01 ppm (between two successive zero calibrations).

The instrument maintenance includes cleaning of the internal measurement cells and IR windows. Immediately after maintenance the impurities accumulate in the measurement cells at a higher relative rate which leads to a fast sensitivity decrease of the instrument. In this case, the zero calibration at 3 hours intervals is not sufficiently frequent to compensate for the fast sensitivity decrease.

Figure 3.4 shows the comparison between the stability of the non-calibrated signal (CO_2 mV) and the calibrated result (CO_2 ppm), around the maintenance date (~ 22 -Aug-2006). A fast decrease of the analyser's direct signal (CO_2 mV in red) occurs in the first weeks after maintenance, and this is reflected in the calibrated result. Note that the range of the left y-scale (for CO_2 mV) is 20 times larger than for the right side scale. This means that the calibration routine does compensate for most of the analyser's drift.

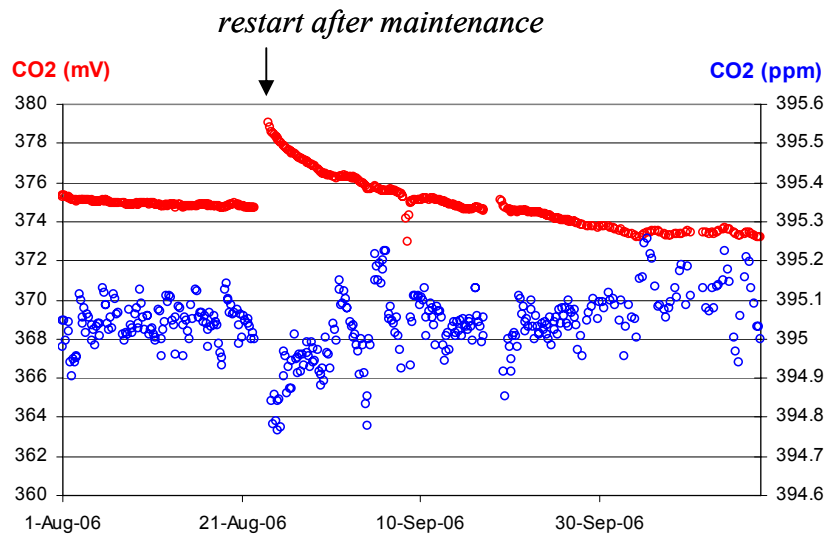


Figure 3.4 Comparison between the evolution of the direct CO_2 analyser response and the calibrated measurement result around the instrument maintenance period.

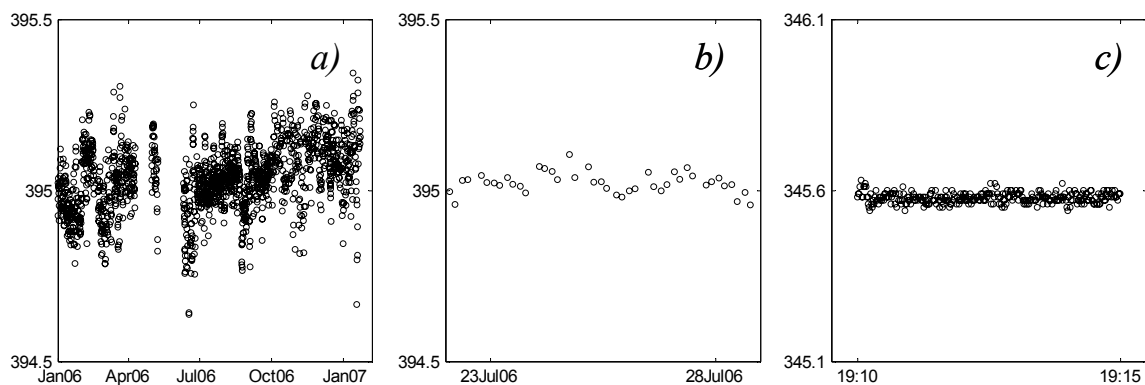


Figure 3.5 Comparison of the CO_2 measurement noise on different time scales: one year (a), one week (b) and five minutes (c)

The level of noise of the CO_2 measurement on different time scales is illustrated for comparison in figure 3.5. The large difference between the noise on short and long

time scales suggest that the measurement precision is below the instrument capability and it can potentially be improved by optimizing the gas handling and the measurement procedures.

The oxygen analyzer

The signal of each measurement cell of the oxygen analyser fluctuates because of intrinsic chemical properties and because of the external influences of temperature and atmospheric pressure. Switching between the two cells every 90 seconds, as described in Chapter 2, cancels out most of the instability. The long term standard deviation of the target measurement is on the same order of magnitude as the noise over few hours or days, and it is mostly caused by the electrical noise of the analyser.

The gas chromatograph (CH₄, CO, N₂O, SF₆)

Both ECD and FID detectors exhibit significant sensitivity variations. For the ECD detector, fluctuations of sensitivity up to 30% have been observed and some of these fluctuations could be explained by variations in carrier gas quality. The sensitivity variations on time scales longer than 20 minutes are counteracted by measuring alternately the sample and the reference gas, thus the measurement results are not affected.

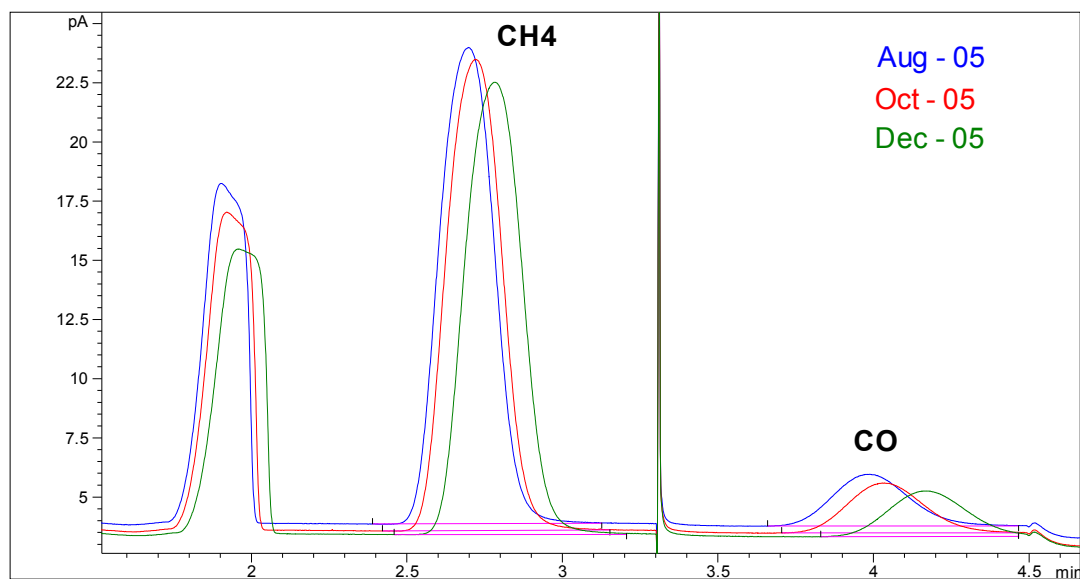


Figure 3.6 Evolution of the chromatogram due to accumulation of impurities inside the gas paths

Because the measurement is running continuously, impurities slowly accumulate inside the filters and the gas paths, causing an increase of the pressure drop and a decrease of the speed of the carrier gases. The result is a slow increase of the retention time and a change of the shape of the measurement signals, as shown in figure 3.6. This can lead to a less stable peak integration and thus to a decrease of the measurement precision, as it happened for CH₄ in the period around March 2006 (see figure 3.2 c, showing the target results for CH₄). The effect has to be corrected periodically by cleaning the filters within the gas paths or by adjusting the measurement method.

3.4 Oxygen fractionation

Oxygen is particularly difficult to measure, partly because of multiple phenomena which can lead to fractionation of oxygen relative to nitrogen and consequently to changes of the composition of the measured gas inside the measurement system. Some of the fractionation mechanisms have been reviewed in Chapter 2 and special gas handling procedures meant to counteract or monitor the effects of fractionation are described in the same chapter. The following paragraphs illustrate two situations where oxygen fractionation has been observed at Bialystok station.

3.4.1 The stability of O₂/N₂ ratio inside the working tanks

As described in Chapter 2, the measurement of CO₂ and O₂/N₂ is differential, i.e. the sample is measured relative to a reference gas. The reference gas originates from a high pressure cylinder referred to in what follows as working tank (WT). The working tanks for the CO₂ and O₂/N₂ measurement are high pressure cylinders (50 L, max. 200 bar) filled with atmospheric air at the MPI-BGC Jena gas facility. The cylinders and regulators are described in detail in Chapter 2, section 2.2.4. With a continuous flow of 100 ml/min, the pressure inside cylinder decreases by about 3 bar/day. One cylinder lasts about eight weeks and is replaced before the pressure decreases below 10 bar.

Since February 2006 the Labview program computes the O₂/N₂ ratio of the working tank after each calibration, using the known values of the four calibration gases. This is done only for verification purpose and the value of the working tank is not used for calculation of measurement results.

Most of the cylinders used so far as working tanks exhibited an obvious decrease of O_2/N_2 , quite uniform along their life time. Figure 3.7 shows as an example the calculated O_2/N_2 ratio of one of the working tanks used at the Bialystok station during July and August 2006. Table 3.3 summarizes the average drifts per day and versus pressure drop of all the cylinders used between February 2006 and February 2007. Some cylinders presented no statistically significant trend (these values are given in parentheses), and there was no cylinder showing O_2/N_2 increase. The cylinder CC173484 is of a different type than all other tanks, with the internal volume of only 29 L. This cylinder showed a faster drift in time, but when scaled with the pressure drop, the result is closer to the results of the other cylinders.

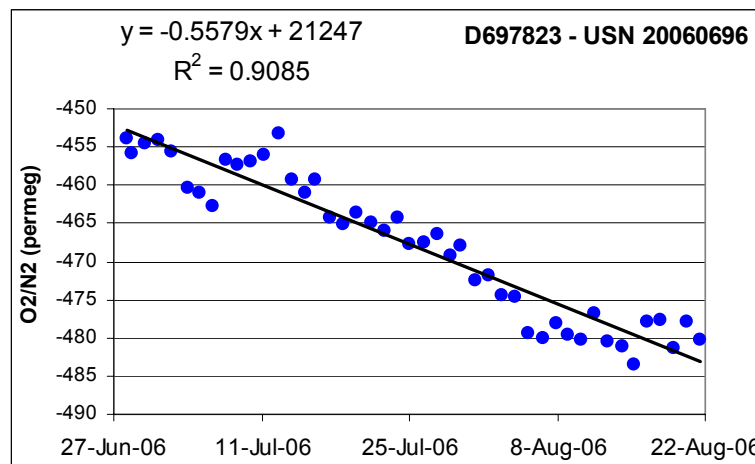


Figure 3.7 Time evolution of the O_2/N_2 ratio calculated for one of the working tanks.

Table 3.3 The O_2/N_2 average drift for each of the working tanks used since Feb-2006. The last column shows the correlation coefficient of the least squares fit. The values in parentheses are not statistically significant. The “USN” is the gas analysis code assigned by the MPI-BGC Gas-Lab, and changes when the cylinder is re-filled and re-analyzed.

Cylinder	USN	Drift/day	Drift / bar	Correlation
D916247	20052086	-0.69	-0.23	0.85
D916246	-	-0.27	-0.09	0.34
CC173484	20060283	-0.99	-0.20	0.59
D697823	20060696	-0.56	-0.19	0.91
D697825	20060697	(-0.19)	(-0.06)	(0.41)
D697830	20060279	(-0.046)	(-0.01)	(0.03)
D916246	20061443	-0.29	-0.10	0.27

A logical next step is to verify the evolution of the cylinders of the same type used for other purposes, for which the O_2/N_2 ratio can be monitored: the ones used for calibration and for the target measurement. One of the cylinders analyzed periodically as target has been totally consumed during this time. The target record for most of the life time of this cylinder is presented in figure 3.8. A step of few permeg between May and June 2006 is due to a small change of the calibration scale. No downwards drift in O_2/N_2 ratio can be observed.

The flow of the target gas is 100 ml/min, similar to the flow of the working gas. The main operation difference between the two cylinders (besides different gas paths) is that the flow out of the working tank is continuous, while the target tank is used for about 20 min every 3-5 hours and in the rest of the time the flow is stopped.

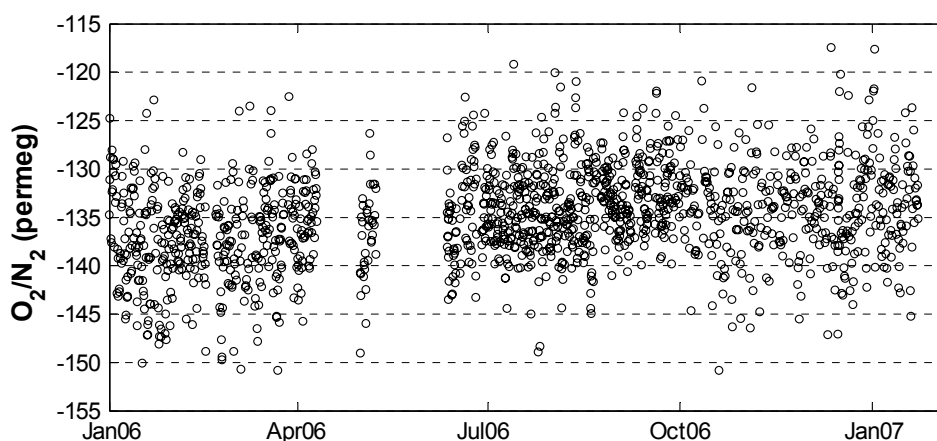


Figure 3.8 O_2/N_2 measurement series of the target cylinder

The drift of the working tanks is observed relative to the calibration gases. At the moment there is no higher level calibration implemented which could signal an eventual drift of the calibration gases themselves. No drifts of the calibration gases relative to each other have been noticed so far.

None of the calibration tanks has been totally consumed during this time. One of the calibration cylinders has been replaced and returned to MPI-BGC after less than one year of use, when the pressure inside decreased by about 50 bar. The cylinder was measured by the MPI-BGC Gas-Lab before and after being used at Bialystok and the results did not reveal a noticeable modification of the O_2/N_2 ratio. A check of the other calibration cylinders will be possible only at the end of their lifetime, when they will be returned to MPI-BGC Jena and re-analyzed by the Gas-Lab.

Discussion and conclusions

Changes of the O_2/N_2 ratio inside high pressure gas cylinders and in glass flasks have already been observed and studied (Keeling et al., 1998, Sturm et al., 2004, Keeling et al. 2004, 2005, 2007). Some of the mechanisms which could possibly produce the observed drifts of the working tanks at Bialystok are discussed in what follows, taking into account the findings of the above mentioned studies.

Oxygen can chemically react inside the cylinder, for example by oxidizing the cylinder walls or impurities. Tests made by Keeling et al. (1998) showed a strong downwards drift of O_2/N_2 in glass flasks unpurified with grease and the drift continued as long as the tests lasted, for almost one year.

Another mechanism is the differential adsorption of oxygen and nitrogen onto the cylinder walls followed by desorption as the pressure inside cylinder decreases (Keeling et al., 1998). If this is the dominant cause of the drifts observed for the working tanks, then the same problem is likely to occur for most of the tanks, including the calibration gases. This mechanism would probably be cylinder specific (because it depends on the roughness of the internal surface), and the amplitude of the decrease will be similar for successive uses of the same cylinder. There is a limited set of cylinders which are filled and used as working tanks at Bialystok. During the period when the O_2/N_2 ratio inside the working tanks was monitored only one of the cylinders was used twice (cylinder D916246 in table 3.3). The drift rate observed for this cylinder was similar for the two use periods, but only one such result is not sufficient to derive a definite conclusion.

A leak of the cylinder can also modify the O_2/N_2 ratio inside the cylinder by preferential escape of the molecules with higher kinetic energy (Knudsen diffusion, see Chapter 2, paragraph 2.2.3). However the existence of a leak would increase the O_2/N_2 ratio inside the cylinder, because the kinetic velocity of O_2 is lower than the one of N_2 . Thus a leak cannot be the reason of the observed decrease of the O_2/N_2 ratio.

Fractionation induced by pressure differences is likely to occur inside the pressure regulator, at the transition between the high pressure side (between 10 and 200 bar) and the low pressure side (typically 1.8 bar abs). As described in Chapter 2, the regulators are separated from the cylinders by a long (1.5 – 2 m) piece of 1/16" Ni tubing. Thus the gradients over the regulator are localized and cannot be transmitted to the cylinder, especially in the case of working tanks where the flow is continuous.

Keeling et al. (2004) observed that the flasks are depleted in oxygen during the measurement, as the pressure decreases, and they also observed a similar effect for high

pressure cylinders. The explanation may be as follows. The pressure decrease leads to adiabatic¹ cooling of the air inside cylinder, while the cylinder walls remain warmer. The mixing of the air at high pressure is slow, thus temperature gradients will appear between the air in the middle of the cylinder (colder) and the air near the cylinder walls (warmer). This thermal gradient induces fractionation of oxygen versus nitrogen, in the sense that the oxygen will tend to accumulate in places with lower temperature, and the air near the cylinder walls will be depleted in oxygen. Thus the air which exits the cylinder can be enriched in oxygen compared to the air which remains inside, and the remaining air will be gradually depleted in oxygen. A simple formula for the thermal diffusion (as used by Keeling et al., 1998) is:

$$\delta O_2/N_2 = -\alpha \Delta T / T;$$

where

$\delta O_2/N_2 - O_2/N_2$ gradient

$\alpha = 0.018$ (Grew & Ibbs, 1952)

ΔT – temperature gradient

T – absolute temperature

A calculation similar to Keeling et al. (1998) shows that a temperature gradient of only 0.2°C is sufficient to induce a difference in O₂/N₂ ratio of about 12 permeg, which is the order of magnitude of the observed changes. The temperature gradient will be larger when the pressure is decreasing faster i.e. for higher flow. This phenomenon is probably at least the partial cause for the observed decrease of the O₂/N₂ ratio inside the working tanks at Bialystok. The temperature gradient is proportional to the speed of the pressure decrease and inversely proportional to the speed of thermal equilibration of the air inside the cylinder. The fact that no change in O₂/N₂ mixing ration has been observed for the target tank could be thus due to the fact that the flow is not continuous and there is sufficient time for temperature equilibration. If this is true, then the calibration gases which are being used even more seldom will not be affected.

It is also possible that thermal gradients exist inside the insulated box where the cylinders are stored. A lower temperature on the side of the cylinder outlets could produce this fractionation effect. Unlike the internal pressure induced temperature gradients discussed above, this externally induced temperature gradient would affect all the cylinders, including the calibration gases, in the same manner.

¹ Adiabatic process is a thermodynamic process in which no heat is transferred to or from the working fluid.

Finally, permeation through the PCTFE sealing of the cylinder is another process which can lead to a decrease of the O_2/N_2 ratio inside the cylinder, because oxygen has a higher permeability than nitrogen through PCTFE (Sturm et al. 2004).

In conclusion, there are multiple possible causes for the observed decrease in O_2/N_2 ratio inside the working tanks: adsorption and desorption onto the cylinder walls, chemical reactions inside the cylinder, thermal fractionation induced either by internal pressure changes or by external temperature gradients, permeation through PCTFE sealing. Depending on which is the real cause, the calibration gases might be affected or not.

The change of the O_2/N_2 ratio inside the cylinders, if the phenomenon only affects the working tanks, does not significantly affect the results and the precision of the air measurements. The average drift of the WT O_2/N_2 ratio for the time interval between two successive calibrations was between -0.45 and -1.15 permeg (for different cylinders), which is small compared to the typical precision of the measurement (~ 5 permeg). Also, no drift of the target measurement results between two calibrations could be observed.

If the cause of the observed variations is thermal fractionation due to pressure decrease inside the cylinder, this is likely to have a negligible effect on the calibration gases. However, if the cause is another phenomenon and calibration gases will suffer the same effect, then the calibration scale will significantly drift over few years. For this reason it is important that the phenomenon is monitored.

The gas cylinders will be re-analyzed by the MPI-BGC Gas-Lab before and after being used at Bialystok. The thermal fractionation hypothesis will be supported if Ar/N_2 will show a drift in the same direction and about 2.5 times larger, as expected based on previous studies (Keeling et al., 2004). Laboratory tests at MPI-BGC Jena are planned in order to understand the causes and to try to quantify and reduce the effect. At Bialystok station, long term archive calibration will be soon implemented (the archive calibration cylinders will have a life time longer than 10 years) with the main purpose to monitor eventual drifts of the calibration gases. Also inter-comparisons between the MPI-BGC Jena Gas-Lab and Bialystok station (e.g. comparisons between in situ measurements and flask samples) will help to discover an eventual calibration scale difference.

3.4.2 Comparison between the main and the control sampling lines

As described in Chapter 2, two air sampling lines have been installed at each of the 30 m and 300 m tower levels. The two sampling lines from each height have different configurations, as shown in figure 3.9.

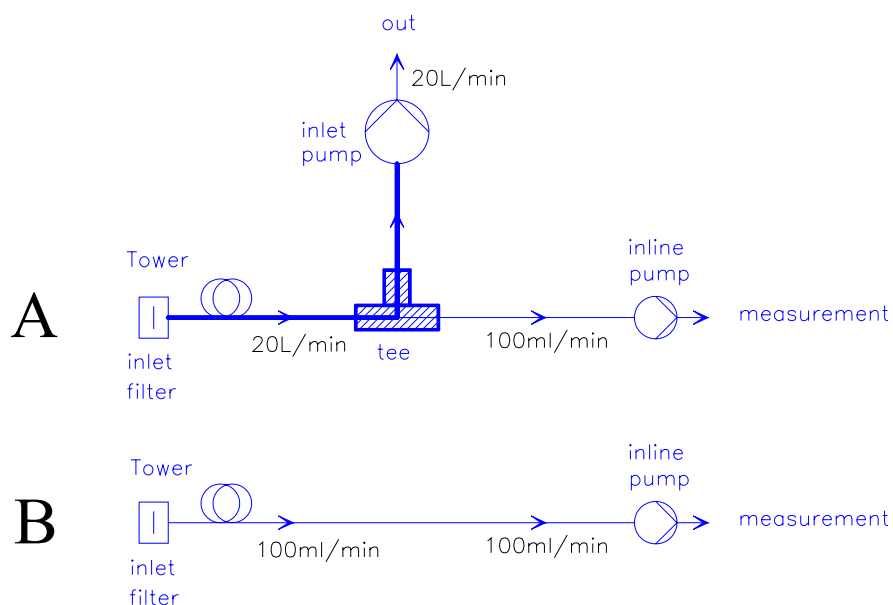


Figure 3.9 The two types of air sampling lines used for CO_2 and O_2/N_2 measurement. “A” is the main sampling line and “B” is the control sampling line (see text).

The lines of type A are the main sampling lines, similar to the ones installed at 90 and 180 m heights of the tower. The lines of type B are the ones additionally installed for verification purpose and referred to in what follows as “control” lines.

One of the main reasons of this design is to have a possibility to detect eventual oxygen fractionation. Some of the phenomena which can lead to fractionation of oxygen relative to nitrogen have been reviewed in Chapter 2, section 2.2.3. Different fractionation mechanisms can affect the two types of sampling lines. The lines of type A contain tee-junctions, in which oxygen can fractionate due to pressure / flow and temperature gradients. Another sensitive place is the air inlet, where thermally induced fractionation can potentially occur. The two types of lines have similar inlet designs (see figure 2.7 in Chapter 2), but the inlet air flow is greatly different: 20 L/min for the type A and 100 ml/min for the type B. The inlet fractionation is known as strongly depending on flow and

is expected to be negligible at a flow of 20 L/min, but significant at the flow of 100 ml/min corresponding to the line type B (Sturm et al., 2006).

In this setup, an eventual fractionation inside the tee junction is expected to be approximately constant on time scales of days or weeks, because the pressure and temperature gradients are stationary in time. However longer-term variations of the room temperature or changes in the system settings can lead to small variations in the tee-junction fractionation. On the other hand, the inlet fractionation is expected to be dependent on the outside temperature, which means periodical variations with the season and with the time of day.

Figure 3.10 shows an example of O₂/N₂, CO₂ and APO results for the air sampled at 300 m height through the two parallel sampling lines, for two selected time intervals in winter (a) and summer (b). APO (Atmospheric Potential Oxygen) is a tracer defined as:

$$APO(\text{permeg}) = O_2 / N_2(\text{permeg}) + 1.1 \times 4.8 \times (CO_2(\text{ppm}) - 350)$$

where: 4.8 is the conversion factor for the CO₂ units (from ppm to permeg)

-1.1 is the assumed average ratio for the land biosphere – atmosphere exchange

The relation above is a simplified version of the definition introduced by Stephens et al. (1998). APO is by definition invariant to the exchange between land biosphere and atmosphere, assuming that this exchange respects the proportion of -1.1 between oxygen and CO₂. Therefore its natural variability is much smaller than the one of O₂/N₂, which makes it a better tool of comparison between sampling lines.

It can be observed that the O₂/N₂ and APO values are different for the two types of sampling lines, while there is no noticeable shift in the CO₂ results. The two selected 5-weeks intervals from winter (plots *a* in figure 3.10) and summer (plots *b*) show differences between the A and B sampling lines in opposite directions.

To check the time variation of the difference between the sampling lines A and B, the measurement time series corresponding to the main sampling lines has been interpolated at the measurement time of the control sampling lines. The difference is calculated between the interpolated values of the main line and the measured values of the control line (figure 3.11). No significant difference between the main and the control lines is found for the CO₂ results. The differences of O₂/N₂ and the APO appear to be dependent on the time of year, with negative values during the cold seasons and positive values in summer of 2006. Though the beginning of the data series (summer 2005) does not show a similar positive difference.

A similar calculation for the 30 m sampling height (figure 3.12, shown only the APO) does not have the same time variations. The difference between the main and the control sampling lines from the 30 m height is almost constant, except for the period around March 2006 when technical problems are suspected.

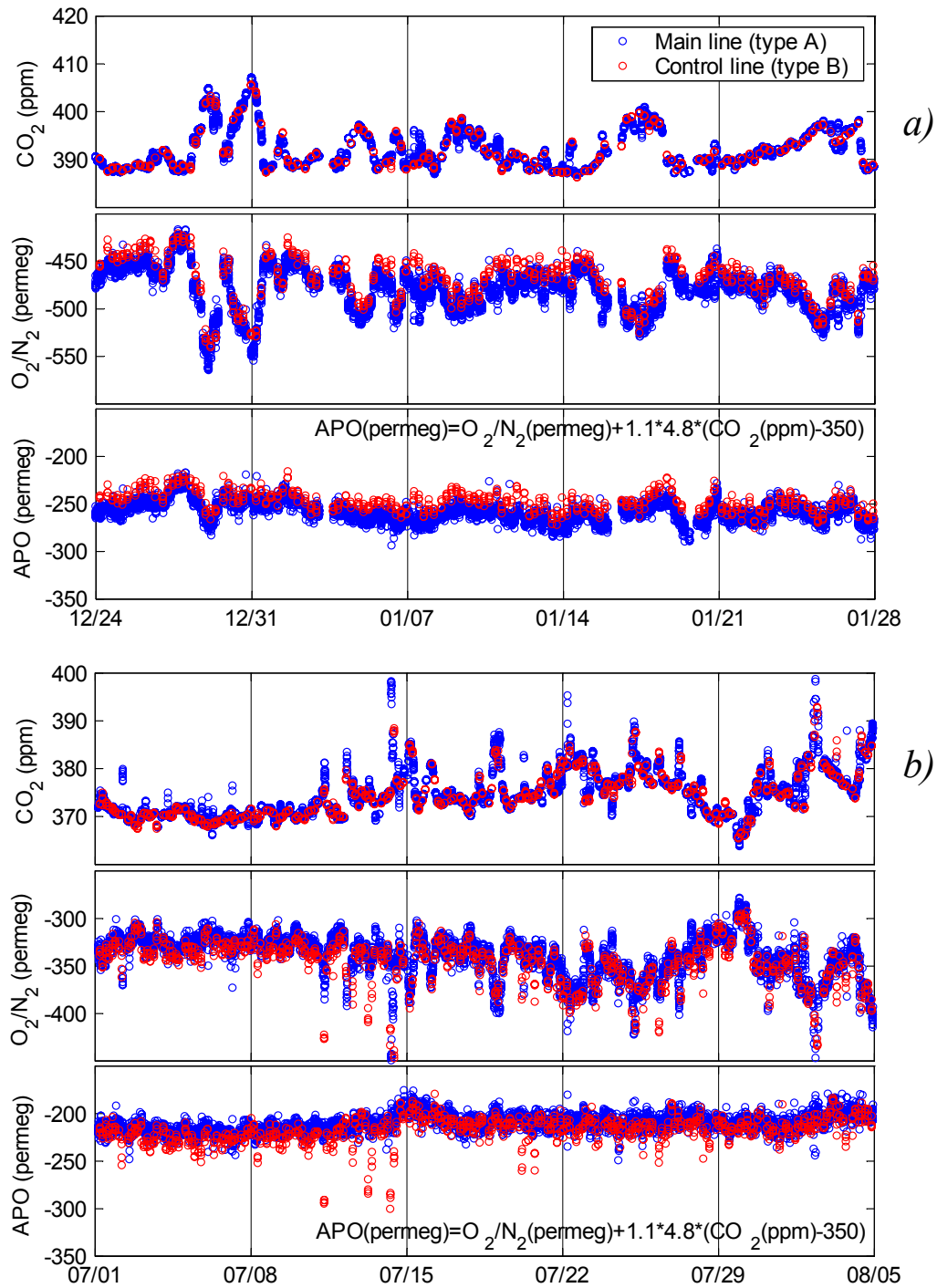


Figure 3.10 CO₂, O₂/N₂ and APO at 300 m agl: comparison between the main (blue) and control (red) sampling lines, for winter (plots a) and summer (plots b)

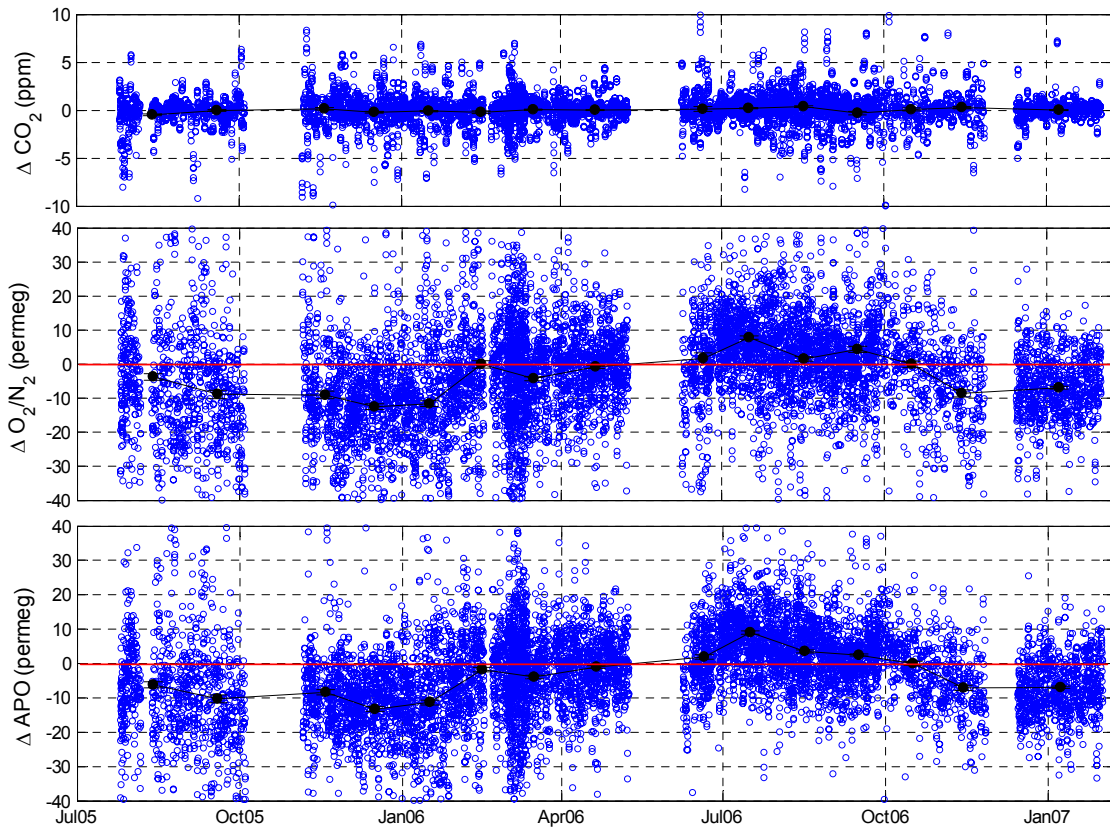


Figure 3.11 The CO_2 , O_2/N_2 and APO differences between air sampled through the main (interpolated values) and control (measured values) lines from 300 m height. The black dots are the averages for time intervals of approximate one month; the error bars represent the standard error of the mean (mostly too small to be seen). The red lines mark the zero level.

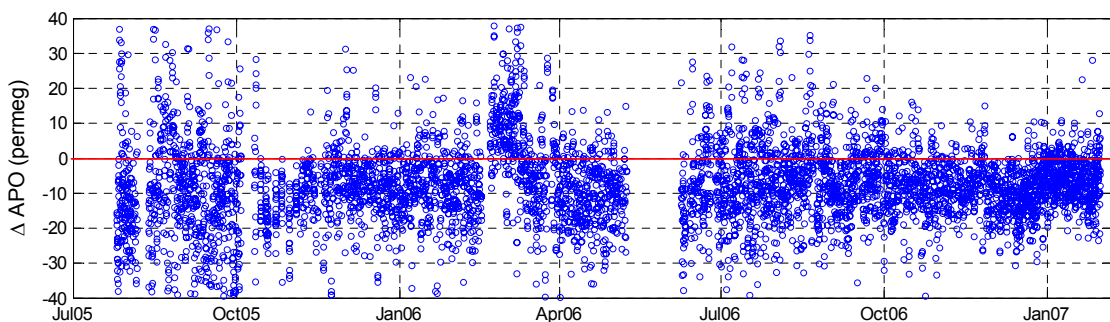


Figure 3.12 The APO difference between air sampled through the main (interpolated values) and control (measured values) lines from 30 m height.

As explained before, the thermal fractionation at inlets is expected to be correlated with the atmospheric temperature, and thus with the time of day of sampling. This effect is expected to be enhanced during summer. The relation of the difference between A and B sampling lines with the time of day and with the atmospheric temperature has been tested for the 30 m and 300 m sampling levels, separately for winter and summer. No

significant dependence could be observed, for any of the sampling lines and for any season. Also, no correlation of the sampling lines difference with any of the system parameters could be observed so far. In conclusion, the results so far suggest that the thermal fractionation at inlets is not a dominant cause, but the cause of these differences could not be determined yet.

On short term (days to weeks), the difference between the two types of sampling lines is constant. This means, the effect is a shift of the signal but the amplitude is not affected. Thus the interpretation of the short term signals is not affected.

For the 300 m height, where the sampling lines difference appears to exhibit a dependence on season, the phenomenon can induce an error on the observed seasonal variation of oxygen. Supposing that the error for the 300 m sampling line A is 20 permeg (\sim the range of the difference between the A and B sampling lines, see figure 3) and the measured seasonal cycle of O_2/N_2 is on the order of 200 permeg, then the amplitude of the seasonal cycle calculated using the main sampling line would appear to be about 10% larger than the real one. The relative effect on the seasonal cycle of APO could be even larger. As it will be shown later Chapter 4 (paragraph 4.5.3), the amplitude of the APO seasonal cycle at 300 m is estimated to be 52 permeg. Assuming like before that the error is 20 permeg, than the real amplitude of the APO seasonal cycle would be only 32 permeg, with about 40% smaller than estimated in Chapter 4.

Comparisons between flasks and the in-situ measurement from the 300 m main line do not show any systematic shift. This comparison is shown in detail in the following section 3.5. The inlet line for the flask sampling system is similar with the main inlet line for the continuous measurement (both are of type A), but the flow used for the flask sampling is between 2 and 4 L/min. Thus an eventual fractionation inside the tee-junction is unlikely to have the same amplitude for the two systems. Also, the Ar/ N_2 values which are measured in flask samples did not suggest so far any fractionation (see explanation in paragraph 3.5). Based on this result, the differences between the main and the control sampling lines are assumed to be due to fractionation phenomena affecting the control lines, and not the main sampling lines. In the rest of this work, the O_2/N_2 results from only the main sampling lines will be used.

This problem needs further investigation. Detailed tests are planned for the summer of 2007. For comparison, flask samples will be filled directly at 30 m height on the tower, with an independent flask sampling apparatus, simultaneous with the in-situ measurement from the main and the control sampling lines.

3.5 Comparison between the in-situ measurement and flask samples results

The comparison of quasi-continuous in-situ measurements with flask samples filled at the same location and analyzed by an independent laboratory is a valuable tool to assess the accuracy of the in-situ measurement. Such a comparison can reveal systematic errors, calibration scale differences or any time period of improper functioning of the in-situ measurement.

The flask samples are analyzed in the MPI-BGC Gas-Lab for CO₂, CH₄, CO, N₂O, SF₆, O₂/N₂, Ar/N₂, ¹³C in CO₂ and ¹⁸O in CO₂. The description of the MPI-BGC Gas-Lab measurement procedures can be found in Jordan & Brand (2003) and Werner et al. (2001).

Flask sampling procedure

The flask sampling is done with an automatic sampling system, as described in Chapter 2. There are two dedicated sampling lines from 300 m and 30 m above ground level. The regular sampling takes place once per week from the 300 m height, at 15:00 local time (which means 13:00 or 14:00 GMT, in summer respective winter). Samples from the 30 m height are filled more seldom, mostly for specific purposes (direct comparisons with the in-situ measurement from the same height or with the flasks samples from 300 m height).

The flasks are installed in the sampling system (during the technician visit) and left with the valves open. The sampling takes place unassisted, at the established date and time. The technician closes the sample valves and uninstalls the filled flasks during a future visit. That means the flasks remain open in the flask sampler between the moment when they are installed in the flasks sampler and the moment when they are uninstalled (the common storage time within the sampler is up to two months). The storage time between the time of filling and the time when flasks are measured varies between one and four months.

The air inlet lines from the tower are continuously flushed. The sampling starts with a sampler “line flushing” step of three minutes at a flow of 4 L/min and pressure of 1.8 bar abs. The flask is then flushed for 10 minutes (flow 2 L/min, pressure 1.6 – 1.8 bar abs), after which the flow is stopped and the flask is left under pressure.

The regular flask sampling is not synchronized with the continuous measurement. This means that when the flask sampling is being done (at fixed time, from 300 m height)

the continuous system can measure air from any height, or any calibration gas. In this case a direct quantitative comparison of individual results is not always possible. For a sufficient number of flasks, however, it would be possible to observe systematic differences or drifts in time. Few supplementary flask samples have been taken at different times of the day, simultaneously with the continuous measurement from the same height, especially for direct comparison of the results. Also some flasks have been filled simultaneously with flight measurements near the tower, for comparison.

Both the in-situ measurement results and the flask samples results have been quality checked and only the results considered good are used for comparison.

The results of the Ar/N₂ measurements are used in this work only as diagnostics. The Ar/N₂ ratio is strongly modified in leaking flasks, due to the fractionation phenomenon of Ar with respect to N₂, which occur when the Ar and N₂ are leaving the flask through a small orifice. Thus the Ar/N₂ ratio measured in air from the flasks is used as indicator for leaking flasks. The results of the flasks which presented abnormal values of Ar/N₂ have been discarded.

Results and discussion

Figure 3.13 shows the difference between results of the in-situ measurement and flask sample analyses, for each of the species measured. The corresponding value for the in-situ measurement was calculated by piecewise interpolation (piecewise cubic hermite interpolating polynomial, Matlab function *pchip*; Fritsch & Carlson, 1980). For this comparison only those flasks were selected for which the continuous measurement was at maximum 3 hours difference in time.

For each species, the plot *a* in figure 3.13 shows the time series of the difference described above and the plot *b* shows the same difference against the species concentration measured in flask. The plots show some expected scattering, partly due to the time difference between the in-situ measurement and the flask filling “moment”. As already explained, because of this time difference, the individual differences cannot be used as quantitative estimation. What is important to find out from this comparison is (1) if there is any time evolution of the difference (plots *a*), (2) if there is any systematic shift between the in-situ and flasks results (plots *a, b*) and (3) if the difference depends on concentration (plots *b*).

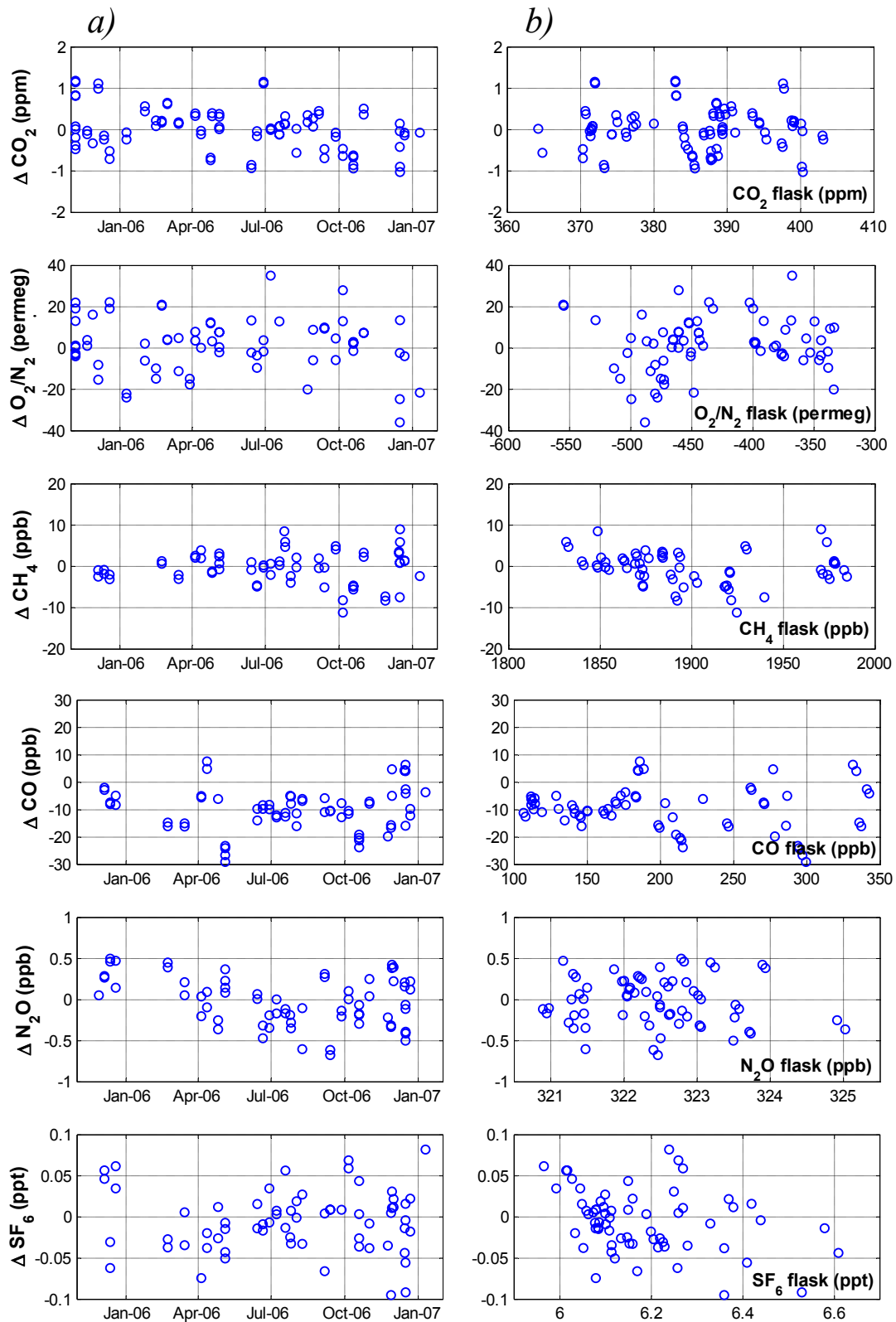


Figure 3.13 Difference between the interpolated value of the in-situ measurement results and the measured flask value. a) (left) time series; b) (right) versus flask concentration

For each species, a t-test was performed to check if the average difference is significantly different from zero. The results of the t-tests are listed in table 3.4. The null hypothesis of the t-test is that the average difference is equal to zero. The t-test takes into account the average of the data set, the number of data points and the variance of the data. If the t-test result is zero (column 5 in table 3.4), it means that the null hypothesis cannot be rejected. In other words, the average difference is not significantly different from zero. The p-value (or significance) shows the probability that the observed value of the difference could be as large or larger by chance under the null hypothesis. The last two columns in table 3.4 are the low and the high limits of the confidence intervals of the mean difference, for a confidence level of 95%.

Table 3.4 Results of the t-tests for the differences between in-situ measurement and the flask samples results

Species	No. flasks	Mean difference in-situ - flask	Stdev difference in-situ - flask	t-test result	p-value	CI_low	CI_high
CO ₂	85	0.004	0.518	0	0.94	-0.108	0.116
O ₂ /N ₂	68	1.392	13.344	0	0.39	-1.838	4.621
CH ₄	63	-0.484	4.012	0	0.34	-1.494	0.527
CO	66	-9.799	7.896	1	6.42E-15	-11.740	-7.858
N ₂ O	67	-0.011	0.324	0	0.79	-0.090	0.068
SF ₆	67	-0.007	0.039	0	0.14	-0.017	0.002

The mean difference between the in-situ and flasks measurements of CO of about 10 ppb is highly significant (note the p-value of 6.42E-15). There is no obvious dependence on concentration (figure 3.13 b).

An increase of the CO mixing ratio in stored flasks has been previously observed. Tests made at MPI-BGC Gas-Lab using similar flasks filled at 2 bar resulted in an average CO increase of 0.047 ± 0.022 ppb/day (A. Jordan, personal communication). The flasks sampled at Bialystok are filled at 1.6 bar and stored on average 73 ± 27 days, between the time of filling and the time of measurement. This would explain a mean difference between the in-situ and flasks results of about 4.2 ppb. Taking this into account there still remains a difference of about 6 ppb to be explained.

A possible reason may be a calibration offset. High pressure cylinders have been measured at Bialystok station for inter-comparison with MPI Gas-Lab and the mean difference between the BIK and the MPI results was -1.31 ± 1.13 ppb. This shows that there is indeed a calibration scale difference, but too small to explain the difference between the in-situ and the flask samples results.

Another possible reason for the observed difference is a contamination source in the flask sampler, where the samples are stored with open valves before and after filling, for a significant period of time.

Looking at the time dependence in figure 3.13a, the CO difference seems more variable during cold seasons and quite constantly centered around -10 ppb during warm seasons. The difference also is more scattered for the higher CO values. An explanation for this is that both the absolute values and the short term variability of CO are higher in the cold seasons, which leads to higher variance of the difference between the two non-synchronous measurements.

For all the other species, the mean difference between the in-situ and flasks measurements is not statistically significant. Also, the absolute value of the differences is on the same order (CH₄) or much smaller than the assigned precision of the in-situ measurement (table 3.2 in paragraph 3.3.1).

Looking at the dispersion of the individual difference results, the N₂O and the SF₆ show the best agreement between the in-situ and the flasks results, better than the precision of the in-situ measurement. This reflects the much lower natural short term variability of the atmospheric concentration of these two species, which means small concentration variations between the flask sampling time and the closest in-situ measurement.

No significant dependence on concentration was found for any of the species.

Conclusions

The results of CO₂, O₂/N₂, CH₄, N₂O and SF₆ comparisons between the in-situ measurement and the flask samples results are satisfactory for the existing data. A synchronized sampling seems however necessary in order to make the direct comparison more meaningful.

CO shows a shift of about 10 ppb between the in-situ and flasks results, independent from concentration. Part of this shift can be explained by an increase of CO

mixing ratio inside the flasks during the flasks storage time and by a calibration scale offset. There is still a difference of about 5 ppb to be explained.

No corrections on the CO measurement results have been done at the moment.

3.6 Summary and conclusions

The data coverage for the first 18 months of measurement is satisfactory, taking into account that during this time the system had still to be adjusted to work in field conditions. A better coverage is expected in the future, as the initial problems have been solved.

The precision estimated from the long term repeatability of the target measurements reaches the project goals, except of the N₂O. Besides the instrumental capability, a careful post-processing of the data is necessary for achieving this level of precision.

This study attested the quality of the measurement performed at Bialystok during the first year and a half of operation, but it also identified some problems which have to be dealt with in the future.

The O₂/N₂ ratio inside some of the cylinders used changed in time due to a yet unclear cause, related to oxygen fractionation. This does not constitute a problem if it only influences the working tanks, but it becomes a serious problem if the calibration gases are affected. Thus the causes of the observed drifts must be studied. This problem shows the importance of introducing the archive calibration for long term monitoring of the gases used for routine calibration.

Differences between the sampling lines of different types, coming from the same height of the tower, are another effect of oxygen fractionation. At the moment the underlying mechanism is not clear, therefore the phenomenon must be further monitored and studied.

The comparisons between the in-situ measurement and the results of flask samples analyzed by the MPI-BGC laboratory are used to monitor the accuracy of the in-situ measurement. No significant differences have been detected so far between the flasks and the in-situ measurements of CO₂, CH₄, O₂/N₂, N₂O and SF₆. In the case of CO, this comparison revealed a systematic difference of about 10 ppb, which can be partly explained by changes of the air composition inside the flasks during storage. Comparisons of high pressure cylinder measurements lead to a much closer agreement

between the Bialystok site and the MPI-BGC GasLab. Additional tests are necessary in order to understand the cause and to decide if data correction is appropriate.

3.7 References

- Fritsch F. N. and Carlson R. E. (1980) Monotone piecewise cubic interpolation. *Siam Journal on Numerical Analysis* 17(2), 238-246.
- Grew K. E. and Ibbs T. L. (1952) *Thermal Diffusion in Gases*. Cambridge Univ. Press, New York. 143 p.
- Jordan A. and Brand W. A. (2003) Technical Report: MPI-BGC, Germany, Proceedings of the 11th IAEA/WMO meeting of CO₂ experts, Tokyo, Sept. 2001. *WMO-GAW Report 148*, ed. S. Toru, 149-153.
- Keeling R. F., Manning A. C., McEvoy E. M., and Shertz S. R. (1998) Methods for measuring changes in atmospheric O₂ concentration and their application in southern hemisphere air. *Journal of Geophysical Research-Atmospheres* 103(D3), 3381-3397.
- Keeling R. F., Blaine T., Paplawsky B., Katz L., Atwood C., and Brockwell T. (2004) Measurement of changes in atmospheric Ar/N₂ ratio using a rapid-switching, single-capillary mass spectrometer system. *Tellus Series B-Chemical and Physical Meteorology* 56(4), 322-338.
- Keeling R. F., Manning A. C., Paplawsky W. J., and Cox A. C. (2005) On the long-term stability of O₂/N₂ reference gases, 12th WMO/IAEA Meeting of Expert on Carbon Dioxide Concentration and Related Tracers Measurements Techniques (Toronto, Canada, 15-18 September 2003). *WMO-GAW Report 161*, ed. S. Toru, 131-140.
- Keeling R. F., Manning A. C., Paplawsky W. J., and Cox A. C. (2007) On the long-term stability of reference gases for atmospheric O₂/N₂ and CO₂ measurements. *Tellus Series B-Chemical and Physical Meteorology* 59(1), 3-14.
- Stephens B. B., Keeling R. F., Heimann M., Six K. D., Murnane R., and Caldeira K. (1998) Testing global ocean carbon cycle models using measurements of atmospheric O₂ and CO₂ concentration. *Global Biogeochemical Cycles* 12(2), 213-230.
- Sturm P., Leuenberger M., Sirignano C., Neubert R. E. M., Meijer H. A. J., Langenfelds R., Brand W. A., and Tohjima Y. (2004) Permeation of atmospheric gases through polymer O-rings used in flasks for air sampling. *Journal of Geophysical Research-Atmospheres* 109(D4), -.
- Sturm P., Leuenberger M. and Valentino F.L. (2006) On thermal fractionation effects at air intakes, 13th WMO/IAEA Meeting of Experts on Carbon Dioxide Concentration and Related Tracers Measurement Techniques, Boulder, Colorado, USA, 19-22 September 2005. *WMO-GAW Report 168*, ed. S. Toru.
- Werner R. A., Rothe M. and Brand W. A. (2001) Extraction of CO₂ from air samples for isotopic analysis and limits to ultra high precision $\delta^{18}\text{O}$ determination in CO₂ gas. *Rapid Comm. Mass Spectrom.* 15, 2152-2167.

Chapter 4.

Overview of the atmospheric data from Bialystok tall tower station

4.1	Introduction	119
4.2	General presentation of the data series	120
4.3	Vertical gradients of the mixing ratios	127
4.4	Diurnal variations of atmospheric mixing ratios	131
4.4.1	Diurnal variations of CO ₂ and O ₂ /N ₂	131
4.4.2	Diurnal variations of CH ₄ , CO, N ₂ O and SF ₆	133
4.5	Seasonal variations of atmospheric mixing ratios	136
4.5.1	Data and data processing	136
4.5.2	Seasonal variation of CO ₂ mole fraction	138
4.5.3	Seasonal variation of O ₂ /N ₂ ratio	141
4.5.4	Seasonal variations of CH ₄ , CO, N ₂ O and SF ₆	146
4.6	Summary and conclusions	149
4.7	References	151

Abstract

I present the record of CO₂, CH₄, CO, N₂O and SF₆ mole fractions, and O₂/N₂ ratios from the first 18 months of in-situ measurements at the tall tower station near Bialystok, in eastern Poland. The data generally present large short term variability due to the intracontinental location of the site, in the proximity of strong sources and sinks. SF₆ is an exception to this, showing strong signals only when the air masses had previously passed through a certain region in Western Europe.

Air sampled from five heights on the tower, between 5 and 300 m, is measured alternately. The observed vertical gradients are highly variable in time. Characteristic for the warm season is the daily periodicity of the vertical gradients. Strong gradients develop during night, with an increase of the mixing ratios near the ground. By day the vertical gradients are diminished due to the strong vertical mixing. CO₂ shows reverse vertical gradients in the afternoon, with lower mole fraction near the ground, due to uptake by the land biosphere. During the cold season, the daily variation of the vertical gradients is replaced by irregular variations. In contrast to the other gas species, SF₆ does not show significant vertical gradients, an observation suggesting that it has no important local sources.

The data show also strong seasonal variations. The seasonality of the atmospheric circulation overlaps with the seasonal variations of sources and sinks. The seasonal cycle of CO₂, mainly due to land biosphere photosynthesis and respiration, is larger at Bialystok than at marine sites, and shifted in time. The O₂/N₂ seasonal cycle includes both land biosphere and oceanic influences. The proportion of the oceanic component at Bialystok is on the order of 20 – 30%, depending on the sampling height. CH₄, CO and N₂O exhibit seasonal cycles with maxima during the cold season and minima during the warm season. The dissimilarities between species are due to spatial and temporal differences in sources and sinks. Comparisons with other continental and marine sampling sites situated at almost the same latitude help to constrain longitudinal partitioning of sources and sinks by atmospheric models.

4.1 Introduction

Results of continuous measurements from several northern mid-latitudes tall tower stations have been described in the literature (e.g. Bakwin et al., 1995, 1998, 2004, Hurst et al., 1997, Haszpra, 1995, Stephens et al., 2007). The data show typically high variability on time scales from hours to weeks, due to the proximity of the strongly localized continental fluxes. Tall tower CO₂ data show strong diurnal cycles and seasonal variations stronger than at marine or mountain stations situated at the same latitudes (e.g. Bakwin et al., 1995), due to the influence of the regional land biosphere.

There are, however, differences between the general variability patterns at tall tower stations from different locations. The amplitude of the CO₂ seasonal cycles is determined by the activity of the land biosphere and thus varies with latitude. The short term variations are influenced by the upstream surface emissions and by the atmospheric transport, and thus by the regional particularities of these.

The tall tower data have been used to infer regional carbon fluxes and anthropogenic emissions of trace gases, to study the boundary layer dynamics and advective transport over the continents. The continental data are particularly useful for modeling studies to resolve the spatial and temporal evolution of the strong continental sources and sinks and to quantify the sources and sinks at regional and country scale.

The Bialystok tall tower measurement station is located in eastern Poland, on the north-eastern margin of the densely populated Western and Central Europe, close to sources and sinks which are highly variable in time and unevenly spatially distributed. Mole fractions of CO₂, CH₄, CO, N₂O and SF₆, and the O₂/N₂ ratio are measured quasi-continuously in air sampled from five heights of the tower, between 5 and 300 m. The O₂/N₂ data available at Bialystok station constitute an addition to most of the results discussed in the literature, with the potential to provide useful constraints on the longitudinal atmospheric transport over the continent.

I present the first 18 months record from the in-situ measurement at the Bialystok tall tower station. The length of data series is insufficient to determine long term trends of the atmospheric mixing ratios. The intention of this chapter is to study some of the shorter term variability patterns, specifically the vertical gradients and the periodical variations on diurnal and seasonal time scales.

4.2 General presentation of the data series

The overall features of the data series for each species are briefly introduced in what follows. Detailed discussions about particular characteristics, like vertical gradients, and variations on different time scales, are the subject of the rest of this chapter.

CO₂ and O₂/N₂ records

The CO₂ and O₂/N₂ records (figure 4.1) show anti-correlated seasonal cycles and superimposed short term (diurnal and synoptic scale) variations. The variability patterns differ with the season and with the sampling height. During the warm season, the diurnal cycles with amplitude of a few tens of ppm clearly dominate the variability at the sampling levels close to the ground (figure 4.1b). The diurnal variation is due to both the diurnal periodicity of atmospheric vertical mixing and the photosynthesis / respiration cycle. The amplitude of the diurnal signal decreases with the sampling height, such that at 300 m above ground level it is comparable with the amplitude of the synoptic scale variations. During the cold season, diurnal signals cannot be distinguished anymore in the CO₂ and O₂/N₂ data series, and this is mainly because the atmospheric vertical mixing is not characterized by diurnal periodicity. During winter the synoptic events become the dominant type of variability.

Vertical gradients are largest in summer time, but appear in all seasons. During summer the vertical gradients follow a daily cycle, while during winter they do not have a regular evolution.

The synoptic scale events (which dominate the variability of the mixing ratios in the air sampled at 300 m) have the same order of magnitude throughout the year; therefore the variance of the data series from 300 m does not show significant seasonal differences. In contrast, the variance of the data from lower sampling levels (5 and 30 m) is much higher during the warm season.

The high variability of the CO₂ and respective O₂/N₂ data series is characteristic to intra-continental measurements, due to the proximity of strong sources and sinks. The enhancements of CO₂ at the lower sampling levels indicate strong local and regional sources. Because of high seasonal and short term variability, any eventual long term trends cannot yet be distinguished from this short data set.

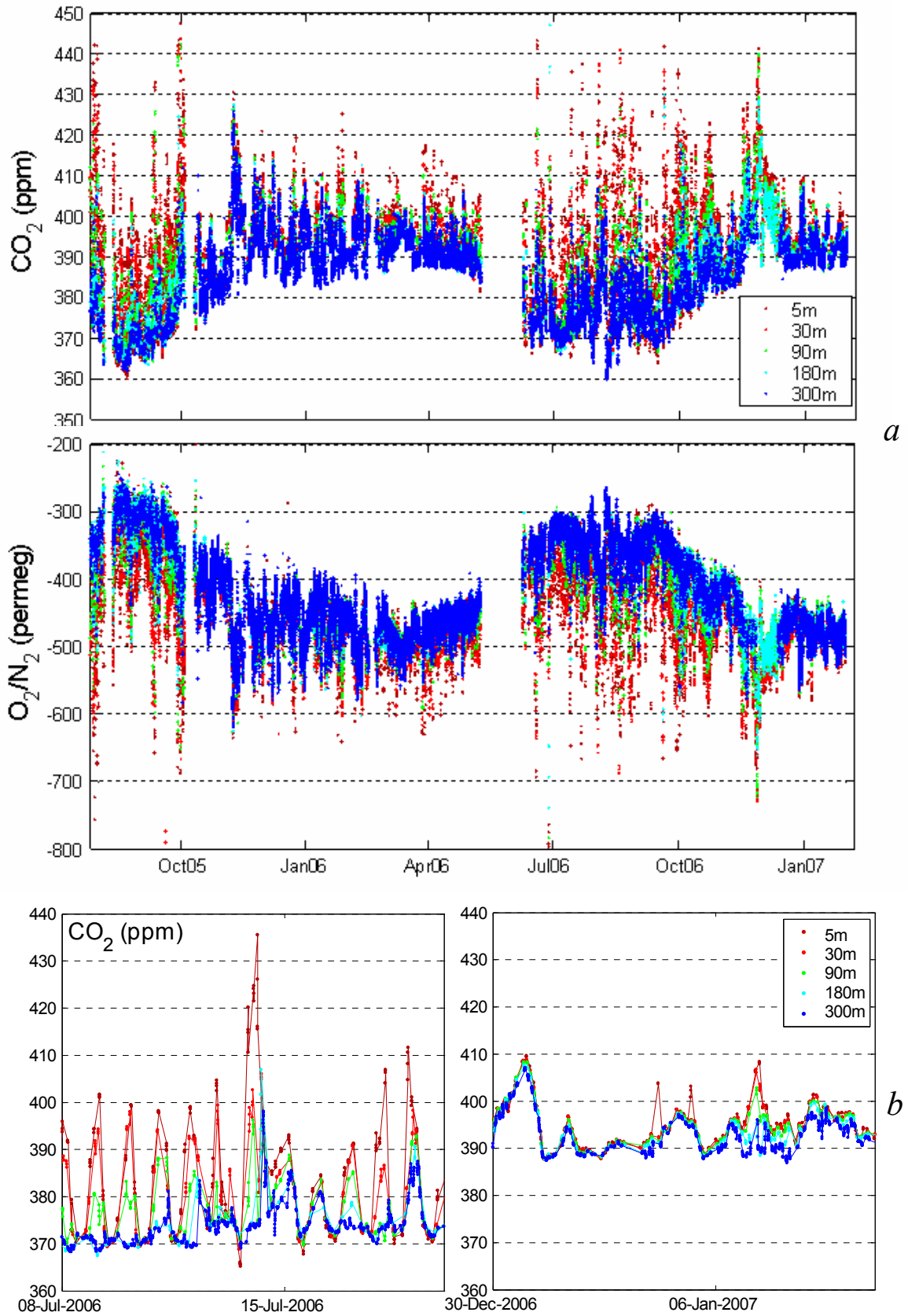


Figure 4.1 a) The CO₂ and O₂/N₂ time series. The colors represent different sampling heights. b) Summer (left) and winter (right) details from the CO₂ measurement series. The y-scales are similar.

CH₄ record

The CH₄ record is characterized by high short term variability, on the order of 200-300 ppb. Strong diurnal signals dominate the variability at low sampling levels during summer. The synoptic signals are stronger during winter than during summer. The difference between the seasons consists mainly in differences in the data variability and in the vertical gradients. The strong vertical gradients, with generally higher mixing ratios at lower sampling levels, suggest the existence of strong local to regional sources.

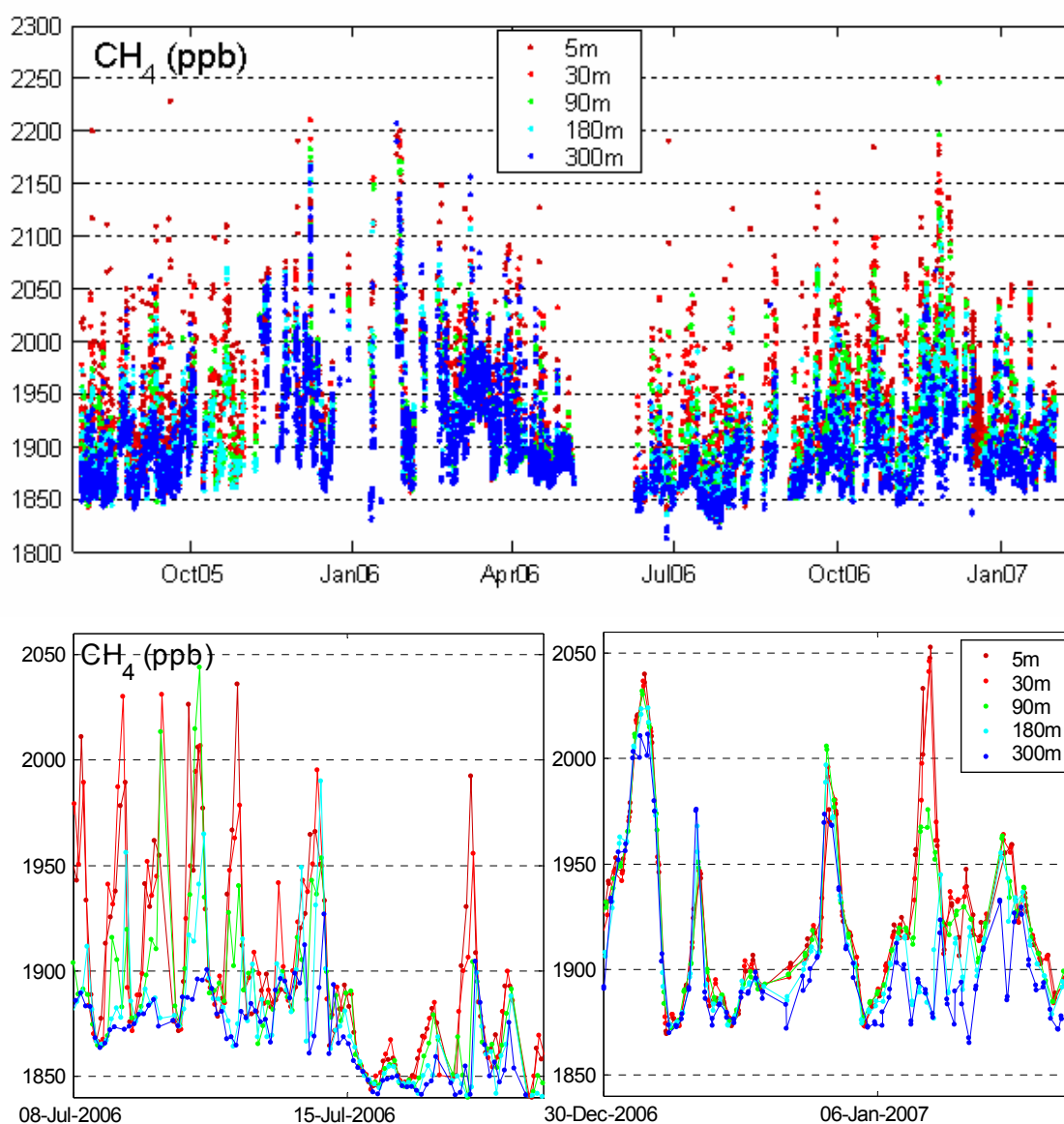


Figure 4.2 Time series of CH₄ measurement. The upper plot presents the whole CH₄ data series. The lower plots present details from summer time (left) and winter time (right). The colors represent different sampling heights. The y-scales of the detail plots are similar.

CO record

CO has seasonally varying atmospheric lifetime, which is reflected in the observed mixing ratios. The seasonality is mostly manifested as difference in variability, although a slight difference in “baseline” can also be observed. During summer, the diurnal variations and the synoptic signal have comparable amplitudes. This is unlike the behavior of CO₂ and CH₄ mixing ratios, for which during summer the diurnal variations are dominating. The strong winter time signals, often above 600 ppb, are probably due to increased anthropogenic emissions combined with a longer CO lifetime during the cold season.

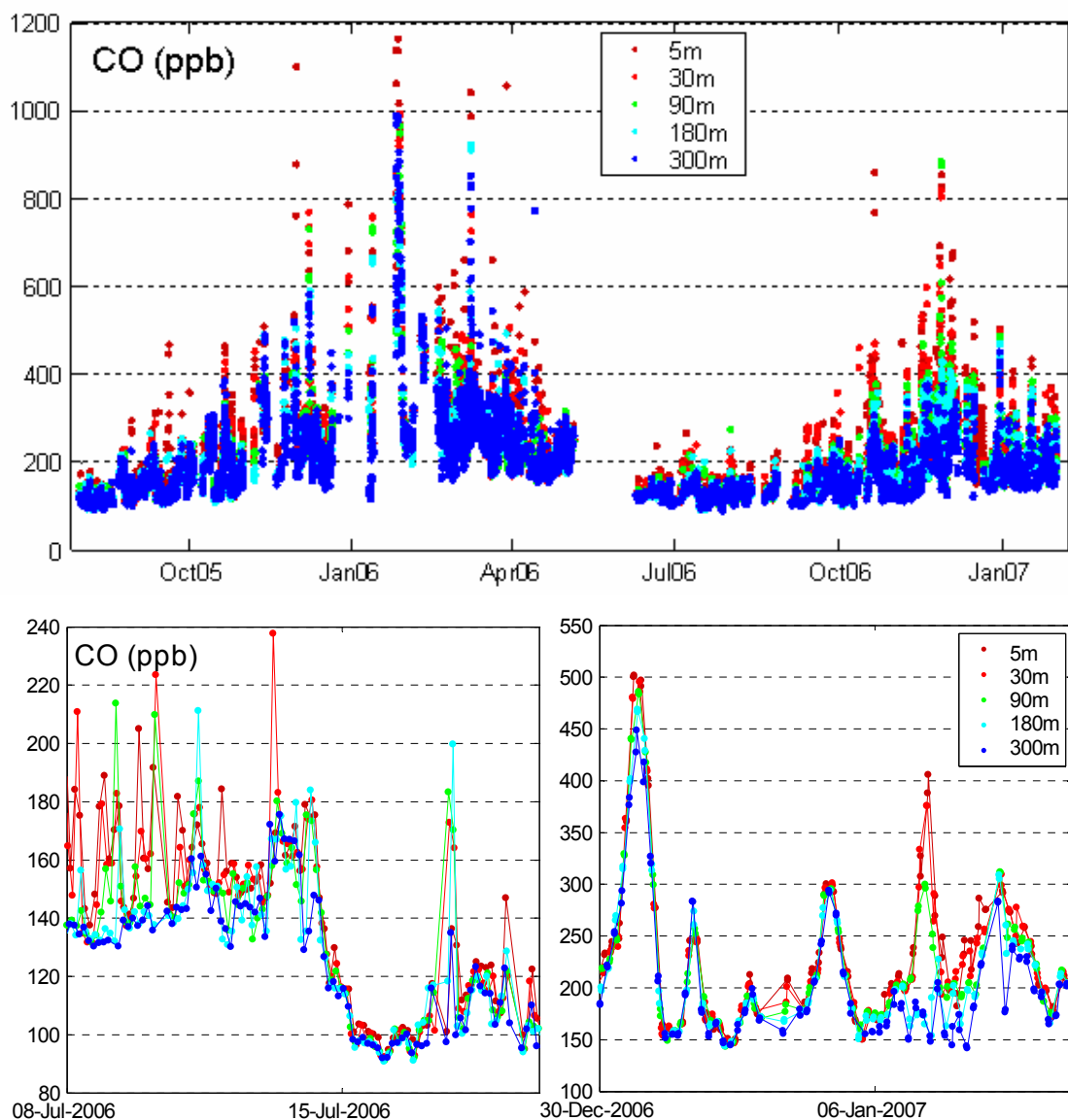


Figure 4.3 Time series of CO measurement. The upper plot presents the whole CO data series. The lower plots present details from summer time (left) and winter time (right). The colors represent different sampling heights. The y-scales of the detail plots are NOT similar.

Vertical gradients with higher mixing ratio at lower sampling levels are apparent through the year but the differences between the sampling levels are normally much smaller than the general data variability. This indicates that the main CO sources are not local, but distributed over a wider area.

N₂O record

The summer time variability of N₂O is dominated by the daily signal, similarly to CO₂ and CH₄. The vertical gradients with higher mixing ratios at lower sampling levels indicate the existence of local to regional sources. The variability is of the same order of magnitude during all seasons.

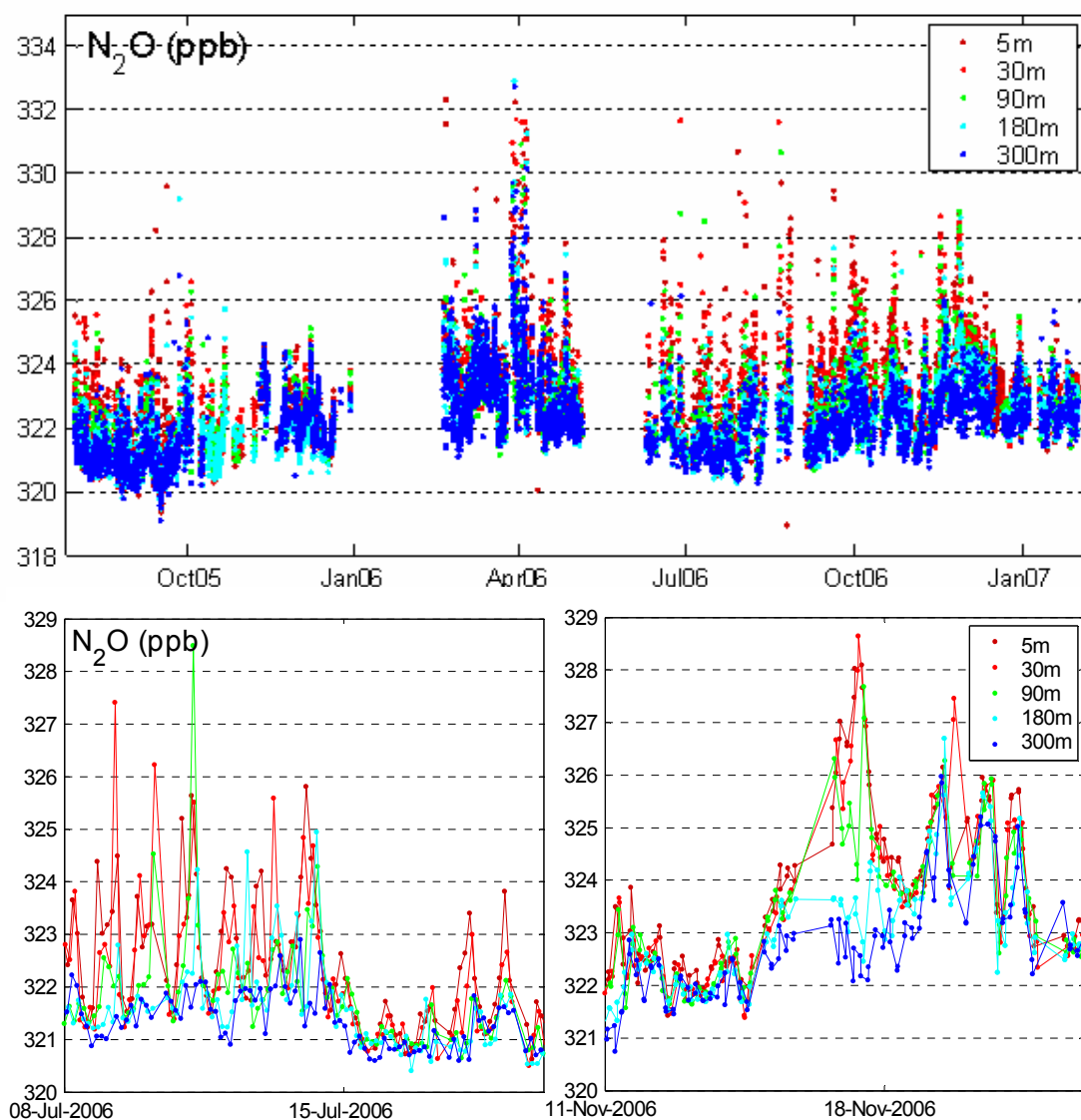


Figure 4.4 Time series of N₂O measurement. The upper plot presents the whole N₂O data series. The lower plots present details from summer time (left) and winter time (right). The colors represent different sampling heights. The y-scales of the detail plots are similar.

SF₆ record

The SF₆ time series is presented in figure 4.5. An immediate feature is a strong and almost constant increase of the atmospheric mixing ratio during the time interval considered. Between August 2005 and Jan 2007, over 1.5 years, the mixing ratio increased by about 0.4 ppt, which means 7%.

The weak seasonal variation which can be observed in the figure is probably due to seasonal differences of atmospheric transport.

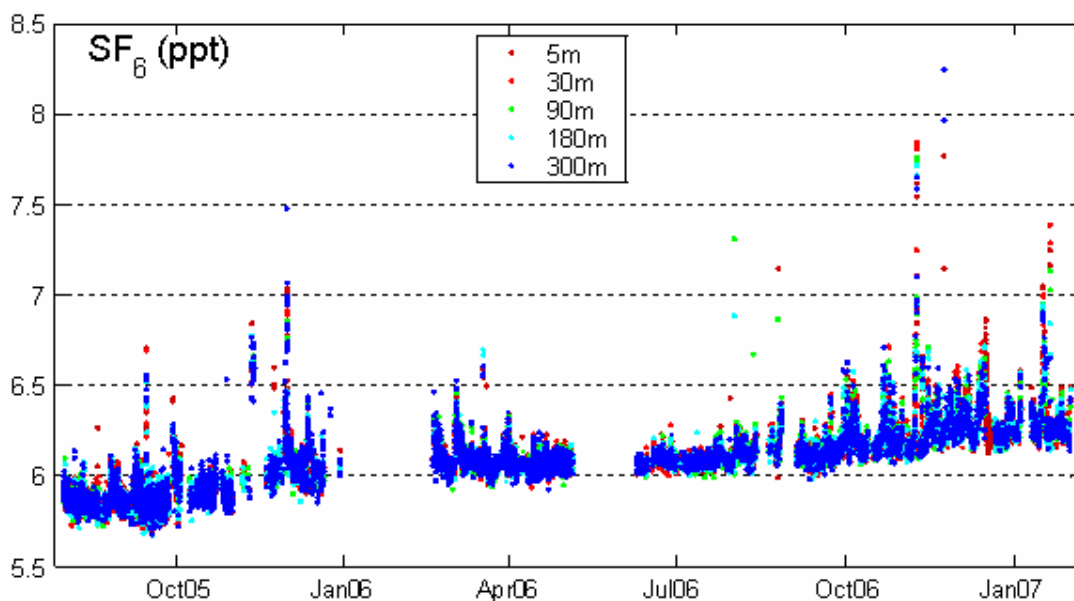


Figure 4.5 Time series of SF₆ measurement. The colors represent different sampling heights.

The general short term variability is quite low, only few mixing ratio increase events have been observed during the measurement period. Air mass back-trajectories have been computed for all the events with amplitude higher than 0.3 ppt, using the model HYSPLIT (<http://www.arl.noaa.gov/ready/hysplit4.html>, Draxler and Rolph, 2003). For all of these events, the corresponding air mass trajectories are confined within a quite narrow angle across the middle of Poland and Germany, which suggest a strong and well localized source along this path.

A notable feature, which can be observed in figures 4.5 and 4.6 a, is the absence of the vertical gradient, which implies that there are no significant local sources of SF₆.

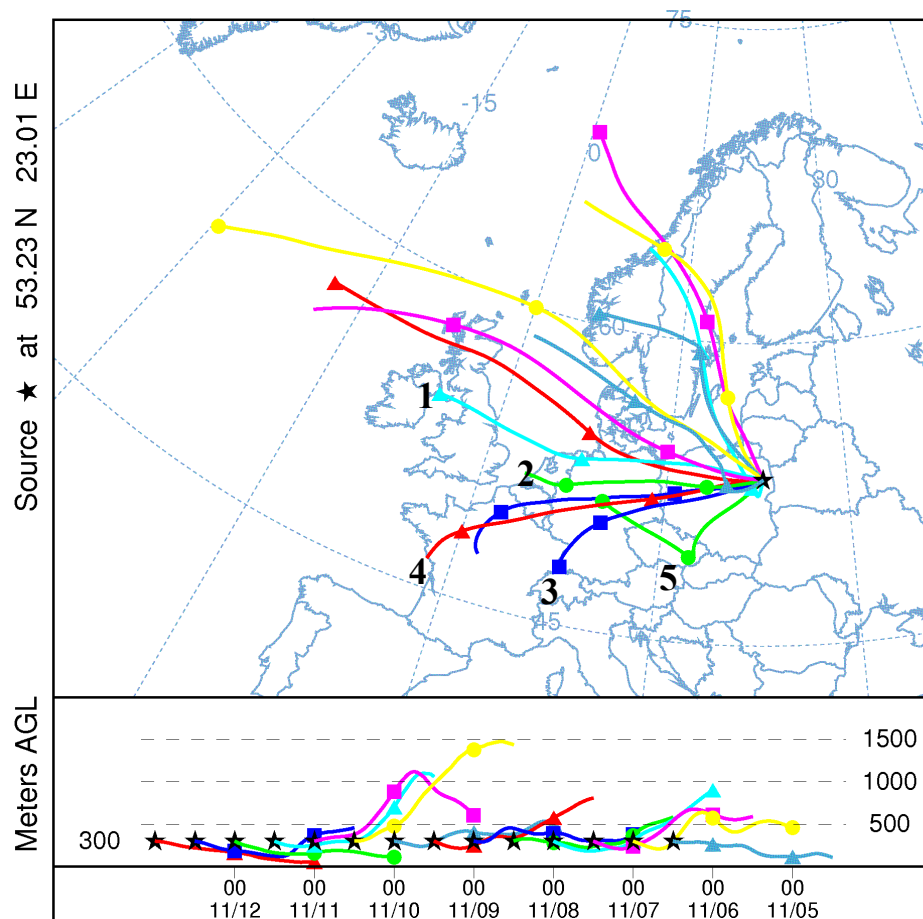
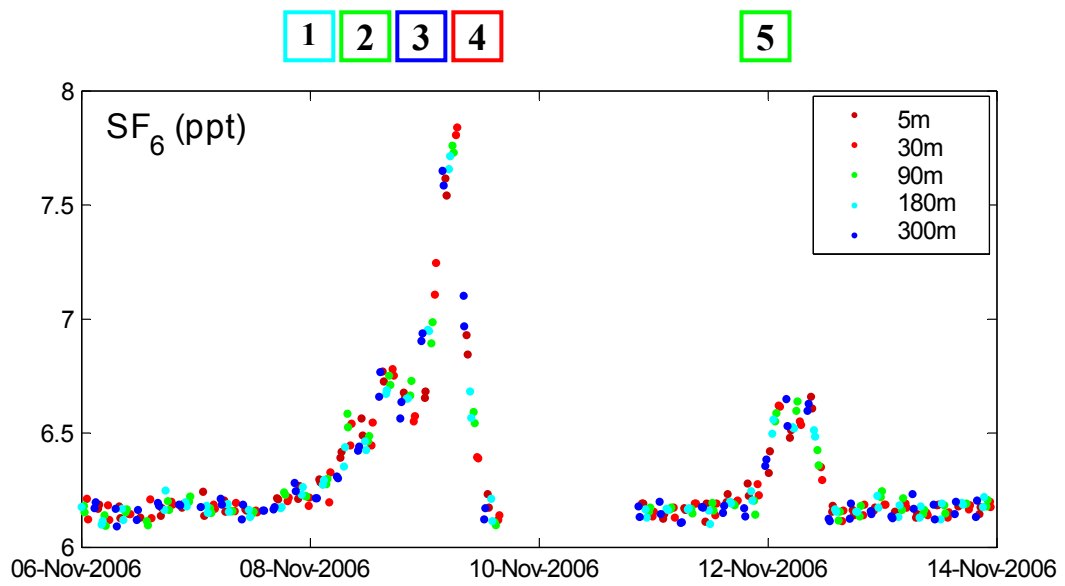


Figure 4.6 a) Interval selected from the SF_6 record, including two pollution events. b) Air mass back-trajectories during the same time interval. The numbers assigned to some of the trajectories correspond to the numbers in the upper plot.

4.3 Vertical gradients of the mixing ratios

Most of the anthropogenic emissions of pollutants and greenhouse gases, as well as the exchange between the land biosphere and the atmosphere take place near the ground. For a given gas flux, the atmospheric vertical mixing determines how the signal is vertically diluted and thus the distribution of the concentration in the air column. Therefore, by observing the vertical profile of the species emitted near the ground, one can learn about atmospheric vertical transport and mixing.

When the vertical mixing is not very strong, the air at different heights above ground carries signals from different influence areas (or different footprints). The footprint of the highest (300 m) sampling height extends typically over few hundred kilometers upwind. The area of influence decreases with the decrease in sampling height and the lowest sampling level (5 m) is mostly representative for few kilometers or tens of kilometers around. The lower sampling levels receive thus stronger signals from local sources and sinks, with high temporal resolution. The higher levels integrate various contributions on regional to continental scale, and the signal is more diluted. Because of this, sampling air from different heights above ground helps to distinguish between local and regional sources and sinks.

The intensity of the vertical mixing is closely related to the vertical gradient of the potential temperature. The potential temperature difference between two levels is proportional to the amount of energy that is necessary to lift an air parcel from the first to the second level. If the potential temperature difference is small or close to zero, the air column is unstable and the vertical mixing is strong. If the potential temperature difference is large (with higher values at the higher level), the air column is stable and the vertical mixing is weak.

The temporal variations of the vertical mixing and accordingly of the observed concentration vertical gradient differ significantly between the warm and the cold seasons. In the warm season, the vertical mixing and the concentration gradient follow a diurnal cycle.

Figure 4.7 shows the record of the CO₂ mole fractions, atmospheric temperature and potential temperature from different heights above ground, over a few days time interval which is typical for the summertime stable weather conditions. The lowest plot of the figure shows the potential temperature differences between different sampling

heights, the 30 m level taken as reference. The potential temperature (θ) is calculated using the following formula:

$$\theta(K) = T(K) \times \left(\frac{1000}{p(\text{mbar})} \right)^k \quad \text{where } k = 0.285857$$

During the afternoon there is a time interval when the gradients of the potential temperature are close to zero and the vertical mixing reduces the vertical gradient of the mixing ratio. As the potential temperature gradient increases in the evening, the vertical mixing declines and the CO_2 which is emitted near the ground accumulates.

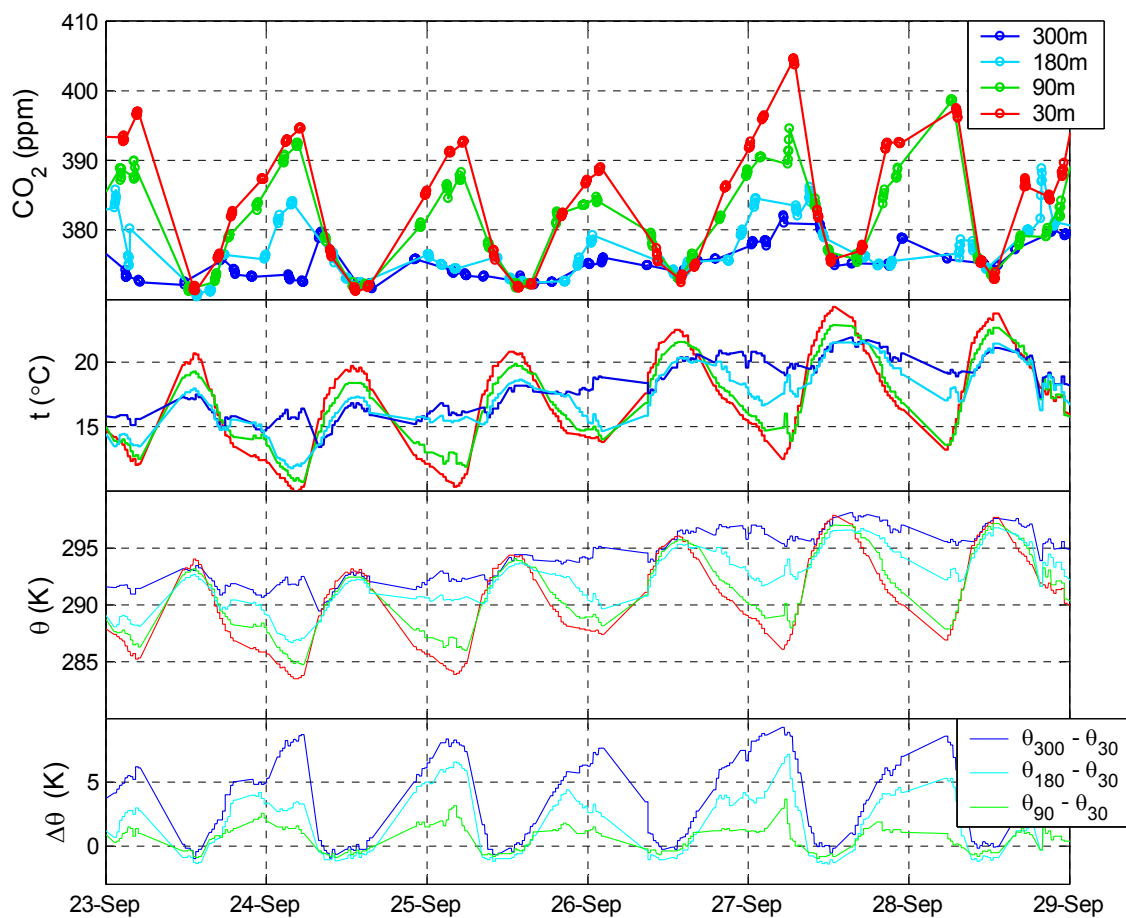


Figure 4.7 Variations of the vertical gradients of the CO_2 mole fraction, atmospheric temperature, potential temperature (θ) and the potential temperature gradients ($\Delta\theta$) typical for the warm season. The gradients of potential temperature are calculated between each sampling height and the sampling height of 30 m chosen as reference. The colors represent the sampling heights.

During winter (figure 4.8) the relationship between the potential temperature and the mixing ratio gradients is similar, but the day-night periodicity is not obvious anymore.

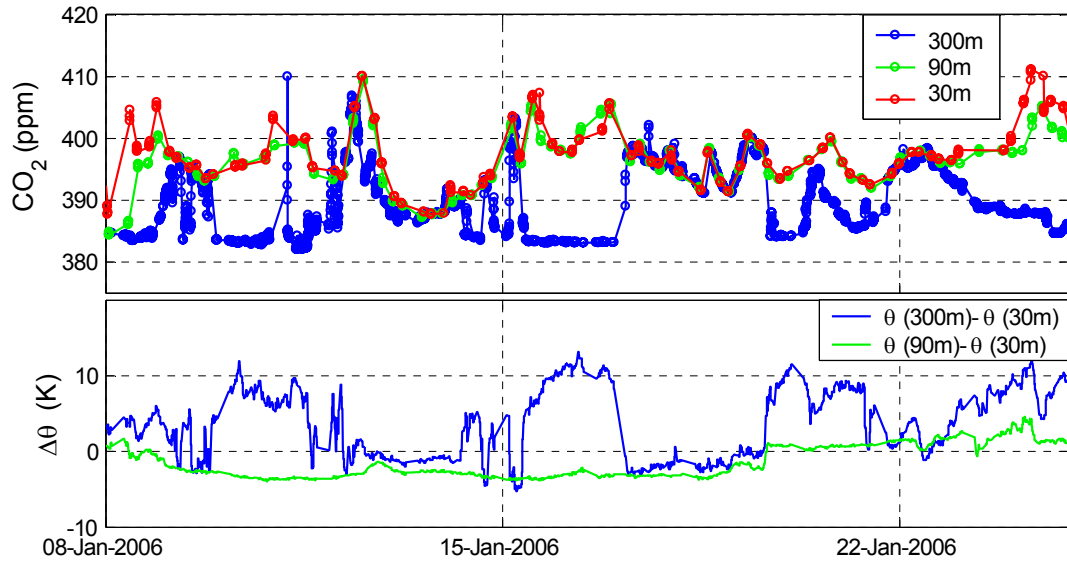


Figure 4.8 Variations of the vertical gradients of the CO_2 mole fraction and the potential temperature gradients ($\Delta\theta$) typical for the cold season. The gradients of potential temperature are calculated between each sampling height and the sampling height of 30 m chosen as reference. The colors represent the sampling heights.

As it can be seen in the figures 4.8 and 4.9, at a fixed sampling point (e.g. at 300 m) large variations of mixing ratios on time scales of few hours can occur due to changes of vertical mixing. However, comparable large mixing ratio changes can however be caused by other phenomena, like advective transport of a pollution plume or the passage of an atmospheric front. The causes of such variations can in some cases be determined by looking at the vertical gradients. From the records in figure 4.9 for example it is evident that the 300 m level is alternately inside and above the surface layer and thus the mixing ratio changes are due to changes in the surface layer height.

The differences between the warm and the cold seasons regarding the amplitude of the vertical gradients, and the evolution of the CO_2 vertical profiles with the time of day are illustrated in figure 4.9. The figure shows the average vertical profiles of the CO_2 mole fraction during summer (25-Jul-2005 – 6-Oct-2005, and 1-Jun-2006 – 1-Oct-2006) and winter (6-Oct-2005 – 1-Apr-2006, and 6-Nov-2006 – 1-Feb-2007), at different times of day. Each line in the figure represents the average of a 3-hour bin for the different sampling heights (5, 30, 90, 180, and 300 m). The dissimilarity between the summer and winter time reflects both differences in sources and sinks and the seasonality of the atmospheric circulation.

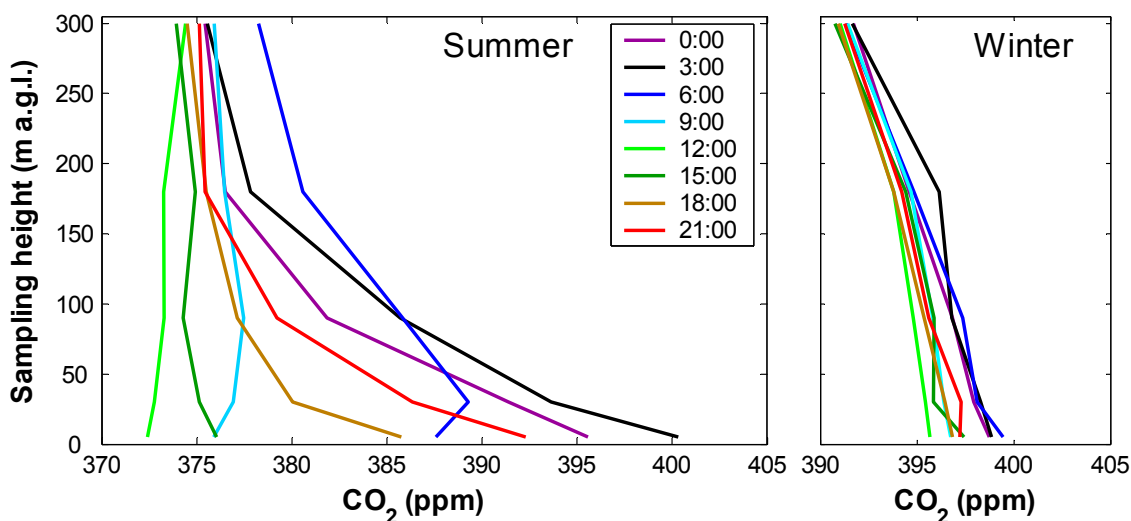


Figure 4.9 Average summer and winter vertical profiles of CO_2 mole fraction at different times of day. The data have been separated in 3-hour bins. The legend shows the start time of each bin (e.g. the line “3:00” represents the average of the data between 3:00 and 6:00 GMT).

As it can be observed in the figure 4.9, during summer time the vertical profile of the CO_2 mole fraction is highly dependent on the time of day. The night time is characterized by strong CO_2 accumulation near ground due to the absence of vertical mixing. The vertical gradient reaches its maximum of almost 25 ppm in the morning before the sunrise (the curve “3:00” in the figure corresponding to the data between 3:00 and 6:00). During afternoon a weak reversed vertical gradient can be observed, the CO_2 mole fraction near the ground being lowered by the photosynthetic uptake. Although the gas flux due to photosynthesis is on the same order of magnitude as the night time fluxes, its effect on the concentration is smaller due to stronger vertical mixing.

The average vertical gradients are much smaller during winter, between 5 and 10 ppm, and the variation of the vertical profiles with the time of day is also reduced. When looking at short time series as the one shown in the figure 4.8, the dependence of the vertical profiles on the time of day is not apparent. The average of longer time series shown in figure 4.9 reveals though a variation with the time of day of about 3 ppm, which is significant when compared to the standard errors of the averages (not shown), which range between 0.1 and 0.5 ppm.

Figure 4.10 shows the comparison between the day and night average vertical profiles of CO_2 , and the ones of CH_4 , CO , N_2O and SF_6 .

By night, the CO₂, CH₄, CO and N₂O concentrations increase at the lower measurement heights. This means that there are emissions close to the ground within the footprint of different heights, which are not dispersed in the absence of vertical mixing. The day time vertical gradients are essentially different: the CO₂ mole fraction is lower at the lower sampling heights and the mole fractions of the other species are still higher near the ground. This shows that during day the region is a sink of CO₂ while being a source for the other species.

SF₆ has no significant vertical gradient at any time of the day. The x-axis of the figure is set to about two times the analytical precision. The differences observed in the figure with the sampling height and with the time of day are not significant by comparison with the variability of the data and with the analytical precision of the measurement. This supports the idea (mentioned before) that there are no significant sources of SF₆ in the region.

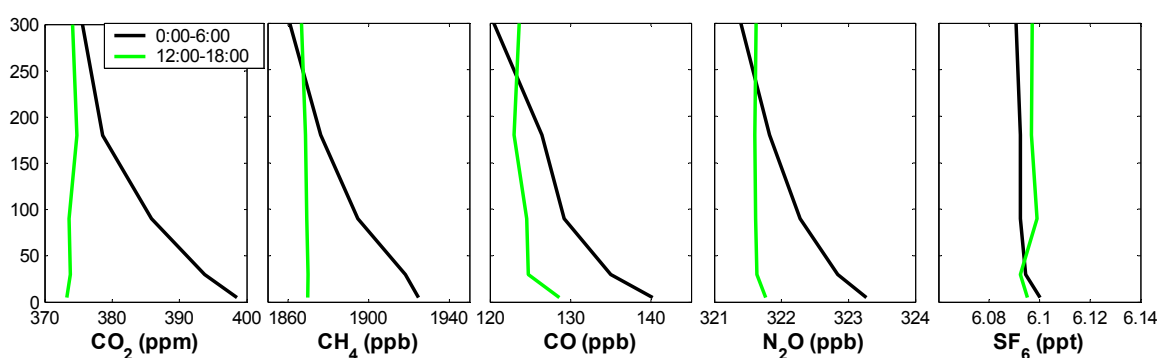


Figure 4.10 Vertical profiles of CO₂, CH₄, CO, N₂O and SF₆ representative for day and night time, during summer.

4.4 Diurnal variations of atmospheric mixing ratios

4.4.1 Diurnal variations of CO₂ and O₂/N₂

During the warm season, the thermally induced vertical mixing follows a diurnal periodicity which overlaps with the diurnal cycle of the release and uptake of CO₂ by the biosphere respiration and photosynthesis and with the diurnal cycle of human activity.

By day, when the net exchange between the biosphere and atmosphere is dominated by photosynthesis, the air is well mixed up to typically 1-3 km. Thus the

decrease of mixing ratio due to photosynthesis is very small, due to strong dilution in the air column. During night, the photosynthesis stops and the vertical mixing is weak, while the respiration is still ongoing. The CO₂ emitted by the respiration accumulates near the ground level. A strong increase of the concentration near the ground, and also strong vertical gradients can be observed. The anthropogenic emissions also add a small contribution to the observed CO₂ summer night-time increase.

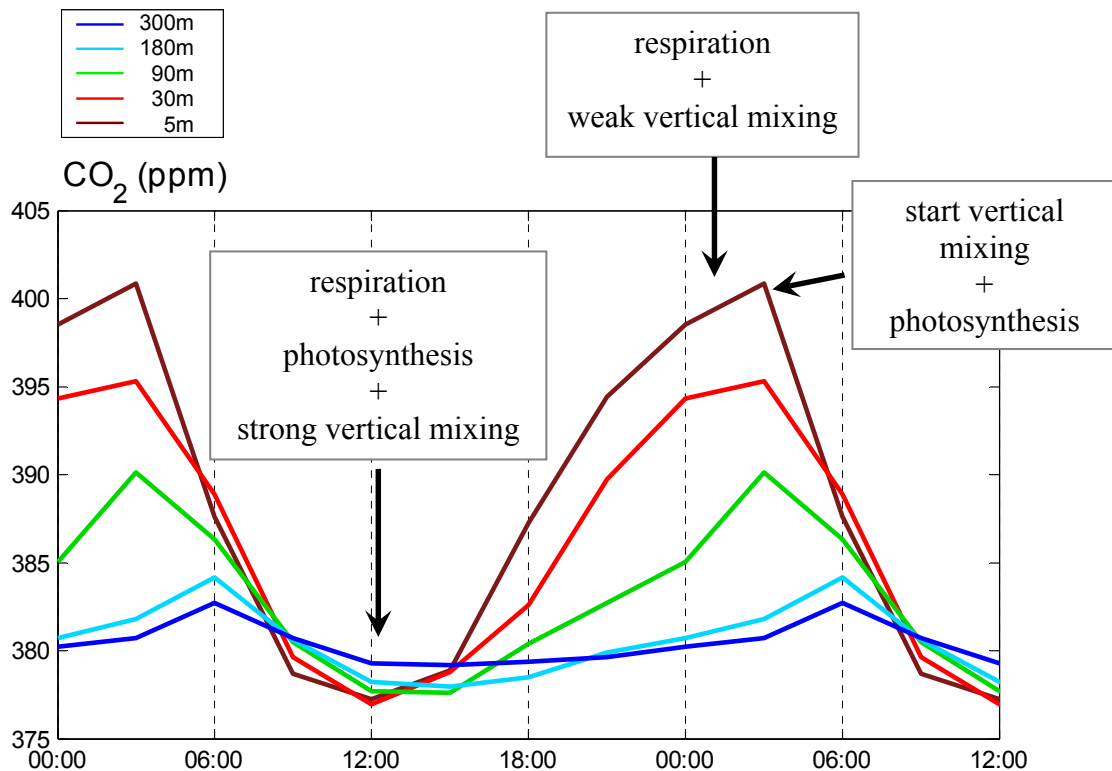


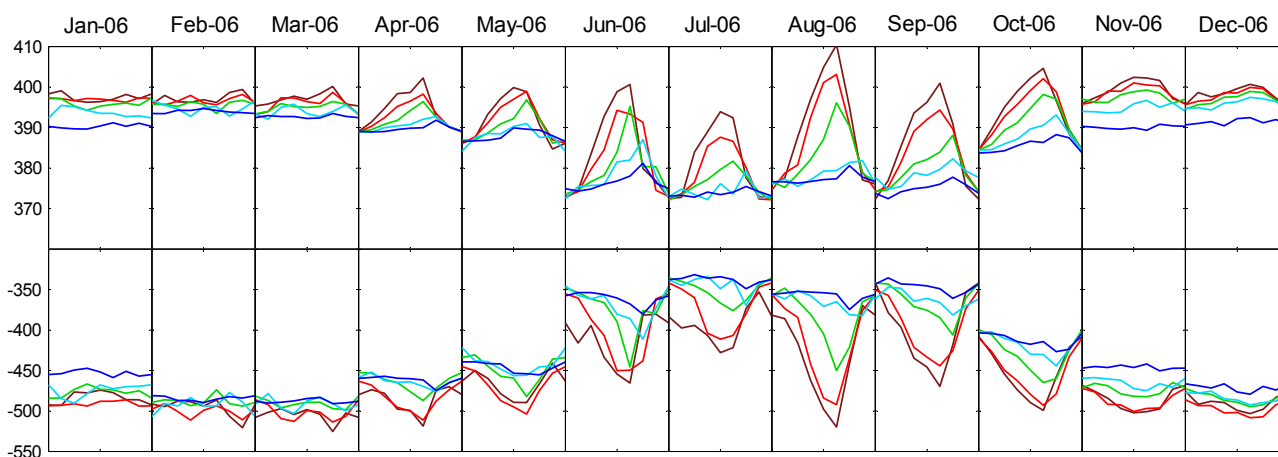
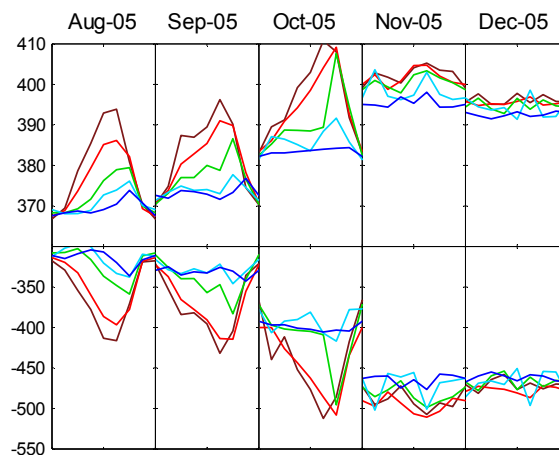
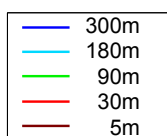
Figure 4.11 Average daily cycle of CO₂ mole fraction during Apr – Sep-2006. X-axis represents GMT time (= local time-2hr). The colors represent different sampling heights. The first half of day was repeated for visual clarity.

The variations of atmospheric oxygen are directly linked to the variations of CO₂, because oxygen is consumed when CO₂ is produced by respiration and photosynthesis, or when fossil fuels are burned. The diurnal cycle of O₂/N₂ ratio is therefore anti-correlated with the diurnal cycle of CO₂.

During the cold season the respiration is reduced and the photosynthesis declines to non-significant level. The anthropogenic CO₂ emissions and the land biosphere respiration are on the same order of magnitude. Also, the diurnal periodicity of vertical mixing disappears; the air column of a few hundred meters above ground is most of the

time well mixed, and temperature inversions appear at non-regular time intervals. As it can be observed in the figure 4.12, the average diurnal variation decreases in amplitude or even becomes indistinguishable during the cold months.

Figure 4.12 Monthly averaged diurnal cycles of CO₂ (ppm) and O₂/N₂ (permeg), for different sampling heights above ground level. The x-axis of each plot covers a 24 hours interval, centered on midnight.



4.4.2 Diurnal variations of CH₄, CO, N₂O and SF₆

Figure 4.13 presents the average diurnal cycle of CO₂, CH₄, CO, N₂O and SF₆ calculated for the same time interval 9-Jun – 30-Sep-2006.

At the first view, the mixing ratios of CH₄, CO and N₂O follow a temporal pattern similar to CO₂. During the day the vertical gradient is reduced by the strong vertical mixing of the air column. During night the vertical gradient increases and there is a strong accumulation at levels close to the ground.

There are, however, dissimilarities of the diurnal variations of different species which reflect the differences in sources and sinks. The weak vertical gradient during the

day has opposite direction for CO₂ than for CH₄, CO and N₂O. During day the net CO₂ flux into the atmosphere is negative due to photosynthesis. Thus the air sampled closer to the ground (where photosynthesis occur) is depleted in CO₂ compared to the higher levels. On the other hand, CH₄, CO and N₂O are being emitted near the ground level, which results in higher mixing ratios at sampling heights closer to the ground, as it can be observed in figure 4.13. Related to this is the night-time evolution of mixing ratios at 300 m sampling height. After the vertical mixing has diminished, the mole fraction of CO₂ at 300 m shows a slight increase, because the consumption of CO₂ by photosynthesis (which lowered the CO₂ mole fraction during day time) has stopped. In the same time, the mole fractions of CH₄, CO and N₂O decrease because the upwards transport of the gases emitted near ground level drastically decreased.

At midnight (= 2:00 local time) a partial minimum can be observed in the CO mixing ratio at the sampling levels close to the ground, bracketed by evening and morning maxima. This evolution is consistent with the temporal variation of human activities. The decrease of the accumulation rate of CH₄ and N₂O near the ground around midnight can also probably be related to the decrease of the anthropogenic emissions. Around 6:00 (= 8:00 local time) the CO₂ mole fraction near the ground decreases due to the joint effect of vertical mixing and photosynthesis. The morning decrease of the mixing ratio of the other species is delayed because the decrease due to vertical mixing is partly counteracted by an increase of anthropogenic emissions.

Although part of the CO₂ accumulated by night is due to anthropogenic emissions, the land biosphere respiration is the main CO₂ source during summer. A rough estimation of the proportion of the anthropogenic CO₂ of the total night time accumulation can be done by comparing the amplitudes of the vertical profiles of CO and CO₂. The CO:CO₂ ratio specific to anthropogenic emissions, estimated by different authors (e.g. Gamnitzer et al., 2006, EMEP/CORINAIR (<http://www.emep.int/emissions.html>), Bakwin et al., 1998), ranges usually between 10 and 25 ppb:ppm for rural areas. Thus the lower limit of the average CO:CO₂ ratio specific to anthropogenic emissions in this region can be reasonably assumed to be about 10 ppb:ppm. The maximum CO accumulation between 5 m and 300 m heights is about 25 ppb. This means that the anthropogenic CO₂ accounts for up to 2.5 ppm of the maximum night time vertical gradient of about 25 ppm. Assuming a higher average CO:CO₂ ratio for the anthropogenic emissions, for example 25 ppb:ppm, leads to an even smaller proportion of anthropogenic CO₂ from the total of 1 ppm, which is 4% from the total CO₂ accumulation.

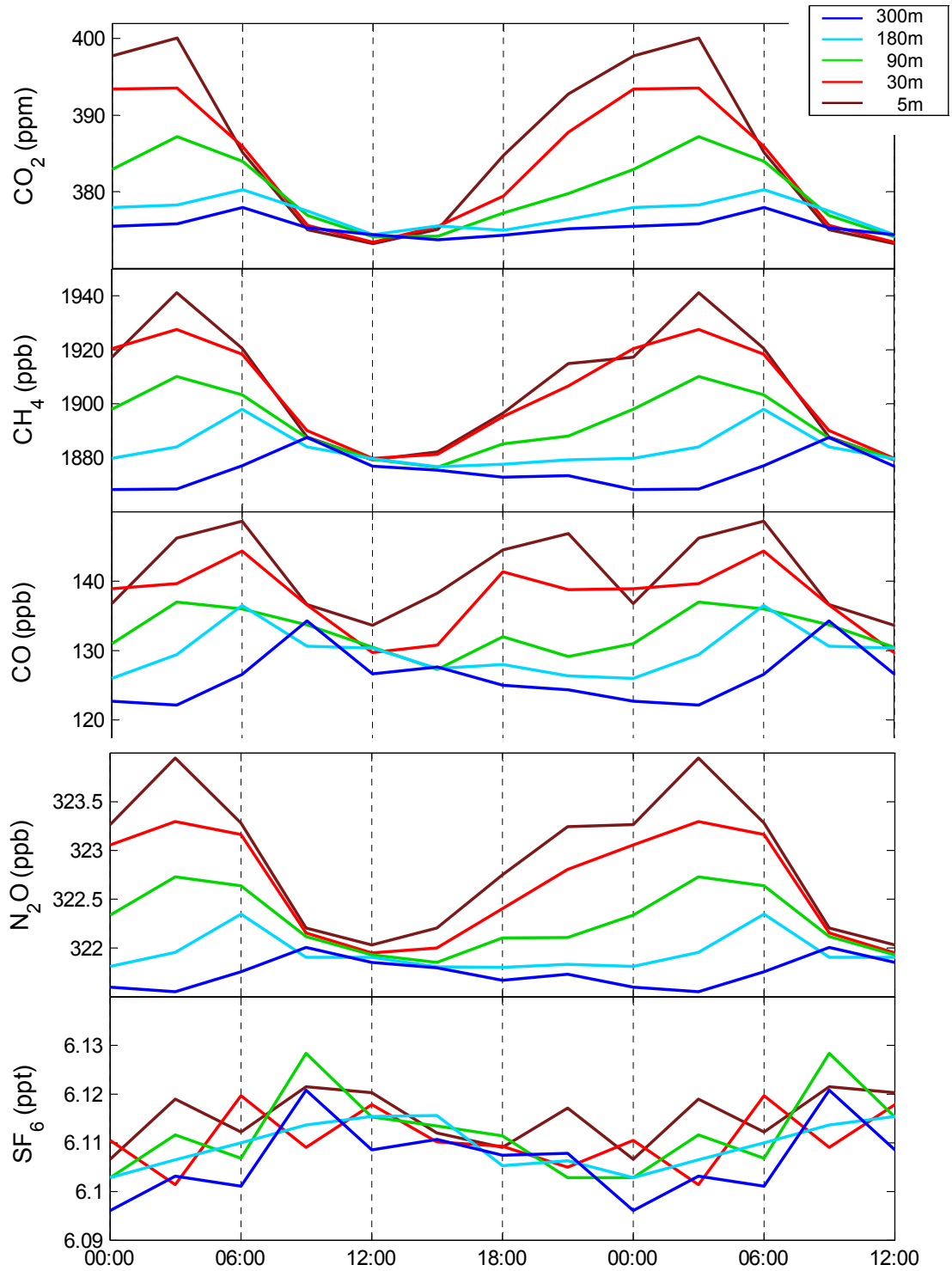


Figure 4.13 Average diurnal variation of CO_2 , CH_4 , CO , N_2O and SF_6 for the period Jun – Sep-2006. X-axis represents GMT time (= local time-2hr). The colors represent different sampling heights. The averages for 3-hour bins are calculated using a robust method, the lowest and the highest 5% of the data being dismissed. The first half of day was repeated for visual clarity.

An interesting feature in figure 4.13 is the strong correlation between CH₄ and N₂O, which suggests that the largest sources are common or have similar diurnal variation pattern. The CH₄:N₂O ratio calculated for different sampling heights varies between 32 (for 5 m) and 40.3 (for 300 m) and the correlation coefficients for all sampling heights are higher than 0.96. Common sources for CH₄ and N₂O could be industry and biomass burning. Sources with similar average diurnal pattern could be temperature dependent emissions from soil (N₂O) and wetlands (CH₄).

SF₆ shows a very weak diurnal variation and no accumulation during night, which confirms that there are no significant local SF₆ sources.

4.5. Seasonal variations of atmospheric mixing ratios

4.5.1 Data and data processing

In what follows, the in-situ measurement data from Bialystok are analyzed together and compared to flask sample data from other locations across Europe. The sampling program at Shetland Islands (SIS) is managed by MPI-BGC and the samples are analyzed by the MPI-BGC Gas- and IsoLab (data provided by M. Heimann, MPI-BGC). Additional flask sample data originate from the NOAA GMD CCGG Cooperative Air Sampling Network (data provided by T. Conway). The flask sampling locations are listed in table 4.1 and shown in figure 4.14. As already mentioned in Chapter 2 (page 61), the calibration gases used at BIK and at MPI-BGC GasLab are traceable to NOAA GMD X2005 CO₂ scale. Thus the results of the two measurement programs managed by NOAA GMD and MPI-BGC respectively can be directly compared.

Table 4.1 Location and coordinates of the sampling stations used for comparison

Station code	Station location	Latitude	Longitude	Altitude (masl)
BIK	Bialystok, Poland	53.23	23.01	180
SIS	Shetland Islands	60.17	01.17	30
BAL	Baltic Sea, Poland	55.35	17.22	3.0
MHD	Mace Head, Ireland	53.33	-9.90	25.0
HUN	Hegyhatsal, Hungary	46.95	16.65	248.0
PAL	Pallas-Sammaltunturi, Finland	67.97	24.12	560.0
IZO	Tenerife, Canary Islands	28.30	-16.48	2360.0
SUM	Summit, Greenland	72.58	-38.48	3238.0

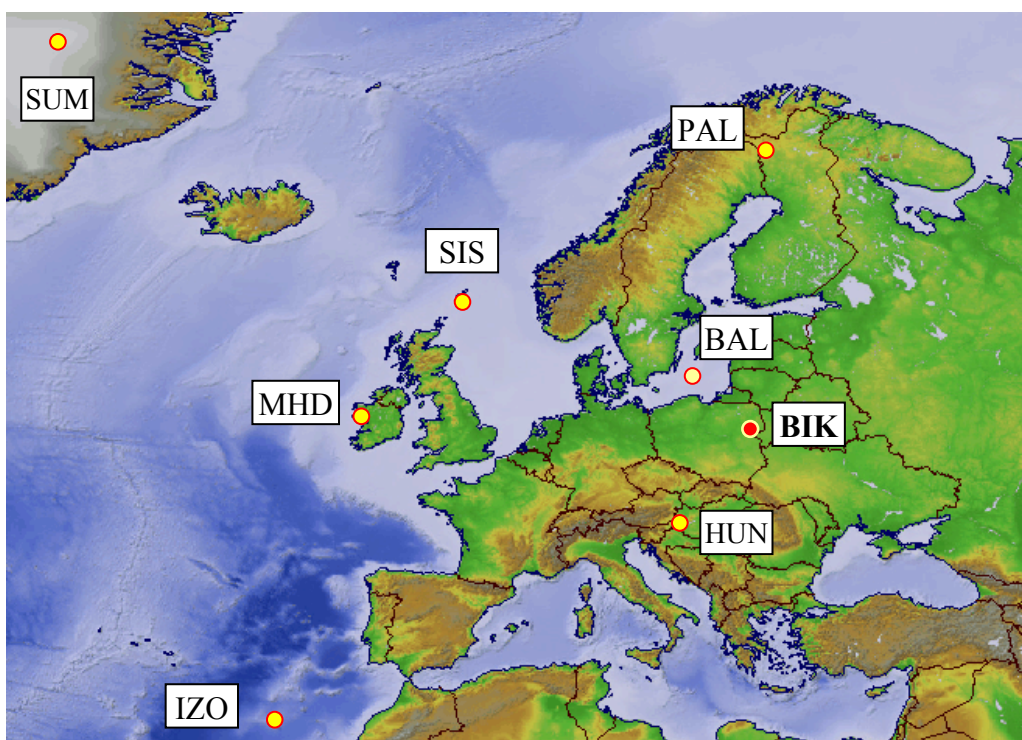


Figure 4.14 Location of the sampling stations. BIK and SIS are the sampling stations managed by MPI-BGC. All other stations belong to NOAA GMD CCGG Cooperative Air Sampling Network.

In order to derive the seasonal variations, the Bialystok data have been processed as follows. First only the afternoon data have been selected, that is, between 13:00 and 15:00 GMT, which during summer means 15:00 – 17:00 local time. Weekly averages are calculated from the selected data excluding the highest and the lowest 25% of the data. The function shown below, consisting in a linear trend and a four harmonics seasonal cycle is fitted to the weekly averages by a least squares method.

$$f(x) = a_0 + a_1x + \sum_{n=1}^4 \left(b_n \sin\left(\frac{2\pi}{365} nx\right) + c_n \cos\left(\frac{2\pi}{365} nx\right) \right)$$

where: x – time in days
 a_0, a_1, b_n and c_n – fitted coefficients

The seasonal variations for the other locations are computed by fitting the same function to the individual flask samples results, without averaging. The data flagged as “bad” or “uncertain” have been excluded. For the station BAL, where the sampling time

is either around midday or around midnight, only the results from the day time samples are taken into account.

The time series from Bialystok is too short for a robust estimation of the interannual trend, thus the linear coefficient a_1 was forced equal to the one calculated for the longer time series from Shetland Islands (SIS). The error induced by this to the seasonal cycle is not significant, because the amplitude of the seasonal cycle is much larger than the long term trend.

4.5.2 Seasonal variation of CO₂ mole fraction

There are several large scale processes which affect the atmospheric content of CO₂ and which are characterized by seasonal variability: the land and ocean biosphere activity, the thermally induced variations of solubility in ocean water, and the seasonal patterns of atmospheric circulation. The seasonal variability of the anthropogenic emissions is very small compared to the processes listed before, thus it is not significant on this time scale.

The gas exchange of the ocean biosphere is on the same order of magnitude and approximately in phase (for a given latitude) with the gas exchange of the terrestrial biosphere. However the activity of the ocean biosphere does not affect significantly the seasonal cycle of the atmospheric CO₂. The reason is briefly explained in what follows. Most of the CO₂ dissolved in sea water does not remain as CO₂, but forms carbonic acid, bicarbonate and carbonate ions. From a certain quantity of CO₂ dissolved, only a very small proportion will remain as CO₂. Assuming for example that only 1% of the CO₂ transferred into the water remains in the non-dissociated form, than an input in the ocean of 100 grams CO₂ will result in disequilibrium between the ocean and atmosphere equivalent to a difference of only 1 gram CO₂. The gas exchange between ocean and atmosphere is controlled by the magnitude of the partial pressure disequilibrium. This chemical process acts as a buffer for the CO₂ exchange between the ocean and the atmosphere and the effect is a long CO₂ equilibration time between the ocean and the atmosphere, of about one year. Because of this, the variations of the dissolved CO₂ due to the marine biosphere seasonal activity are not transferred into the atmosphere in significant proportion. The thermal variation of CO₂ solubility is affected by the same chemical buffer. Moreover, the solubility variation and the biosphere activity are in

opposite phase, so they counteract each other. In consequence the seasonal variations of atmospheric CO₂ are mainly due to the land biosphere and to the seasonal pattern of atmospheric circulation.

Figure 4.15 presents the fitted curve to the Bialystok CO₂ data corresponding to the 300 m sampling height. The curve was computed as described before, imposing the linear trend from the SIS data.

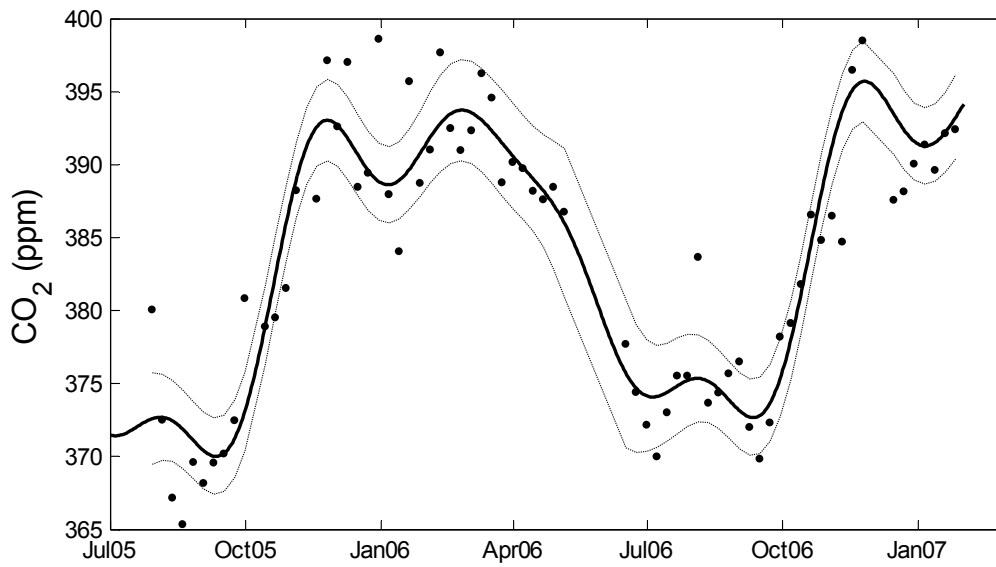


Figure 4.15 Harmonic fit to the CO₂ data from Bialystok (sampling height 300m). The dots represent the weekly robust averages of CO₂ mole fraction. The continuous line is a linear trend plus four harmonics of the annual cycle. The dotted line represents the 95% confidence bounds for the fit.

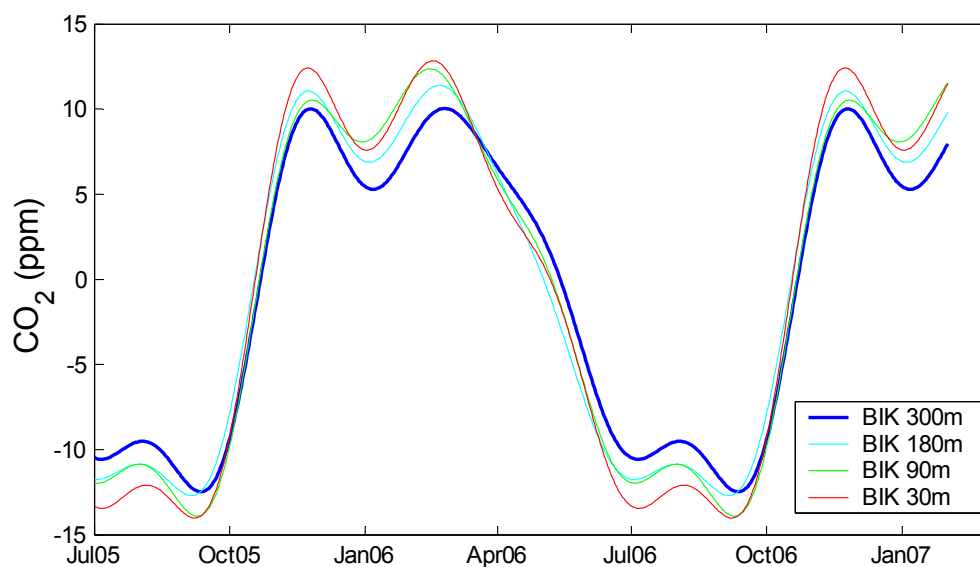


Figure 4.16 Four-harmonic seasonal components of the CO₂ mole fraction at BIK. The colors represent different sampling heights above ground level.

The CO₂ measured at Bialystok presents a seasonal cycle of about 23 ppm when considering the sampling height of 300 m (blue line in figure 4.16), which increases for lower sampling heights, up to about 27 ppm at 30 m (red line in figure 4.16). The lower sampling heights have larger seasonal amplitude due to the stronger influence from local CO₂ emissions during winter and from the CO₂ biosphere uptake during summer.

Figure 4.17 shows the comparison between the CO₂ seasonal variation at Bialystok (BIK) and results from other continental and oceanic stations. The locations of the stations considered have been shown in figure 4.14. As the subject of this comparison is the shape and timing of the seasonal cycle at Bialystok relative to the other locations, the seasonal fits for all the stations have been computed using the data covering the same time interval as the data series from BIK (Jul-05 to Feb-07).

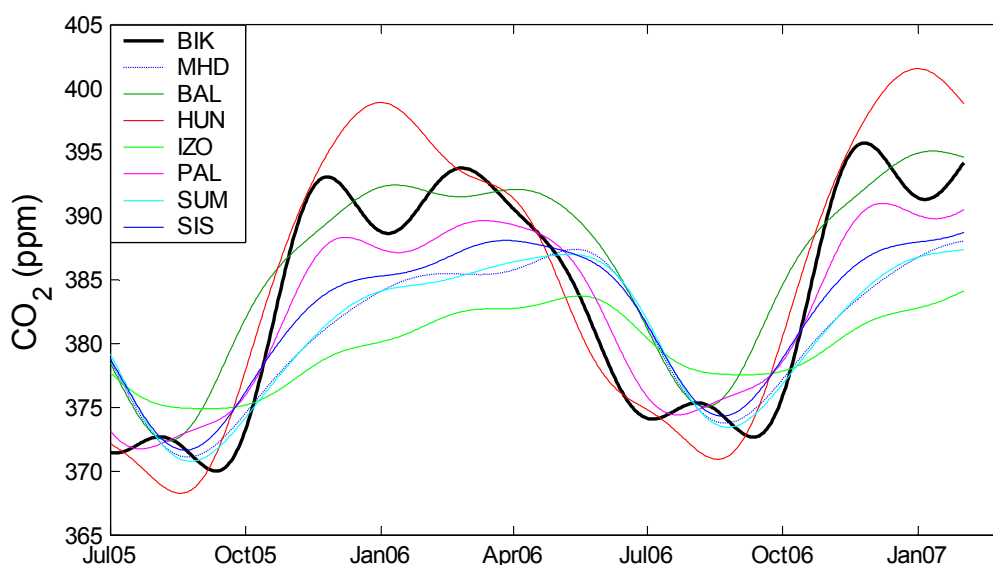


Figure 4.17 Linear trend plus four-harmonic seasonal fits of the CO₂ mole fraction at different sampling stations. The curve BIK corresponds to the 300m sampling height.

The seasonal shape of the seasonal variation at BIK is not well constrained because of the shortness of the time series. It is however possible that the presence of double maxima during the cold season is a systematic feature. A possible explanation for the first peak is the enhanced heterotrophic respiration in autumn after the leaf fall, when the available quantity of fresh organic matter increased. The second peak could be due to an increase of the gas exchange with the soil after the snow melted. A similar shape

during the cold season can be distinguished in the curve corresponding to the PAL station.

The two minima of the BIK curve during summer are however peculiar. The time series used here contains only one full length summer, in 2006. During this summer a heat wave affected most of Europe up to the end of July, and August was a cold and rainy month. The atmospheric CO₂ was influenced by the weather conditions and by the reaction of the land biosphere to heat and drought. The partial maximum of CO₂ which can be seen in the BIK record around the end of July is most likely due to the large influence of this particular summer on the curve fit, and thus probably not a general feature of the seasonal cycle in this region.

An interesting aspect which can be observed in figure 4.16 is the delay of about one month in the spring decrease of the marine stations (MHD, BAL, IZO, PAL, SUM, SIS) compared to the continental stations (BIK, HUN, PAL). As explained before, the CO₂ seasonal cycle is mainly due to the land biosphere activity. Thus the CO₂ spring time decrease at the marine stations is due to transport of continental air masses which have been depleted in CO₂ by the land biosphere. The delay observed is comparable to the intra-hemispheric mixing time of the troposphere. The station SUM is located in Greenland, at 3238 m above sea level, thus most likely representative for the free troposphere. MHD and SIS are situated on the east side of Atlantic, close to the continent. The fact that the spring decrease takes place at the same time at the station SUM and at the marine stations MHD and SIS, suggests that this decrease is due to homogenization of the land biosphere signal throughout the hemisphere rather than to direct air transport from the continent.

4.5.3 Seasonal variation of O₂/N₂ ratio

The seasonal variations of atmospheric oxygen are due to the same seasonal processes which involve the CO₂: the land and ocean biosphere activity, the thermally induced variations of solubility in ocean water, and the seasonal patterns of atmospheric circulation. There is, however, an essential difference regarding the gas exchange between ocean and atmosphere. While the CO₂ exchange is buffered by the chemical reactions of CO₂ in sea water, the oxygen is not affected by similar chemical processes. This translates into a large difference of equilibration time between the ocean and

atmosphere for the two species: about one year for CO₂ and about three weeks for oxygen (Broecker and Peng, 1982). The ocean biosphere absorbs CO₂ and releases oxygen during summer, which generates an oxygen flux from the ocean to the atmosphere, without a parallel CO₂ flux from the atmosphere into the ocean. During winter a reverse oxygen flux takes place, again with no corresponding CO₂ flux.

The seasonal warming and cooling of the ocean lead to variations in gas solubility. For the same reasons as explained before, the out-gassing and in-gassing of oxygen during warming respective cooling periods is much larger than of CO₂. Moreover, the thermal effect on oxygen acts in the same direction as the ocean biosphere: out-gassing during summer and in-gassing during winter.

In summary, the gas exchange between ocean and atmosphere on seasonal time scale has a significant effect on the atmospheric oxygen content and has no significant effect on the atmospheric content of CO₂. Thus, while the CO₂ seasonal cycle is mostly due to the land biosphere, the seasonal variation of atmospheric oxygen has an important oceanic component.

The oceanic component has been computed in previous works (e.g. Keeling et al 1998) by subtracting the land biosphere component from the total oxygen seasonal cycle. The land biosphere component is calculated based on the seasonal cycle of CO₂, assuming an average ratio between the oxygen and CO₂ variations due to the land biosphere of -1.1 (Severinghaus, 1995). The oceanic component of the oxygen seasonal cycle calculated in this way is approximately equivalent to the tracer APO (Atmospheric Potential Oxygen) defined by Stephens et al., 1998. The simplified definition of APO is:

$$APO(\text{permeg}) = O_2 / N_2(\text{permeg}) + 1.1 \times 4.8 \times (CO_2(\text{ppm}) - 350)$$

where: 4.8 is the conversion factor for the CO₂ units (from ppm to permeg)

-1.1 is the assumed average ratio for the land biosphere – atmosphere exchange

APO is by definition invariant to the exchange between land biosphere and atmosphere, assuming that this exchange respects the proportion of -1.1 between oxygen and CO₂. Fossil fuel burning, which can induce variations of APO (because the average O₂:CO₂ ratio specific to fossil fuel burning is more negative than -1.1) does not have a significant seasonality. Therefore it can be considered that the seasonal variations of APO are largely caused by the ocean – atmosphere gas exchange.

Figure 4.18 shows the four-harmonic seasonal cycles of CO₂, O₂/N₂ and APO at BIK station, corresponding to two sampling heights: 300 m and 30 m above ground level. The curves have been detrended but not normalized, in order to observe the evolution of the vertical gradient during the year.

The CO₂ and oxygen cycles are approximately anticorrelated, which means that the main drivers are the processes which involve both species. A notable difference between the shapes of the CO₂ and oxygen curves is the minimum in oxygen around March 2006 that is much stronger than the corresponding CO₂ maximum.

APO, which represents the oceanic component of the O₂/N₂ seasonal cycle, has a seasonal variation with a peak to peak amplitude of 52 permeg at 300 m and 41 permeg at 30 m. Compared to the amplitude of the O₂/N₂ seasonal variation of 162 permeg at 300 m and 175 permeg at 30m, the oceanic component represents 32% respective 23% from the total seasonal cycle.

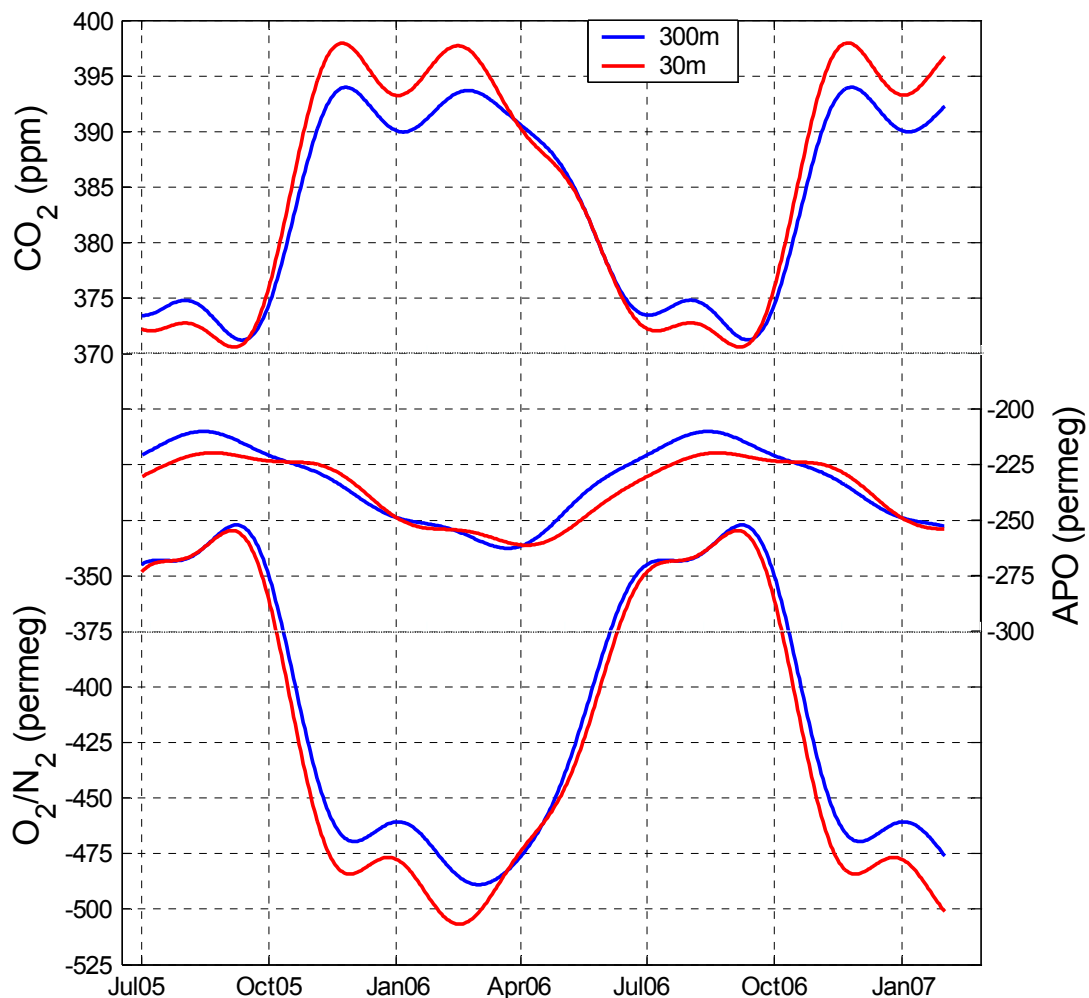


Figure 4.18 Seasonal cycles of CO₂, O₂/N₂ and APO at BIK, for two sampling heights.

During winter, the CO₂ difference of about 3-4 ppm between the two sampling heights is mirrored by an O₂/N₂ difference of about 15-20 permeg. The resulting APO has similar values for the two sampling heights. During summer, the CO₂ gradient of about 2 ppm is not balanced by a corresponding gradient in oxygen, resulting in an APO gradient on the order of 10 permeg. The lower CO₂ at the 30 m sampling level is due to the stronger influence of the land biosphere uptake at this height. Accordingly the oxygen should be enhanced at 30 m compared to the 300 m height. The missing gradient can be explained if another source of oxygen acts in opposite direction and it has a slightly stronger influence on the air at 300 m compared to the air at 30 m. It seems reasonable to explain this by an oceanic influence: since this influence is transmitted by long range atmospheric transport, it is likely to influence stronger the higher layers of air. A reciprocal phenomenon should happen in winter, i.e. a stronger oceanic induced O₂/N₂ depletion at the higher sampling level. A hypothesis is that the difference between the summer and winter seasons is related to different atmospheric circulation patterns or seasonally dependent proportions of local and large scale influence areas for the two sampling levels.

At the 30 m height, the fast decrease in oxygen in September and October is not accompanied by any important change in APO, which indicates as reason for the oxygen decrease the land biosphere activity. This is consistent with the hypothesis formulated in the previous paragraph, that the CO₂ maximum during autumn is due to a peak in the heterotrophic respiration following the litter fall. In contrast, the APO at 300 m does have a decrease of about 15 permeg during this period.

Figure 4.19 presents the seasonal cycles of CO₂, O₂/N₂, APO and the residual terrestrial component of the O₂/N₂ at BIK and SIS. The seasonal amplitude of the CO₂ at SIS is lower than at BIK, but the seasonal amplitude of O₂/N₂ is almost the same. The oxygen minimum which appears in the BIK curve around March, and which is not balanced by a CO₂ maximum of the same strength, corresponds to a minimum of oxygen and APO at SIS. The overall shape of the BIK APO curve is more similar to the O₂/N₂ and APO at SIS than to the O₂/N₂ at BIK. This is not surprising since the seasonal cycle of APO is assumed as having oceanic origin. The APO seasonal amplitude at SIS is about 90 permeg, while at BIK it is only 52 permeg. Also, the APO seasonal cycle at BIK is slightly delayed in comparison with the one from SIS, which is consistent to a transport of oceanic signal to the continent. Reversely, the CO₂ cycle is delayed and attenuated at SIS

in comparison with the one from BIK, which is consistent to a transport of land biosphere signal from the continent.

The proportion of oceanic and land biosphere components of the O_2/N_2 seasonal cycle at SIS (each of them about half of the total signal) is similar to findings of other studies, for marine or high altitude stations in the mid latitude Northern Hemisphere (e.g. Keeling and Shertz, 1992, Sturm et al., 2005a, 2005b). Quantifying the attenuation of the oceanic signal at BIK and the variation of this attenuation with the sampling height constitute information about the spatial representativity of this sampling location and can help to constrain the longitudinal transport in atmospheric transport models.

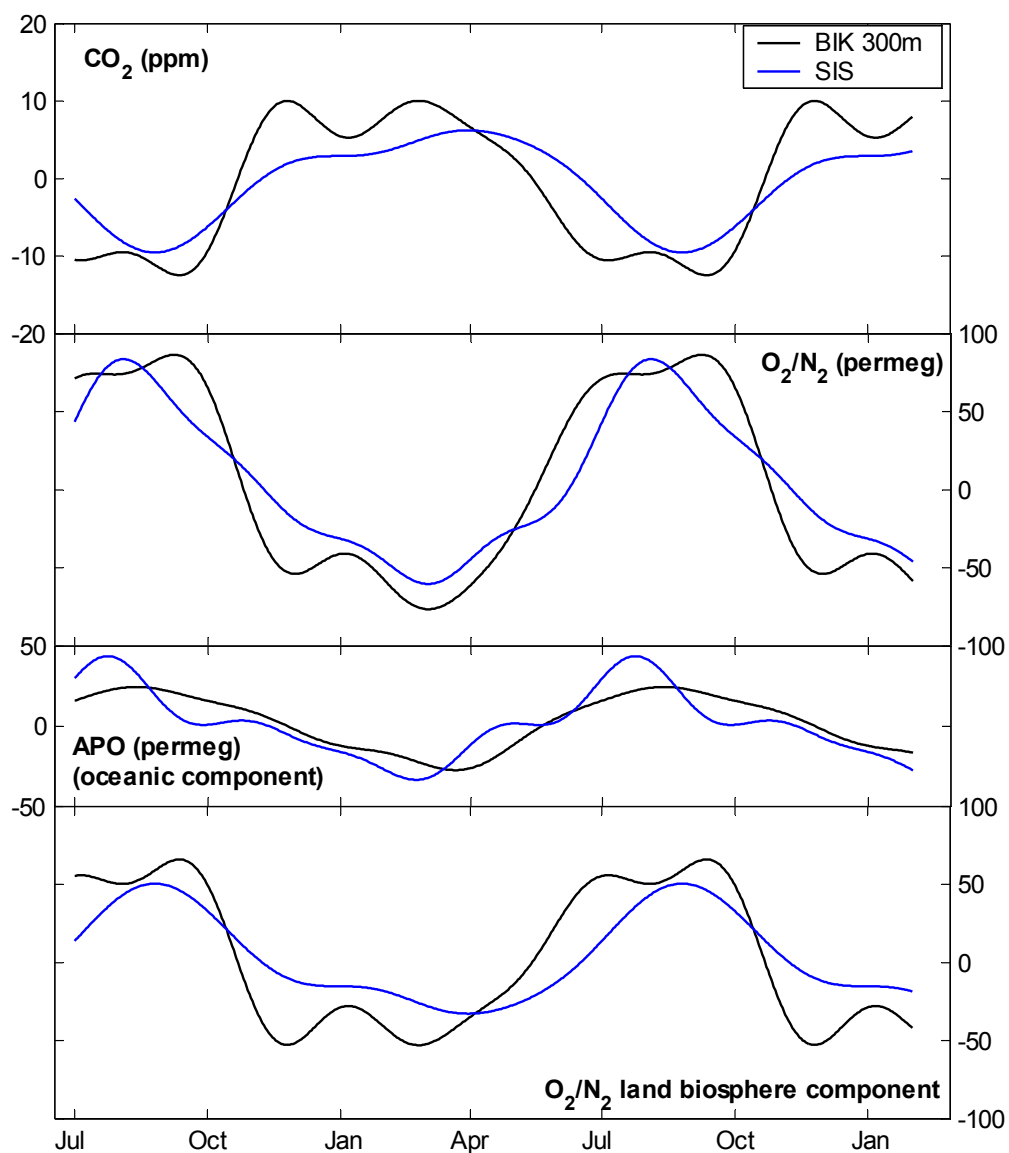


Figure 4.19 Seasonal cycles of CO_2 , O_2/N_2 , and the oceanic (APO) and land biosphere components of the O_2/N_2 , at BIK (300 m sampling height) and SIS. The curves are detrended and centered to zero mean.

In figure 4.20 the seasonal variations of O_2/N_2 are plotted against CO_2 mole fractions, both in ppm units. The slopes calculated by a robust least squares regression method and expressed in units of mol O_2 / mol CO_2 are -1.39 ± 0.07 for BIK and -1.65 ± 0.12 for SIS. These values are less negative than the values around -2 mol O_2 / mol CO_2 observed by Sturm et al., 2005a and 2005b at two sampling stations in Europe (Jungfraujoch, 3580 masl, $46^\circ33'N$, $7^\circ59'E$, and Puy de Dôme, 1480 masl, $45^\circ46'N$, $2^\circ58'E$) and during flights above Griffin Forest, UK ($56^\circ37'N$, $3^\circ47'W$). The difference could be partly due to the interannual variations in the air-sea gas exchange, given that the data series used here is short and covers a different time interval than the data used by Sturm et al. The difference in the slopes for SIS and BIK is however consistent with results of model simulations of the dilution of ocean signal over the continent (Heimann, 2001).

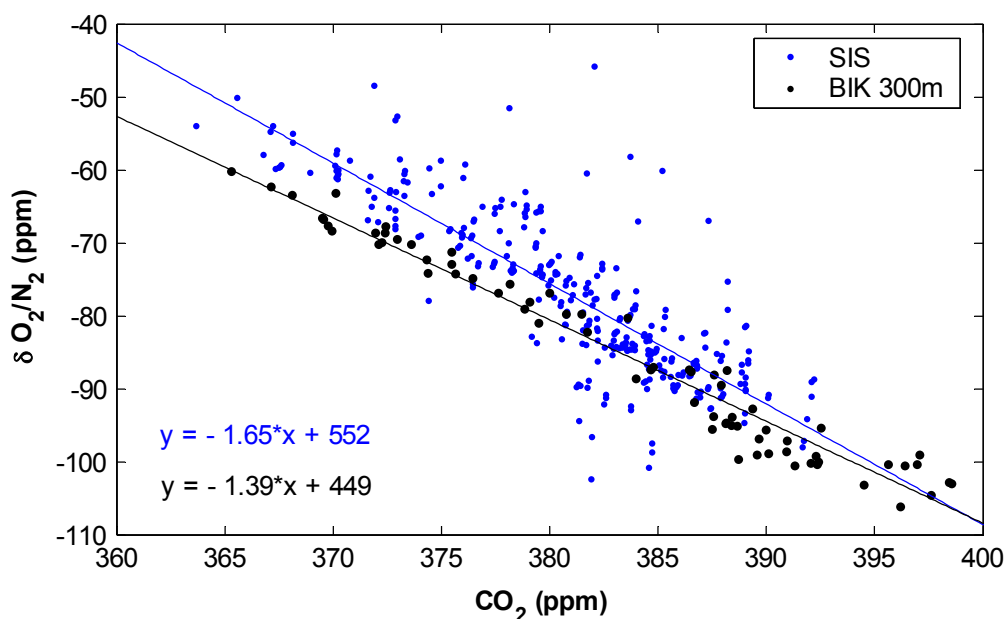


Figure 4.20 O_2/N_2 versus CO_2 for SIS and BIK (sampling height 300m).

4.5.4 Seasonal variations of CH_4 , CO , N_2O and SF_6

In order to derive the seasonal variations, the CH_4 , CO , N_2O and SF_6 data have been processed in a slightly different manner than the CO_2 and O_2/N_2 data. The time interval for selecting the afternoon data was expanded to 11:00 to 16:00 GMT, because the frequency of the data for the GC measured species is much lower. Weekly averages

have been calculated from the afternoon results in the same way as for CO₂ and O₂/N₂, excluding the highest and the lowest 25% of the data. A function with consisting in a linear trend and only two harmonics to the annual cycle was fitted to the weekly averages by a least squares method.

Figure 4.21 presents the curve fits to the CH₄, CO, N₂O and SF₆ time series. All the curves have been detrended using the linear component corresponding to only one sampling height (300 m), and have not been centered to zero mean, in order to observe the seasonal evolution of the vertical gradient. It is evident from the figure that the amplitude of the seasonal cycle varies with the sampling height in case of CH₄, CO and N₂O, while the difference between the sampling heights in case of SF₆ is not significant.

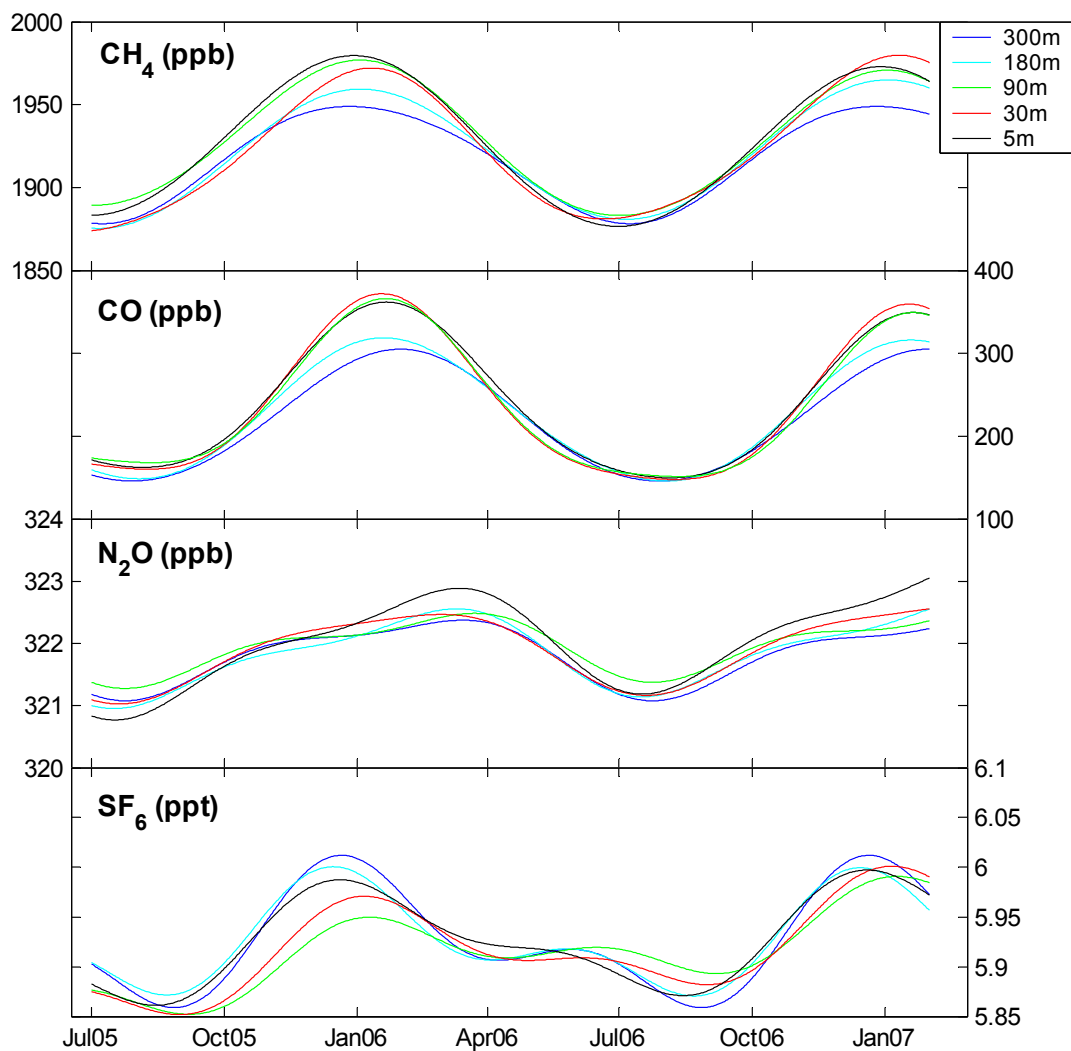


Figure 4.21 Two harmonic components of the curve fits to the CH₄, CO, N₂O and SF₆ afternoon data. The colors represent the sampling heights.

The peak to peak amplitude of the CH₄ seasonal cycle ranges from 70 ppb at 300 m to about 100 ppb at 5 and 30 m above ground, with the maximum in December – January and the minimum at the beginning of July.

The CO seasonal cycle has an amplitude of 160 ppb at 300 m, that increases to about 200 ppb at 5 and 30 m. The maximum is in January, slightly delayed compared to the maximum of the CH₄ mixing ratios. In autumn CO starts increasing later than CH₄, the low CO concentration level season is longer, and the minimum of the seasonal cycle is with about one month delayed compared to CH₄. The explanation for the difference might be as follows: the photochemical sink strengths for both species have their maximum in summer (maximum day time duration in June); for CH₄ the major sources are also temperature dependent and thus higher in late summer, whereas the main CO source is probably the combustion process that increase when it is getting colder.

The N₂O seasonal cycle is strongly asymmetrical. The minimum is in July, about half month later than the CH₄ minimum. There is a fast mixing ratio increase between July and October, which continues at a lower rate until it reaches a maximum in March. The peak to peak seasonal amplitude is of about 1.3 ppb at 300 m, and the amplitude is not significantly different at the other sampling heights, except for the lowest level which shows an amplitude of about 1.9 ppb.

The detrended seasonal variation of SF₆ is shown in the figure 4.21; for clarity, the SF₆ variation without removing the linear trend is shown in the figure 4.22. The SF₆ seasonal variation presents two distinct phases (see figures 4.21, 4.22): a fast increase of the mixing ratio between September and December, followed by a relatively stagnating

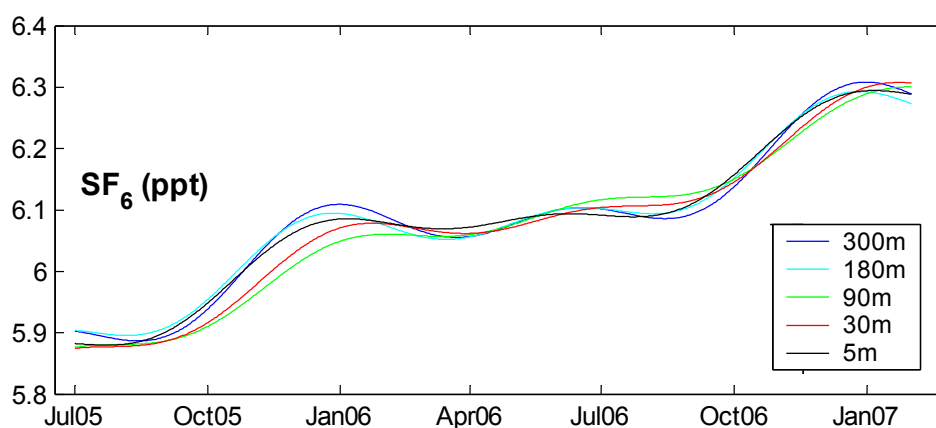


Figure 4.22 Curve fit (linear plus two annual harmonics) to the SF₆ afternoon data. The colors represent the sampling heights, similarly to the previous figure.

period between January and September. The decrease between January and September which is apparent in figure 4.21 is mostly due to the subtraction of the linear trend. In contrast to the other species, the SF₆ seasonal cycle seems to have the maximum peak to peak amplitude of 0.15 ppt at the highest sampling level, while the 90 m sampling level shows the minimum seasonal amplitude of about 0.8 ppt. However, this small variation of the seasonal cycle with the sampling height is cannot be well constrained with the available data, therefore it might be not representative as long term characteristic.

The seasonal variation of each species has a component due to the seasonality of the atmospheric circulation, overlaid by a species characteristic component which is the sum of the sources and sinks variability. The variability of the species which have no strong seasonally varying sources, like SF₆, carries information about the seasonality of the atmospheric transport. Thus the multispecies approach can be useful to evaluate the contribution of the atmospheric transport to the seasonal cycles of different species.

Regarding the representativity of the seasonal cycles presented here, some remarks must be made. The shortness of the data series combined with the large short term variability of the mole fractions lead to potentially large error in computing the curve fits. The resulting amplitude and shape of the seasonal cycles are sensitive to the data selection (afternoon, between 11:00 and 16:00 GMT), data processing (50% weekly averages) and to the fitting method (linear + two seasonal harmonics). The interannual trends are also not well defined and cannot be expected to be representative on long term (for example the decreasing trends obtained in the case of CH₄ and CO). When a longer record will be available, it will be possible to verify which of the features described here are representative on long term.

4.6 Summary and conclusions

The observed signals result from an overlaying of long term trends, with seasonal, synoptic and diurnal variations. The mixing ratios of all species with the exception of SF₆ show high variability on time scales of hours to weeks, a fact which is expectable from continental measurements in the lower troposphere. Large variations of the species abundances are due to the proximity of sources and sinks variable in time and with irregular spatial distribution. Because of this large variability, eventual long term trends

cannot be distinguished from the data series covering only 18 months. For SF₆ only a clear trend can be observed, with a growth rate of about 0.3 ppt / year, consistent with the results of other monitoring stations in the recent decades.

The vertical profiles of the mixing ratios are closely related to the vertical transport and mixing; therefore the measurement of tracers which have sources near the ground provide a tool for studying the boundary layer dynamics and improving its representation by atmospheric transport models.

The highest sampling level is alternately located in the mixed boundary layer or in the free troposphere. Thus information about both the free troposphere and the planetary boundary layer can potentially be obtained with a careful data selection. The representativity of the sampled data can be determined by comparison with the lower sampling levels and / or using the vertical gradients of the potential temperature.

The differences between sampling heights which have different influence areas can help to determine the spatial distribution of sources and sinks. For example, the increase of the CO₂, CH₄, CO and N₂O mixing ratios at lower sampling levels in the absence of strong vertical mixing proves the existence of significant local and regional sources for these gases. In the same time, the absence of a vertical gradient in the SF₆ mixing ratio shows that there are no significant sources in the region. In this context a modeling study to characterize the extent and the variability of the influence areas for each of the sampling heights at this location would be useful.

The summer diurnal variations of the vertical profile of mixing ratios are driven by the diurnal variations of the air columns vertical mixing, but in the same time they reflect the variations of sources and sinks.

The correlation with the CO mixing ratio suggests that the summer night time CO₂ accumulation is mainly due to the land biosphere respiration, anthropogenic sources accounting for less than 10%. This result is in good agreement with model simulations for this location (TM3 model, Christian Roedenbeck, personal communication). On the other hand, anthropogenic emissions contribute substantially to the diurnal variations of CH₄, CO and N₂O. The absence of night time accumulation in case of SF₆ supports the hypothesis that there are no significant local sources of SF₆.

Seasonal cycles can be observed for all in-situ measured species at Bialystok. The CO₂ seasonal cycle has a peak to peak amplitude between 23 ppm at the sampling height of 300 m and 27 ppm at 30 m. The lower sampling levels show higher seasonal amplitude due to stronger local influence. The comparison with marine stations suggests that the region is a sink for CO₂ during summer. Unlike CO₂, the oxygen seasonal cycle is due to the combined effect of the land biosphere and the gas exchange between atmosphere and ocean. The tracer APO can be used to quantify the oceanic component of the oxygen seasonal cycle. The comparison with the marine station SIS permits to quantify the dilution of APO over the continent and thus to constrain the longitudinal transport in the models. This is particularly important for determining the distribution of the CO₂ sink in the northern mid-latitudes.

The seasonal cycle of each species has a component which is due to seasonal variations in the atmospheric circulation. Thus observing the seasonal cycle of compounds which have no seasonally varying sources can help to constrain the seasonality of the atmospheric transport and to separate this component from the seasonal cycles of the other species.

Some of the features presented in this chapter are similar to results from other continental tall tower stations (e.g. Bakwin et al., 1995). There are, however, attributes which are location specific, like the low SF₆ variability or the attenuation of the oceanic signal. In summary, the results presented here make clear that studying the general variability patterns of the data at each sampling location is important for the further use of these data, and also for decisions regarding the measurement strategy.

4.7 References

- Bakwin P. S., Tans P. P., Hurst D. F., and Zhao C. L. (1998) Measurements of carbon dioxide on very tall towers: Results of the NOAA/CMDL program. *Tellus Series B-Chemical & Physical Meteorology* 50(5), 401-415.
- Bakwin P. S., Tans P. P., Zhao C. L., Ussler W., and Quesnell E. (1995) Measurements of carbon dioxide on a very tall tower. *Tellus Series B-Chemical & Physical Meteorology* 47(5), 535-549.

- Bakwin P. S., Davis K. J., Yi C., Wofsy S. C., Munger J. W., Haszpra L., and Barcza Z. (2004) Regional carbon dioxide fluxes from mixing ratio data. *Tellus Series B-Chemical and Physical Meteorology* 56(4), 301-311.
- Broecker W. S. and Peng T.-H. (1982) *Tracers in the Sea*. Lamont-Doherty Geological Observatory, Palisades, N.Y.
- Draxler, R.R. and Rolph, G.D. (2003) HYSPLIT (HYbrid Single-Particle Lagrangian Integrated Trajectory) Model access via NOAA ARL READY Website (<http://www.arl.noaa.gov/ready/hysplit4.html>). NOAA Air Resources Laboratory, Silver Spring, MD.
- Gamnitzer U., Karstens U., Kromer B., Neubert R. E. M., Meijer H. A. J., Schroeder H., and Levin I. (2006) Carbon monoxide: A quantitative tracer for fossil fuel CO₂? *Journal of Geophysical Research-Atmospheres* 111(D22), -.
- Haszpra L. (1995) Carbon dioxide concentration measurements at a rural site in Hungary. *Tellus Series B-Chemical and Physical Meteorology* 47(1-2), 17-22.
- Heimann M. (2001) The cycle of atmospheric molecular oxygen and its isotopes. In Schulze ED (Eds.): *Global biogeochemical cycles in the climate system*. Academic Press, San Diego. pp. 235-244
- Hurst D. F., Bakwin P. S., Myers R. C., and Elkins J. W. (1997) Behavior of trace gas mixing ratios on a very tall tower in North Carolina. *Journal of Geophysical Research-Atmospheres* 102(D7), 8825-8835.
- Keeling R. F. and Shertz S. R. (1992) Seasonal and interannual variations in atmospheric oxygen and implications for the global carbon cycle. *Nature* 358(6389), 723-727.
- Keeling R. F., Stephens B. B., Najjar R. G., Doney S. C., Archer D., and Heimann M. (1998) Seasonal variations in the atmospheric O₂/N₂ ratio in relation to the kinetics of air-sea gas exchange. *Global Biogeochemical Cycles* 12(1), 141-163.
- Severinghaus J. P. (1995) *Studies of the terrestrial O₂ and carbon cycles in sand dune gases and in biosphere 2*. Ph.D. thesis, Columbia University, 148 pp.
- Stephens B. B., Bakwin P. S., Tans P. P., Teclaw R. M., and Baumann D. D. (2007) Application of a differential fuel cell analyzer for measuring atmospheric oxygen variations. *Journal of Atmospheric and Oceanic Technology* 24(1), 82-94.
- Stephens B. B., Keeling R. F., Heimann M., Six K. D., Murnane R., and Caldeira K. (1998) Testing global ocean carbon cycle models using measurements of atmospheric O₂ and CO₂ concentration. *Global Biogeochemical Cycles* 12(2), 213-230.
- Sturm P., Leuenberger M., Moncrieff J., and Ramonet M. (2005a) Atmospheric O₂, CO₂ and δ¹³C measurements from aircraft sampling over Griffin forest, Perthshire, UK. *Rapid Communications in Mass Spectrometry* 19(17), 2399-2406.
- Sturm P., Leuenberger M., and Schmidt M. (2005b) Atmospheric O₂, CO₂ and δ¹³C observations from the remote sites Jungfraujoch, Switzerland, and Puy de Dome, France. *Geophysical Research Letters* 32(17), -.

Chapter 5.

Correlations between diurnal variations of atmospheric oxygen and carbon dioxide

5.1	Background and introduction	155
5.2	Methods	156
5.2.1	Measurement site and data	156
5.2.2	Data processing	159
5.2.3	Errors affecting the calculated O ₂ :CO ₂ ratio	160
5.3	Results and discussion	161
5.4	Summary and conclusions	166
5.5	References	167

Abstract

The correlation between the variations of atmospheric oxygen and carbon dioxide is currently used to constrain sources and sinks of atmospheric CO₂. This utilization relies on the fact that, for land sources and sinks (fossil fuel and land biosphere), the gas exchange of the two species is linked by stoichiometric factors. For the exchange between land biosphere and atmosphere, the presently assumed O₂:CO₂ ratio is -1.1 ± 0.05 (Severinghaus, 1995). How precise is the estimation of this ratio, what is its natural variability and which are the potential influence factors – these questions are still open.

The present work tries to partly answer these questions, by looking at CO₂ and O₂ signals from a continental tall tower measurement, with focus on diurnal time scale variations. The continental location has the advantage of strong land biosphere signals, with good time resolution.

The observed O₂:CO₂ ratio for diurnal signals affected mainly by land biosphere is systematically less negative than expected. The temporal variation of this ratio suggests possible influences of meteorological conditions.

5.1 Background and introduction

Atmospheric oxygen measurements have been used increasingly in the past years to distinguish between sources of CO₂ and causes of its variability (Keeling, 1988b). The oxygen variation helps to partition the carbon uptake between land and ocean (e.g. Keeling and Shertz, 1992, Bender et al., 2005, Manning and Keeling, 2006), to estimate the biological productivity in the ocean (Keeling and Shertz, 1992, Bender et al., 1996, Balkanski et al., 1999), the gas exchange between the ocean and the atmosphere (Keeling et al., 1998) and oceanic transport (Stephens et al., 1998, Gruber et al., 2001).

The main sources / sinks for both atmospheric CO₂ and oxygen are land biosphere (mainly photosynthesis and respiration), fossil fuel combustion and the gas exchange with oceans. Whereas the land biosphere and the fossil fuel combustion influence the oxygen and CO₂ in a stoichiometric proportion, the exchange between ocean and atmosphere of the two gases is driven by non-correlated factors.

The ratio in which oxygen is consumed when CO₂ is produced by fossil fuel burning (the oxidative ratio) is depending on composition of fuel. For example, complete burning of pure carbon would consume 1 mol of oxygen for each mol of CO₂ produced; in case of methane two moles of oxygen are needed to obtain one mol of CO₂. The global average ratio for the fossil fuel burning was estimated at about 1.4 moles of O₂ consumed per mole of CO₂ produced (Keeling, 1988a).

For land biosphere two approaches have been used to infer the oxidative ratio. The first one is based on chemical plant and soil organic matter composition (Severinghaus, 1995, Randerson et al., 2006). The second approach is based on direct observations of correlation between measured atmospheric oxygen and CO₂ variations (Severinghaus, 1995, Luecker et al., 2001, Seibt et al., 2004). However, the estimations done so far by both methods suffered from scarcity of data. Following these studies, the average oxygen to CO₂ ratio for the land biosphere - atmosphere exchange presently used is:

$$\text{O}_2(\text{mol}) : \text{CO}_2(\text{mol}) = - 1.1 \pm 0.05$$

Stephens et al., 1998 defined the tracer APO (Atmospheric Potential Oxygen). A simplified definition of APO, without accounting for the small influences of CH₄ and CO, is:

$$\text{APO (permeg)} = \text{O}_2/\text{N}_2 \text{ (permeg)} + 1.1 \times 4.8 \times (\text{CO}_2 \text{ (ppm)} - 350);$$

where:

4.8 is conversion factor for CO₂ units;

-1.1 is the specific ratio for land biosphere – atmosphere exchange

APO is by definition invariant to land biosphere – atmosphere exchange of CO₂ and O₂, as long as this exchange respects the proportion of -1.1 between O₂ and CO₂. This makes it useful to distinguish the oceanic influence and in a smaller amount, the fossil fuel influence.

On the other hand, atmospheric measurements at ecosystem level on short time scale (hours to weeks) had shown significant variability of soil exchange and assimilation O₂:CO₂ ratio (e.g. Seibt et al., 2004). Such results must be taken into account when using APO on small spatial or temporal scales. Also, more investigation appears necessary for better understanding and constraining the spatial and temporal variability of the oxidative ratios of organic matter involved.

This chapter presents CO₂ and O₂/N₂ measurement results from the tall tower station at Bialystok, Poland. The intra-continental location, in the proximity of land sources, provides strong land signals with good time resolution. Oxygen and carbon dioxide are measured in air sampled from five heights of the tower; the footprint of different sampling heights ranging between few km and few hundreds of km. The measured air carries both fossil fuel and land biosphere signals in variable proportions. By using a large amount of continuous, high precision measurement data it is possible to learn more about the O₂:CO₂ ratio for different temporal and spatial scales, specific to different processes affecting the two gas species.

5.2 Methods

5.2.1 Measurement site and data

The source of the CO₂ and O₂/N₂ data is the quasi-continuous in-situ measurement from the Bialystok tall tower station (53°13'N, 23°01'W, 180 masl). Because of intra-continental location of the station, the short term signal contains both anthropogenic and local biosphere signatures. The area surrounding the tower on a radius of few tenths of kilometres is flat, covered by forests, crops and pastures. The population density is low; the nearest town Bialystok with about 300000 inhabitants is situated about 20 km SE. The

land biosphere influence strongly dominates the variations observed at lower sampling heights in the vegetation period.

The time series used here cover the time interval between 26-Jul-2005 and 1-Feb-2007. The air is sampled from five heights of the tower: 5, 30, 90, 180 and 300 m. The CO_2 mole fraction and O_2/N_2 ratio are measured from the same air sample, after the air has been dried at a dewpoint of about -82°C . The sampling lines from different heights are measured alternately and intercalated with calibration and target gases measurements. In this way, the air from each height gets to be measured once every few hours and the time distribution is not regular. Also, the data density for different heights is not similar. Figure 5.1 shows an example of CO_2 and O_2/N_2 measurement results for a 24-hours interval. Different colours represent the different sampling heights. As it can be observed in the figure, the measurement for each sampling line is repeated few times before switching to another line; this is being done for quality check purpose. Each measurement point represents the average over a three minutes interval.

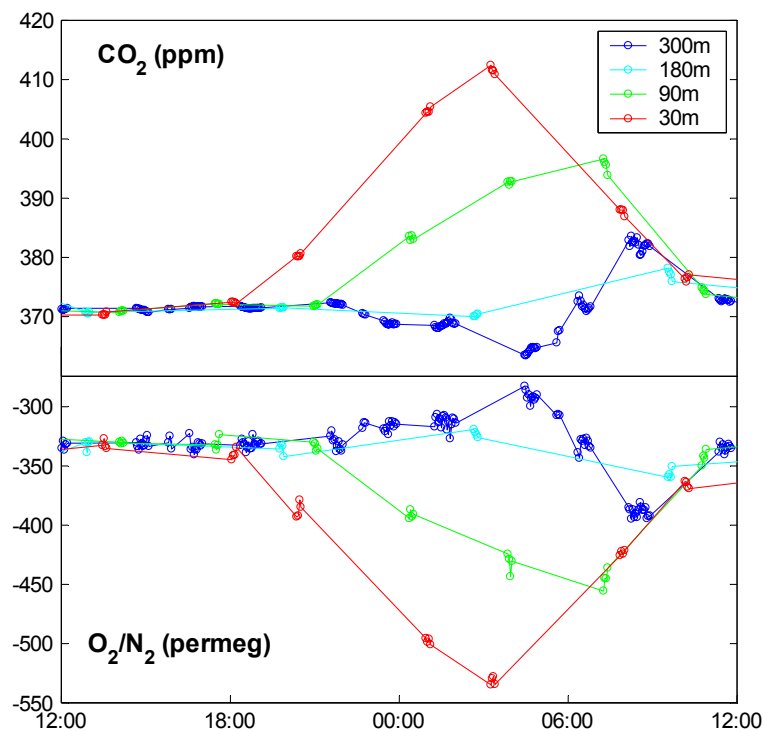


Figure 5.1 Summer typical day – night variation of CO_2 (up) and O_2/N_2 (down) for different sampling heights. The colours represent different sampling heights.

The data have been quality checked and flagged. The precision assumed is 0.1 ppm for CO₂ and 5 permeg (~1 ppm) for O₂/N₂ data, resulted from the long term standard deviation of the results of the target measurements. Comparisons with flasks sampled at the same location and measured by the MPI-BGC Gas- and IsoLab showed no scale shifts or systematic deviations, in the limits of the assumed precision. The data from lowest sampling level (5 m) are not used because of a suspected oxygen fractionation problem.

The CO₂ and O₂/N₂ measurement method has been explained in detail in Chapter 2, and Chapter 1 includes a more extended description of the site. Detailed information about the data precision, accuracy and validation can be found in Chapter 3.

The meteorological data are provided by the meteorological station Bialystok (station code 122950, 53°06'N, 23°10'E, 151 masl), situated at about 20 km distance. The parameters available are: air temperature, air pressure, dewpoint, precipitation quantity, wind speed and direction. The data have hourly time resolution, except for the precipitation which is being measured once every 6 to 24 hours.

General features of the measurement data

During the vegetation period there is a strong diurnal variation in the CO₂ mixing ratio and O₂/N₂ ratio for the air sampled close to the ground level, which attenuates with the increase of the sampling height. The lower levels suffer a stronger local influence and the land biosphere has a significant contribution to it.

There are few hours in the afternoon when the air column is well mixed, while by night the vertical gradient becomes significant, with an increase of CO₂ close to the ground, associated oxygen depletion. The largest part of the CO₂ accumulation is due to the land biosphere respiration. The CO₂ concentration at 300 m level remains almost stable by night and increases sharply in the morning, due to vertical transport from lower levels. By day, when the net exchange between the biosphere and atmosphere is dominated by photosynthesis, the air is well mixed up to typically 1-3 km. Thus the decrease of mixing ratio due to photosynthesis which is very small due to strong dilution in the air column.

In winter months the vegetation signal is less significant and the synoptic signals much stronger. The night time vertical gradient becomes less evident, partly due to the decrease in local CO₂ biospheric source and partly because of increased atmospheric instability. However, there is still a small diurnal variation, caused probably by a small biospheric activity and by periodic human emissions from transport, energy use etc.

5.2.2 Data processing

The ratio between the oxygen and CO₂ variations ($\Delta O_2(\text{ppm}) : \Delta CO_2(\text{ppm})$), named in what follows O₂:CO₂) was calculated as slope of a MODEL-2 least squares fit (York et al., 2004); the method is described in detail in Appendix 4. In summary, it uses a least squares fit function which minimizes the perpendicular distance of measurement points to the fitted line, taking into account for the weighting function the measurement errors on both x and y axes. The function is symmetrical on x and y e.g. is invariant at axes interchange (in case of axes switch, the new slope is the reciprocal of the old one). The measurement uncertainty assigned for linear fit calculation is 0.1 ppm for CO₂ and 1 ppm for oxygen, resulted from the overall target tank standard deviation.

The ratio for the diurnal variation (for each height of the tower separately) was calculated for each 24-hours interval of the vegetation period, for data between 12:00 GMT and the same hour next day. For this data set, the vegetation periods considered are: 25-Jul-2005 to 1-Oct-2005 and 1-Apr-2006 to 1-Oct-2006; there is a gap in data from 9-May-05 until 9-Jun-05 caused by technical problems.

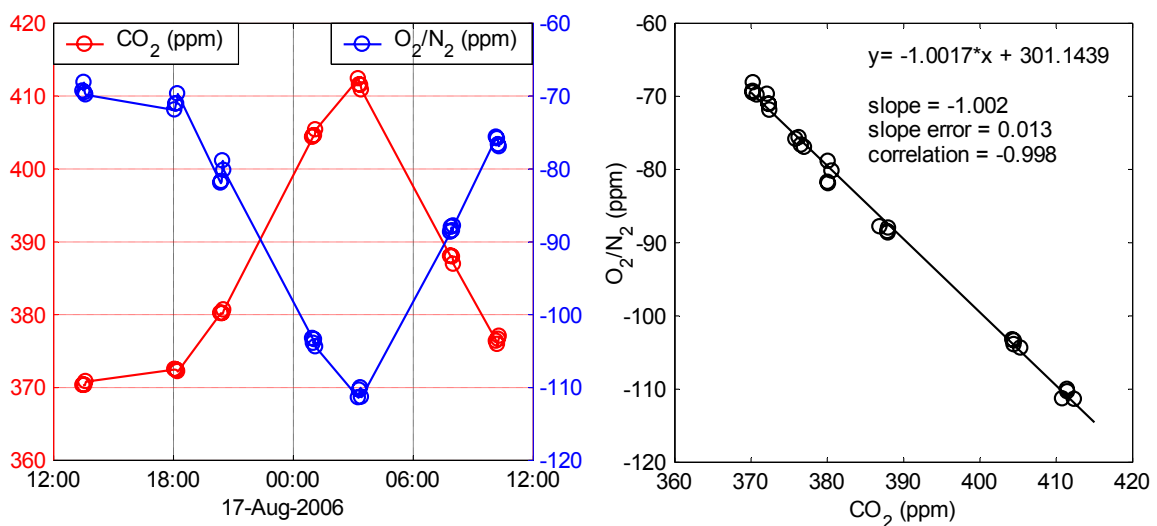


Figure 5.2 Illustration of CO₂ and O₂/N₂ variations over 24-hours (sampling height 30 m) and the corresponding O₂:CO₂ ratio calculated as slope of a linear fit.

For each sampling height the 24-hours intervals have only been used when at least five measurement points for the respective height were available. Also the results of poorly defined fitted lines were excluded: 20 from 208 results have been rejected because

the standard error for the O₂:CO₂ slope was larger than 0.1 or the correlation between the CO₂ and O₂/N₂ data was smaller than 0.9.

5.2.2 Errors affecting the calculated O₂:CO₂ ratio

The linear fit is affected by the measurement error and the “natural” error. The measurement error includes the measurement noise and the sampling error. The “natural” error comes from the fact that, even with perfect measurement, the real O₂ and CO₂ would not have a perfect linear relationship. The resulting error for the fit is estimated based on the data variability as described in Appendix 1.

A supplementary error for the linear fit in this particular case comes from the assignment of uncertainties for the measured O₂ and CO₂ (1 ppm for O₂, 0.1 ppm for CO₂). The result of the fitting is depending on the ratio between x-axis and y-axis “known” errors. In this case, the error for each data point is not known and the mean standard deviation of the target measurement over the whole interval was assigned as uncertainty for each data point. This approximation does not affect the mean result over the whole dataset considered. However, it is possible that proportion between x and y errors for a certain time interval was in reality different from the considered one.

To test the effect of erroneous error attribution, the linear fits were recalculated for different pairs of CO₂ and O₂ uncertainties, in the intervals [0.03, 0.2] ppm for CO₂ and [0.5, 2] ppm for O₂. This cover the range considered possible for our measurement system. The mean difference between the new calculated slopes and the initial ones was smaller than 0.01, which can be considered negligible. Supplementary tests showed that the slope error due to the approximation in error assignment is negligible, as long as one of the errors is at least three times bigger than the other, like in this case.

5.3 Results and discussion

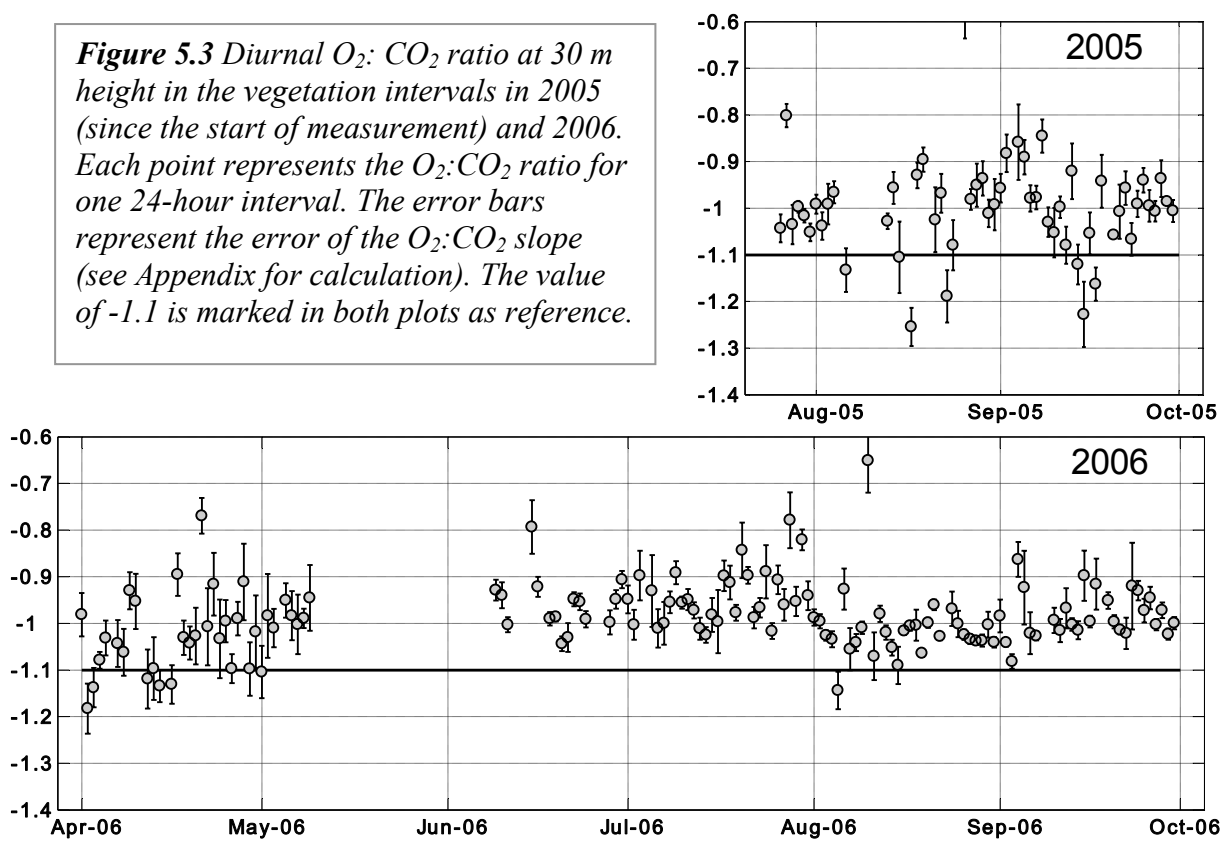
Absolute values of O₂:CO₂ ratio

Figure 5.3 shows the O₂:CO₂ ratio results for the diurnal signal at 30 m above ground. Each data point represents the ratio calculated for one 24-hours interval (starting

at 12:00 GMT), as slope of the MODEL-2 least squares fit. The error bars represent the estimated error of the slope.

The absolute value of calculated ratio is consistently lower than expected. The measured air carries mostly land biosphere and fossil fuel signal. Ocean influence is not strong at this location and not significant on such short time scales like the diurnal variations. For the 30 m level, model results and the CO variation (measured in parallel) suggest that the anthropogenic sources account on average for less than 10% of the total diurnal signal, the rest being due to land biosphere respiration (see Chapter 4, section 4.4.2). As already mentioned, the generally accepted values for O₂:CO₂ corresponding to the land biosphere is -1.1, and -1.4 for fossil fuel combustion. The observed ratios should mostly result from a combination of these two factors and consequently range within this interval (-1.4, -1.1). This is obviously not the case here, as most of the results are significantly less negative than -1.1. That means that the current knowledge on O₂:CO₂ ratios for the land biosphere is not well describing the situation for the Bialystok tall tower site.

Figure 5.3 Diurnal O₂: CO₂ ratio at 30 m height in the vegetation intervals in 2005 (since the start of measurement) and 2006. Each point represents the O₂:CO₂ ratio for one 24-hour interval. The error bars represent the error of the O₂:CO₂ slope (see Appendix for calculation). The value of -1.1 is marked in both plots as reference.



While the cause determining these values for the O₂:CO₂ ratio is not clear, there are some possible processes that could result in these values.

It is possible that an ecosystem dominated by herbaceous crops and deciduous tree species has a lower oxidative ratio than the global average. The fast growing plants contain in a bigger proportion chemicals with lower oxidative ratios, like cellulose and starch. Also, the ploughing and grazing can cause an increase in the oxidation state of carbon in plants and so a decrease in the oxidative ratio (Randerson et al., 2006).

The plant nitrogen fixation in the absence of light is done by mitochondrial dissimilation of carbohydrates, which has as result a release of CO₂ but it does not involve any exchange of oxygen with the atmosphere (Galloway et al., 2004). This is a source of CO₂ not compensated by any oxygen uptake.

The lowest sampling height considered here is 30 m above ground level. If the oxygen released by photosynthesis during day accumulates in or near the soil and is used preferentially by night, this could lead to observing a lower O₂:CO₂ ratio at 30 m height. For example, Seibt et al (2004) found that the canopy air O₂:CO₂ ratios were significantly lower than the exchange ratios of net turbulent fluxes between the ecosystem and the atmosphere.

Soil respiration can also show a quite wide range of O₂:CO₂ ratios, depending on the soil composition (nitrogen content), water content and different diffusion coefficients of oxygen and carbon dioxide from the soil.

Temporal variation of O₂:CO₂ ratio

The results show also a significant temporal variation which cannot be explained by the assigned errors. These variations could be linked to variations of meteorological parameters in the same time interval, as can be seen in figure 5.4. An illustrative example is the comparison of the months of July and August 2006: July was dry and hot, with low relative humidity (and consequently high vapour pressure deficit, VPD) and the O₂:CO₂ ratio less negative (~ -0.95); August was wetter and colder and the corresponding O₂:CO₂ ratio became more negative (~ -1.05).

There are some mechanisms by which the observed O₂:CO₂ ratio variability could be linked to variations of the meteorological variables. These mechanisms do not exclude each other and it is likely the results observed are determined by a combination of phenomena. Some of the possible paths by which the meteorological situation could have influenced the observed O₂:CO₂ ratios are discussed in what follows.

A first hypothesis is that there is a connection between atmospheric temperature or humidity and the chemistry of the land biosphere respiration, generating the observed temporal variation in the O₂:CO₂ ratio. The atmospheric temperature and humidity could affect directly the chemical processes involved in dark respiration, or the proportion in which different chemical reactions or different carbon pools contribute to respiration. Also the proportion between the autotrophic and heterotrophic respiration could change. For example, the respiration increases approximately exponentially with the temperature (e.g. Lloyd and Taylor, 1994) but high temperature associated with drought leads to a decrease in respiration, because the water becomes the limiting factor. If the above ground vegetation is strongly affected by drought but the soil still contains sufficient water, the proportion of the soil respiration increases.

If the plant nitrogen fixation is affected, this could also change the O₂:CO₂ ratio by changing the quantity of CO₂ released into the atmosphere which is not balanced by a corresponding oxygen uptake.

Another dry period, at the end of August 2005, shows also O₂:CO₂ ratio around -0.95, although the temperature and the VPD were not as high as in July 2006. This would suggest a second hypothesis, that the precipitation has a direct effect on O₂:CO₂ ratio, not only by changing the atmospheric humidity. The influence of precipitation on O₂:CO₂ ratio could be related to the gases circulation in soil. The quantity of water in soil could affect the CO₂ and O₂ transport in different ways and would also dissolve the two gases in different proportions, modifying the ratio of exchange with the atmosphere without the actual soil respiration being changed. The upper layer of the soil in this region is sandy and thus quite susceptible to loose easily the water, which gives importance to precipitation.

Another mechanism which could potentially affect the ratio between the oxygen and CO₂ variations is the gas exchange between the soil and the atmosphere, driven by fluctuations in the atmospheric pressure. The two gases CO₂ and O₂ have different diffusivity coefficients in soil. In case of atmospheric pressure variations, the in- or out-gassing of the soil air would transport CO₂ and oxygen in proportions dependent on their soil diffusivities.

The third hypothesis is that the atmospheric transport could induce the temporal variations of O₂:CO₂ ratio, by bringing air masses which had suffered different influences. Although the air at 30 m above ground is by night mostly locally influenced, the vertical transport partly mixes it with air from higher altitude which has a much larger

influence area. Comparing again the months of July and August 2006 one can observe the stable weather in July, which implies lower vertical mixing during night, while the August weather was unstable, dominated by strong synoptic events and low atmospheric pressure.

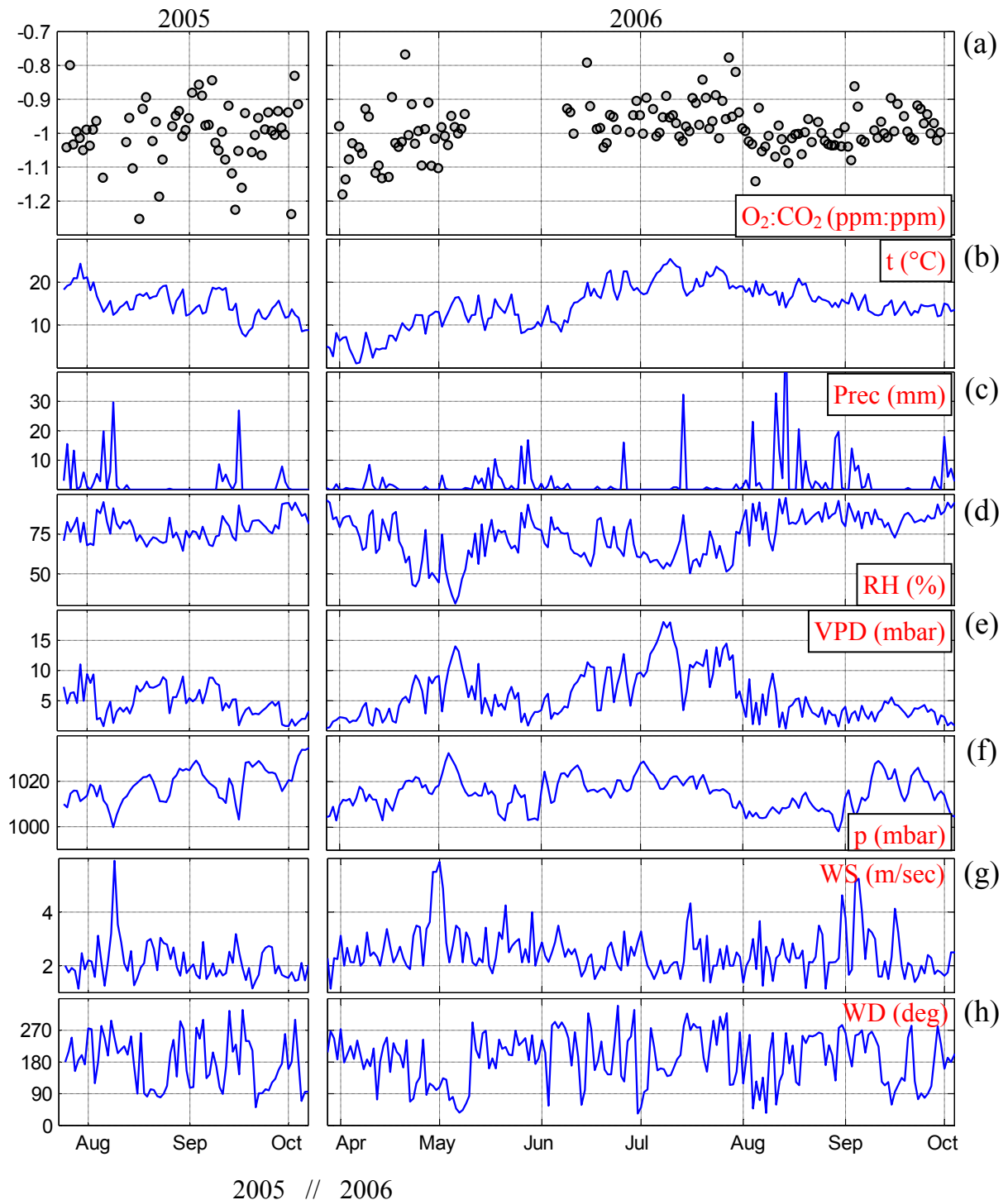


Figure 5.4 a) Diurnal $O_2:CO_2$ ratio at 30 m height in the vegetation intervals in 2005 and 2006; b-h) Daily averaged meteorological parameters: b) atmospheric temperature; c) precipitation; d) relative humidity; e) vapour pressure deficit; f) atmospheric pressure; g) wind speed; h) wind direction

Figure 5.5 shows the comparison between the O₂:CO₂ ratios calculated for the 30 m sampling height with the ratios calculated in similar manner for 90 and 300 m sampling heights. The colours represent different sampling heights.

In summer and on such short time scale (24 hours) the variation in CO₂ concentration at higher levels is strongly influenced by the vertical transport. In consequence, the origin of the CO₂ signal is at least partly the local biosphere respiration. However, in the absence of night time vertical mixing, a bigger proportion of the CO₂ at higher levels is horizontally transported from other places, potentially with a stronger anthropogenic or oceanic influence.

Looking at figure 5.5, the vertical gradient of the O₂:CO₂ ratio seems to confirm the differences in the vertical mixing between July and August 2006. In July, the vertical gradient is evident, the ratio becoming more negative with the increase in sampling height. Considering that the O₂:CO₂ ratio is typically more negative for anthropogenic sources than for land biosphere gas exchange, the more negative ratio observed at higher sampling levels suggests a higher proportion of anthropogenic CO₂. In August 2006 the vertical gradient of the O₂:CO₂ ratio is not very obvious. The ratio at 30 m level is more negative than in July and the ratio at 300 m level is less negative, so probably the lower sampling level receives via vertical mixing more anthropogenic influence while the highest level sees more of the respired CO₂. This is giving clear evidence that the time variations of the O₂:CO₂ ratio at 30 m above ground are at least partly due to differences in the vertical mixing. However it does not exclude the other possible influence factors mentioned before.

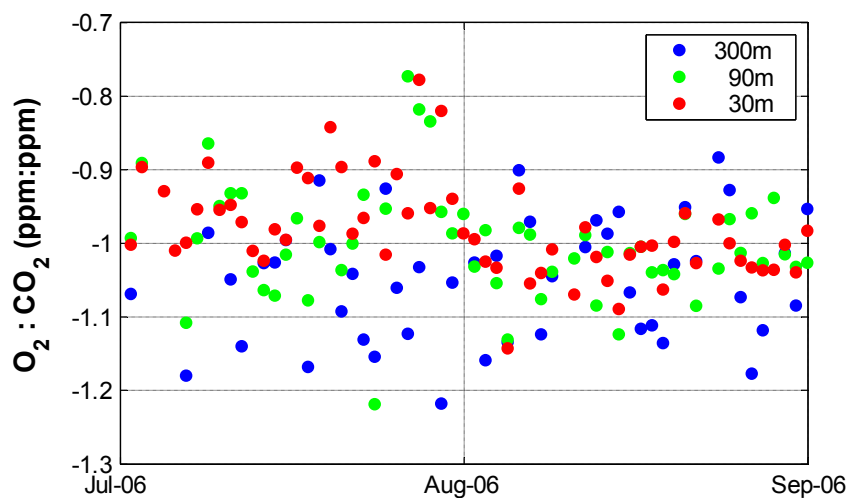


Figure 5.5 Daily O₂:CO₂ at 30, 90 and 300 m above ground level

5.4 Summary and conclusions

The observed O₂ to CO₂ ratio for the day – night variation in the vegetation period is systematically less negative than -1.1. This does not correspond to a combination of the two generally accepted mean oxidative ratios, -1.1 for the land biosphere and -1.4 for the fossil fuel burning. A periodical ocean influence on this short time scale (24 hours) and close to the ground is improbable.

The results presented here for the O₂:CO₂ ratio are apparently not consistent with the generally used land biosphere specific factor of -1.1, but they are in agreement with other more recent studies (e.g. Seibt et al., 2004, Stephens et al., 2007). However, these observations do not necessarily imply a higher than expected oxidative ratio of the local land biosphere. A combination of different processes with different temporal variations could lead to the same results.

Land biosphere processes have up to now been thought not to have any impact on APO. In this situation, interpreting the variations of APO in the data set presented here as oceanic or fossil fuel influence would be erroneous. If APO is calculated using the -1.1 factor and in reality the integrated signal of exchange between land biosphere and atmosphere has for example an average ratio of -1.0, then the APO will present a significant diurnal cycle even without any oceanic or anthropogenic influence.

The fact that the APO is assumed invariant to the land biosphere is frequently used to separate the oceanic and the land biosphere components of the seasonal cycle of O₂/N₂. This approach is applied in Chapter 4, section 4.5.2 for the O₂/N₂ seasonal variation observed at Bialystok. The partition based on APO lead to an estimation of the oceanic component at 23% from the seasonal cycle, the rest of 77% being due to the land biosphere. Supposing that the real O₂:CO₂ ratio of the land biosphere signal at this location is -1 instead of -1.1, and changing this factor into the APO definition, leads to a new estimate of the oceanic component at 29%, which is a significant change compared to the previous estimate of 23%.

However, generalizing the results obtained here for the short term O₂:CO₂ ratios to seasonal time scale must be done carefully, since different processes may be dominating on such different time scales. Moreover, the present analysis is limited to the night time evolution of atmospheric components, when respiration fluxes are dominating. Day time fluxes with the same magnitude do not lead to strong vertical gradients and to large variations of mixing ratios, because of the dilution due to the vertical mixing.

Therefore day time fluxes with different characteristic O₂:CO₂ ratios could lead to a net O₂:CO₂ ratio different from the one observed here.

Regarding the observed temporal variations of the O₂:CO₂ ratio, it is not clear from the available data if they are due to reactions of the land biosphere respiration to meteorological factors, changes in soil gases transport due to water content or atmospheric pressure variations, or variations of the atmospheric transport and of the footprint of the sampled air. Most probable is the combination of all these factors. Measurements in the canopy of the surrounding forest in parallel with the ones from the tall tower could potentially provide a better understanding on this subject.

5.6 References

- Balkanski Y., Monfray P., Battle M., and Heimann M. (1999) Ocean primary production derived from satellite data: An evaluation with atmospheric oxygen measurements. *Global Biogeochemical Cycles* 13(2), 257-271.
- Bender M., Ellis T., Tans P., Francey R., and Lowe D. (1996) Variability in the O₂/N₂ ratio of southern hemisphere air, 1991-1994 - implications for the carbon cycle. *Global Biogeochemical Cycles* 10(1), 9-21.
- Bender M. L., Ho D. T., Hendricks M. B., Mika R., Battle M. O., Tans P. P., Conway T. J., Sturtevant B., and Cassar N. (2005) Atmospheric O₂/N₂ changes, 1993-2002: Implications for the partitioning of fossil fuel CO₂ sequestration. *Global Biogeochemical Cycles* 19(4), B4017.
- Galloway J. N., Dentener F. J., Capone D. G., Boyer E. W., Howarth R. W., Seitzinger S. P., Asner G. P., Cleveland C. C., Green P. A., Holland E. A., Karl D. M., Michaels A. F., Porter J. H., Townsend A. R., and Vorosmarty C. J. (2004) Nitrogen cycles: Past, present, and future. *Biogeochemistry* 70(2), 153-226.
- Gruber N., Gloor M., Fan S. M., and Sarmiento J. L. (2001) Air-sea flux of oxygen estimated from bulk data: Implications for the marine and atmospheric oxygen cycles [review]. *Global Biogeochemical Cycles* 15(4), 783-803.
- Keeling R. F. (1988a) *Development of an interferometric oxygen analyzer*. Ph.D. thesis, Harvard University, Cambridge, Mass., 178pp.
- Keeling R. F. (1988b) Measuring correlations between atmospheric oxygen and carbon dioxide mole fractions - a preliminary study in urban air. *Journal of Atmospheric Chemistry* 7(2), 153-176.
- Keeling R. F., Najjar R. P., Bender M. L., and Tans P. P. (1993) What atmospheric oxygen measurements can tell us about the global carbon cycle. *Global Biogeochemical Cycles* 7(1), 37-67.
- Keeling R. F. and Shertz S. R. (1992) Seasonal and interannual variations in atmospheric oxygen and implications for the global carbon cycle. *Nature* 358(6389), 723-727.

- Keeling R. F., Stephens B. B., Najjar R. G., Doney S. C., Archer D., and Heimann M. (1998) Seasonal variations in the atmospheric O₂/N₂ ratio in relation to the kinetics of air-sea gas exchange. *Global Biogeochemical Cycles* 12(1), 141-163.
- Lueker T. J., Keeling R. F., and Dubey M. K. (2001) The oxygen to carbon dioxide ratios observed in emissions from a wildfire in Northern California. *Geophysical Research Letters* 28(12), 2413-2416.
- Manning A. C. and Keeling R. F. (2006) Global oceanic and land biotic carbon sinks from the Scripps atmospheric oxygen flask sampling network. *Tellus Series B-Chemical and Physical Meteorology* 58(2), 95-116.
- Randerson J. T., Masiello C. A., Still C. J., Rahn T., Poorter H., and Field C. B. (2006) Is carbon within the global terrestrial biosphere becoming more oxidized? Implications for trends in atmospheric O₂. *Global Change Biology* 12(2), 260-271.
- Seibt U., Brand W. A., Heimann M., Lloyd J., Severinghaus J. P., and Wingate L. (2004) Observations of O₂:CO₂ exchange ratios during ecosystem gas exchange. *Global Biogeochemical Cycles* 18(4), B4024.
- Severinghaus J. P., 1995: *Studies of the terrestrial O₂ and carbon cycles in sand dune gases and in Biosphere 2*. Ph.D. thesis, Columbia University, 148 pp.
- Stephens B. B., Bakwin P. S., Tans P. P., Teclaw R. M., and Baumann D. D. (2007) Application of a differential fuel-cell analyzer for measuring atmospheric oxygen variations. *Journal of Atmospheric and Oceanic Technology* 24(1), 82-94.
- Stephens B. B., Keeling R. F., Heimann M., Six K. D., Murnane R., and Caldeira K. (1998) Testing global ocean carbon cycle models using measurements of atmospheric O₂ and CO₂ concentration. *Global Biogeochemical Cycles* 12(2), 213-230.
- York D., Evensen N. M., Martinez M. L., and Delgado J. D. (2004) Unified equations for the slope, intercept, and standard errors of the best straight line. *American Journal of Physics* 72(3), 367-375.

Chapter 6.

Estimation of night time ecosystem respiration

6.1	Introduction	171
6.2	Data	172
6.3	Methods for the calculation of night time CO ₂ emission	174
6.3.1	The principle	174
6.3.2	Method 1 – daily estimation	174
6.3.3	Method 2 – monthly average	175
6.3.4	Method 3 – moving time window	177
6.4	Results and discussion	178
6.4.1	Time series	178
6.4.2	Comparison with the temperature function from Lloyd and Taylor (1994)	180
6.4.3	Calculation errors	181
6.4.4	Comment: Using the atmospheric temperature as predictor for ecosystem respiration	183
6.5	Conclusions	183
6.6	References	184

Abstract

I present a test procedure to estimate the nocturnal ecosystem respiration using only the evolution of the CO₂ vertical profile between 5 m and 300 m above ground level. One of the basic assumptions is that, during night time, the highest sampling level is located above the inversion layer and no CO₂ is vertically transported across this border.

Three calculation methods are compared, which have different time steps and are affected by different errors. The results estimated by all the three methods are in the range expected for the ecosystem respiration in a temperate region. The night time respiration shows an increase with the temperature which can be approximated by an exponential function, and a decrease in conditions of high water vapor deficit, when the humidity becomes the limiting factor. The dependence on the atmospheric temperature agrees well with the function proposed by Lloyd and Taylor (1994).

The similarity of the results of the three calculation methods gives confidence that none of them is affected by large systematic errors. Although the data series is too short to get definite conclusions, the results so far suggest that this approach can be developed into a complementary technique for the usual eddy covariance measurements.

6.1 Introduction

Land biosphere respiration accounts globally for the second largest exchange of CO₂ with the atmosphere, following the gross primary production (Prentice et al., 2001, Raich and Schlesinger 1992). Because of its higher potential variability, respiration may be more important than photosynthesis in controlling the carbon balance of the land biosphere (Valentini et al., 2000).

Up to 75% of the total ecosystem respiration is represented by the autotrophic and heterotrophic soil respiration (Law et al., 2001a, Goulden et al., 1996b, Lavigne et al., 1997, Janssens et al., 2001). The ecosystem and soil respiration depend on the availability of organic matter, soil composition and texture, water availability and temperature. For a given location, the last two explain most of the short and medium term variability.

The variation of respiration with the temperature has been extensively studied (e.g. O'Connell, 1990, Jenkinson, 1990, Schlentner & Van Cleve, 1985, Lloyd & Taylor, 1994, Fang & Moncrieff, 2001, Atkin et al., 2005) and mostly exponential type relationships have been suggested. One of the results widely used at present is the relationship proposed by Lloyd & Taylor, 1994:

$$R = Ae^{\frac{-E_0}{T-T_0}} \quad \text{where:} \quad \begin{array}{l} E_0 = 308.56 \text{ K} \\ T_0 = 227.13 \text{ K} \end{array} \quad (1)$$

Expressing the relation above relative to the respiration R_{10} at the temperature $T_{\text{ref}} = 10^\circ\text{C}$ results:

$$R = R_{10} e^{E_0 \left(\frac{1}{T_{\text{ref}} - T_0} - \frac{1}{T - T_0} \right)} \quad \text{where:} \quad T_{\text{ref}} = 283.15 \text{ K} \quad (2)$$

The usual techniques to quantify respiration are based on direct CO₂ eddy covariance flux measurements or respiration chambers. A known problem of the eddy covariance measurements is the systematic underestimation of the night-time flux, especially under low turbulence conditions (e.g. Goulden et al., 1996b). The small measurement footprint is another disadvantage, especially for the respiration chambers, making it difficult to up-scale the estimates to ecosystem or regional scale.

An alternative approach to estimate the night time carbon flux from land biosphere respiration, based on nighttime evolution of CO₂ mole fraction vertical gradients, is presented in this chapter.

6.2 Data

This study uses quasi-continuous CO₂ mole fraction measurement data from the Bialystok tall tower station (53°13'N, 23°01'W, 180 masl). The area surrounding the tower within a radius of few tenths of kilometers is flat, and covered by crops, forests, and pastures. The population density in the region is low (60/km²); the nearest town Bialystok with about 300000 inhabitants is situated about 20 km SE. The measurement series covers the time between 26-July-2005 and 1-Feb-2007.

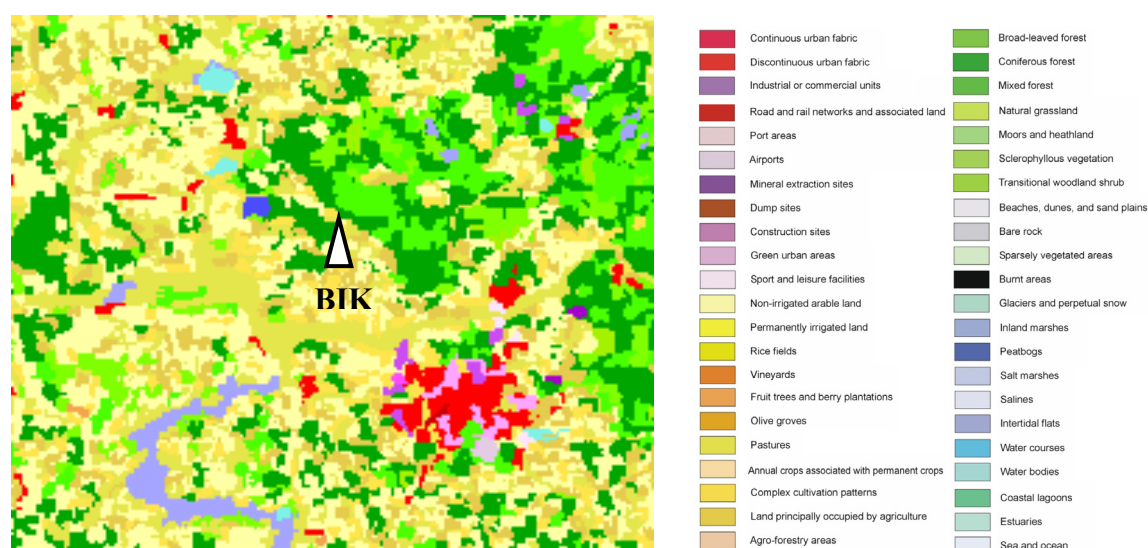


Figure 6.1 Land cover map of the area surrounding the BIK tall tower station (approx. 70 x 50 km). Map source: Corine land cover 2000 (CLC2000), <http://www.eea.europa.eu>, © EEA, Copenhagen, 2004

Air is sampled from five heights of the tower: 5, 30, 90, 180 and 300 m agl. The sampling lines from different heights are measured alternately and intercalated with calibration and target gases measurements. In this way, air from each height is measured once every few hours and the time distribution is not regular. Also, the data density for different heights is not similar. Figure 6.2 shows an example of measurement results for a 24-hour interval. Different colors represent the different sampling heights. As it can be

observed in the figure, the measurement for each sampling line is repeated several times before switching to another line; this is being done for quality check purpose. Each measurement point shown represents the average of the CO₂ mole fraction over 3 minutes.

The typical summer vertical profile reveals a night-time CO₂ accumulation at the levels close to the ground, which is released in the morning by vertical mixing. Usually there is no or little night-time increase in the CO₂ mole fraction at 300 m height, which means that no significant amount of CO₂ is vertically transported above this height. Day-time consumption of CO₂ by photosynthesis is difficult to observe, because the signal is strongly diluted by vertical mixing. In contrast, the night time respired CO₂ accumulates close to the ground in the absence of strong turbulent vertical mixing. In the warm months, most of the CO₂ accumulated by night can be assumed to be due to the local and regional land biosphere respiration, the fossil CO₂ accounting for less than 10% from total (see paragraph 4.4.2, page 134).

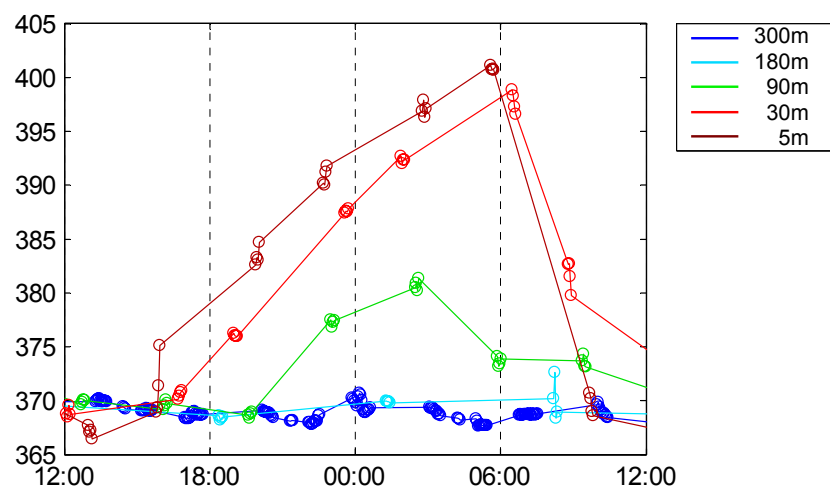


Figure 6.2 Example of CO₂ measured in air sampled at different heights above ground, over a 24-hours interval.

The meteorological data are provided by the meteorological station situated in Bialystok, at about 20 km distance (station code 122950, 53°06'N, 23°10'E, 151 masl). The parameters available are: atmospheric temperature, pressure, humidity, wind speed and direction and precipitation. The data have hourly time resolution, except for the precipitation which is being measured once every 6 to 24 hours. The time intervals

corresponding to the gaps in the CO₂ mole fraction have been eliminated also from the meteorological data.

There are no available measurements of soil moisture and leaf area index.

6.3 Methods for the calculation of night time CO₂ emission

6.3.1 The principle

During daytime when the lower atmosphere is well mixed the CO₂ mole fraction has no or little vertical gradient. By night, when the vertical mixing is low, the CO₂ emitted mostly accumulates near the ground level. Assuming that no CO₂ is transported above 300 m, the integral over height of the CO₂ mole fraction (which is the CO₂ accumulated in the air column) is proportional to the CO₂ emission rate and to the accumulation time. It is then straightforward to calculate the average CO₂ emission per time unit. The existence of a well mixed day time is an important condition for this calculation, because in the absence of a previous mixing time period, the accumulation time is not well defined.

Because of the irregular data distribution shown in figure 6.2, the estimation of the CO₂ emission for each individual night is difficult. Three different methods have thus been tested, for which the calculation procedure is described in what follows.

6.3.2 Method 1 – daily estimation

The start of the accumulation time is chosen as the time of the measurement from 5 m height which is the closest to 19:30. The time when the 5 m level reaches its maximum mole fraction is taken as the end of the accumulation time. Because the different heights are not measured at the same time, the mole fraction values at the respective moments for all levels except for the 5 m level are calculated by linear interpolation. The integrals over height at both the start and the end time of the accumulation are calculated (figure 6.3). The difference between the two integrals represents the total CO₂ accumulated in the respective time interval. The mole fraction between 0 and 5 m above ground is assumed to be constant.

From the total data series have been selected only the “stable” nights (for which the measurement from 300 m had a variability of less than 5 ppm), with sufficient data coverage and preceded by a well mixed day time. Following this data selection, only a number of 48 nights are considered. None of the winter nights satisfied these conditions.

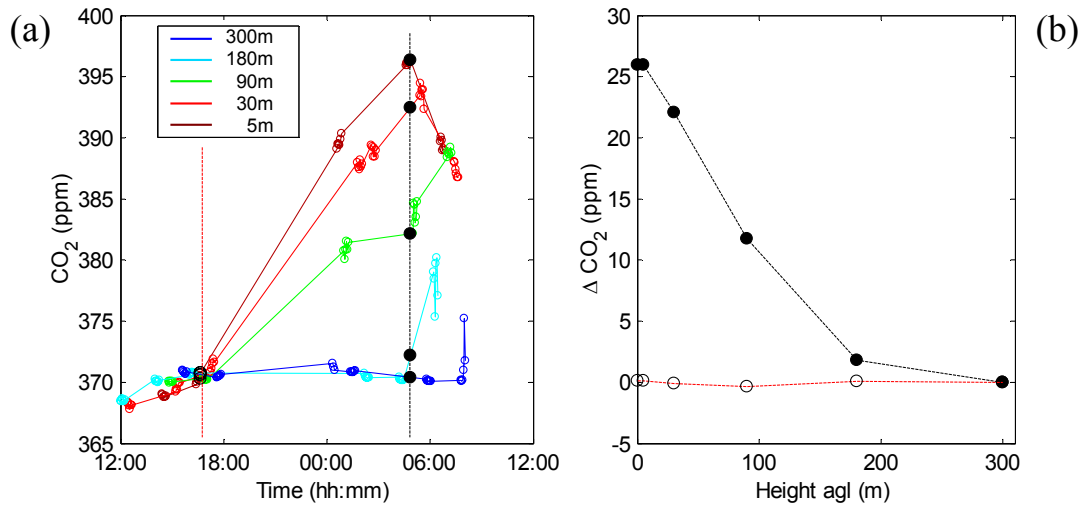


Figure 6.3 Illustration of night time CO₂ emission calculation for method 1. (a) CO₂ mole fraction at different heights above ground. The dashed lines mark the start and the end time of the accumulation. (b) CO₂ vertical gradient (referenced to the CO₂ mole fraction at 300 m agl) corresponding to the start (red dashed line) and end time (black dashed line) of accumulation. ΔCO_2 is the difference between the CO₂ mole fraction at each height and the mole fraction at 300 m. The area between the two lines represents the total CO₂ accumulated in the air column.

6.3.3 Method 2 – monthly average

The data series of each month has been separated in 3-hourly bins and the average CO₂ mole fraction was calculated for each bin and sampling height (figure 6.4a). The vertical gradient was calculated taking as reference the mole fraction at 300m (figure 6.4b). The integral of the CO₂ mole fraction over height was then computed, for the 18:00 bin (which is the average of the data between 18:00 and 21:00) and at the time bin of the maximum mole fraction at 5 m level. The difference between the two integrals gives the total CO₂ accumulated in the air column per surface unit, starting from 18:00 until the

maximum mole fraction at 5 m is reached by night. The CO₂ mole fraction between 0 and 5 m above ground is assumed constant.

Figure 6.5 shows the average CO₂ daily variation for each month, for the whole measurement time. Only the months for which well mixed daily intervals exist have been selected: Aug – Sep-05 and Apr – Oct-06. The absence of any significant diurnal cycle in the cold months is due to the absence of a regular diurnal cycle of the vertical mixing, and should not be interpreted as absence of CO₂ emission.

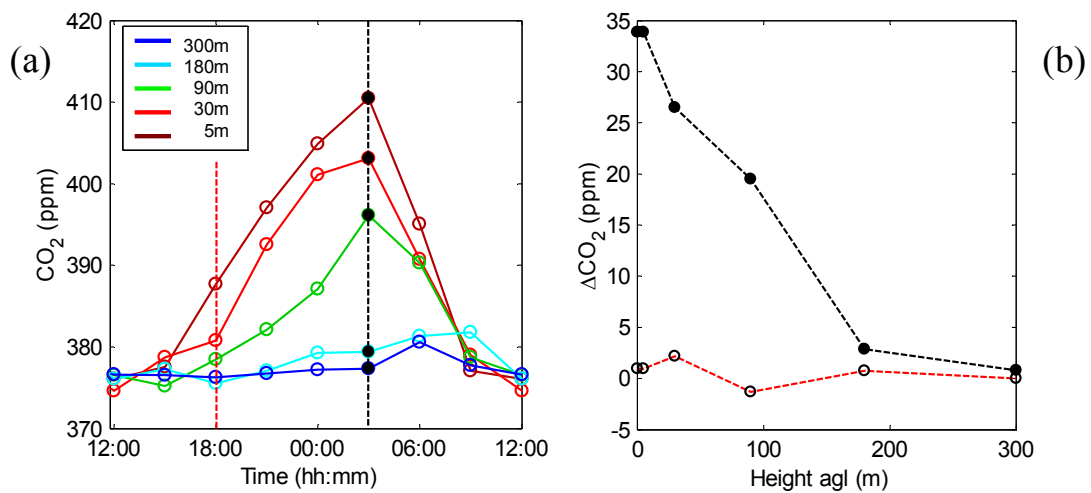


Figure 6.4 Illustration of the monthly calculation method.

(a) Mean CO₂ mole fraction for each 3-hourly bin, for each measurement height (data July-2006);

(b) Vertical mole fraction gradients corresponding to the start and the end accumulation times. Reference is the mole fraction at 300 m.

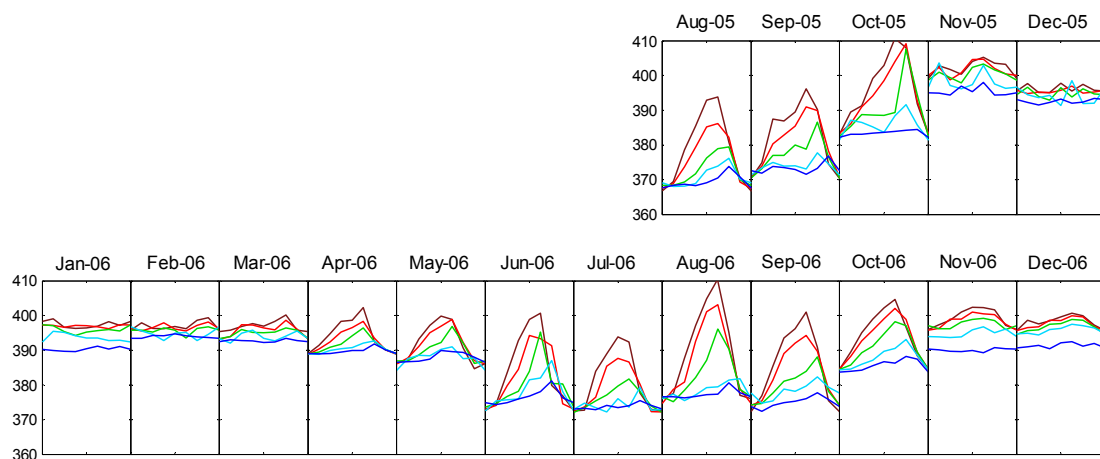


Figure 6.5 Monthly averaged diurnal CO₂ variation

6.3.4 Method 3 – moving time window

The mean nocturnal CO₂ accumulation was calculated similar as for the method 2, but for a moving time window (see figure 6.6). Different lengths of the time window and different time steps have been tested. Choosing a shorter time window decreases the number of measurement points for each time bin and thus increases the error of the estimation. A longer time window for the same time step decreases the number of final results. A shorter time step for the same time window length increases the autocorrelation of the results, while a longer time step reduces the number of the final results.

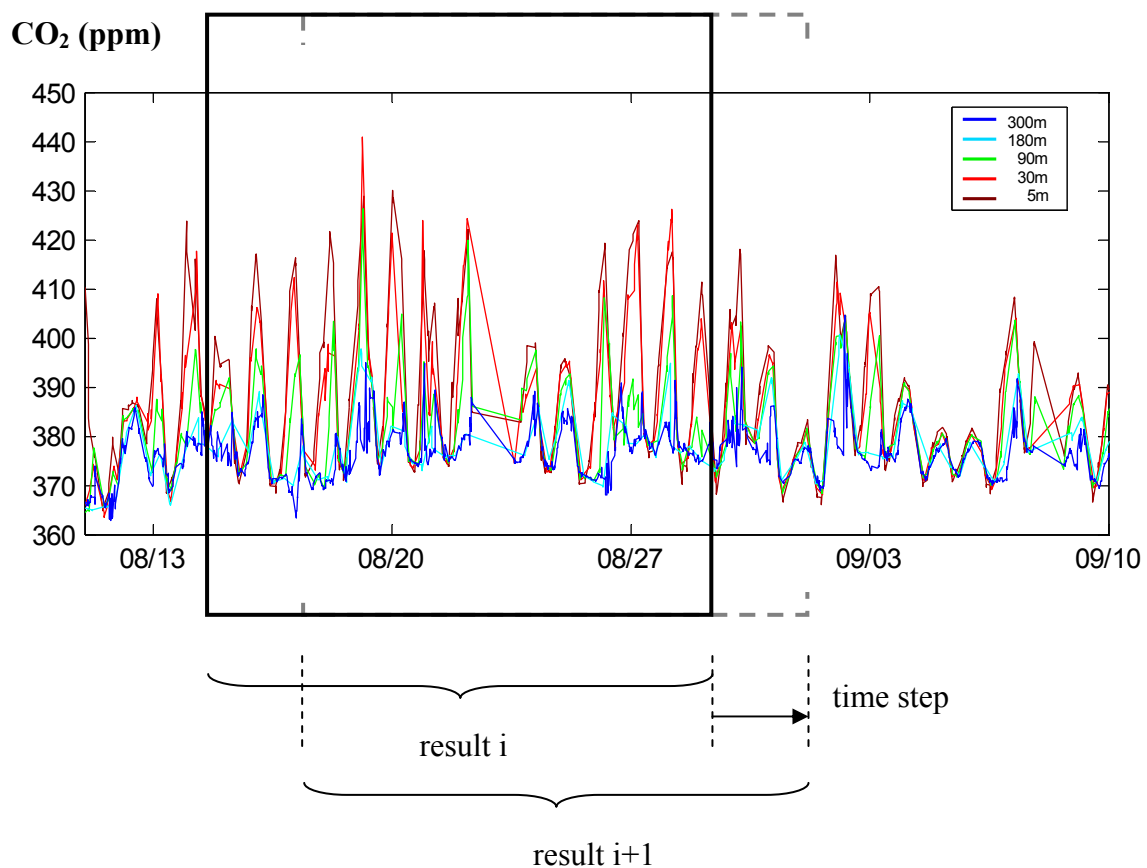


Figure 6.6 Illustration of the moving time window method

6.4 Results and discussion

6.4.1 Time series

The CO₂ emission per square meter per second, calculated by each of the three methods described, is shown in figure 6.7, together with the mean daily temperature and precipitation.

For the daily estimation (method 1), a number of 48 nights have been taken into account. Each point from the “daily” series in figure 6.7 represents the result for one night. The monthly averages (method 2) are calculated for the months Aug – Sep-2005 and Apr – Oct-2006. For the moving average (method 3) the time window was set to 20 days and the time step to 6 days (thus each point of the series “moving average” is calculated using the average of 20-nights data).

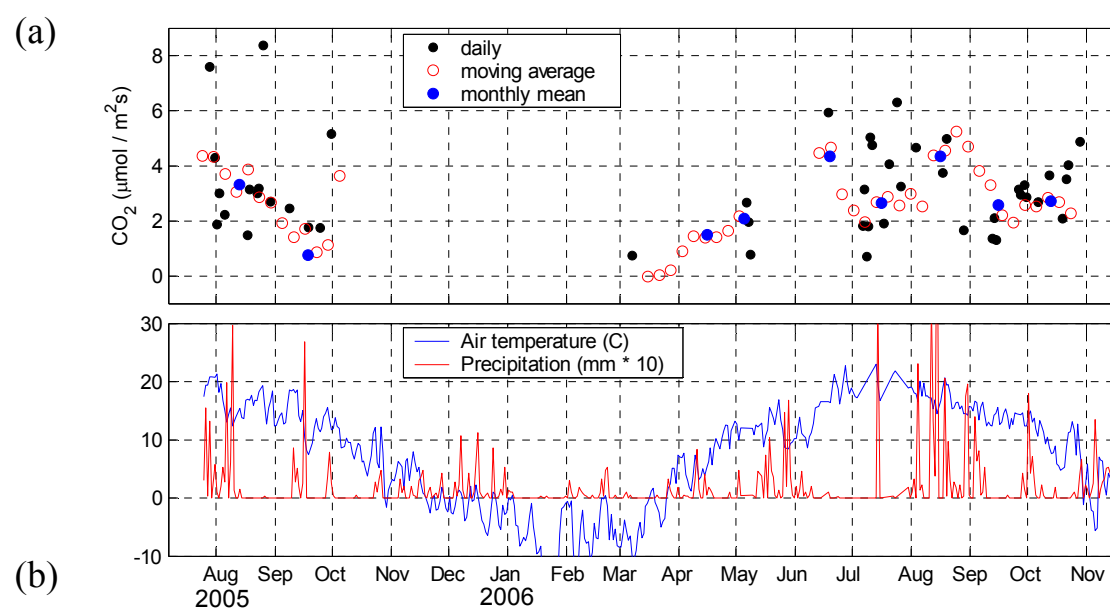


Figure 6.7 (a) Night time respiration calculated by the three methods
(b) The daily mean air temperature and daily precipitation

There are no apparent systematic differences between the results of the three methods. The calculated flux values are realistic for a temperate region (e.g Valentini et al., 2000, Kutsch et al., 2005).

As expected, the respiration calculated by each method is positively correlated with the atmospheric temperature. However there are two time intervals which seem to make an exception. In July 2006, although the temperature was high, the respiration decreased. The precipitation plot in the lower panel suggests a drought effect, which could explain the low respiration. October 2006 shows an opposite unexpected high value for the corresponding temperature.

In the following figure 6.8 the carbon flux is plotted versus atmospheric temperature, separately for the three calculation methods. Each data set has been separated in two categories based on the water vapor pressure deficit, which is taken as a measure of the water stress (the limit between the two categories was chosen arbitrarily $VPD = 10$ mbar). It is evident in the figure that the water stress decreases the respiration, balancing or dominating the temperature effect in part of the warm season. This is probably the explanation for the reduced respiration in July-2006.

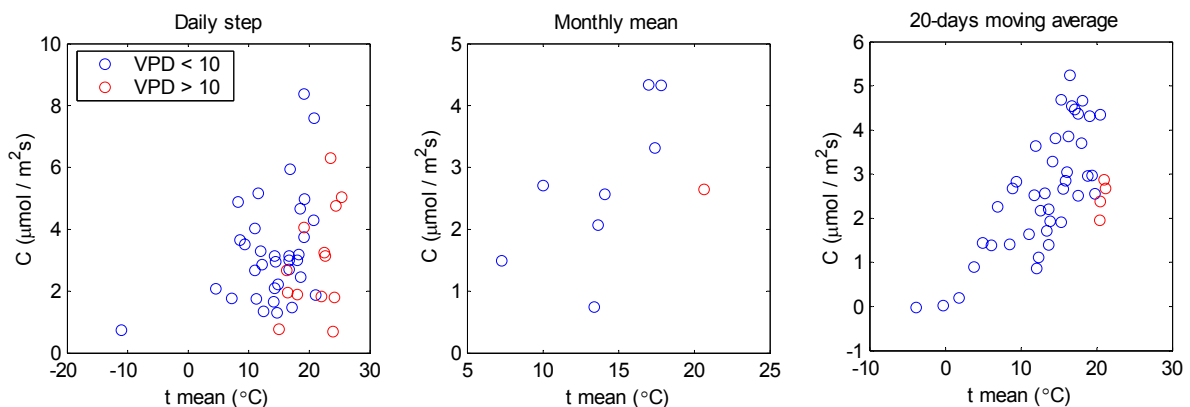


Figure 6.8 The CO_2 emission versus mean atmospheric temperature, for each of the calculation methods. The data are separated into two categories by the corresponding mean water vapor pressure deficit (VPD); the separation limit was $VPD = 10$ mbar. Note that the scales are different for the three plots.

The high respiration in Oct-2006 might be explained as follows. [1] When the atmospheric temperature decreases in autumn, the soil temperature decrease is delayed compared to the air temperature. The temperature dependence of ecosystem respiration is mostly related to the soil temperature, since the soil respiration is the largest fraction of the total respiration. [2] The leaf fall increase the available recent organic matter in the upper layer of the soil. [3] The rain in the beginning of October after a dry period

stimulates the respiration. The concomitance of the three phenomena above can lead to the effect observed in Oct-2006.

6.4.2 Comparison with the temperature function from Lloyd and Taylor (1994)

Lloyd & Taylor (1994) proposed a temperature function for soil and ecosystem respiration which gives good results for various ecosystems when the water availability is not a limiting factor (equations 1, 2, page 171). For comparison, the equation (1) was fitted to the results obtained here, excluding the respiration values for which the corresponding atmospheric water vapor pressure deficit (VPD) was greater than 10 mbar. The parameters E_0 and T_0 are the same as used by Lloyd & Taylor ($E_0 = 308.56$ K, $T_0 = 227.13$ K) and only the proportionality factor A was calculated by a robust least squares method. The reference respiration at 10°C (R_{10}) was then calculated from the fitted curve. The resulting R_{10} values based on the daily calculation, the moving average and the monthly mean results were $1.90 \mu\text{mol}/\text{m}^2\text{s}$, $1.80 \mu\text{mol}/\text{m}^2\text{s}$ and $1.89 \mu\text{mol}/\text{m}^2\text{s}$ respectively.

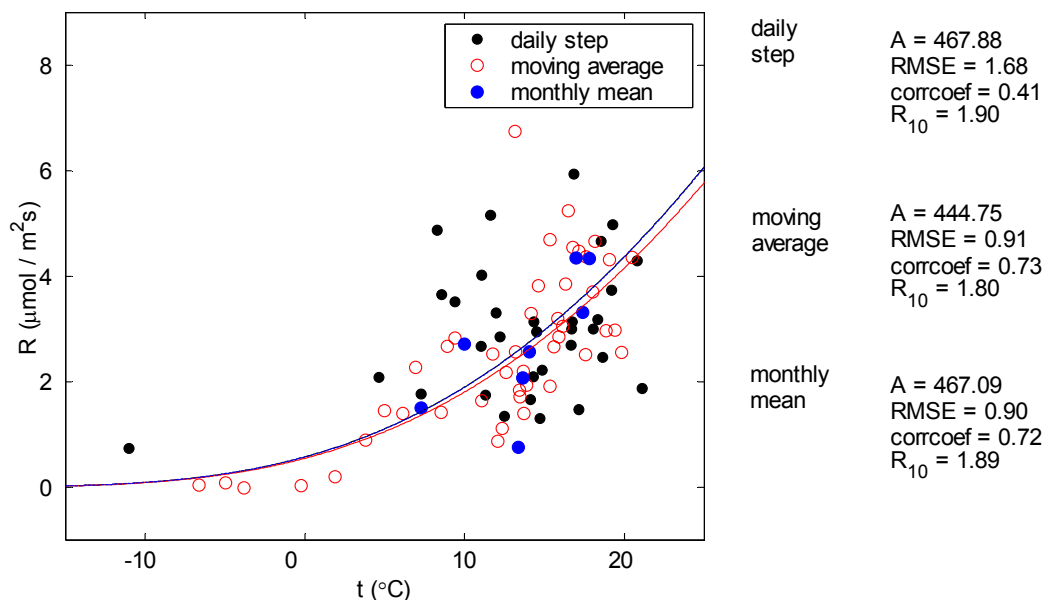


Figure 6.9 The respiration versus atmospheric temperature and the fitted Lloyd curves for the three calculation methods. The curves for the daily and the monthly step results overlap. The fitting statistics are written on the right side of the figure.

Figure 6.9 shows the respiration calculated by the three methods versus mean temperature, and the corresponding fitted curves. Some fitting parameters are listed on the right side of the figure. The three R_{10} values are similar within the error range.

Figure 6.10a shows the respiration results normalized to the corresponding R_{10} , together with the normalized respiration function (equation 2). The residuals are plotted in figure 10b. The function calculated with the parameters from Lloyd & Taylor ($E_0 = 308.56$ K, $T_0 = 227.13$ K) seems to underestimate the respiration at temperatures around 10°C , but the effect is not statistically significant for the noise range of the data. However, most of the data in this temperature range are the data from Oct-2006, for which the respiration rate is higher than expected from the temperature values, as explained before. A longer data set is probably necessary to get a clear conclusion.

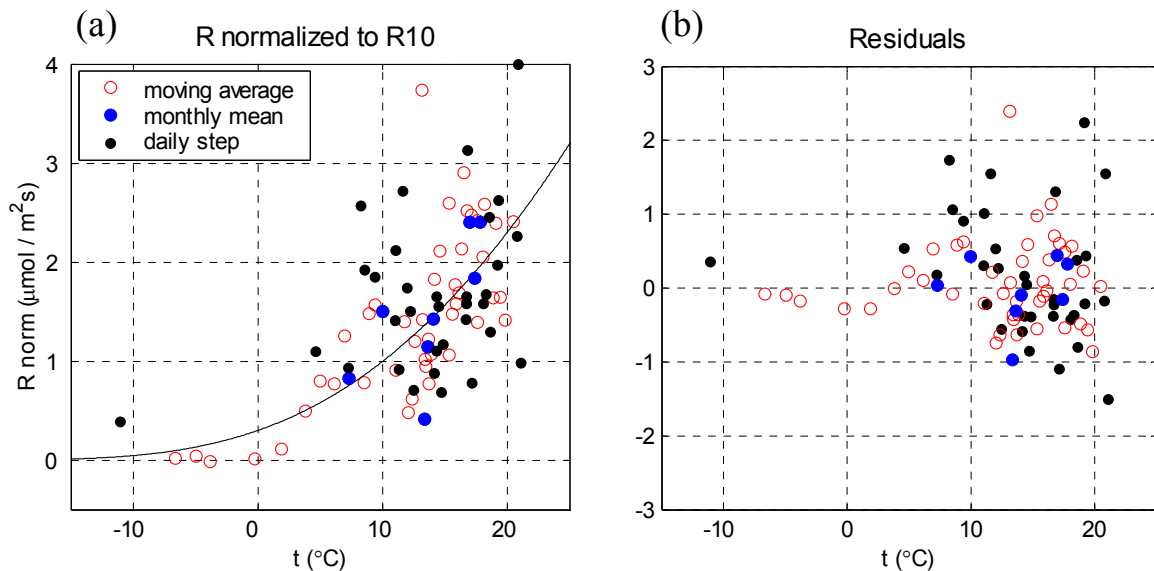


Figure 6.10 (a) The respiration normalized to R_{10} and the normalized function of temperature (equation 2); (b) Residuals of the normalized respiration

6.4.3 Calculation errors

Some of the errors possibly affecting the results presented are listed in what follows, without a quantitative estimation being possible at this stage.

In reality some of the CO_2 emitted near the ground can be transported above the 300 m height. In this case, assuming that no CO_2 is transported over the 300 m height

leads to an underestimation of CO₂ emission.

The effect of CO₂ variations due to horizontal transport is mostly cancelled by averaging, when method 2 or method 3 are used. These CO₂ variations are likely to induce some noise for the daily estimation (method 1) but the overall features, like the dependence on temperature are not strongly affected. For the daily estimation method effect is diminished by selecting only the stable nights, as described in the paragraph 6.3.2.

The assumption that the CO₂ mole fraction between the ground level and the 5m level is constant will also result into an underestimation of CO₂ emission, because most of the CO₂ is emitted from the soil and thus the CO₂ mole fraction will be higher near the ground.

For the diurnal step calculation, the use of interpolated values for the CO₂ mole fraction leads to errors with an approximately normal distribution, which means that overestimation and underestimation of the emission are equally possible. For the overall features like the temperature dependence this is seen as noise.

The same effect is produced by the CO₂ variations due to advective transport. The effect of such variations is mostly cancelled by averaging in case of the other two calculation methods.

Even in the warm periods, not all the CO₂ accumulated is produced by biosphere respiration. During summer the proportion of anthropogenic CO₂ can be reasonably assumed on the order of 5 – 10%. Thus the real respiration signal is smaller than calculated here. During the colder months, a higher proportion of CO₂ is likely to come from anthropogenic sources, thus the overestimation is even larger. The result will be improved if any supplementary constraint on the proportion of the anthropogenic CO₂ (e.g. modeling results or estimations based on CO measurements) is used for corrections.

The meteorological measurements performed at 20 km distance may induce biases as well as additional scatter on the temperature functions, but it does not affect the absolute values of CO₂ emission.

The area is in large proportion used for agriculture and grazing. It is thus possible that some of the variations observed in the CO₂ emissions time series are actually the results of some events like ploughing or harvesting.

6.4.4 Comment: using the atmospheric temperature as predictor for ecosystem respiration

On a seasonal time scale, the CO₂ function of air temperature is likely to show a hysteresis shape. That means: in the spring the soil temperature will be lower than the air temperature, and so the respiration will be lower than the prediction based on air temperature. Reversely, in autumn the decrease in soil temperature is delayed compared to the air temperature and the respiration can be higher than the prediction based on air temperature.

The soil temperature is usually higher in winter than the atmospheric temperature. In summer, the forest soil buffers the temperature extremes, but the bare soil can get warmer than the air because of lower albedo. Using the atmospheric temperature leads thus to shifting the variation of respiration function of temperature.

On a short time scale, on the order of days, the amplitude of the soil temperature variations is smaller than the amplitude of atmospheric temperature variations, the soil is thus buffering the fast changes. Looking at this time scale the apparent variation of the respiration with the temperature would be smaller than predicted by the atmospheric temperature variations.

In conclusion, the prediction of respiration based on atmospheric temperature is limited and is not suitable for fundamental respiration studies.

6.5 Conclusions

The three calculation methods yield compatible results, in terms of absolute values and in terms of dependence on temperature, although they are affected by partly different errors. This may suggest that none of them is affected by extreme errors. The choice of the calculation method should therefore be based on the data available and on the purpose of the research.

The daily step calculation method had better temporal resolution but applicability limited by the atmospheric conditions. The most precise results are obtained in case of low turbulence atmospheric conditions, contrary to the eddy covariance measurements. Thus this method could potentially be used complementarily to flux measurements. An

interesting next step would be a comparison with eddy covariance and respiration chamber measurements, for different atmospheric conditions.

However, for direct comparisons with eddy covariance or respiration chamber measurements, the representativity for each of the methods must be estimated. The eddy covariance measurements have typically an influence area of few hectares. The respiration chamber method has a representativity limited to a range between few cm² to few m². The air sampled on the tall tower at different heights has, except for the 5 m sampling level, a larger footprint area than the eddy covariance measurements. Moreover, the footprint varies with the sampling height. These differences have to be taken into account for an eventual comparison between the results of different methods.

The temperature function with the parameters from Lloyd & Taylor (1994) corresponding to $Q_{10} = 2.3$ fits well the data when the humidity is not a limiting factor for respiration. Nevertheless the air temperature alone is not the best predictor for ecosystem respiration, especially in spring and autumn. Probably the soil temperature or a combination between soil and atmospheric temperature would give better results.

6.6 References

- Atkin O. K., Bruhn D., Hurry V. M., and Tjoelker M. G. (2005) The hot and the cold: unravelling the variable response of plant respiration to temperature. *Functional Plant Biology* 32(2), 87-105.
- Fang C. and Moncrieff J. B. (2001) The dependence of soil CO₂ efflux on temperature. *Soil Biology & Biochemistry* 33(2), 155-165.
- Goulden M. L., Munger J. W., Fan S. M., Daube B. C., and Wofsy S. C. (1996a) Exchange of carbon dioxide by a deciduous forest: Response to interannual climate variability. *Science* 271(5255), 1576-1578.
- Goulden M. L., Munger J. W., Fan S. M., Daube B. C., and Wofsy S. C. (1996b) Measurements of carbon sequestration by long-term eddy covariance: Methods and a critical evaluation of accuracy. *Global Change Biology* 2(3), 169-182.
- Janssens I. A., Lankreijer H., Matteucci G., Kowalski A. S., Buchmann N., Epron D., Pilegaard K., Kutsch W., Longdoz B., Grunwald T., Montagnani L., Dore S., Rebmann C., Moors E. J., Grelle A., Rannik U., Morgenstern K., Oltchev S., Clement R., Gudmundsson J., Minerbi S., Berbigier P., Ibrom A., Moncrieff J., Aubinet M., Bernhofer C., Jensen N. O., Vesala T., Granier A., Schulze E. D., Lindroth A., Dolman A. J., Jarvis P. G., Ceulemans R., and Valentini R. (2001) Productivity overshadows temperature in determining soil and ecosystem respiration across European forests. *Global Change Biology* 7(3), 269-278.

- Jenkinson D. S. (1990) The turnover of organic carbon and nitrogen in soil. *Philosophical Transactions of the Royal Society of London Series B-Biological Sciences* 329(1255), 361-368.
- Kutsch W. L., Liu C. J., Hormann G., and Herbst M. (2005) Spatial heterogeneity of ecosystem carbon fluxes in a broadleaved forest in Northern Germany. *Global Change Biology* 11(1), 70-88.
- Lavigne M. B. and Ryan M. G. (1997) Growth and maintenance respiration rates of aspen, black spruce and jack pine stems at northern and southern BOREAS sites. *Tree Physiology* 17(8-9), 543-551.
- Law B. E., Thornton P. E., Irvine J., Anthoni P. M., and Van Tuyl S. (2001a) Carbon storage and fluxes in ponderosa pine forests at different developmental stages. *Global Change Biology* 7(7), 755-777.
- Lloyd J. and Taylor J. A. (1994) On the temperature dependence of soil respiration. *Functional Ecology* 8(3), 315-323.
- O'Connell A. M. (1990) Microbial decomposition (respiration) of litter in eucalypt forests of South-Western Australia: An empirical model based on laboratory incubations. *Soil Biology and Biochemistry* 22(2), 153-160.
- Prentice I. C., Farquhar G. D., Fasham M. J. R., Goulden M. L., Heimann M., Jaramillo V. J., Kheshgi H. S., Le Quéré C., Scholes R. J., Wallace D. W. R. (2001): The carbon cycle and atmospheric carbon dioxide. In: *Climate Change 2001: The Scientific Basis*. Cambridge University Press, 183-237.
- Schlentner R. E. and Cleve K. van (1985) Relationships between CO₂ evolution from soil, substrate temperature, and substrate moisture in four mature forest types in interior Alaska. *Canadian Journal of Forest Research-Revue Canadienne De Recherche Forestiere* 15(1), 97-106.
- Valentini R., Matteucci G., Dolman A. J., Schulze E. D., Rebmann C., Moors E. J., Granier A., Gross P., Jensen N. O., Pilegaard K., Lindroth A., Grelle A., Bernhofer C., Grunwald T., Aubinet M., Ceulemans R., Kowalski A. S., Vesala T., Rannik U., Berbigier P., Loustau D., Guomundsson J., Thorgeirsson H., Ibrom A., Morgenstern K., Clement R., Moncrieff J., Montagnani L., Minerbi S., and Jarvis P. G. (2000) Respiration as the main determinant of carbon balance in European forests. *Nature* 404(6780), 861-865.

Chapter 7.

Weekly variations of atmospheric CO₂, CO, CH₄, N₂O and SF₆

7.1	Introduction	189
7.2	Data	189
7.3	Data processing and results	190
7.3.1	Correlations between the weekly cycles of the mixing ratio of different species	195
7.3.2	Correlations between the weekly cycle of mixing ratios and the meteorological parameters	198
7.4	Discussion	202
7.5	Summary and conclusions	204
7.6	References	206

Abstract

Statistically significant weekly cycles have been detected in the atmospheric mixing ratio of CO₂, CO, CH₄, N₂O and SF₆ measured at Bialystok tall tower station. Such variations can only be attributed to anthropogenic influences, as they cannot be explained by any natural phenomenon.

The weekly signals show different features for cold and warm seasons, due to the predominance of different sources and sinks and to different atmospheric circulation patterns. For winter data, the ratio between the amplitude of the weekly signals of CO and CO₂ is in the range typical to fossil fuel burning.

The amplitude of the weekly variations does not attenuate with the increase of sampling height, fact which suggests a large scale effect, rather than the influence of local emissions.

Correlations between the weekly variation of mixing ratios and weekly variations of some of the meteorological parameters can also be distinguished. Although a mathematical correlation does not necessarily imply dependence, there are mechanisms by which the meteorological parameters and the weather conditions can influence the atmospheric mixing ratios of trace gases.

It is not possible from this short record to get definite conclusions about the mechanisms which lead to the observed variations of the mixing ratios. The cause is most probable a combination between the direct effect of the periodical anthropogenic emissions and the indirect, still anthropogenic effect via weekly variations of meteorological factors and atmospheric transport.

7.1 Introduction

There is no known natural phenomenon which would lead to a weekly cycle of CO₂ concentration or any atmospheric parameters. The existence of such a weekly periodicity can only be related to the weekly cycle of human activity.

Various authors found weekly cycles in the concentrations of anthropogenic pollutants (Broennimann and Neu, 1997, Marr and Harley, 2002, Beirle et al., 2003) and in various meteorological parameters, e.g. temperature, rainfall, hail severity (Simmonds and Keay, 1997). Most of these studies considered locations close to or in areas with high population density and the weekly variations of the meteorological parameters were explained by local pollution, heat emissions and aerosol – cloud interactions. Cerveny and Coakley (2002) identified a weekly cycle of CO₂ at Mauna Loa, Hawaii and attributed it to local emissions.

On a larger scale, Gordon (1994) studied satellite data for the years 1979 – 1992 and found a weekly cycle in the lower troposphere temperature over the Northern Hemisphere. Recently, Baeumer and Vogel (2007) showed the existence of a significant weekly cycle of more meteorological parameters (temperature, sunshine duration, precipitation) at different locations in Germany, including the station on Mount Zugspitze which is situated above the polluted planetary boundary layer most of the time. They suggested that the weekly periodicities are not fully explained by local pollution but by a larger scale anthropogenic effect on the atmosphere.

This chapter presents results regarding the weekly variations of atmospheric mixing ratio of greenhouse gases measured at Bialystok tall tower station. The air is sampled at different heights above ground level, between 5 and 300m, fact which allows studying the weekly variations for different footprints and helps thus to distinguish between local and larger scale influences.

7.2 Data

We use the CO₂, CH₄, CO, N₂O and SF₆ mixing ratio data measured at the Bialystok tall tower (53°13'N, 23°01' W, 180 masl), in the time interval between 25-Jul-2005 and 1-Feb-2007. The sampling heights are: 5, 30, 90, 180 and 300 m above ground level.

The meteorological measurement at the Bialystok tall tower station was not available for about half of the time interval considered. Thus meteorological data provided by the meteo station Bialystok (WMO station code 122950, coordinates 53.06N, 23.20E, 151 masl), situated at about 20 km distance away, are used instead. The parameters available are: air temperature, air pressure, dewpoint, wind speed and direction. The measurement is done near the ground level and the data frequency is in general 1 measurement per hour.

Examples of typical CO₂ variations at different heights above ground are shown in figure 7.1, for the summer (1a) respective the winter period (1b). Because of the intra-continental location of the station, the short term signals are strong, containing both anthropogenic and local biospheric signatures. The different aspect of the time variations between the cold and the warm seasons are due to different atmospheric circulation and mixing, and to differences in sources and sinks. The land biosphere influence strongly dominates the diurnal variations observed at lower sampling heights in the vegetation period.

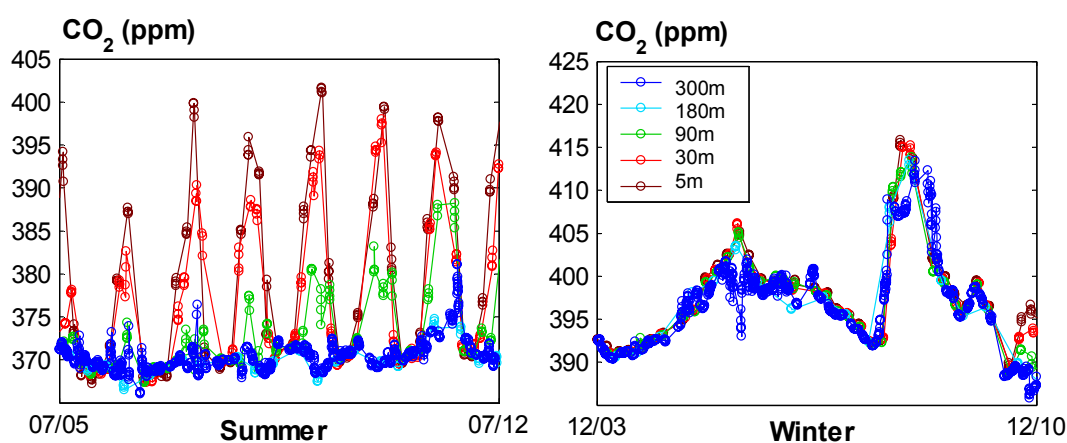


Figure 7.1 Example of CO₂ measurement results in the cold and warm seasons (data from the year 2006)

7.3 Data processing and results

The CO₂ concentration series (between 26-Jul-2005 and 1-Feb-2006) was averaged for each day of the week, separated for the different heights above ground level.

Figure 7.2 shows the results; the error bars represent the standard error of the mean. The much smaller standard error of the data from 300 m height is partly explained by smaller variance of the data at this height and partly due to a much larger number of measurement points. The number of samples from each sampling height and the standard deviation of the respective data series are listed in table 7.1.

Table 7.1 Sample characteristics for each sampling height

Height (m agl)	No. Samples	Standard deviation (ppm)
5	12406	13.10
30	18303	12.11
90	12833	11.68
180	9463	11.39
300	57487	9.39

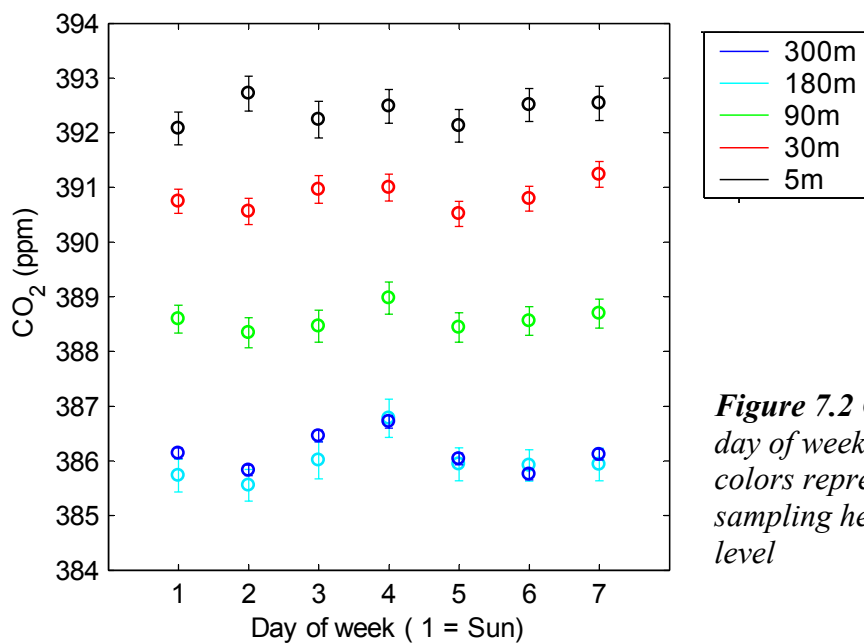


Figure 7.2 CO₂ averages for each day of week (day 1 = Sun); the colors represent different sampling heights above ground level

Figure 7.2 visually suggests the existence of a weekly cycle in the CO₂ mole fractions, with similar patterns for all sampling heights except for the 5 m level.

A more quantitative evaluation must be done by statistical analysis of variance. The statistical distribution of the CO₂ data is illustrated by the histogram in figure 7.3, compared with the normal distribution with the same mean and variance. Such a

distribution excludes the possibility of using a normal analysis of variance (ANOVA) procedure, since one of the main ANOVA assumptions (normally distributed data) is not fulfilled.

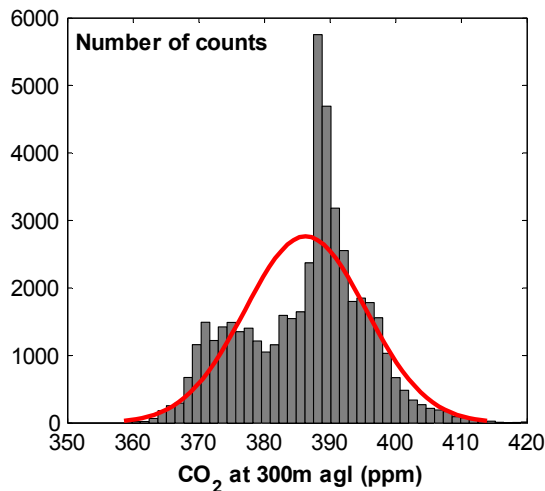


Figure 7.3 The distribution of the CO₂ mole fraction data (300 m agl) compared with the normal distribution with the same mean and variance (red line).

A Kruskal-Wallis non-parametric test was used for data analysis (Hollander and Wolfe, 1973). The Kruskal-Wallis analysis of variance method uses the ranks of the data instead of their numeric values and the usual F statistic is replaced by a chi-square statistic. For the multiple comparison, the critical intervals assigned are based on Tukey's honestly significant difference criterion (Studentized range distribution, Hochberg and Tamhane, 1987). The analysis for the CO₂ data from 300 m agl is illustrated in figure 7.4.

The averages for different days are considered significantly different when the critical intervals (shown by bars in the right side figure) do not overlap. For the 300 m sampling height, a significant difference can be observed between the week days, with the maximum occurring on Wednesday. The weekend days' means are lower than the total average, but the minimum occurs on Monday.

Similar analysis for the other heights above ground level is summarized in figure 7.5. The differences between the days of the week cannot be proved for all the heights, although some significant differences can be observed. This does not mean there are no differences, just that the hypothesis of equal means cannot be excluded for the given data distribution.

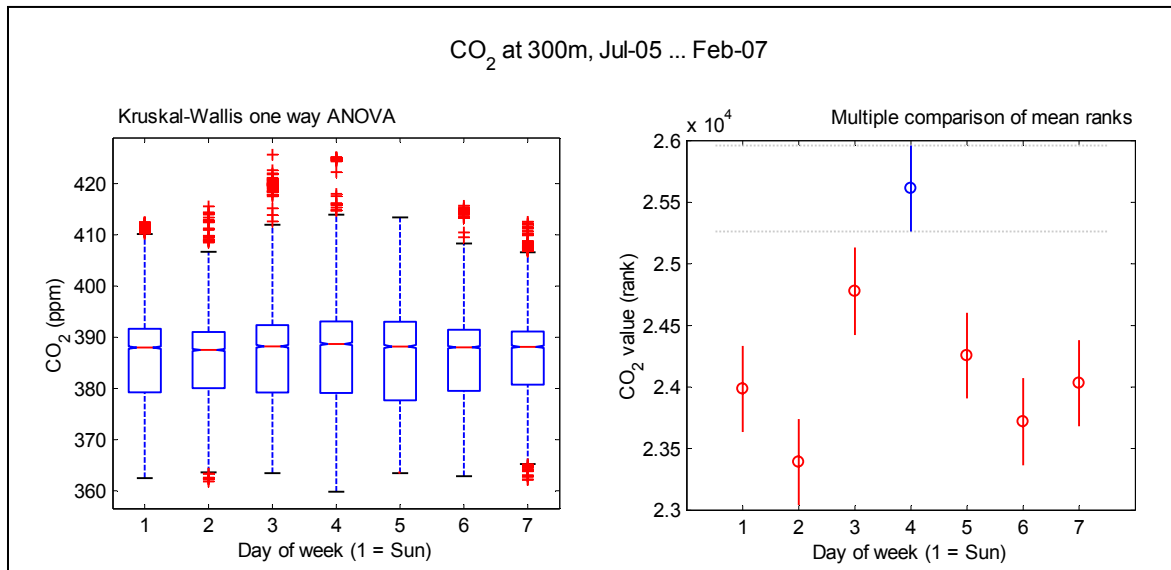


Figure 7.4 The multiple comparison based on Kruskal-Wallis ANOVA for the CO₂ concentration in air sampled at 300m agl.

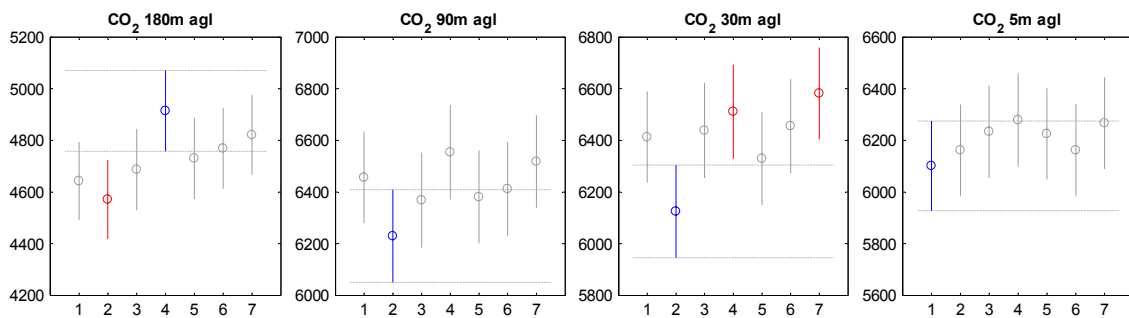


Figure 7.5 Multiple comparison tests for the CO₂ concentration versus day of week, for the sampling heights 5, 30, 90 and 180m agl. The x-axis is the day of the week (day 1 = Sun); the y-axis represent the mean ranks compared. The red and blue markers show the days which were found significantly different.

Theoretically, a potential influence on the result could be the functioning of the measurement system itself. There are no weekly cycles in the routine of the measurement system. The system runs unattended and a technician visit takes place at few days irregular intervals, with no preference for any of the week days. Also, the weekly results of the target measurement show that there is no weekly pattern in the performance of the instrument.

An uneven distribution of the sampling time over the day time could also affect the result, by the preferential sampling of lower or higher concentration time intervals.

The mean and the distribution of the sampling time have been checked for all the sampling heights. The figure 7.6 shows for example the distribution of the sampling time for different days of week, for the 300 m height. No significant difference concerning the sampling time distribution has been found for any of the sampling heights, between the days of the week.

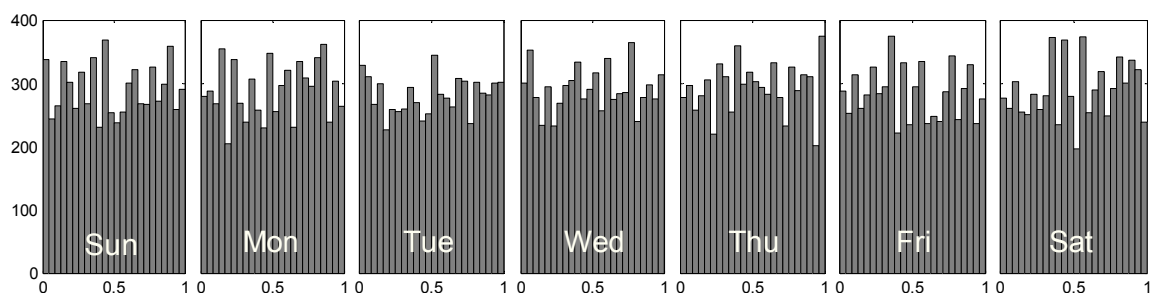


Figure 7.6 Distribution of the measurement time for each day of the week, for the 300m sampling height. The x-axis represents the time of the day; y-axis is number of counts.

The first analysis showed statistically significant differences between the days of the week for the CO₂ data series. The next steps will try to answer the following questions:

- (1) is there any seasonal dependence of the weekly variation?
- (2) is there any significant weekly variation for other species measured (CH₄, CO, N₂O, SF₆), and if yes, what is the connection between the CO₂ and the other species' weekly cycles?
- (3) what is the relationship between the observed weekly cycle of mixing ratios and meteorological factors?

There are two almost independent measurement systems, one measuring CO₂ and the other (based on gas chromatograph) measuring CH₄, CO, N₂O and SF₆. The two measurements are not synchronized and the different data series have gaps over different time intervals. Thus for direct comparison between species a data selection was necessary. Only those days were considered, when all the species, from all the five sampling heights, have been measured (a total of 343 days).

In order to look for any possible seasonal variation of the weekly cycle, the data have been separated into two categories, corresponding to the cold, respective the warm seasons. In what follows, winter data are considered the time intervals 6-Nov-2005 – 1-Apr-2006 and 26-Oct-2006 – 1-Feb-2007. The summer data are between 26-Jul-2005 – 6-

Oct-2005 and between 1-Jun-2006 – 1-Oct-2006. There are no available data before 26-Jul-2005 (start of the measurement) and after 1-Feb-2007 (end of the measurement data series used here). The data between 6-Oct and 6-Nov-2005 and between 1-Apr and 8-Jun-2006 could not be used because of technical reasons.

The same verifications like for the whole set of data have been made. The distribution of the sampling time over the day time was found uniform. The results of the target measurements do not show any dependence on the day of week (see for example the figure A5.1 in Appendix 5, page 223).

7.3.1 Correlations between the weekly cycles of the mixing ratio of different species

For each species, for each sampling height, the average was calculated for each day of the week. The results for winter and summer are presented separately in what follows.

a. Winter data (6-Nov-2005 – 1-Apr-2006; 26-Oct-2006 – 1-Feb-2007)

Figure 7.7 presents the averages of CO₂, CO, CH₄, N₂O and SF₆ mole fractions for each day of the week and each sampling height, for the winter data. The error bars represent the standard error of the averages. The statistical significance of the difference between the days of the week was tested using the previously described Kruskal-Wallis method. The figures illustrating these tests are not shown because they are not essentially different from figure 7.7 and therefore do not provide additional information.

As can be seen in figure 7.7, a general feature for all species is a significant increase of the concentration in the middle of the week.

The shape of curves and the gradient between sampling heights in the case of CO and CH₄ are quite similar; the two highest sampling levels have the strongest and most symmetric variation with the day of week.

The shape of the CO₂ curves looks quite similar to CO and CH₄, although the sampling time of CO₂ is not simultaneous with the other species considered here. CO₂ measured in air sampled at 300 m above ground is an exception to this, the amplitude of the weekly variation being much smaller. Also, the difference between the two highest sampling levels (300 and 180 m agl) is much larger for CO₂ than for CH₄ and CO. N₂O shows a similar pattern for the first four days of the week (starting with Sun) but the decrease at the end of the week is less pronounced than for CO₂, CO and CH₄.

The SF₆ curve has also a peak in the middle of the week (Wed), but unlike the other species, the third day does not show any significant difference compared to the previous species. Like for CO₂, the 300 m sampling level seems disconnected from the others, having a significantly lower concentration and a slightly different shape.

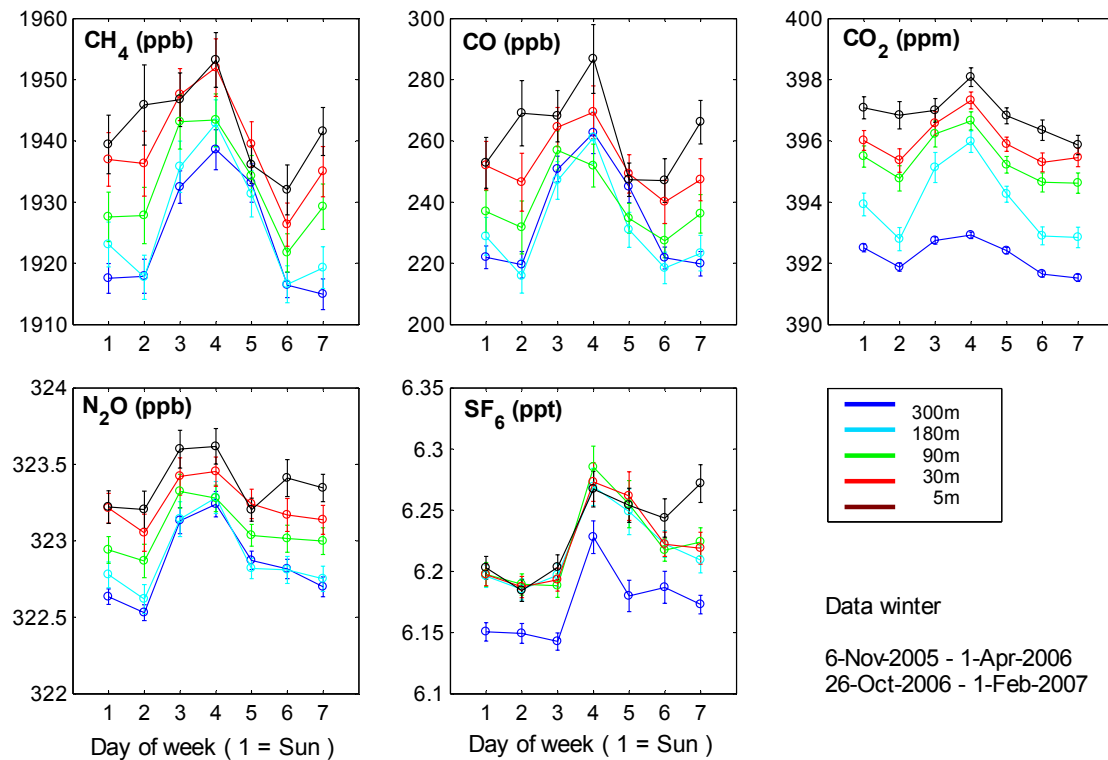


Figure 7.7 Winter weekly variation for CH₄, CO, CO₂, N₂O and SF₆; the colors represent different sampling heights. The x-axis for each plot represents the day of the week, starting with Sunday.

In figure 7.8, the CH₄ and CO averages for each day of the week are plotted versus the corresponding CO₂ values. The colors represent different sampling heights. For each sampling height there is a strong correlation between CO, CH₄ and CO₂. The data from 5, 30, 90 and 180 m are in good agreement regarding the ratio between CO and CO₂, respective CH₄ and CO₂ variations. The CO (ppb) : CO₂ (ppm) ratios for the 5, 30, 90 and 180 m sampling heights between 12 and 14 ppb:ppm, are in the range which would be expected for the fossil fuel emission in this region. This fact suggests that the fossil fuel burning is the origin of the observed weekly variations.

The CO (ppb) : CO₂ (ppm) and CH₄ (ppb) : CO₂ (ppm) ratios for the 300 m sampling height are much higher, due to the lower weekly variability of CO₂ at 300 m (as noted before).

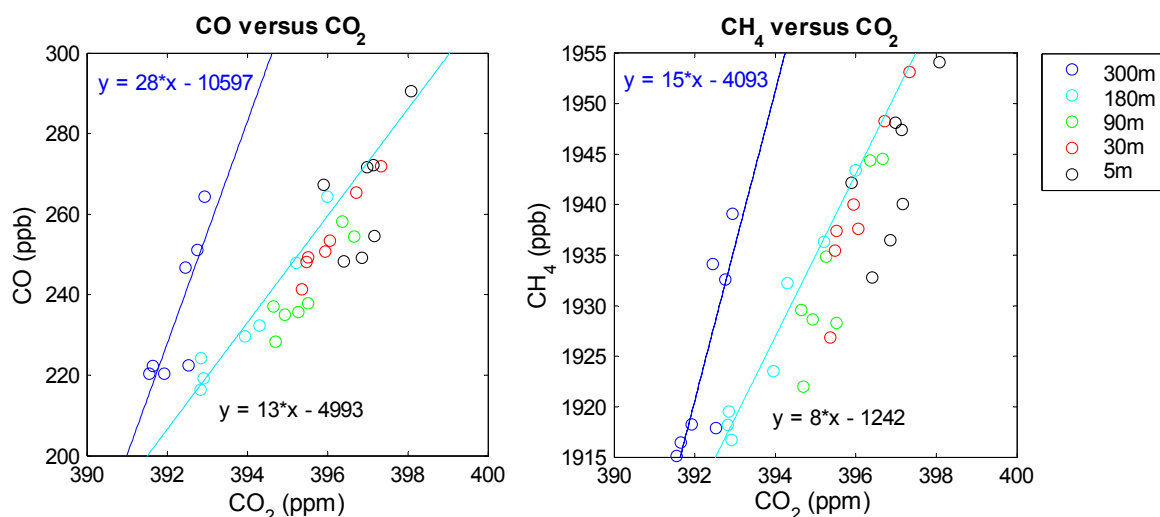


Figure 7.8 CO and CH₄ versus CO₂ (each point represents one day of week). The light blue line is a least squares fit through the data from 180 m height (equation shown in black).

b. Summer data (26-Jul-2005 – 6-Oct-2005; 1-Jun-2006 – 1-Oct-2006)

Figure 7.9 presents the averages of CO₂, CO, CH₄, N₂O and SF₆ mole fractions for each day of the week and each sampling height, for the summer data. The error bars represent the standard error of the averages. The statistical significance of the difference between the days of the week was tested using the Kruskal-Wallis method. The figures illustrating these tests are not shown because they are not essentially different from figure 7.9 and therefore do not provide additional information.

Comparing to the winter results, there are no more maxima in the middle of the week. Moreover, the first two days tend to show a higher concentration, which decreases slightly through the week and rises again at the end of the week.

Unlike the winter data, the correlation between CH₄ and CO is not very high, while the N₂O and CH₄ look more similar. From all species CO₂ shows the most significant differences between days, with clear minima in the middle of the week. The SF₆ mixing ratio shows a significant maximum on Thursday, which is not correlated with any of the other species.

Contrary to the winter data, the summer weekly cycles of CO₂, CH₄, CO and N₂O appear to be stronger for the lower sampling levels, which suggests that part of the cause is local.

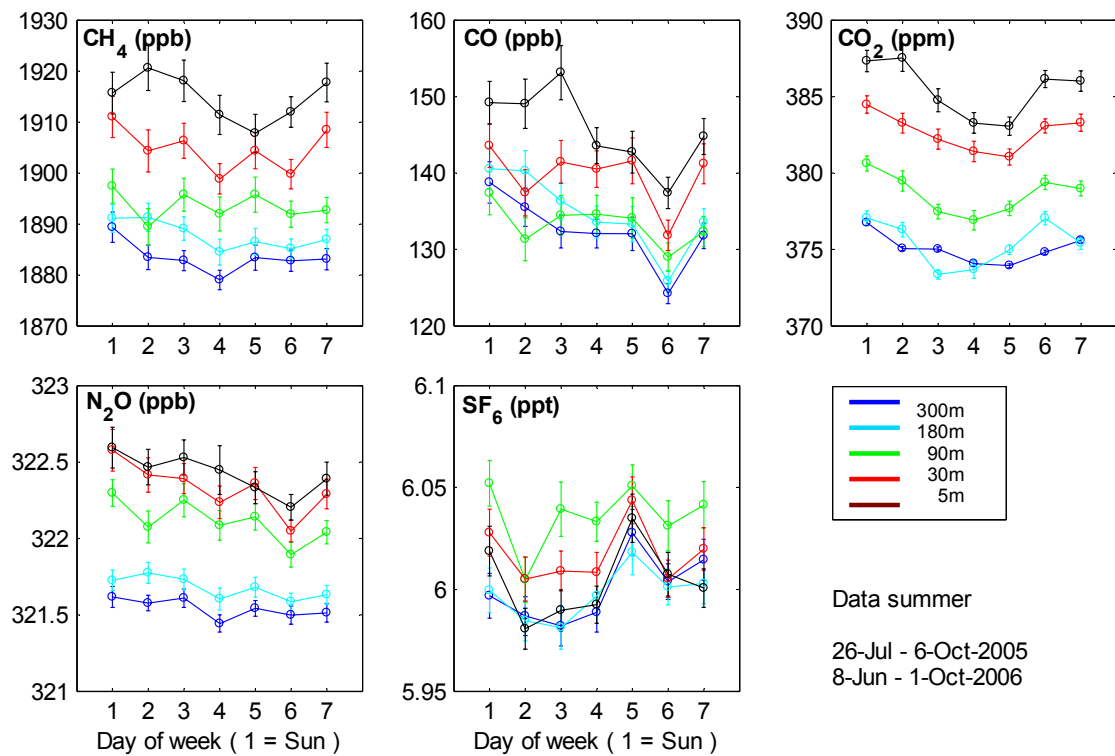


Figure 7.9 Summer weekly variation for CH_4 , CO , CO_2 , N_2O and SF_6 ; the colors represent different sampling heights. The x-axis for each plot represents the day of the week, starting with Sunday.

7.3.2 Correlations between the weekly cycle of mixing ratios and the meteorological parameters

The corresponding weekly variation of the available meteorological parameters has been tested next, in order to find eventual correlations. The summer and winter time intervals are treated separately.

As already mentioned, the meteorological parameters used here are not measured at the same location with the mixing ratio data. This can be a limitation for the quantitative interpretation of the following results.

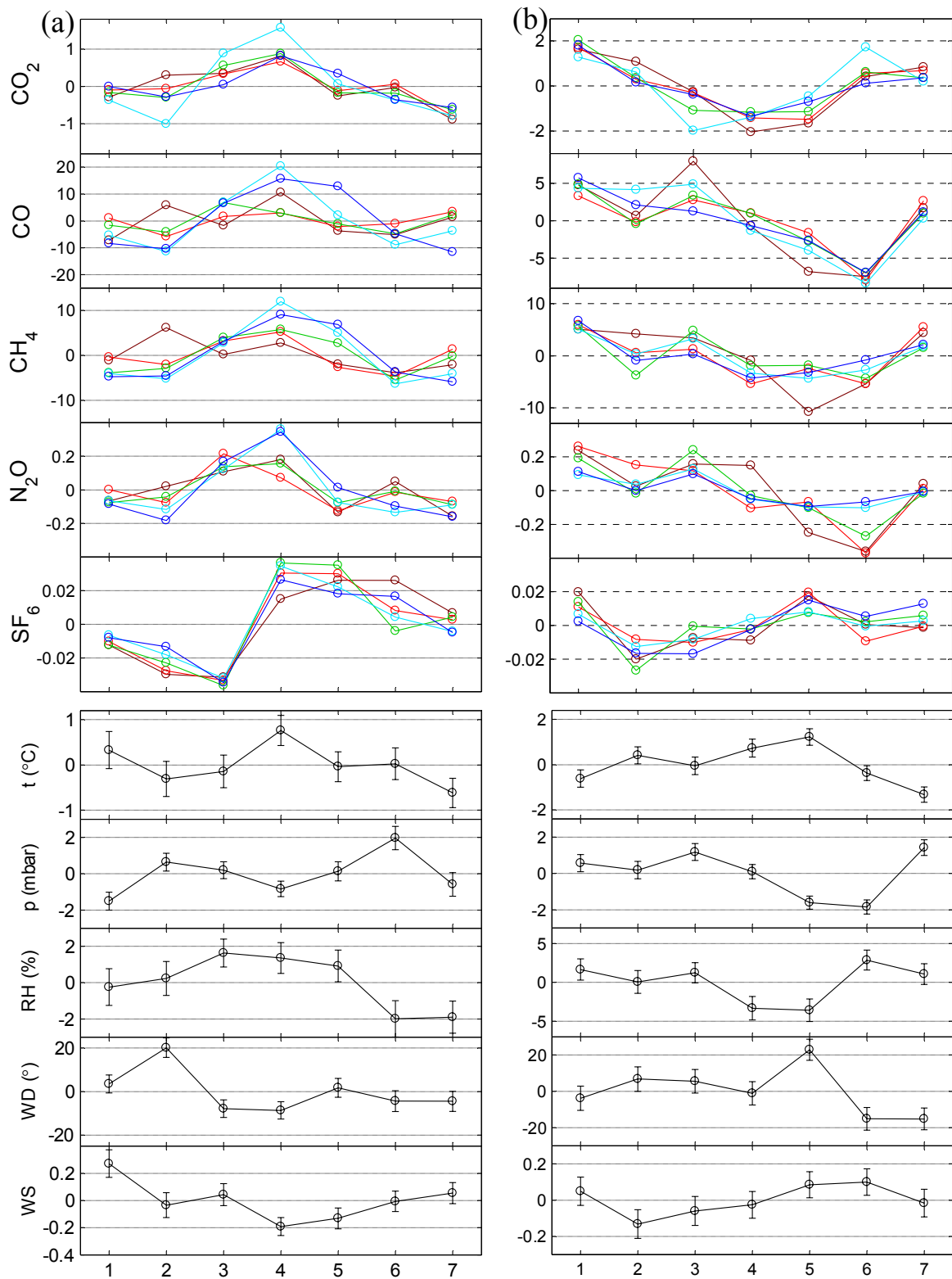


Figure 7.10 Anomalies of mixing ratio and meteorological parameters function of day of week (day 1 = Sun) for a) winter and b) summer time intervals

Because the CO₂ data, the GC measured species (CH₄, CO, N₂O and SF₆) and the meteorological data are not time synchronized, a different data processing was necessary. First only those days were selected, for which mixing ratio data for all species, from all sampling heights and meteorological data for all parameters exist. The data for the selected days were then averaged in two-hourly steps. These two-hourly averages are used in the following section, to calculate the averages for each day of the week.

The figures 7.10a and 7.10b show the anomalies (deviations from the average) of the mixing ratio and meteorological data, for winter respective summer time. Some slight differences between figure 7.10 and the previous results (figures 7.7 and 7.9) are mainly due to the different data selection.

As it can be observed in figure 7.10, the meteorological parameters also present significant differences between the days of the week. For example, in winter the temperature and the relative humidity have a maximum in the middle of the week, similar to the mixing ratios. The higher temperature in the middle of the week is consistent with other studies (Baeumer and Vogel, 2007). The mean wind direction anomaly has here only qualitative importance, because it was computed as arithmetic mean which is not well suitable for wind direction averaging.

The correlation coefficients between each of the meteorological parameters and the mixing ratio weekly series (r^2) have been calculated independently, by a least squares method. The resulted correlation coefficients are plotted in figure 7.11 for winter (fig. 11a) and summer (fig. 11b).

In case of the winter data, the CO₂ mixing ratio anomaly has a quite strong positive correlation with the atmospheric temperature and relative humidity, while the correlations with the atmospheric pressure, wind direction and wind speed are not significant. The CH₄, CO and N₂O present the same overall features but the correlation with the atmospheric temperature and relative humidity decrease with the decrease in sampling height. The SF₆ does not show any significant correlations with the meteorological parameters. The correlations between the mixing ratios and meteorological parameters tend to be stronger for the higher sampling levels, although the meteorological measurement is done close to the ground level.

For summer data, the correlation between temperature and mixing ratio anomalies is negative. A strong correlation between atmospheric pressure and the CH₄, CO and N₂O anomalies can be observed, which is not apparent for the winter data. The relative humidity is still correlated with CO₂ and with CH₄ from the highest sampling levels. The

SF₆ anomaly is correlated with the wind speed, but not with the other meteorological parameters.

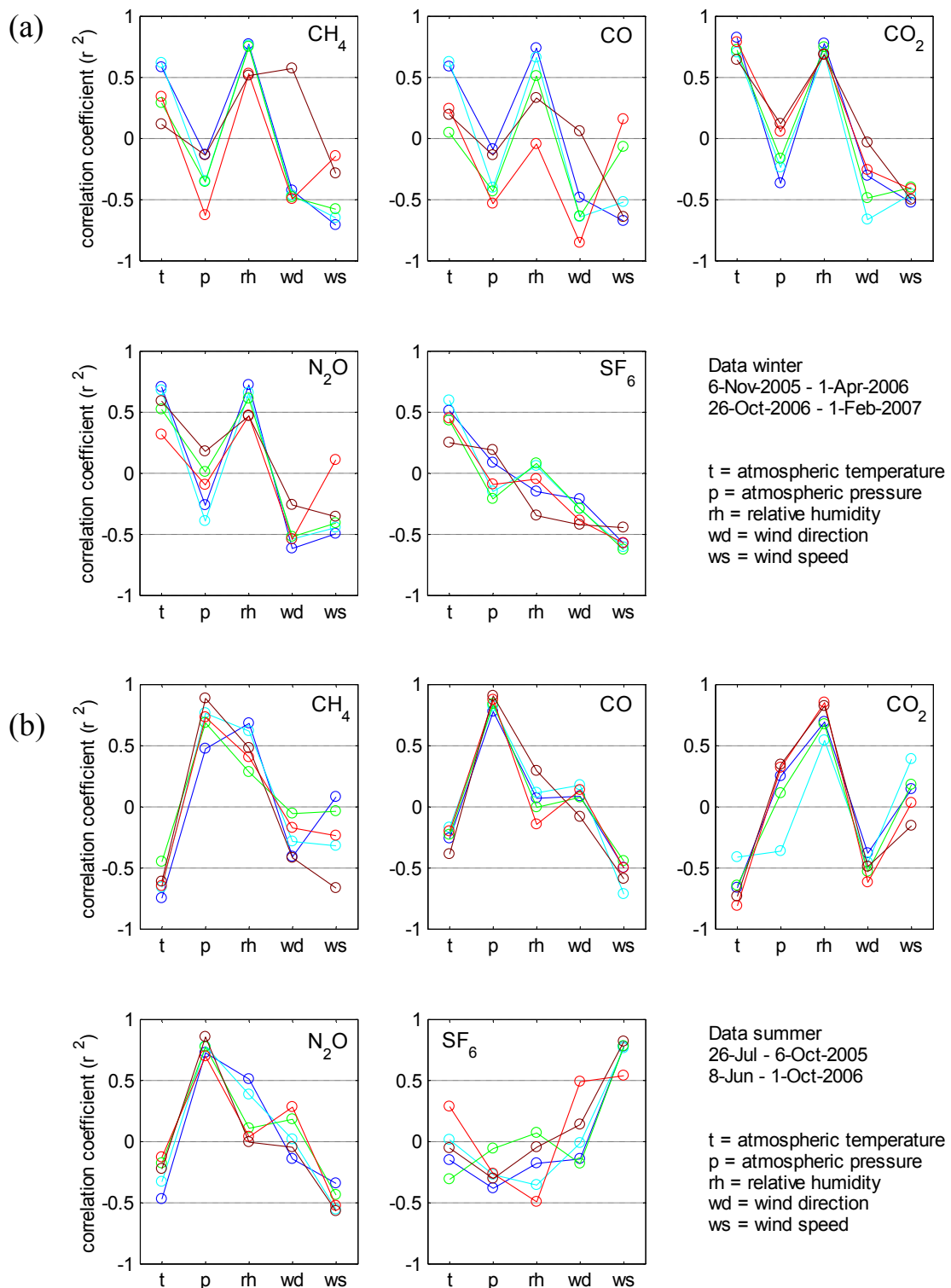


Figure 7.11 Correlations between the weekly cycle of each species (from each height) and the weekly cycle of the meteorological parameters, for winter (a) and summer (b). The y-axis represents the correlation coefficients calculated; the colors represent the sampling heights.

7.4 Discussion

Robustness of results

Different data processing methods have been tested, in order to verify the robustness of the results. When using a robust averaging method (e.g. eliminating the highest and the lowest 25% of the data) or when the data are binned in hourly or 2-hourly steps (as described in the paragraph 8.3.2) the results do not change essentially.

The results are more sensitive to the selection of the time intervals taken into account. For example, in figure 7.10a, the weekly cycle of CO from 300 m in winter time has the amplitude of about 25 ppb. The weekly cycle for the same parameter in figure 7.7 has the amplitude of about 40 ppb. The difference is due to the fact that for the figure 7.10, some more days have been eliminated from the total time series.

Trying to look at each summer or winter separately leads to quite different pictures. The main features of the weekly variations are maintained (e.g. the general mixing ratio increase in the middle of the week for each winter and the decrease for each summer) but the weekly curves have different shapes. These data series are not long enough to cancel out the strong synoptic-scale events by averaging.

In conclusion, the information extracted from the available data is likely to be real (result robust to data processing) but it might be not fully representative for long term (result not robust to data selection).

Correlations between species

A similar weekly pattern for CO, which is a marker of anthropogenic pollution, and CO₂, CH₄ and N₂O, leads to the conclusion that at least part of the weekly variation is directly related to anthropogenic emission cycle. For winter, the ratio between the CO and CO₂ weekly anomalies for the sampling heights between 5 and 180 m (between 12 and 14 ppb:ppm) is comparable to the expected fossil fuel signature for this region. The fact that SF₆ is not correlated with the other trace gases can be explained by totally different sources (still anthropogenic) with different spatial distribution and temporal variability.

Correlation with meteorological parameters

The mathematical correlation between two variables does not necessarily involve a direct cause-effect relationship. It is possible that the two variables are independent from each other, but they are both influenced by a common factor. In this particular case,

it is possible that the meteorological parameters and the trace gases mixing ratios are independent, and both directly influenced by weekly human activities. Thus a possible explanation of at least part of the correlation between the weekly cycles of some of the meteorological parameters and the weekly cycles of trace gases is as follows. Greenhouse gases, heat, pollutants, aerosols are emitted with synchronized weekly periodicity from human activities like transport, industry, fossil fuel burning. The meteorological situation on local or regional scale can be independent from the evolution of the trace gases but dependent on any other emissions (for example aerosols and heat) which are source-coupled with the trace gases emissions. For example, one might find correlations between CO₂ and temperature, just because the CO₂ was produced by the same source which emitted the aerosols which actually increased the temperature.

However, the possibility of direct cause-effect relation cannot be excluded, since there are natural mechanisms by which the meteorological and the weather situation can directly influence or be influenced by atmospheric mixing ratio of the trace gases considered here. Some of these mechanisms are shortly discussed in what follows, although probably not all the possibilities are covered.

CO₂ atmospheric concentration is connected with the local meteorological situation via multiple paths. Important especially in the warm season is the direct influence of meteorological parameters on ecosystem functions and thus on the gas exchange with the atmosphere. The biosphere respiration is depending on atmospheric and soil temperature and humidity. Some of the controlling factors for photosynthesis are the radiation (and cloud coverage), the atmospheric humidity and the temperature.

In summer, when the net exchange between regional land biosphere and atmosphere is dominated by photosynthesis (the region is a net sink of CO₂ during summer) the increase of temperature in the middle of the week or an eventual increase in cloud coverage during weekend could have as effect a higher CO₂ uptake by photosynthesis and thus a decrease of atmospheric CO₂ mixing ratio during the week. Such phenomenon could cause the observed vertical gradient of the summer CO₂ weekly cycle, with higher amplitude for the lower sampling levels. In cold seasons, when the respiration is dominating, the increase of temperature would lead to an increase in CO₂ released by respiration and thus to an increase in atmospheric CO₂ concentration. There is though no vertical gradient to support the last hypothesis regarding the winter data.

The gas exchange between the soil and the atmosphere is significantly influenced by atmospheric pressure and soil moisture (which is connected to the quantity of rain).

The concentrations of CO₂, CO, CH₄ and N₂O in soil air are different from the atmospheric concentration, thus a variation of the gas exchange between soil and atmosphere leads to variations of the atmospheric concentrations of these species.

All species considered here have sources at the ground level. The dilution of concentration by vertical mixing of the PBL during stable weather conditions is influenced by atmospheric pressure, temperature and humidity. This would however have opposite effect on CO₂ during the summer (an increase in concentration in case of stronger mixing), if the lower atmospheric layer is depleted in CO₂ by photosynthesis. Also the mixing ratios of all species can be affected by changes of the wind speed and direction, which would bring air masses from different regions.

In case of SF₆ there are no significant local sources, thus the measured concentration at this location is mainly dependent on horizontal atmospheric transport, i.e. on wind direction and speed, and on vertical mixing at regional level.

In conclusion there are many interactions which could combine and lead to the observed variations. Also the meteorological parameters are not independent, which makes it more difficult to separate the eventual causes. Weekly cycles of atmospheric temperature, pressure, humidity or the wind speed or direction could all theoretically induce weekly cycles of atmospheric mixing ratios. However the weekly cycles of the meteorological parameters are too small to be the main drivers of the large weekly cycles of trace gases, like CO and CH₄. It is hard to conclude at this moment if any of the mentioned effects could be strong enough to have a significant influence.

7.5 Summary and conclusions

There are statistically significant variations with the day of the week in the measured atmospheric mixing ratios of CO₂, CO, CH₄, N₂O and SF₆ over the time interval considered.

When the data are separated in two subsets corresponding to the cold (“winter”) respective the warm (“summer”) seasons, even stronger weekly cycles of the mixing ratios can be observed. The summer and winter weekly cycles have different characteristics. Possible reasons for this are the differences in the dominant sources and sinks between summer and winter and the differences in the atmospheric circulation.

For this particular dataset, the overall weekly cycle seems dominated by the

winter weekly cycle, but this could be due to a larger number of data points corresponding to the winter data selection.

The amplitude of the weekly variations does not strongly attenuate with the sampling height. This suggests that the local emissions are not the dominant cause of the observed weekly cycles, but a larger scale interaction between anthropogenic emissions and atmosphere.

There are significant correlations between the weekly variations of different species, but these correlations are also different for the summer and winter intervals. For winter, the ratio between the CO and CO₂ weekly anomalies for the sampling heights between 5 and 180 m agl (12 to 14 ppb:ppm) is comparable to the expected fossil fuel signature for this region.

Significant correlations have also been found between the weekly anomalies of the mixing ratios and those of the meteorological parameters. Although a mathematical correlation does not necessarily imply dependence, there are mechanisms by which the meteorological parameters and the weather conditions can influence the atmospheric mixing ratios of trace gases. The correlations differ with the season, the gas species and the sampling height, which is predictable since different species are in different ways affected by the meteorological conditions.

The results are not sufficiently robust to data selection methods to make precise quantitative estimations. Also the 1.5 years record is not long enough to conclude which of the observed features are representative over long term.

Given the shortness of the data series, it is not possible to fully clarify the mechanisms which lead to the observed variations of the mixing ratios. The cause is most probable a combination between the direct effect of the periodical anthropogenic emissions and the indirect, still anthropogenic effect via weekly variations of meteorological factors and atmospheric transport.

7.6 References

Baumer D. and Vogel B. (2007) An unexpected pattern of distinct weekly periodicities in climatological variables in Germany. *Geophysical Research Letters* 34(3), -.

- Beirle S., Platt U., Wenig M., and Wagner T. (2003) Weekly cycle of NO₂ by GOME measurements: a signature of anthropogenic sources. *Atmospheric Chemistry and Physics* 3, 2225-2232.
- Bronnimann S. and Neu U. (1997) Weekend-weekday differences of near-surface ozone concentrations in Switzerland for different meteorological conditions. *Atmospheric Environment* 31(8), 1127-1135.
- Cerverny R. S. and Coakley K. J. (2002) A weekly cycle in atmospheric carbon dioxide. *Geophysical Research Letters* 29(2), -.
- Gordon A. H. (1994) Weekdays Warmer Than Weekends?. *Nature* 367(6461), 325-326.
- Hochberg Y. and Tamhane A. C. (1987) *Multiple comparison procedures*. Wiley.
- Hollander M. and Wolfe D. A. (1973) *Nonparametric statistical methods*. Wiley.
- Marr L. C. and Harley R. A. (2002) Spectral analysis of weekday-weekend differences in ambient ozone, nitrogen oxide, and non-methane hydrocarbon time series in California. *Atmospheric Environment* 36(14), 2327-2335.
- Milliken G. A. and Johnson D. E. (1984) *Analysis of Messy Data, Volume 1: Designed Experiments*. Chapman & Hall.
- Searle S. R., Speed F. M., and Milliken G. A. (1980) Population Marginal Means in the Linear-Model - an Alternative to Least-Squares Means. *American Statistician* 34(4), 216-221.
- Simmonds I. and Keay K. (1997) Weekly cycle of meteorological variations in Melbourne and the role of pollution and anthropogenic heat release. *Atmospheric Environment* 31(11), 1589-1603.

Chapter 8.

Final conclusions and remarks

The data value

On long term, the measurement data from the Bialystok tall tower station will be used with inverse atmospheric transport models to determine the intensity and distribution of sources and sinks of greenhouse gases at continental, regional and national level (as required by Kyoto Protocol) and to evaluate the effectiveness of carbon emissions reduction policies. However, the use of the data is not limited to this.

The position of the Bialystok station on the north-eastern border of the highly populated region of the western and central Europe is particularly suitable for monitoring the anthropogenic emissions. The predominant westerly circulation brings background oceanic air masses which gradually accumulate gases emitted from surface sources, and lose the oceanic signature, while mixing with the continental air masses. Comparisons with other monitoring stations permit to observe for example the progressive increase of gas species with anthropogenic origin, and the CO₂ decrease during the summer when the land biosphere uptake dominates. The attenuation of the APO signals in the interior of the continent, as shown in Chapter 4, can be used to constrain the longitudinal atmospheric transport, which is particularly important for resolving the spatial distribution of the mid-latitudes CO₂ sink.

The high temporal resolution of multiple species measurements, from different sampling heights, offers numerous possibilities of studying the shorter term signals. Only some of these possibilities have been reached in this thesis. For example, the evolution of the vertical gradients of trace gases emitted near the ground provides a tool to study the boundary layer dynamics. The study of the short term variability of the data (on time scales of hours to days), combined with information about the influence area for the air masses arriving at the sampling location (back-trajectories or footprint models) can provide information about the spatial distribution of sources and sinks. The multitracer approach helps to distinguish between the periodicity of sources and sinks, and the periodicity of the atmospheric circulation in the case of the CO₂ seasonal and diurnal variations.

An important domain of research is the land biosphere, which has the capability to store part of the anthropogenic CO₂, but it also has the capability to release CO₂. Its reactions to changes of the environment and climate can drive the net balance of the gas exchange with the atmosphere to either uptake or release of CO₂. It is therefore important to observe the gas exchange between the land biosphere and atmosphere and to understand the underlying processes. Examples of knowledge which can be extracted

from the presented data, regarding the gas exchange between the land biosphere and atmosphere, are Chapter 5 and Chapter 6 of this thesis.

As a future perspective, the Bialystok data can potentially be used as complementary measurement and high precision point validation for other types of measurements, like ground based FTIR (Fourier transform infrared spectrometer), airborne and satellites.

The technological value

At the moment of writing this thesis, the measurement system installed at Bialystok has already been operated for two years. The performance evaluation after the first one and a half years shows that the measurement reaches the high precision levels requested by the project and is in the same time robust and reliable enough for long term unassisted operation.

Besides the scientific value of the atmospheric data provided, the measurement system installed at Bialystok constitutes a technical achievement in itself, contributing to the general technological expertise in the field of atmospheric measurements. It is at the moment one of the few continuous, high precision, unattended oxygen measurement capabilities in the world. It also provides useful experience for the measurement community at instrumental level, for example concerning the adaptation of a gas chromatographic system to continuous and unattended field operation. Additionally it provides a base for long term studying specific technical issues, like oxygen fractionation.

Measurement errors and the importance of quality assurance

The measurement system was built around commercially available analysers. The high precision achieved (for some of the gas species much above the factory specifications of the instruments) is the result of the systematic, long term optimization of the measurement and calibration procedures and of the continuous monitoring of the system performance. Methodical quality assurance procedures and the existence of specific quality check means proved essential for attesting and maintaining the high quality standard.

Still the high precision (typically estimated based on the measurement repeatability) does not exclude the possibility of errors and does not necessarily mean a high accuracy. As shown in Chapter 3 regarding the CO mixing ratio results, the precision on the measurement is about 0.5 ppb, but the potential systematic error as inferred from

comparisons with flask samples results is on the order of 10 ppb. In case of O₂/N₂ measurements, systematic differences between parallel sampling lines from the same height of the tower show that at least one of them is affected by systematic measurement errors. This shows that assessing the measurement uncertainty at the level of the estimated precision is erroneous. In general it is important to be aware of the fact that the measurement uncertainty is not limited by the measurement precision. In this context the quality assurance strategies including verifications by e.g. regular inter-comparisons are indispensable for estimating the overall uncertainty of the data.

Another important aspect of the quality assurance is the ability to propagate the calibration scales on long term and to maintain the traceability to the primary calibration scale from the central laboratory. The gas cylinders which define the on-site calibration scale have to be monitored in such way that any eventual drift can be observed and quantified. The archive standard gases will have the role to propagate the on-site calibration scale on long term by periodical comparisons with the routine calibration standard gases. The connection between the on-site calibration scale and the central laboratory has to be maintained and attested by intercomparisons, using high pressure cylinders and flask samples.

When data from several measurement stations are used to infer spatial gradients, one of the important requirements is that no systematic shifts between the different stations exist. An important step in achieving this goal was made by the CHIOTTO project through the partial standardization of the equipment and of the calibration and measurement procedures, as well as by the inter-comparison programs initiated under CHIOTTO and continued under CarboEurope IP. As different measurement methods are likely to be affected by different systematic errors, the use of similar equipments helps diminish the intra-network measurement shifts which could be incorrectly interpreted as spatial gradients.

During the last two years I have learned that installing a high-quality measurement system is far from being the end of the work. The most difficult part is to maintain the measurement at high quality standards, and to be able to prove it.

Remarks concerning the atmospheric measurements strategy

A high precision measurement system implies a big time, money and effort investment at the beginning, careful maintenance and high running costs for the whole lifetime. Also usually a high precision system is complex and sensitive, which means

higher probability of breakdowns and thus more frequent data gaps. Thus such a measurement is less suitable for field or unassisted use.

Lowering the precision requirements permits to use simpler measurement systems, which have lower construction and operation costs, are more robust and more suitable for unassisted field use.

The spatial density of the actual in-situ measurement network is limited by the high costs and vulnerability of the measurements. Thus a higher measurement density could be achieved using cheaper and more robust equipments. The optimal measurement network should provide in the same time the adequate precision and spatial coverage.

Strong horizontal gradients of mixing ratios over the continent are due to uneven distribution of sources and sinks. These gradients are reflected in the measurement data as fast temporal variations of the mixing ratios, and high dependence on the air masses origin. In this context a denser monitoring network could be useful to determine the spatial distribution of sources and sinks. In the same time the amplitude of the signals is for most of the species much larger than the precision (ex. CO₂, CO, CH₄). This leads to the idea that the continental monitoring network could incorporate few high precision stations (as there are already the CHIOTTO tall towers and the other stations in CarboEurope), and a higher number of lower precision stations, with the condition that no large systematic shifts exists between stations. Given a dense network one could for example follow the evolution of the same signal over few successive points, but this would require a distance between stations (in air travel time) smaller than the diurnal periodicity of the vertical mixing. Simple and robust measurement systems are also a potential option for remote locations, where the logistic aspects are important.

On multi-annual time scales the signal which has to be distinguished gets much smaller, e.g. the atmospheric CO₂ increase is on the order of 1-2 ppm per year and the average continental gradient is also on the order of 1 ppm. In such situations high precision measurements are necessary. On this time scale however the high spatial and temporal resolution is not compulsory and the necessary information can be obtained from a less dense network of measurement stations.

High precision is also necessary when looking at the vertical gradients in the planetary boundary layer. The diurnal vertical gradient during summer is typically on the magnitude of less than two ppm, and that is when the land biosphere is at maximal amplitude of CO₂ uptake. That means, the whole land biosphere uptake during summer only provides a less than 2 ppm signal on this time and space scale. This small vertical

gradient is important as it can provide constraints on the spatial distribution of sources and sinks of CO₂.

Although high precision measurements exist at this moment for many gas species, the instruments are in many cases complicated and suitable mostly for laboratory use. An idea is that part of the work from now on should focus not only on the increase in precision, but on optimizing the measurements in a way that the same precision can be achieved with simpler, cheaper and more robust instruments.

In-situ, continuous measurements versus flask sampling

The in-situ continuous measurement obviously provides much better temporal resolution than the usual weekly flask sampling. The flask results are just momentary snapshots of a variable situation. Inside the continents, where short term variations are large, continuous measurements give significantly more representative information. At clean, background locations, where temporal variations on short term are not very important, the difference in information content between flask samples and eventual continuous measurement decreases.

One of the advantages of flask sampling is that the samples can be measured in laboratory, which means the possibility to measure more species, and usually higher precision can be achieved. On the other hand, flask samples can be affected by contamination and storage artifacts, and the intervention time in case of malfunctions of the sampling apparatus is much longer.

In conclusion, in areas with strong spatio-temporal gradients a continuous measurement can be more valuable. Supplementary flask sampling at continuous monitoring stations provides information about additional species and, as evident from Chapter 3, it is essential for the validation of the in-situ measurement.

Appendix 1

Maps of Europe (*Globalis.gvu.unu.edu*)

The location of Bialystok tall tower station is marked by blue triangle.

1. Topography

Source: The Global Land One-km Base Elevation (GLOBE) Project ETOPO 2 Worldwide Bathymetry (topography)

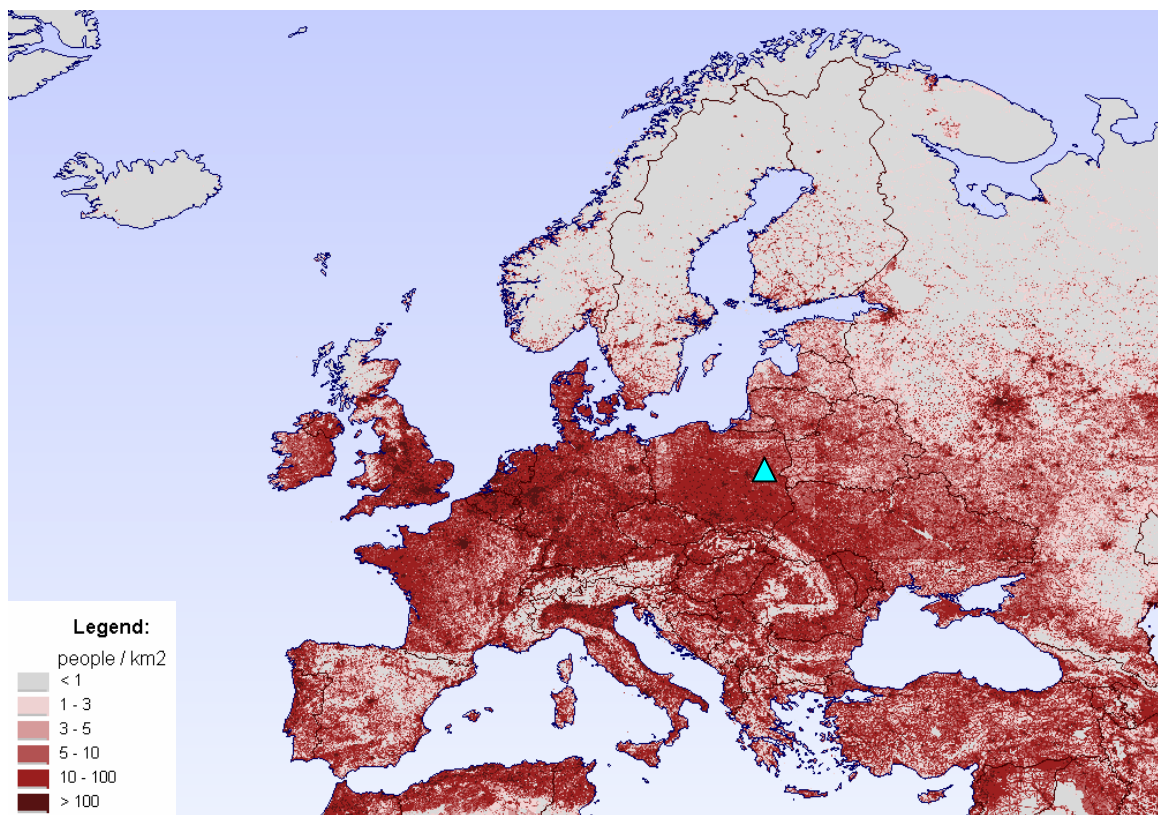
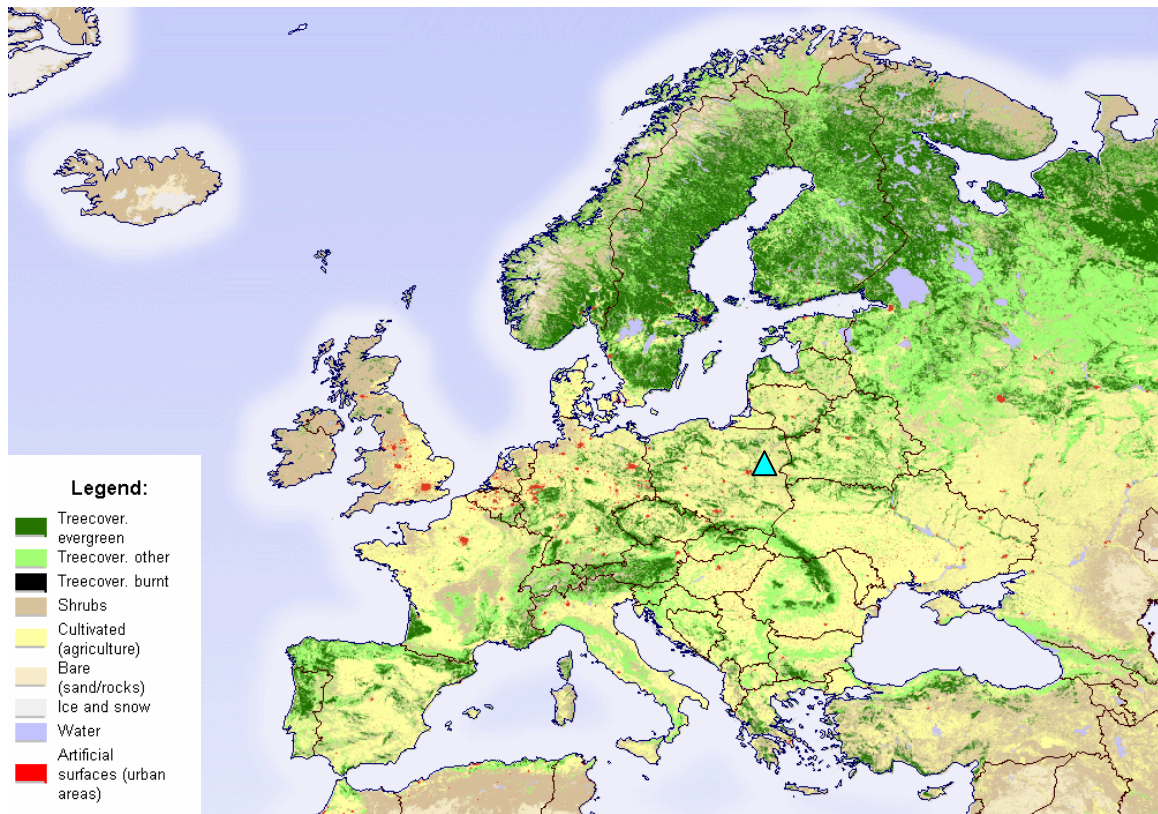
2. Land cover

Source: Global Land Cover 2000 database. European Commission, Joint Research Centre, 2003. (land cover)

3. Population density

Source: Landsat 2001(population)





Appendix 2

Derivation of formula used to calculate the variation of O₂ mole fraction (ppm) knowing the variation of O₂/N₂ ratio (permeg)

Concentrations: O₂, N₂, CO₂, Ar (*mol/m³*)

Mole fraction:

$$X_{O_2} = \frac{O_2}{N_2 + O_2 + Ar + CO_2 + \dots} \times 10^6, (\mu\text{mol} / \text{mol}) \quad (1)$$

$$X_{O_2} - X_{O_2}^0 = \Delta X_{O_2} \approx \frac{dX_{O_2}}{dN_2} \Delta N_2 + \frac{dX_{O_2}}{dO_2} \Delta O_2 + \frac{dX_{O_2}}{dCO_2} \Delta CO_2 + \frac{dX_{O_2}}{dAr} \Delta Ar + \dots \quad (2)$$

Assumption: $\frac{dX_{O_2}}{dN_2} \Delta N_2$ negligible

Permeg definition:

$$\delta O_2 / N_2 (\text{permeg}) = \left(\frac{(O_2 / N_2)_{\text{sample}}}{(O_2 / N_2)_{\text{reference}}} - 1 \right) \times 10^6 \quad (3)$$

Assumption: the change in O₂/N₂ is produced only by change in oxygen

$$\delta O_2 / N_2 = \frac{\frac{X_{O_2}}{1 - X_{O_2}} - \frac{X_{O_2}^0}{1 - X_{O_2}^0}}{\frac{X_{O_2}^0}{1 - X_{O_2}^0}} = \frac{X_{O_2}(1 - X_{O_2}^0) - X_{O_2}^0(1 - X_{O_2})}{(1 - X_{O_2})(1 - X_{O_2}^0)} \times \frac{(1 - X_{O_2}^0)}{X_{O_2}^0} = \frac{X_{O_2} - X_{O_2}^0}{X_{O_2}(1 - X_{O_2})} \quad (4)$$

from (4) $\rightarrow \frac{dX_{O_2}}{dO_2} \Delta O_2 = X_{O_2}^0(1 - X_{O_2}^0) \delta(O_2 / N_2)$ (5)

$$\frac{dX_{O_2}}{dCO_2} \Delta CO_2 \approx -X_{O_2}^0 \Delta X_{CO_2} \quad (6)$$

$$\frac{dX_{O_2}}{dAr} \Delta Ar \approx -X_{O_2}^0 \Delta X_{Ar} \quad (7)$$

By replacing (5), (6), (7) in (2), assuming all other air components stable or negligible:

$$\rightarrow \Delta X_{O_2} \approx X_{O_2}^0 [(1 - X_{O_2}^0) \Delta \delta(O_2 / N_2) - \Delta X_{Ar} - \Delta X_{CO_2}] \quad (8)$$

Appendix 3

Description of the gas chromatographic method - 170206.M

GC oven temperature (ECD columns): 76°C
Auxiliary oven temperature (FID columns): 60°C
Run time: 7.02 min

FRONT DETECTOR (FID)

Temperature: 175°C (On)
Hydrogen flow: 50.0 mL/min (On)
Air flow: 320.0 mL/min (On)
Mode: Constant makeup flow
Makeup flow: 5.0 mL/min (On)
Makeup Gas Type: Nitrogen
Flame: On
Lit offset: 1.0

BACK DETECTOR (ECD)

Temperature: 385°C (On)
Anode purge flow: 6.0 mL/min (On)
Mode: Constant makeup flow
Makeup flow: 5.0 mL/min (On)
Makeup Gas Type: Nitrogen
Adjust offset: 60.00

AUX PRESSURE 3

Gas Type: Nitrogen
Initial pressure: 1.000 bar (On)

AUX PRESSURE 4

Gas Type: Argon methane 5%
Initial pressure: 3.000 bar (On)

AUX PRESSURE 5

Gas Type: Argon methane 5%
Initial pressure: 4.200 bar (On)

METHANISER

Temperature: 385°C (On)

VALVES TABLE

Valve	Type	Description	Initial position	OFF	ON
1	switching	FID injection	OFF	Sample load	Sample inject
2	switching	ECD injection	OFF	Sample load	Sample inject
3	switching	FID methaniser bypass	OFF	no bypass	bypass
4	switching	ECD bypass	OFF	bypass	no bypass
5	switching	signal to Labview	OFF	0	1
6	switching	between sample loops	ON	closed	open
7	switching	MFC valve control	OFF	closed	open
8	switching	Sample inlet	ON	closed	open

TIME TABLE

Time	Specifier	Parameter & Setpoint	Detector	Comment
0.01	Aux 3 Pressure	0.00 bar	FID	pressure decrease needed for Valve 3 switching, otherwise the FID flame is blown off
0.01	Valve 5	On		start signal to Labview program
0.01	Valve 6	On	FID, ECD	start sample load
0.01	Valve 8	On	FID, ECD	start sample load
0.02	Valve 7	On	FID, ECD	start sample load
0.50	Valve 3	On	FID	methaniser bypassed
0.50	Valve 5	Off		stop signal to Labview program
0.55	Aux 3 Pressure	3.80 bar	FID	back to work pressure after Valve 3 switch
1.00	Valve 8	Off	FID, ECD	end sample injection
1.15	Aux 4 Pressure	0.15 bar	ECD	pressure adjustment according to valves position
1.20	Valve 1	On	FID	FID sample injection
1.20	Valve 2	On	ECD	ECD sample injection
3.30	Valve 3	Off	FID	sample through methaniser for CO detection
4.48	Valve 1	Off	FID	FID pre-column back-flushing
4.48	Valve 6	Off	FID, ECD	separate FID and ECD sample loops
4.50	Aux 3 Pressure	4.00 bar	FID	pressure adjustment according to valves position
4.50	Aux 4 Pressure	3.00 bar	ECD	pressure adjustment according to valves position
4.50	Aux 5 Pressure	4.80 bar	ECD	pressure adjustment according to valves position
4.50	Valve 2	Off	ECD	ECD pre-column back-flushing
4.50	Valve 4	On	ECD	lead sample to ECD, after the oxygen was flushed outside
4.80	Valve 6	On	FID, ECD	start sample load for next run
5.00	Valve 8	On	FID, ECD	start sample load for next run
7.00	Aux 5 Pressure	4.20 bar	ECD	pressure adjustment according to valves position
7.00	Valve 4	Off	ECD	ECD bypass
7.00	Valve 7	Off	FID, ECD	MFC valve closed

INTEGRATION EVENTS

FID Signal Specific Integration Event Table

Event	Value	Time
Initial Slope Sensitivity	0.900	Initial
Initial Peak Width	0.220	Initial
Initial Area Reject	1.000	Initial
Initial Height Reject	0.100	Initial
Initial Shoulders	OFF	Initial
Integration	OFF	0.000
Integration	ON	2.200
Integration	OFF	3.200
Integration	ON	3.450
Slope Sensitivity	0.600	3.500
Fixed Peak Width	0.400	3.500
Integration	OFF	4.450

ECD Signal Specific Integration Event Table

Event	Value	Time
Initial Slope Sensitivity	0.800	Initial
Initial Peak Width	0.400	Initial
Initial Area Reject	3.915	Initial
Initial Height Reject	0.190	Initial
Initial Shoulders	OFF	Initial
Integration	OFF	0.000
Integration	ON	4.600
Baseline Now		4.650
Baseline Now		5.750
Integration	OFF	6.800

Appendix 4

MODEL-2 least squares fit (York et al., 2004)

The method iteratively minimizes the weighted residuals in both x and y . The x - and y -errors are assumed independent. The weight function is based on the assigned x and y uncertainty vectors. In this particular case the individual uncertainties for each measurement point are not known. The x - and y - uncertainties for all the data points are based on the estimated average analytical precision (0.1 ppm for CO₂ and 1 ppm for O₂/N₂).

The equations (1) – (4) are used to determine the slope, intercept and the corresponding errors according to York et al., 2004. Equation (2) must be solved iteratively.

$$a = \bar{Y} - b\bar{X} \quad (1)$$

$$b = \frac{\sum W_i \beta_i V_i}{\sum W_i \beta_i U_i} \quad (2)$$

$$\sigma_a^2 = \frac{1}{\sum W_i} + \bar{x}^2 \sigma_b^2 \quad (3)$$

$$\sigma_b^2 = \frac{1}{\sum W_i u_i^2} \quad (4)$$

where:

a, b – y -intercept and slope for the best line, $y = a + bx$

\bar{X}, \bar{Y} – weighted averages of the observed values X_i and Y_i

W_i – weight function

β_i – defined below (point 5.)

V_i, U_i – residuals for x and y

σ_a, σ_b – LSE standard errors of the intercept and slope

\bar{x} – adjusted weighted average for x

Calculation sequence

Note: the index i refers to the element i of the data vectors X and Y , and it is not the iteration index.

1. Calculate an initial value of b by ordinary least squares method
2. Determine the partial weights $\omega(X_i)$ and $\omega(Y_i)$ for each of the measurement points, based on the assigned uncertainty vectors σ_x and σ_y :

$$\omega(X_i) = 1/\sigma_x^2; \quad \omega(Y_i) = 1/\sigma_y^2$$

3. Compute the weight function W_i for each point based on the weights $\omega(X_i)$ and $\omega(Y_i)$ and the last estimated slope b :

$$W_i = \frac{\omega(X_i)\omega(Y_i)}{\omega(X_i) + b^2\omega(Y_i)}$$

4. Calculate \bar{X} and \bar{Y} using the observed points (X_i, Y_i) , and W_i

$$\bar{X} = \frac{\sum W_i X_i}{\sum W_i} \quad \bar{Y} = \frac{\sum W_i Y_i}{\sum W_i}$$

5. Calculate U_i , V_i and β_i

$$U_i = X_i - \bar{X}; \quad V_i = Y_i - \bar{Y}; \quad \beta_i = W_i \left[\frac{U_i}{\omega(Y_i)} + \frac{bV_i}{\omega(X_i)} \right]$$

6. Calculate a new value for b , using equation (2) and the last estimated W_i , U_i , V_i and β_i

7. Use the new b and repeat the steps 3, 4, 5 and 6 until successive estimates of b agree within a chosen tolerance (in this case the tolerance was set at 10^{-6})

8. From the final values of b , \bar{X} and \bar{Y} calculate a using equation (1)

9. For each point X_i calculate the adjusted values x_i

$$x_i = \bar{X} + \beta_i$$

10. From x_i and W_i calculate \bar{x} and u_i

$$\bar{x} = \frac{\sum W_i x_i}{\sum W_i}; \quad u_i = x_i - \bar{x}$$

11. From W_i , \bar{x} and u_i calculate σ_b and σ_a using the equations (4), respective (3)

Appendix 5

Supplementary figure for Chapter 7

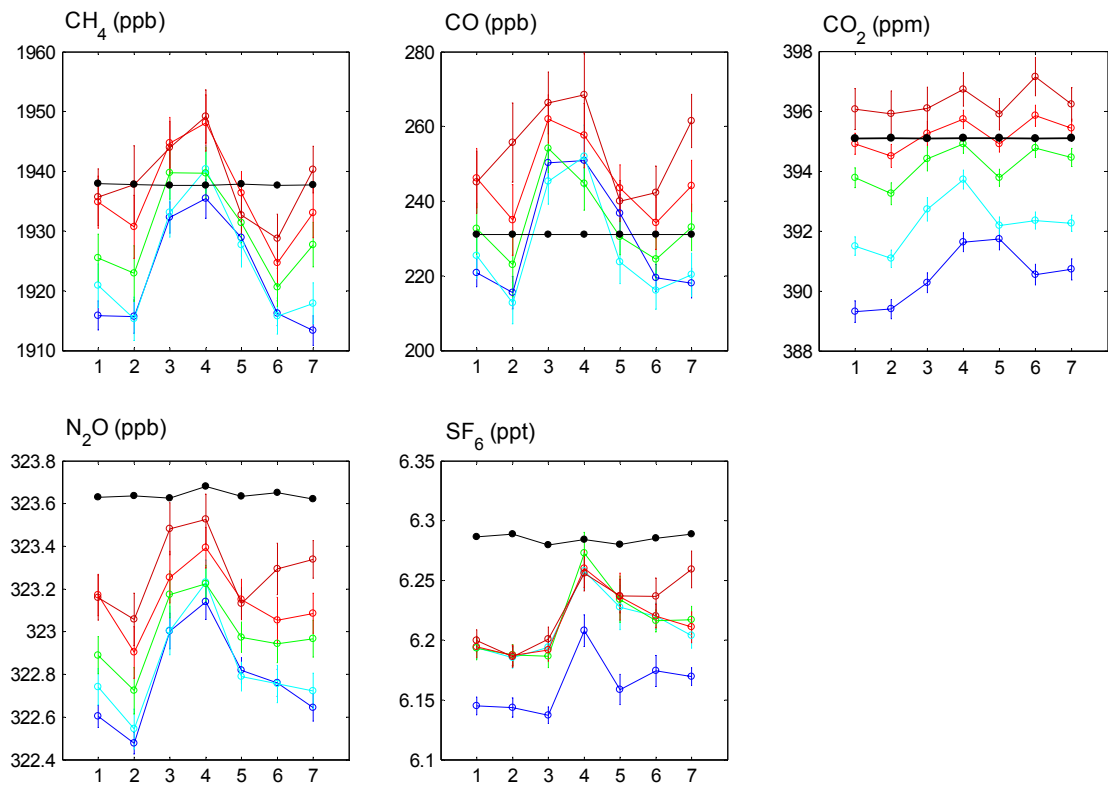


Figure A5.1 Comparison between the weekly variations of each species with the target measurements. The results show that the weekly variations observed in the air measurement are not due to a weekly periodicity of the measurement system functioning.

List of abbreviations and acronyms

MPI-BGC	– Max-Planck Institute for Biogeochemistry (Germany)
NOAA	– National Oceanic & Atmospheric administration (USA)
- CMDL	– Climate Monitoring and Diagnostics Laboratory
- GMD	– Global Monitoring Division
- ESRL	– Earth System Research Laboratory
SIO	– Scripps Institute of Oceanography (USA)
CSIRO	– Commonwealth Scientific and Industrial Research Organization (Australia)
NIWA	– National Institute of Water and Atmospheric Research (New Zealand)
WMO	– World Meteorological Organization
GAW	– Global Atmosphere Watch
IPCC	– Intergovernmental Panel of Climate Change
UNEP	– United Nations Environment Programme
CHIOTTO	– Continuous High-precision Tall Tower Observations of Greenhouse Gases in Europe
CE-IP	– CarboEurope Integrated Project
GWP	– Global Warming Potential
HFC	– Hydro-fluoro-carbon
PFC	– Per-fluoro-carbon
CFC	– Chloro-fluoro-carbon
APO	– Atmospheric Potential Oxygen
PCTFE	– Poly-chloro-tri-fluoro-ethylene
IR	– Infrared (radiation)
NDIR	– Non-Dispersive InfraRed (CO ₂ analyzer)
WT	– Working Tank (reference gas)
GC	– Gas Chromatograph

FID – Flame Ionization Detector

ECD – Electronic Capture Detector

ppm (ppb, ppt)– part per million (per billion, trillion)

Definitions

Atmospheric lifetime - the burden (Tg) divided by the mean global sink (Tg/yr) for a gas in a steady state (i.e., with unchanging burden) (IPCC 2001, page 247).

Radiative forcing - has been employed in the IPCC Assessments to denote an externally imposed perturbation in the radiative energy budget of the Earth's climate system. Definition as given in IPCC 2001:

“The radiative forcing of the surface-troposphere system due to the perturbation in or the introduction of an agent (say, a change in greenhouse gas concentrations) is the change in net (down minus up) irradiance (solar plus long-wave; in Wm^{-2}) at the tropopause AFTER allowing for stratospheric temperatures to readjust to radiative equilibrium, but with surface and tropospheric temperatures and state held fixed at the unperturbed values”.

Global warming potential (GWP)

The GWP has been defined as the ratio of the time-integrated radiative forcing from the instantaneous release of 1 kg of a trace substance relative to that of 1 kg of a reference gas, taken usually to be CO_2 (IPCC, 1990).

Fractionation is a separation process in which a certain quantity of a mixture (solid, liquid, solute or suspension) is divided up in a large number of smaller quantities (fractions) in which the composition changes according to a gradient.

Definitions of terms related to the data quality

[according to EUROMET - the Regional Metrology Organisation for Europe under the CIPM MRA]

Measurand: Particular quantity subject to measurement.

Measuring result: Value attributed to a measured measurand by measurement.

Corrected result: Measuring result after correction for systematic error.

Measuring error: Result of a measurement minus a true value of the measurand.

Measuring (working) range: Set of values of measurands for which the error of a measuring instrument is intended to lie within specified limits.

Accuracy of measurement: Closeness of the agreement between the result of a measurement and a true value of the measurand.

Random error: Result of a measurement minus the mean that would result from an infinite number of measurements of the same measurand carried out under repeatability conditions.

Relative error: Error of measurement divided by a true value of the measurand.

Repeatability (of results of measurements) Closeness of the agreement between the results of successive measurements of the same measurand carried out under the same conditions of measurement.

Reproducibility (of results of measurements) Closeness of agreement between the results of measurements of the same measurand carried out under changed conditions of measurement.

Experimental standard deviation: Parameter for a series of n measurements of the same measurand, characterises the dispersion of the results and is given by the formula for standard deviation.

Systematic error Mean that would result from an infinite number of measurements of the same measurand carried out under repeatability conditions minus a true value of the measurand.

Traceability: Property of the result of a measurement or the value of a standard whereby it can be related to stated references, usually national or international standards, through an unbroken chain of comparisons all having stated uncertainties.

Uncertainty of measurement: Parameter, associated with the result of a measurement that characterizes the dispersion of values that could reasonably be attributed to the measurand. The estimation of uncertainty in accordance with GUM guidelines is usually accepted.

Acknowledgements

I came almost five years ago from Romania, in a world which was totally foreign to me. I had the will to learn and to do things, but this would not have been enough to be successful. I met people who helped me to make it possible and getting to know these people is one of the most valuable things I achieved during this years. Some of them I admire and respect, some of them became my friends. I also lost some friends, but I will try to remember about them only the moments of joy.

It is not possible to list here all the people who influenced my life and work during this time. I will only mention some of them, and I hope the others will forgive my choice.

Martin Heimann is my MPI-BGC supervisor and the director of the institute. The strategic position of my office vis-à-vis of Martin's office led to many interruptions of his work by me; Martin received most of them with a smile and with readiness to help, to discuss and to make future plans. I thank Martin for having almost always five minutes to see an interesting graph, even when he knew that the five minutes might become two hours. I thank him also for the trust and support he gave me in some of the most difficult moments of my PhD time.

Wolfgang Weigand, my PhD supervisor from Friedrich-Schiller University, had always the door open for me when I was "spontaneously" visiting his office. Short visits became long discussions about my work and molecular orbitals. I am grateful for his time, his interest in my work and his kind willingness to help.

Andrew Manning was my supervisor during the first two years of my PhD, and the leader of the project until he left the institute in 2005. As leader of the group, he oversaw the design of the measurement system for Bialystok, the equipment choice and part of the practical work. Andrew also gave me the opportunity to learn a lot by working for his already existing measurement station at Ochsenkopf, and he helped me to get a clear idea about what science is, and about how I want and how I don't want to be as a scientist.

Manuel Gloor was one of my official supervisors during the first few months of my PhD, until he left the institute. After he left, he continued voluntarily to be my advisor; he helped me during my whole PhD time, and had an important role in improving my work and this thesis. As an example of his almost unlimited willingness to help, I want to mention this: Manuel, a pure "computer guy", came from USA to Poland,

to help me with the installation of the measurement system at the tower site. I want to thank Manuel for helping me to believe that everything has a solution, and that mathematics and computers do not hurt. I also thank him for giving me trust and example that science can and has to be clean.

Armin Jordan was in fact my advisor long before he became my official advisor. The setup of the gas chromatograph at Bialystok is in large part based on his previous work for Ochsenkopf. He spent many hours teaching and helping me, and the general setup of the Bialystok measurement greatly benefited from his experience in measurement and quality assurance strategy. I learned a lot from Armin, about gas chromatographs, about the honesty of measurements and about helping the others without making them feeling uncomfortable. He spent also a lot of time reviewing my thesis and his effort greatly improved the result. One of my hopes for the future is to have again opportunities to work with Armin.

Uwe Schultz is for me the representative of the German engineering talent. Uwe participated to the design and installation of almost all the measurement equipment for Bialystok. Among other contributions, Uwe designed and built the meteorological measurement system, the electrical and air conditioning installations and supervised the installation of the sampling lines on the tower. Moreover, during the time of building and installing the Bialystok measurement system, Uwe was the person who would fix any machine which refused to function with me. During my PhD, Uwe became one of the people I trust the most and one of the people I am proud to call friend. I thank Uwe for all his work, for coffee breaks with “realistic” moral support and for being my friend even when he knew that this was not the best strategy.

Falk Haensel is one of the most remarkable people I know, and I’m glad I had the chance to know him. Falk is an infinite source of energy and good mood for the people around, and organizes and gets things moving when everybody else is exhausted. Even when he is tired, sad or ill, Falk still keeps working, smiling and supporting the others. I am grateful for the huge work he did and keeps doing with the gas cylinders, generators and many other things, work that not many people could do. I thank Falk more than all for being the Sunny-Boy, for having energy and chocolate to give, for supporting me when almost nobody did, and for saying openly what he thinks.

I thank Thomas Seifert for making the complex Labview based program which controls most of the operation of the Bialystok measurement system, and for his

important contribution to managing the communication between computers and equipment.

Willi Brand is the specialist in oxygen measurements and another colleague I learned a lot from. I thank Willi for his readiness to discuss, for the never-ending measurements of our gas cylinders and for all the help and trust he gave me.

I thank Michael Hielscher for his help with the meteorological measurement, and for recovering our lost data, when none of the computer people could help. I still owe him a lot of cakes – I did not forget.

Kristina Trusilova is one of the people who I like and admire, and I hope her to be my friend for very long time. I thank her for measurements versus modeling coffee breaks, small and big talks, motivating postcards, good advices which I agreed to, although almost never followed. More than all, I want to thank her for never letting me down, in good as in bad times.

I am grateful to Rona Thompson for offering me a view on the meandering ways of New Zealand type English politeness, and for accepting that I'm neither English nor particularly polite. I appreciate her strength to declare that she is my friend when she was required not to be, although she knew that this means troubles.

Antje Moffat was always a kind and supportive friend and colleague, and an example that one can go on even when the situation is hard. I thank Antje for the nice time we spent together with her and her family, and I wish her not to change.

Karen Schindler is the master of organizing and solving problems, and she took me out of a lot of papers-related troubles. I thank Karen for all and I hope she will help me to solve the upcoming problems...

Julia Steinbach is always a source of good mood and energy, and I enjoyed the reading clubs and various social events she organized.

Galina Churkina and Christian Roedenbeck are colleagues I never directly worked with, yet we had long discussions about my work and not only. Their interest in my work and their moral support gave me trust, enthusiasm and helped me to go on.

I am grateful to Doug Worthy for his advice regarding the gas chromatograph setup, and I thank CHIOTTO project participants for useful discussions during conferences and workshops. I also thank Ralph Keeling for interesting and helpful discussions regarding the oxygen measurements.

Aelita Wagner was the best possible flat mate, and large part of this thesis was written in our garden, in Aelita's working company. I will always miss Aelita and our garden...

And most of all, I thank to my family in Romania, who accepted to let me go and keeps waiting for me since then.

CURRICULUM VITAE

Maria Elena Popa

Date and place of birth: 14-Nov-1974, Oradea, Romania

Citizen of Romania

Education and employment

- 2005: PhD student – Friedrich-Schiller University, Jena, Germany
- 2003: PhD student – Max Planck Institute for Biogeochemistry, Jena, Germany
- 2001 - 2003: Project engineer for technical security systems – Argus Standard Security SA, Bucharest, Romania
- 1999 - 2001: Technological engineer for electronic components – Baneasa SA, Discrete Device Division, Bucharest, Romania
- 1998 - 1999: FoxPro databases operator – I.S.C.I.R., Bucharest, Romania
- 1998: License and Diploma of Physicist Engineer – Physics Faculty, University of Bucharest, Romania
- 1997 - 1998: Non-destructive testing technician – S.C. NAMICON, Bucharest, Romania
- 1996 - 1998: Specialization in Technological Physics – Metrology & Non-destructive testing department, Physics Faculty, University of Bucharest, Romania
- 1993 - 1998: Physics studies – Physics Faculty, University of Bucharest, Romania
- 1993: Baccalaureate
- 1989 – 1993: Lyceum – I. L. Caragiale, Bucharest, Romania

Presentations

Talks

“Progress report on Ochsenkopf and Bialystok tall towers”

E. Popa, A. Manning, M. Gloor, U. Schultz, T. Seifert, A. Jordan, M. Heimann, E. D. Schulze

CHIOTTO First Annual Meeting, Budapest, 6-7 November 2003

“Tall Tower Measurements of Greenhouse Gases”

E. Popa, A. Manning, M. Gloor, U. Schultz, T. Seifert, R. Krause, A. Jordan, M. Heimann

Communication Seminar MPI-BGC, 12 December 2003, Jena

“Progress report on Ochsenkopf and Bialystok tall towers”

E. Popa, A. Manning, M. Gloor, U. Schultz, T. Seifert, F. Haensel, A. Jordan, M. Heimann, E. D. Schulze

CHIOTTO 2nd annual meeting, 17 September 2004, Schagen, Netherlands

“Tall Tower Measurement Bialystok, Poland”

E. Popa, A. Manning, M. Gloor, U. Schultz, F. Haensel, T. Seifert, R. Krause, A. Jordan, M. Heimann, D. Schulze

Institute retreat, 26-Jan-2005, Oberhof

“Bialystok (BIK) report”

E. Popa, M.-Gloor, U. Schultz, F. Haensel, T. Seifert, A. C. Manning, A. Jordan, M. Heimann

CHIOTTO 3rd Annual Meeting, 19 October 2005, CEA, Paris

“Bialystok (BIK) report”

E. Popa, M.-Gloor, U. Schultz, F. Haensel, T. Seifert, A. C. Manning, A. Jordan, M. Heimann

CHIOTTO Final workshop: The potential of tall tower concentration data for improvement of greenhouse gas emission estimates, 09-10 March 2006, Amsterdam

“Tall tower measurement – Bialystok, Poland (BIK)”

E. Popa, M.-Gloor, U. Schultz, F. Haensel, T. Seifert, A. C. Manning, A. Jordan, M. Heimann

MPI-BGC Retreat, 20 March 2006, Kloster Nimbschen

“Tall tower measurement – Bialystok, Poland (BIK)”

E. Popa, M.-Gloor, U. Schultz, F. Haensel, T. Seifert, A. Jordan, M. Heimann

CarboEurope Atmospheric Component - Data flagging workshop, 21 September 2006, Heidelberg

“Greenhouse gases measurements – Bialystok tall tower station”

E. Popa, U. Schultz, F. Haensel, T. Seifert, A. Jordan, M. Gloor, M. Heimann

MPI-BGC Retreat, 12 – 14 February 2007, Oberhof

Posters

“CHIOTTO – Continuous High-precision Tall Tower Observations of Greenhouse Gases in Europe”

E. Popa, A. Manning, M. Gloor, U. Schultz, T. Seifert, A. Jordan, R. Krause, C. Rödenbeck, M. Heimann, D. Schulze

MPI-BGC Scientific Advisory Board Meeting, Jena, 2005

“First results from a 300 m tower atmospheric measurement station for greenhouse gases – Bialystok, Poland (BIK)”

E. Popa, M.-Gloor, A. C. Manning, U. Schultz, F. Haensel, T. Seifert, A. Jordan, R. Krause, E.D.-Schulze, M. Heimann

Seventh International Carbon Dioxide Conference (ICDC7) 26 – 30 September 2005, Broomfield, Colorado

“BIK TALL TOWER (Bialystok, Poland) – Greenhouse gases concentration measurement”

E. Popa, M. Gloor, U. Schultz, F. Haensel, T. Seifert, A. Jordan, A. C. Manning, C. Roedenbeck, M. Heimann

Open Science Conference on the GHG Cycle in the Northern Hemisphere, 14-18 November 2006, Sissi-Lassithi, Crete

“Monitoring atmospheric greenhouse gases – Results from a continental tall tower measurement (Bialystok, Poland)”

E. Popa, E. Gloor, A. Jordan, U. Schultz, F. Haensel, T. Seifert, A. Manning, M. Heimann
European Geosciences Union, General Assembly 2007, Vienna, Austria, 14 - 21 April 2007

“Results from a tall tower measurement station – Bialystok, Poland (BIK)”

E. Popa, M. Gloor, A. Jordan, U. Schultz, F. Haensel, T. Seifert, A. Manning, M. Heimann
14th WMO/IAEA Meeting of Experts on Carbon Dioxide, Other Greenhouse Gases, and Related Tracer Measurement Techniques, 10-13 September 2007, Helsinki

Selbständigkeitserklärung

Ich erkläre, dass ich die vorliegende Arbeit selbständig und unter Verwendung der angegebenen Hilfsmittel, persönlichen Mitteilungen und Quellen angefertigt habe.

Jena, den 13.10.2007

Maria Elena Popa